Design, synthesis and biological evaluation of sphingosine kinase inhibitors for the treatment of prostate cancer

By

Salha M Tawati

A thesis submitted to the Strathclyde Institute of Pharmacy and Biomedical Sciences

In conformity with the requirements for the degree of Doctor of Philosophy

University of Strathclyde

Glasgow, UK, 2018

Declaration

This thesis is the result of the author's original research. It has been composed by the author and has not been previously submitted for examination, which has led to the award of a degree.

The copyright of this thesis belongs to the author under the terms of the United Kingdom copyright Acts as qualified by University of Strathclyde Regulation 3.49. Due acknowledgement must always be made of the use of any material contained in, or derived from, this thesis.

Signed:

Date:

Acknowledgements

First, I would like to express my deepest sense of gratitude to my supervisors, Prof. Nigel Pyne, Prof. Simon Mackay, and Prof. Susan Pyne for their inspiration, support, encouragement, and excellent advice throughout this project and for their detailed and constructive comments and invaluable guidance toward the writing of my thesis.

I would like to thank all the members (current and past) of the Mackay's and Pyne's research groups who have skillfully assisted me during my studies in different ways: Dr Jessica Baiget (co-worker), Paula Lopez Rivas (co-worker), Dr. Giacomo Berretta, Dr Chris Lawson, Dr Dave Breen, Dr Nahoum Anthony, Dr Neil MacRitchie, Dr Stephanie Boomkamp and Dr Stuart Cochrane.

My thanks must also go to Mrs Louise Young and Ms Gráinne Abbott for their help with my ADP-Glo assays.

Many thanks to my postgraduate colleagues in Mackay's and Pyne's labs for their support and useful time experiences and information we have shared. I offer my regards and blessings to all my friends in Glasgow, the writing-up rooms and in SIPBS who supported me in many respects during my study.

My thanks go to my special friend Ms. Aisha Alsfouk for her motivating company during my PhD journey. You are a true friend and my time in SIPBS would not have been the same without you.

I would like to thank the Libyan embassy and Institute of Higher education in Libya for offering me a scholarship to pursue my studies at the University of Strathclyde.

 My infinite appreciation and thanks goes to mum and to all my sisters and brothers, especially my sister Dr Mabrouka and my brother Dr Ali: thanks a lot for your motivation, love and caring.

I am eternally grateful for my husband (Elbibani) for his endless love, kindness, caring, patient and extensive support in completing my PhD, for always believing in me and making me feel that everything is achievable.

Finally, my greatest thanks go to my beloved sons (Almontiser and Aboubaker); you are a precious gift. I am so grateful for having you and I am very regretful for giving you so little time throughout my PhD.

Dedication

This thesis is dedicated in loving memory of my father and my brother (Almontiser), who encourage my curiosity toward science, I'm so sorry that even I have not got the chance to say thanks for you. I know that you would love to see me getting my PhD degree.

Table of Contents

List of Figures

xii

List of Tables

List of Schemes

Abbreviations

Å	Angstrom(s)
ABC294640	3-(4-Chlorophenyl)-adamantane-1-carboxyliacid(pyridin-4-ylmethyl)amide
Ala	Alanine
AMP	Adenosine monophosphate
Asp	Aspartic acid
ATP	Adenosine triphosphate
BSA	Bovine serum albumin
°C	Degree (s) Celsius
cAMP	Cyclic adenosine monophosphate;
$CDCl_3$	Deuterated chloroform,
Cer	Ceramide
CerS	Ceramide synthase
CERT	Cer transfer protein
CH_2Cl_2	Dichloromthane
^{13}C NMR	Carbon NMR
C-terminus	Carboxylic acid-terminus,
Cys	Cysteine
D	Doublet
Da	Kilo Dalton(s),
DAG	Diacylglycerol
DCE	Dichloroethane,
Des1	Dihydrocermide desaturase
dd	Doublet of doublet,
DIBAL-H	Diisobutylaluminiumhydride,
DMSO-d_6	Deuterated dimethyl sulfoxide,
DMSO	Dimethyl sulphoxide;

DNA	Deoxyribonucleic acid
EFCS	European foetal calf serum;
EGF	Epidermal growth factor;
ER	Endoplasmic reticulum
ERK	Extracellular signal-regulated kinase
Et_3N	Triethylamine
Et_2O	Diethyl ether
Eq	Equivalent(s)
eV	Electron volt(s),
FTY720	2-amino-2-[2-(4-octylphenyl)ethyl]-1,3-propanediol
g	Gramme(s)
GCerase	Glucosyl ceramidase
Glu	Glutamic acid,
GOLD	Genetic optimization for ligand docking
h	Hour(s)
H-bond	Hydrogen bond
HDAC	Histone deacetylase
HER2	Human epidermal growth factor receptor-2
^{1}H NMR	Proton NMR
hPASMC	human pulmonary aortic smooth muscle cells
HRMS-ESI	High resolution mass spectrometry-electrospray ionization
H_2SO_4	Sulphuric acid
HTS	High throughput study
Hz	Hertz
IC_{50}	Half maximal inhibitory concentration
Ile	Isoleucine
IP3	Inositol trisphosphate
J	Coupling constant
JNK	C-Jun N-terminal kinase
Kg	Kilogram

K_2CO_3	Potassium carbonate
K_{ic}	Competitive inhibition constant
K_{iu}	Uncompetitive inhibition constant;
Km	Michaelis constant
LC-MS	Liquid chromatography-mass spectrometry
Leu	Leucine
LPP	Lipid phosphate phosphatase
MAPK	Mitogen-activated protein kinase
MeCN	Acetonitrile
MEK	MAPK/ERK kinase
Met	Methionine
MG132	Carbobenzoxy-L-leucyl-L-leucyl-L-leucinal
mg	Milligramme(s),
$MgSO_4$	Magnesium sulphate,
MHz	Mega hertz
µg	Microgram
µM	Micromolar
µL	Microlitre(s)
mins	Minutes
mL	Millilitre(s)
mM	millimole(s)
M	Molar
m	Multiplets
MS	Mass spectrometry
$NaBH(OAc)_3$	Sodium triacetoxyborohydride
nM	Nanomolar
NA	Not Active
NMR	Nuclear Magnetic Resonance
NAC	*N*-acetyl *L*-cysteine
PARP	Poly ADP ribose polymerase

PBS	Phosphate buffered saline
PDGF	Platelet derived growth factor
PI3K	Phosphatidylinositol 3-kinase
pKa	Acid dissociation constant
PA	phosphatidic acid
PLC	Phospholipase C
Pgp	P-glycoprotein
PMA	Phorbol 12-myristate 13-acetate
PMSF	Phenylmethylsulphonyl fluoride
PP2A	Protein phosphatase 2A
ppm	Parts per million
PS	phosphatidylserine
q	Quartet
RIP1	Receptor interacting protein 1
rt	Room temperature
s	Singlet
SAR	Structure activity relationship
SDS	Sodium dodecyl sulphate
SDS-PAGE	Sodium dodecyl sulphate-polyacrylamide gel electrophoresis
Ser	Serine
SiO_2	Silicon dioxide
siRNA	Small interfering RNA
SK	Sphingosine kinase
SKi	2-(p-Hydroxyanilino)-4-(p-chlorophenyl)thiazole
SMase	Sphingomyelinase
SMS	Sphingomyelin synthases
Sph	Sphingosine
S1P	Sphingosine 1-phosphate
S1PP	S1P phosphatase
S1PR	S1P receptor

t	Triplet
TFA	Trifluoroacetic acid
Thr	Tyrosin
TRAF2	Tumor necrosis factor receptor-associated factor 2
Val	Valine
VEGF	Vascular endothelial growth factor.

Abstract

Sphingosine is phosphorylated via the action of the enzymes sphingosine kinase 1 (SK1) and sphingosine kinase 2 (SK2) to produce the bioactive signalling molecule sphingosine 1-phosphate (S1P). S1P drives cancer cell proliferation and migration whilst also promoting cell survival. Many studies have demonstrated that SK is a promising target for the treatment of cancer and the development of novel isoform-selective SK inhibitors to treat human cancers is of major interest. To date, inhibitors for this enzyme have either been selective for SK1 or non-selective for both isoforms. However, most SK inhibitors have only weak potency. This project involves the design and synthesis of small molecule inhibitors of SK as potential anti-cancer compounds.

In this drug discovery project, a series of potent and selective inhibitors of SK (SK1 or SK2 or SK1/SK2) were developed based on the structure of PF-543, a known potent SK1 selective inhibitor. Analogues of PF-543 were prepared that were potent selective inhibitors of SK1 over SK2 and nM potent SK2 inhibitors with selectivity over SK1. These compounds represent some of the first nM potent SK2 inhibitors with selectivity over SK1. Indeed, the studies identified a structural determinant in the catalytic site of SK1 and SK2 that confers selectivity, with the heel and toe regions of the so-called J-channel in either enzyme providing a means toward selectivity.

Exemplars from the series were shown to have potent cellular activity but poor *in vitro* microsomal stability. Effective target engagement and selectivity for SK1 in prostate cancer cell lines (LNCaP and LNCaP-AI) and proliferating human pulmonary artery smooth muscle cells (hPSMAC) were also established. A variety of biological assays associated with SK inhibition were used to evaluate their ability to induce cancer cell death, which was shown to involve a caspase-3/7-independent mechanism.

Our SK1 and SK1/SK2 inhibitors, but not SK2 inhibitors, also reduced expression of dihydroceramide desaturase 1 (Des1) in a dose dependent manner, causing growth arrest and caspase-independent cell death. This project highlighted the importance for combining SK1 with Des1 inhibition in terms of endowing compounds with cytotoxicity against cancer cells.

.

Chapter 1. General Introduction

1.1 Sphingolipids metabolism

Sphingolipids are a class of lipids that are commonly found in cell membranes. [1,2] The sphingolipid metabolites ceramide (Cer), sphingosine (Sph), and sphingosine-1-phosphate (S1P) play a significant role in the regulation of several vital cellular processes such as cell proliferation, survival, senescence, migration and differentiation under both physiological and pathological conditions. [3]

Sphingolipid metabolism (**Figure 1.1**) involves several reactions utilising enzymes at different subcellular localizations to form a multitude of lipids with signaling functions. [4] Ceramide (Cer) is positioned at the center of sphingolipid biosynthesis and catabolism and is therefore defined as a metabolic hub. [3] There are four main metabolic pathways of Cer formation; [4]

1) First, the *de novo* pathway (in the endoplasmic reticulum) leads to the formation of 3-ketodihydrosphingosine via the use of palmitoyl-CoA and serine, and in turn, reduction of 3-keto-dihydrosphingosine to produce dihydrosphingosine. This is then acylated by dihydroceramide synthase to produce dihydroceramides of different chain lengths. [4] There are six different isoforms of ceramide synthases (CerS1-6) and each one selectively binds to acyl chains of varying lengths (C16-C26) coupled to coenzyme A that are required for *N*-acylation of the sphingosine base. [5] The final step is the formation of Cer species via the introduction of a double bond by dihydroceramide desaturase (des1). [6] Cer is then translocated to the Golgi via vesicles or by Cer transfer protein (CERT) [7] where it can be metabolised to other sphingolipids such as sphingomyelin, which is a major component of the plasma membrane, Sph and ceramide-1-phosphate. [8]

2) The sphingomyelinase pathway (in the plasma membrane, Golgi and mitochondria) involves conversion of sphingomyelin into Cer by the action of sphingomyelinase (SMase). Sphingomyelinase activation happens in response to various stimuli, such as vitamin D. [9–14] Cer can then be converted back into sphingomyelin via the action of sphingomyelin synthases (SMS) and exchange of the phosphoryl choline head group of phosphatidylcholine can produce diacyglycerol.

3) The salvage pathway (in endosomes and lysosomes), includes the deacylation of Cer via the action of ceramidases and results in the formation of sphingosine (Sph). Phosphorylation of Sph at the 1-OH position by sphingosine kinases (SK) results in S1P formation. [3] There are two types of sphingosine kinase, namely SK1 and SK2 which are described in detail in **section 1.2**. Cells also have S1P phosphatase (S1PPs) [15] and Cer synthase (CerS) activities that are able to convert S1P back into Sph and Sph to Cer respectively. Alternatively, S1P can be irreversibly metabolised by S1P lyase (S1PL). to ethanolamine phosphate and hexadecenal.[4,15]

4) The glycosphingolipids pathway involves transfer of complex glycosphingolipids in the Golgi to the plasma membrane by vesicular transport followed by metabolism to glucosylceramides that can also be converted to Cer by the action of by glucosyl ceramidase (GCerase) (**Figure 1.1**). [16,17]
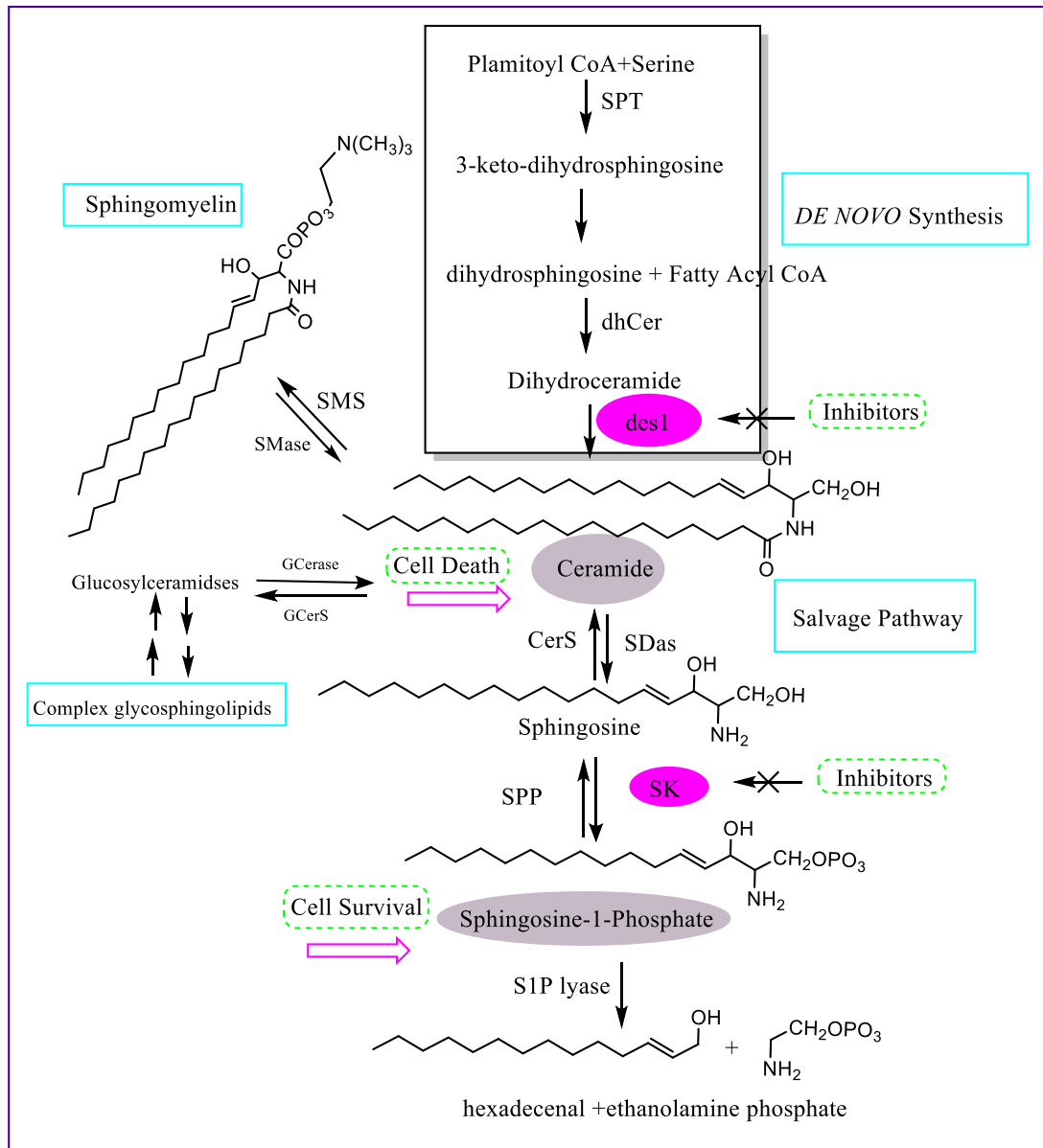
Figure 1.1. Sphingolipid /Ceramide (Cer) metabolism pathways. *De novo* synthesis of Cer and production of sphingosine-1-phosphate (S1P). Key enzymes that are controlling the Cer/S1P rheostat are shown in pink. Also, shown are the chemical structures of Cer, sphingosine (Sph) and (S1P).

1.1.1 Physiological role of sphingolipids: the sphingolipid rheostat

Physiologically, Cer and Sph both promote apoptosis or cell growth arrest. [18–21] S1P, on the other hand, stimulates cell proliferation, growth, and migration. [18,20,22] Cer and S1P are pro-death and pro-survival messengers respectively (**Figure 1.2**); Cer promotes apoptosis through a direct disruptive effect on mitochondria thereby

4

inhibiting cell division. [23] S1P stimulates a number of different pro-survival pathways (mainly the Akt and ERK pathways), the crucial consequence being the production of proteins that inhibit apoptosis. S1P has been implicated in several physiological and cellular processes. [24] For example, S1P is involved in regulating cell survival, and adhesion. [25] In addition, S1P has a role in regulating vascular development, atherosclerosis, inflammation and immunity, tumourgenesis and metastasis. [25,26]

The interconversion of Cer to Sph and S1P is termed the sphingolipid rheostat. [22,27] The balance between signaling by ceramide and sphingosine and S1P is vital in determining cell fate. [3,28] In normal healthy cells, a balance is achieved between pro-survival and pro-death messages, which are dependent on the status of the rheostat. [29] Cellular stress, such as inflammation and irradiation increases Cer production, [30] while cancer is one example where the balance shifts in favour of S1P through the up-regulation of SK.[31]
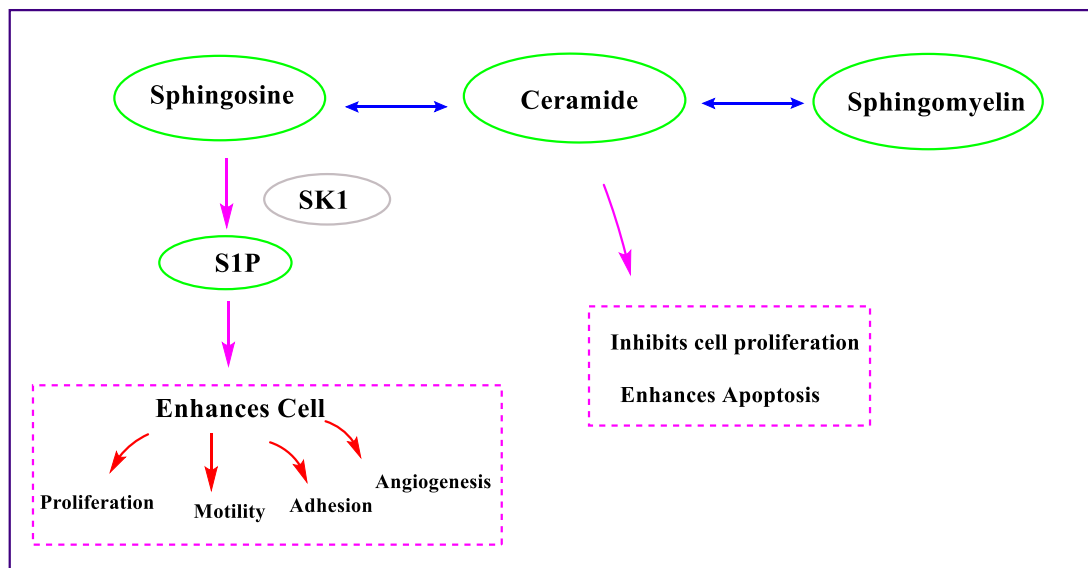
Figure 1.2. Physiological role of Ceramide (Cer) and sphingosine-1-phosphate (S1P). The apoptotic role of Cer by inhibition of cell proliferation and the anti-apoptotic function of S1P via enhancing of cell proliferation, controlled by the sphingolipid rheostat.

Although regulation of the sphingolipid rheostat involves several enzymes (**Figure 1.1**), many studies provide evidence that SK has a crucial role in regulating cell survival. [32–38] In addition, recent studies highlight that dihydroceramide desaturase (Des1)

5

is another crucial enzyme involved in the regulation of cell survival as inhibition of Des1 would reduce pro-apoptotic Cer but could increase dihydroceramides;[39] providing evidence that modulation of both the *de novo* Cer pathway and the sphingolipid rheostat are able to affect cell growth.

1.1.2 Sphingosine 1-phosphate receptors and inside-out signaling

S1P has well-established roles in both normal physiology and pathophysiology.[28] S1P can be used to signal inside the cell or it can be transported outside of the cell, where it binds to S1P receptors with high affinity.[40] S1P receptors (S1PRs) are a family of plasma membrane G-protein coupled receptors that have crucial roles in the sphingolipid pathway.[41] S1P can bind to S1PRs in both a paracrine and autocrine manner in a process termed 'inside-out` signalling. ATP-binding cassette (ABC) transporters[1] and the spinster homologue 2 (Spns2) transporter[42,43] are capable of transporting S1P out of the cell, where it then binds to any one of the five SIPRs (S1P$_1$–S1P$_5$) (**Figure 1.3**). S1P$_1$, S1P$_2$ and S1P$_3$ are expressed in most tissues.[2] S1P$_4$ is commonly found in immune cells and the lungs, while S1P$_5$ is expressed in the central nervous system and skin.[2,40] The S1P receptor subtypes are coupled to a wide range of distinct G proteins (G$_i$, G$_q$ and G$_{12/13}$) that trigger different primary messenger pathways. They can activate phospholipase C (PLC), phosphatidylinositol 3-kinase (PI3K), extracellular signal-regulated kinase (ERK) and Rho pathways or inhibit adenylate cyclase (AC) and Rac signaling (**Figure 1.3**).[2,44]
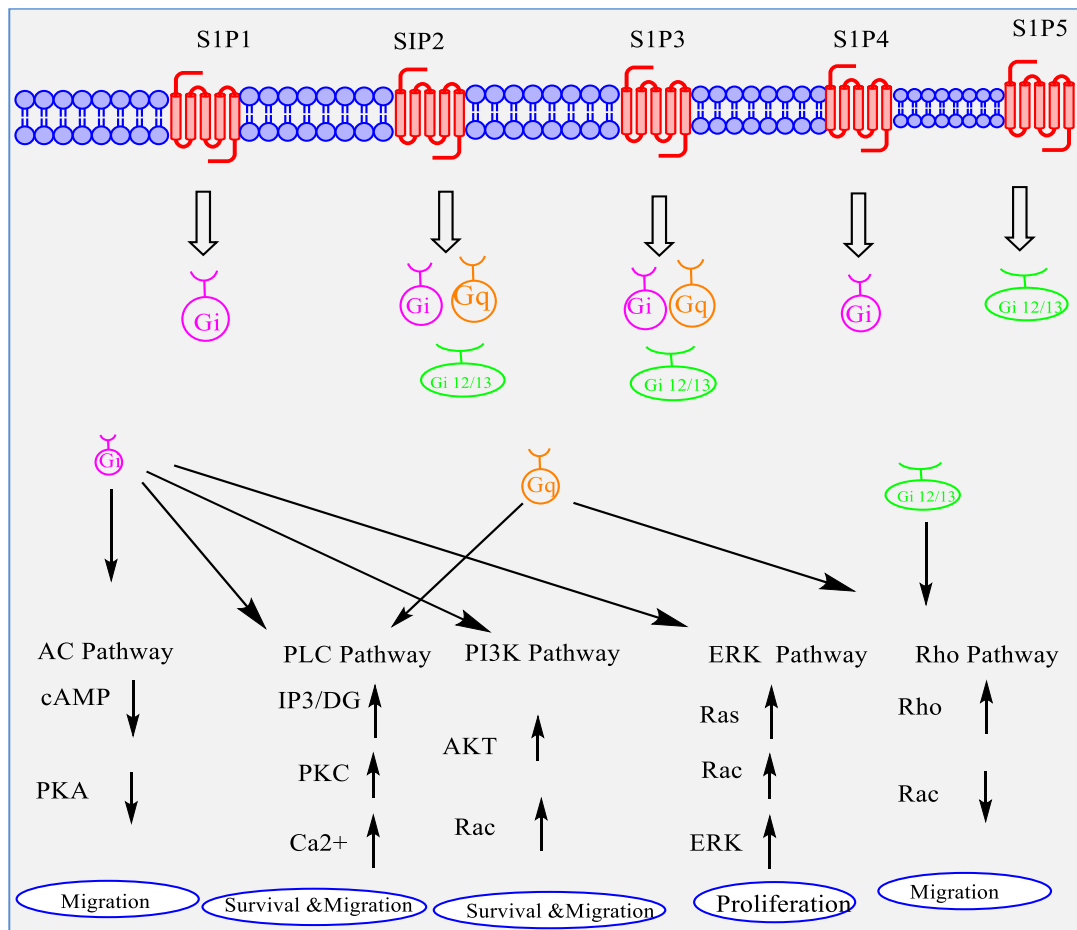
Figure 1.3. The major roles of sphingosine 1-phosphate receptors (S1PRs). Summary of signalling pathways activated upon S1P stimulation of its five GPCR subtypes.

$S1P_1$ couples to G_i and inhibit the AC pathway whilst activating PI3K, PLC and ERK pathways. $S1P_1$ uses both G_i and β-arrestin to regulate the ERK pathway. [2,44–46] The ERK and PLC pathways are responsible for cell proliferation, [3,22] while the PI3K pathway is responsible for migration by increasing Rac expression [2] and cell survival pathways. Indeed, PI3K signalling (increased via Akt) up-regulates the expression of anti-apoptotic proteins including Bcl-2 and Mcl-1, and down-regulating pro-apoptotic proteins such as BAD and BAX. [47–49] $S1P_1$ is widely expressed and has a major role in angiogenesis and vascular maturation, [50] vascular tone, [51] and endothelial barrier function. [52]

Unlike $S1P_1$, $S1P_2$ couples primarily to $G_{12/13}$ and stimulates the Rho pathway to inhibit cell migration. [2,53,54] $S1P_2$ can also couple with G_q to activate PLC[55] and with G_i to

mediate cell proliferation via activation of ERK. [56] $S1P_2$ is predominantly expressed in the vascular smooth muscle cells [55] and plays a key role in the development and/or mediation of neuronal excitability. [57] It is also crucial for the appropriate performance of the auditory and vestibular systems and its underexpression causes deafness. [58,59]

Similar to $S1P_2$, $S1P_3$ can also couple to G_i, G_q and $G_{12/13}$. [30] $S1P_3$ couples most efficiently to G_q to activate PLC and enhance cell angiogenesis. [30] In contrast to $S1P_2$, $S1P_3$ binds to G_i and promotes cell migration via activation of Rac. [2,53] It is highly expressed in the heart, lungs, spleen, kidney, intestine, diaphragm and certain types of cartilage. [60]

$S1P_4$ also couples to G_i and $G_{12/13}$ and stimulates PLC and ERK resulting in cytoskeletal rearrangements after stimulation with S1P. [2,53] Its expression is limited to the immune compartments and leukocytes. [61,62]

$S1P_5$ mediates the inhibition of cell migration through coupling to $G_{12/13}$, resulting in the subsequent stimulation of the Rho pathway. $S1P_5$ also couples to G_i and may also induce cell migration via activation of the Rac pathway. [63] It is highly expressed in the central nervous nervous system and is the predominant receptor in oligodendrocytes, the myelinating cells of the brain. [64,65]

1.1.3 Sphingosine 1-phosphate as an intracellular effector

Choi *et al*., provided the first evidence for the existence of intracellular targets of S1P, reporting an S1PR-independent regulation of intracellular calcium levels.[66] More recently, intracellular S1P produced by SK1 (in the cytosol) was found to activate TRAF2, an E3-ubiquitin ligase involved in the K63 polyubiquitination of receptor interacting protein 1(RIP1). [26] The TRAF2/SK1 complex acts as a scaffold that allows the binding and phosphorylation of IκB kinase, which leads to its subsequent polyubiquitination and degradation and activates NF-κB, a transcription factor regulating the expression of proteins involved in cell survival and the immune response. [26,67,68]

Nuclear S1P formed by SK2 regulates epigenetic-mediated gene expression through inhibition of histone deacetylaces. [26] The enzymatic activity of histone deacetylases HDAC1 and HDAC2 is inhibited by direct binding of S1P, which in turn promotes transcription of tumour suppressors and proto-oncogenes such as the senescence marker p21 and the transcription factor c-fos. [69] Prohibitin (PHB)2, a tumor suppressor protein that regulates mitochondrial assembly and function that mediates mitochondrial respiration via the assembly of the cytochrome-c oxidase, has been reported to bind to SK2-produced S1P. [70]

1.2 Sphingosine kinase

Sph, obtained from Cer (synthesised either *de novo* or via the salvage pathway), is phosphorylated in an ATP-dependent reaction catalysed by the enzyme sphingosine kinase (SK) on its primary hydroxyl group to generate S1P. Two isoforms of SK have been identified: (SK1 [32,71,72] and SK2 [50]). In humans, three splice variants of SK1 (SK1a, SK1b and SK1c) and three splice variants of SK2 (SK2a, SK2b, SK2c) have been reported that differ by their *N*-terminal extensions. [50,73,74] Almost all of the SK1 sequence aligns with regions of the larger SK2, with 47% and 43% amino acid sequence identity for the *N*- and *C*-terminal regions of SK1 [74] as shown in **figure 1.4**. SK1 and SK2 genes are located on different chromosomes: the SK1 gene is on chromosome 17 (17q25.2), while the SK2 gene is on chromosome 19 (19q13.2).
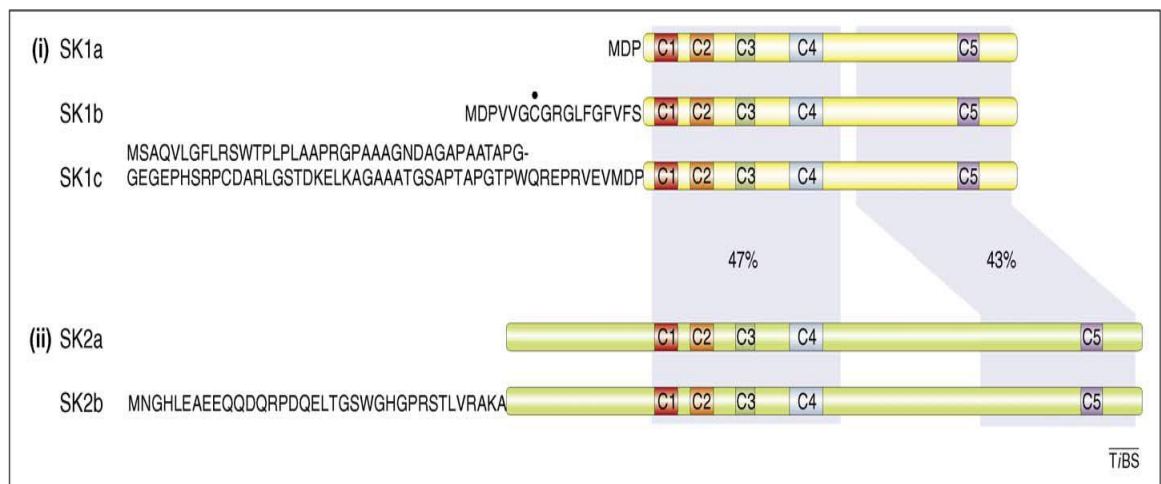
Figure 1.4. **Human sphingosine kinase (SK) isoforms.** C1 – C5 are the highly conserved regions that are evolutionarily conserved within sphingosine kinases. [74]

1.2.1 General structure of human SK

SK has been classified as an evolutionary conserved lipid kinase family that has five conserved domains C1-C5 (**Figure 1.4**). The C1-C3 domains are the putative catalytic regions (nucleotide binding domain) of the enzymes, in common with diacylglycerol (DGK) and Cer kinases. [75] The C4 domain is specific to sphingosine kinases and appears to be less conserved in DGKs.[76] The C5 domain is also conserved in Cer kinase[77] and DGKs[76]. hSK1 consists of three major *N*-terminal variants that are 384, 398, and 470 amino acids in size, while the SK2 enzymes consist of two variants comprising 618 and 654 amino acids. [78] The ATP-binding site in SK1 was shown to reside in the C2-C3 domains of the enzyme within the consensus sequence SGDGx17-21K and only have weak sequence similarity to the well characterised and highly conserved glycine-rich loop motifs of protein kinases. [75,79,80] The Sph binding site in the enzyme was reported to involve a conserved aspartic acid residue (Asp178 in hSK1b, Asp264 in hSK1a and Asp177 in mouse SK1) in the C4 domain.[76,81,82]

1.2.2 Distribution and localization

Interestingly, SK1 and SK2 have almost identical tissue distribution, although SK1 is mainly expressed in the brain, heart, thymus, spleen, kidney, and lung [83] whereas SK2 is more highly expressed in the kidneys and liver. [50] The cytosolic localisation of SK1 is consistent with the lack of a hydrophobic domain. [84] SK2 is localised at the endoplasmic reticulum (ER) and mitochondria and can also shuttle between the cytoplasm and nucleus. [4,85] In rat kidney homogenates, SK activities have been found at the plasma membrane, the endoplasmic reticulum and the cytosol. [86]

1.2.3 Translocation and regulation of SK1

The activation of ERK-1/2 catalyses phosphorylation of Ser225 in hSK1. [36] The consequent increase in enzyme activity is accompanied by its translocation from the cytosol to the plasma membrane, where it is tethered by the direct interaction of specific residues (Thr54 and Asn89) with phosphatidylserine (PS). [87] hSK1 also interacts with phosphatidic acid (PA) at the plasma membrane and in the Golgi; this interaction maps to its *C*-terminus and is independent of catalytic activity or of the

DGK-like domain of the enzyme. [88] hSK1 is also activated by its interaction with TRAF2 via a PPEE379-382 motif and accompanied stimulation by TNFα. [89] The *C*-terminus of hSK1 has a proline-rich domain (the last 17 amino acids) which has been proposed as an SH3-binding sequence. [90,91] Also, translocation of SK1 to and from the nucleus might involve two nuclear export sequences (NES).[92] NES1 lies between amino acids 147-155 while NES2 lies between amino acids 161-169. [92] The export of SK1 from endothelial cells, leading to the extracellular presence of SK1 that affects the vascular S1P gradient, has also been reported. [93]

1.2.4 Translocation and regulation of SK2

hSK2 is phosphorylated by ERK1/2 on either (or both) Ser351 and Thr578 in response to arrange of growth factors and cytokines. [94] Localizationof SK2 to the ER can occur in response to serum deprivation and the S1P 'salvage' pathway that leads to the generation of pro-apoptotic Cer via ER-localized S1P phosphatase and ceramide synthase. [38,95] SK2 localization to the nucleus is regulated by nuclear localization and nuclear export sequences with export being enhanced by PKD-mediated phosphorylation. [85] Cellular release of active SK2 can occur following cleavage at the *N*-terminus by caspase-1 and this allows extracellular generation of S1P. [96] Although there is only little information about hSK2 regulation by phospholipids, the presence of hSK2 at the ER in response to serum starvation suggests that SK2 might also be regulated by phospholipids. [97] It has been suggested that the *N*-terminus (residues 1–175) of hSK2 interacts with 3-*O*-galactosylceramide and phosphoinositides. Indeed, the ability of SK2 to bind these lipids is reduced following deletion of this region. [98] The physiological consequences of these interactions have not been defined. [98]

1.2.5 The SK /S1P pathway in inflammation and immunity.

The SK/S1P pathway is known to play a critical role in many inflammatory responses in diseases such as multiple sclerosis. Furthermore, augmented activity of the SK/S1P pathway is associated with the trigger and perpetuation of ulcerative colitis (UC) and inflammatory bowel disease (IBD). [99] The effects of SK and S1P on epithelial cells, haematopoeitic cells and endothelial cells contribute to their role in inflammatory processes. In cells of the immune system, SK activation occurs after cross-linking of

immunoglobulin surface receptors, a process necessary for downstream signaling. [66,100] Moreover, in epithelial cells, key pro-inflammatory mediators, such as TNFα, IL-11α and LPS cause SK1 activation, which in turn mediate the activation of several proteins such as cyclooxygenase-2 and monocyte chemoattractant protein-1 (MCP-1). [20,49]

1.3 SK/S1P pathway in cancer

Overexpression of SK1 and increased S1P levels is a factor in promoting carcinogenesis, inhibiting apoptosis and increasing the ability of the cells to migrate to produce the development of new blood vessels which are both principal supporting factors of tumour growth and cancer metastasis (**Figure 1.5**). [26]
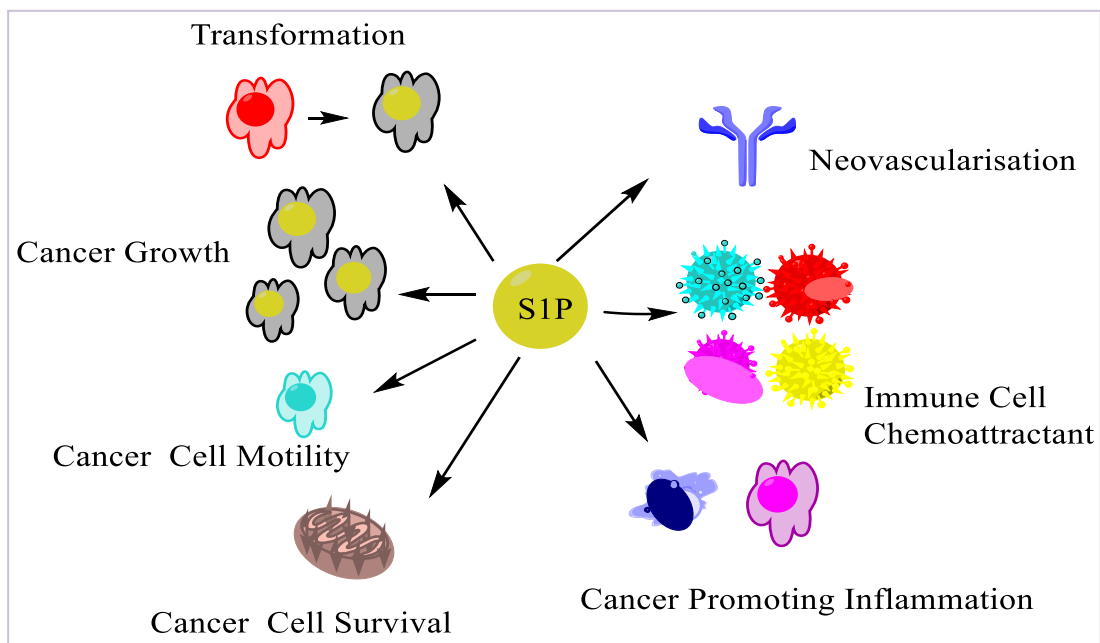
Figure 1.5. The role of S1P action in cancer. S1P engages with its receptors ($S1P_{1-5}$) to facilitate a range of signaling pathways, affecting vital biological processes that are fundamental to cancer pathogenesis.

1.3.1 Cancer cell proliferation and survival

Stimulation of $S1P_1$ and $S1P_3$ receptors enhance cell growth and proliferation through activation of pro-apoptotic ERK, PI3K and NF-kB pathways, while $S1P_2$ promotes cell apoptosis by activating the Rho pathway, which then stimulates small G protein Ras and inhibits Akt signaling. [9,101,102]

Overexpression of $S1P_4$ and SK1 in oestrogen receptor-negative (ER^-) breast tumours was found to be linked to shorter disease-specific survival times and decreased recurrence time in patients. [103] In addition, over-expression of $S1P_1$ and $S1P_3$ has been found to be associated with oestrogen-dependent tumourigenesis of human breast cancer cells. [103] The mechanism underlies oestrogen-dependent tumourigenesis involving the functional interaction between S1P and growth factor signalling pathways, as estradiol stimulates the release of S1P from breast cancer cells which then promotes the release of growth factors such as epidermal growth factor (EGF). [34] The high expression of $S1P_1$ and $S1P_3$ receptors were also linked to poor prognosis in estrogen receptor α (ERα) positive breast cancer patients. [104] Hsu and co-workers found that maintaining tumour growth in lung adenocarcinoma cells induced by $S1P_3$ receptor stimulations increased the expression of the EGF receptor (EGFR) via activation of Rho-associated kinase (ROCK). [105]

$S1P_4$ has been found to stimulate ERK1/ERK2 in MDA-MB-453 breast cancer cells by its interaction with human EGFR 2 (HER2), which results in enhancement of tumour growth. [106] Furthermore, it has been shown that a positive correlation exists between the survival of glioblastoma patients and high expression of $S1P_1$. [107]

1.3.2 Effect of SK/S1P on migration, invasion and metastasis

Tumour metastasis includes both cell migration and invasion. $S1P_1$, $S1P_2$ and $S1P_3$ receptors have been shown to have significant roles in the regulation of cell migration. [54,56] The Rho family of GTPases, particularly RhoA and Rac has been identified as a central controller of cell migration. [9,101,108,109] In various cell types, activation of the $S1P_1$ and/or $S1P_3$ receptor by S1P enhances cell migration through activation of Rac via Gi, while activation of the $S1P_2$ receptor exerts an inhibitory effect on cell migration due to the suppression of Rac activation via $G_{12/13}$. [110,111] Cell migration regulated by S1P receptors ($S1P_1$ and $S1P_3$) includes $G_{i/o}$-mediated stimulation of phosphatidylinositol 3-kinase (PI3K) and Rac. For example, S1P promotes ML-1 thyroid carcinoma cell and MCF-7 breast cancer cell migration via activation of $S1P_1$ and $S1P_3$ and downstream G_i and PI3K-Akt activation. [110]

Long and co-workers found that S1P binding to $S1P_3$ induces a migration of ER+MCF-7 via an SK1-dependent mechanism. [112] Many studies in human glioblastoma cells support the concept of a pro-migratory effect of S1P. [113,114] In addition, S1P was found to enhance the invasiveness of glioblastoma cells by activation of plasminogen activator inhibitor-1 (PAI-1). [115] The activation of RhoA/Rho-kinase is essential for the anti-migratory effect of $S1P_2$ receptor signalling. It was observed that S1P also had inhibitory effects on migration of glioblastoma cells which predominately expressed $S1P_2$ receptors. [116] Therefore, the balance between S1P receptor subtypes seems to be a crucial factor in the metastatic response to S1P; in particular, there is speculation that the balance between signals from the G_i and $G_{12/13}$-Rho pathways has a direct modulation effect on cell migration, either in a positive or negative way. [110,117]

1.3.3 S1P in vasculogenesis and angiogenesis

S1P promotes blood vessel formation through its interaction with vascular endothelial growth factor (VEGF) signaling. [118] VEGF stimulates SK1 activity in T24 bladder cancer cells, which is essential for VEGF-induced activation of Ras and mitogen-activated protein kinase (MAPKs). [119] The suggestion that S1P has an efficient role in vascular physiology originates from the fact that platelets have a high content of S1P [120] and erythrocytes produce S1P as a normal constituent in plasma and serum. [40] A recent study has shown that angiogenesis is enhanced by SK1/S1P-induced proliferation and migration of endothelial cells. [121] $S1P_1$ receptor expression is essential for the maturation of blood vessels during embryonic development [50] and for tumour angiogenesis to support tumour growth. [122]

1.4 Inhibition of S1P receptor signalling for the treatment of cancer

Inhibition of dysregulated S1P signalling in cancer can be targeted using three approaches. The first strategy involved the use of an antibody to eradicate/reduce circulating levels of S1P. [123,124] Secondly, antagonists have been used to prevent S1P binding to S1P receptors to block downstream signaling. The final option involves pharmacological inhibition of SK1 and/or SK2 within the cell using SK inhibitors to reduce the supply of S1P. [22] The murine derived anti-S1P monoclonal antibody (mAB, Sphingomab™) was the first S1P-neutralising antibody developed to reduce the

bioavailability of S1P at its receptors.[123,124] A humanised version of the anti-S1P mAB (Sonepcizumab™) has since been developed and is currently in Phase I clinical trials in cancer.[124]

To date, a number of S1P receptor antagonists have been reported. One such inhibitor, FTY720 (fingolimod (Gilenya™), has been extensively studied. It is an analogue of Sph that upon *in vivo* administration is phosphorylated by SK2 into (*S*)-FTY720 phosphate, which binds to $S1P_{1,3,4,5}$ receptors (but not $S1P_2$) and acts initially as an agonist. However, it acts as a functional antagonist of $S1P_1$ by causing the receptor to be targeted for proteasomal degradation. [125–127] Notably, FTY720 also acts as an SK1 inhibitor [128] by inducing its proteasomal degradation. [129] FTY720 reduces metastasis in a breast cancer mouse model that is correlated with collapsed and decreased filopodia formation in the cancer cells.[130]

FTY720 is currently approved by the FDA for the treatment of multiple sclerosis. Its immunosuppressant activity again involves phosphorylation by SK2 to from FTY720-phosphate, which then induces down-regulation of $S1P_1$ by proteosomal degradation resulting in T cell-trapping in lymph nodes. [131] Other antagonists include JTE 013, which has been described as an $S1P_2$ receptor antagonist with an IC_{50} of 17 nM. It can inhibit S1P-induced cell migration and invasion. [112,132] VPC23019 is a selective antagonist for $S1P_1$ and $S1P_3$ with IC_{50} values of 25 and 300 nM, respectively. [133] VPC23019 can reverse S1P-prompted migration of ovarian cancer cells and thyroid cancer cells.[40]

1.5 Role of SK in cancer

SK1

The SKs have a significant role in many cancers. SK1 is implicated in the main mechanisms supporting cancer growth such the enhancement of cellular survival, proliferation, prevention of apoptosis and the stimulation of angiogenesis. For example, stomach, lung, kidney, and colon cancer have been found to have elevated levels of SK. [35] Furthermore, overexpression of SK1 has been shown to be associated with poorer survival in breast cancer patients. [106,134] In addition, SK1 plays a role in

cancer cell migration in pancreatic carcinoma cells. [135] SK1 activation by EGF is also required for EGF-directed breast cancer cell migration. [136]

A recent study has found that endogenous SK1 controls motility, growth, and tamoxifen resistance of MCF-7 cells. [112,137] Moreover, the enforced overexpression of SK1 in NIH 3T3 fibroblasts causes the acquisition of a transformed phenotype and tumour formation in nude mice, demonstrating the growth promoting potential of this enzyme. [33] Both SK1 and SK2 are involved in EGF-mediated activation and migration of MDA-MB-453 breast cancer cells. [138]

These findings suggest that SK1 and SK2 might be critical for the growth, metastasis and chemo-resistance of human breast cancers. Similarly, several studies have shown that SK1 has led to an increase in tumourigenic potential in a transgenic mouse model of erythroleukaemia. [139] S1P was found to be prominent in the plasma and malignant ascites of ovarian cancer patients. [140,141] Interestingly, over-expression of SK1 also reduced etoposide-induced apoptosis in HL-60 acute myeloid leukaemia cells. [142] In addition, activation of SK1 by VEGF in T24 bladder-tumour cells increased DNA synthesis. [143] Furthermore, inhibition of SK1 led to the suppression of cell growth and enhanced apoptosis in PC3 prostate cancer cells as a consequence of decreased S1P levels and increased Cer levels. [129,144,145] These findings support the possibility that the growth-promoting effect of S1P in cancer is primarily mediated by SK1. Several *in vitro* and *in vivo* studies have confirmed that SK1 has major role in the acquisition of resistance to apoptotic effects of γ-irradiation and chemotherapeutic drugs in prostate cancer cells. [145–149]

SK2

Unlike SK1, the role of SK2 in cancer is not well defined. Some studies have revealed that SK2 is pro-apoptotic, whereas others have it to be anti-apoptotic. Indeed, the role of SK2 in cancer might be linked to its localisation in the nucleus and its interaction with histone deacetylase (HDAC). In the nucleus, S1P produced by SK2 inhibits HDAC, causing augmented histone acetylation and the consequent expression of the cyclin dependent kinase inhibitor p21, an inhibitor of cell cycle progression and the transcriptional regulator, c-Fos. [69]

SK2 can be exported from the nucleus into the cytoplasm by protein kinase D [85] and plays a pro-apoptotic role. It is a putative BH3-only protein capable of stimulating apoptotic signaling; [73] i.e. it has a 9-amino acid motif similar to that present in Bcl$_2$-homology domain 3 (BH3)-only proteins. Like other BH3-only proteins, there is a physical interaction between SK2 and the anti-apoptotic member Bcl-xL. SK2 down regulates anti-apoptotic Bcl-$_2$ and Bcl-xL to promote apoptosis. [78] SK2 can associate with the ER and generate S1P to produce the pro-apoptotic ceramide, [38] while S1P formed by SK2 affects mitochondrial membrane permeability and cytochrome C release to induce apoptosis. [150] Similar to SK1, SK2 has been found to have a protective role against chemotherapeutic treatments. [151]

In contrast, many other more recent studies have revealed an anti-apoptotic role for SK2 as its knockdown promoted apoptosis and increased the sensitivity of cancer cells to chemotherapy. [152] Gao and Smith [153] have established that some cancer cell types might depend on SK2 rather than SK1 for survival. For example, in kidney and breast cancer cells, the siRNA-mediated knockdown of SK2 has a greater anti-cancer effect than the knockdown of SK1.

In addition, it has been shown that in glioblastoma cells, knock-down of SK2 expression inhibited cell proliferation to a higher extent than down-regulation of SK1. [154] While the clinical implication of SK2 in cancer patients' survival and prognosis is not well established, several novel roles for it have been revealed recently through the use of the chemical tool compound ABC294640, a selective and competitive SK2 inhibitor with a K_i of 10 μM reduced S1P level in intact cells. [155] In contrast to its role in BH3 signalling, inhibition of SK2 with ABC294640 promoted apoptosis and exhibited effective anti-proliferative activity in different types of tumour cell lines, indicating a crucial role for SK2 in cancer cell survival. [156] ABC294640 also induced dose-dependent apoptosis via the increase of caspase cleavage in Kaposi's sarcoma-associated herpes virus positive patient-derived primary effusion lymphoma cells. [157] It induced autophagic death in A498 kidney carcinoma cells, PC-3 prostate cancer cells and MDA-MB-231 breast adenocarcinoma cells. [153,155,158,159] Studies have demonstrated that ABC294640 has significant anti-proliferative effects, including the arrest of cell-cycle progression in prostate cancer cells. [160] A recent study has found

that the anti-tumor effect of ABC294640 could be due to its ability to induce the proteasomal degradation of both SK1 and dihydroceramide desaturase (Des1). [39]

1.5.1 The role of the Cer/Des1 and the S1P/SK pathway in the regulation of cancer cell growth

As mentioned above, maintaining a "sphingolipid rheostat" of Cer, Sph and S1P is a crucial factor in controlling cell growth. For instance, exposure of cells to stress stimuli results in the accumulation of Cer due to the stimulation of *de novo* biosynthesis or sphingomyelin hydrolysis. [161] Cer has been reported to stimulate stress-activated protein kinases, such as p38 mitogen-activated kinase (p38 -MAPK) and c-Jun *N*-terminal kinase (JNK) via the activation of protein kinase C (PKC). [162] In addition, Cer accumulation has been shown to induce the release of pro-apoptotic proteins such as cytochrome C and pro-caspases by the formation of channels at the mitochondrial membrane. [102,163–165] Furthermore, Cer promotes apoptosis by controlling the activity of members of the Bcl-2 protein family. Cer activates the pro-apoptotic Bax [166] and inhibits the anti-apoptotic Bcl-2, [167] which results in the subsequent activation of caspases and onset of apoptosis. [168] Similar to Cer, Sph also has pro-apoptotic properties. Indeed, Sph initiates apoptosis in several cell lines by the activation of BAX via PKC and stimulation of caspase-3/9. [169,170] In contrast to Cer and Sph, S1P and SK1 have the opposite effect on the Bcl-2 family members; S1P has been reported to inhibit caspase activation and apoptosis. [13,22] Generally, S1P activates anti-apoptotic proteins (e.g. Bcl-2) while deactivating pro-apoptotic proteins (e.g. Bad, Bim and Bax). [47–49]

Dihydroceramide desaturase (Des1) is the last enzyme in the *de novo* synthesis of Cer and regulates the balance between dihydroceramides and Cers. Despite the fact that it has not been studied as extensively as SK, both SK and Des1 have become of major interest as therapeutic targets. [171] Recent studies have revealed that Des1 ablation can trigger pro-survival, anabolic cellular responses and inhibition of cancer cell growth. For example, inhibition of Des1 and the consequent accumulation of dihydroceramides induced autophagy and delayed the cell cycle in gastric cancer cells via modulation of cyclin D1 expression. [172] Furthermore, siRNA knockdown of Des1 in SMS-KCNR neuroblastoma cancer cells increased dihydroceramide levels and

inhibited cell growth with promoted cell cycle arrest at G_0/G_1. [173] This was linked to a protein phosphatase 1-induced dephosphorylation of retinoblastoma protein, which regulates cell cycle transition. [173] In general, cancer cells utilise several strategies to overwhelm Cer/Sph-mediated apoptosis, such as down-regulation of Cer synthesis via the *de novo* and sphingomyelin pathways and/or over-expression of enzymes that convert Cer into non-apoptotic sphingolipids (**Figure 1.1**). For example, Cer kinase, and SK1 over-expression in various cancer cells was associated with stimulation of cancer cell survival, proliferation and drug resistance. [134,174] In contrast, sphingomyelinase and serine palmitoyl transferase have been found to be down-regulated in human colon cancer cell lines. [175]

1.5.2 Role of p53 and p21 in growth arrest

p21 and p53 are tumour suppressor genes that induce growth arrest. Transactivation of p21 by p53 stimulates DNA damage, which in turn promotes cell cycle arrest. [176] p21 is predominantly a key effector of p53 and is an inhibitor of cyclin-dependent kinases CDK2 and CDK1 which inhibit DNA synthesis. [176]

Recently, a functional interaction has been identified between SK1 and the tumour suppressor p53. [177] SK1 degradation has been shown to be induced by p53, [37] whereas, SK2 stimulates the induction of the cell cycle inhibitor p21. [69,151] SK1 degradation by p53 in response to DNA damage could shift the sphingolipid balance toward ceramide accumulation and result in ceramide-induced growth inhibition and cell senescence. [177] Others have demonstrated that Des1 and SK1 are involved in regulating LNCaP-AI prostate cancer cell growth via p53/p21-dependent and -independent pathways. In one study, siRNA knockdown of Des1 increased p53 expression, while a combined Des1/SK1 siRNA-based intervention increased the expression of p21. [39]

1.6 Prostate cancer: an overview

Prostate cancer is the most common cancer in men worldwide and an estimated 46,700 in the UK were diagnosed in 2014. [178] Over the last few years, advances in early detection methods have brought about a decrease in the prostate cancer death rate, although related mortality is still high. Worldwide, more than 307,000 men died from

the disease in 2012. [179] This mortality rate is because there is currently no available curative treatment for locally advanced or metastatic cancers, which are invariably fatal.

Androgen stimulation is the initiator of prostate cancer cell growth and survival. [180] Inhibition of the expression or down-regulation of androgen receptor (AR)-regulated genes is a key therapeutic strategy for the treatment of locally advanced or metastatic disease. This involves suppressing androgen production via surgical and/or chemical castration (androgen ablation therapy) and/or by blocking AR activation by administration of AR antagonists (anti-androgen therapy). [181] Despite initial efficacy, the ultimate failure of these AR-directed treatments in the large majority of patients is due to the development of an androgen-independent (also termed hormone-refractory or castration-resistant) prostate cancer, which usually occurs within 18 months from starting treatment. [182] Currently, castration-resistant prostate cancer (CRPC) is incurable and is fatal with a median survival of approximately 18 months from its onset. [182] The exact mechanisms responsible for the development of androgen independence are still not fully understood.

1.7 Role of SK in prostate cancer

SK1 and S1P signaling exert multiple effects on prostate cancer cells that are conducive to cancer progression. The role of SK1 in enhancing the proliferation and survival of prostate cancer cells has been widely investigated. Inhibition of cell proliferation and activation of apoptosis in prostate cancer cells has been linked to SK1 expression through siRNA knock-down that causes elevation in the Cer/S1P ratio to activate apoptosis, whereas pharmacological inhibition of SK has been unsuccessful at activating apoptosis due to its inability to increase the Cer/S1P ratio and shift the balance toward Cer. [129,145,146,149,183] A recent study found that chronic treatment of LNCaP cells (a cellular model of androgen-sensitive prostate cancer) with the SK inhibitor SKi induced proteasomal degradation of SK1 and consequent activation of apoptosis associated with accumulation of Cer. [129] In addition, SK1 inhibition is connected with a major decrease of metastasis in prostate cancer animal models. [145,146,183] More importantly, SK1 down-regulation has been shown to

increase the sensitivity of prostate cancer cells to anti-cancer treatments. [145,146,183] Over-expression of SK1 significantly enhances prostate prostate cancer cell proliferation by causing a substantial reduction in the Cer/S1P ratio. [183] *In vivo* studies have confirmed a function of SK1 in regulating the survival of prostate cancer. For instance, large tumours with increased vascularisation in nude mice were associated with a reduced Cer/S1P ratio after injection of prostate cancer cells over-expressing SK1 comparing to control cells that had only normal endogenous SK1. [145,146,183] Over-expression of SK promotes cancer progression by enhancing the survival and growth of cancer cells. A 2-fold increase in SK1 expression has been observed in human prostate specimens obtained from cancer patients compared to control specimens and this increase in SK1 activity was associated with an increase in tumour size and poor response to treatment. [174]

Recent studies have established that SK2 might also have a significant role in prostate cancer. Tonelli *et al.,* showed that SK1 and SK2 had different effects on intracellular sphingolipid levels in LNCaP prostate cancer cells Treatment of LNCaP cells with the inhibitor SKi induced Cer-dependent apoptosis and inhibited autophagy, whereas a specific inhibitor of SK2, (*R*)-FTY720-OMe, failed to promote apoptosis while stimulating autophagy in these cells. [184] However, the pharmacological inhibition of SK2 via ABC294640 decreased prostate cancer cell proliferation,[155] although a recent study found that it induced growth arrest of LNCaP-AI cells that was linked to proteosomal degradation of both SK1 and Des1 and subsequent accumulation of p21 and p53. This study suggests that both the SK1 and Des1 pathways are modulated to affect the *de novo* Cer and sphingolipid rheostat pathways to induce growth arrest of cancer cells. [39] SK inhibitors may represent a novel class of compounds with the potential to intervene in prostate cancer progression, but their poor potency to date has precluded clinical application.

1.8 Crystal structure of SK1

In 2013, the crystal structure of human SK1 was first solved by Wang *et al.,* hSK1 (residues 9–364, nine α helices, 17 β strands and a 3_{10}-helix) was crystallised in the apo (unbound) form and in complexes with ATP, ADP, Sph and the SK inhibitor SKi;

2-(*p*-hydroxyanilino)-4-(*p*-chlorophenyl)thiazole [35] at 2.0–2.3 Å resolution. [81] The crystal structure of SK1 in its apo form consists of two-domains: the *C*-terminal domain (CTD), the *N*-terminal domain (NTD) and the catalytic site (ATP binding site) situated in the cleft between the two domains. The hydrophobic lipid-binding pocket is found in the *C*-terminal domain (**Figure 1.6 A**). [81] The *N*-terminal domain (NTD) containing the C1–C3 domains (residues 9–150 and 357–364) has six β strands (β1–β5 and β17) and six α helices (α1-α6) (**Figure 1.6 B**). [81] The core of the NTD is four-stranded β sheets (strand order, β2, β1, β3, β4) which are arranged parallel to each other, while strands β17 and β5 have an anti-parallel arrangement, with strand β17 running in part parallel to strand β4. Three α helices (α2, α3, and α4) edge the central β sheet on one side, with three others (α1, α5, and α6) on the opposite side. [81] The CTD (**Figure 1.6 B**) (residues 151–356) contains the C4 and C5 domains and consists of 11 β strands and 4 α helices. The 11 β strands are arranged into a two-layer anti-parallel sheet, with the ''back'' sheet containing β7, β6, β16, β13, and β9 and the ''front''sheet comprising β15, β14, β8, β10, β11, and β1

2. Three α helices, α 7– α 9, and a 3_{10} helix following helix α 9, pack onto the front sheet whereas a long coiled loop (loop β9–β10, residues 214–256) covers the back sheet.[81]
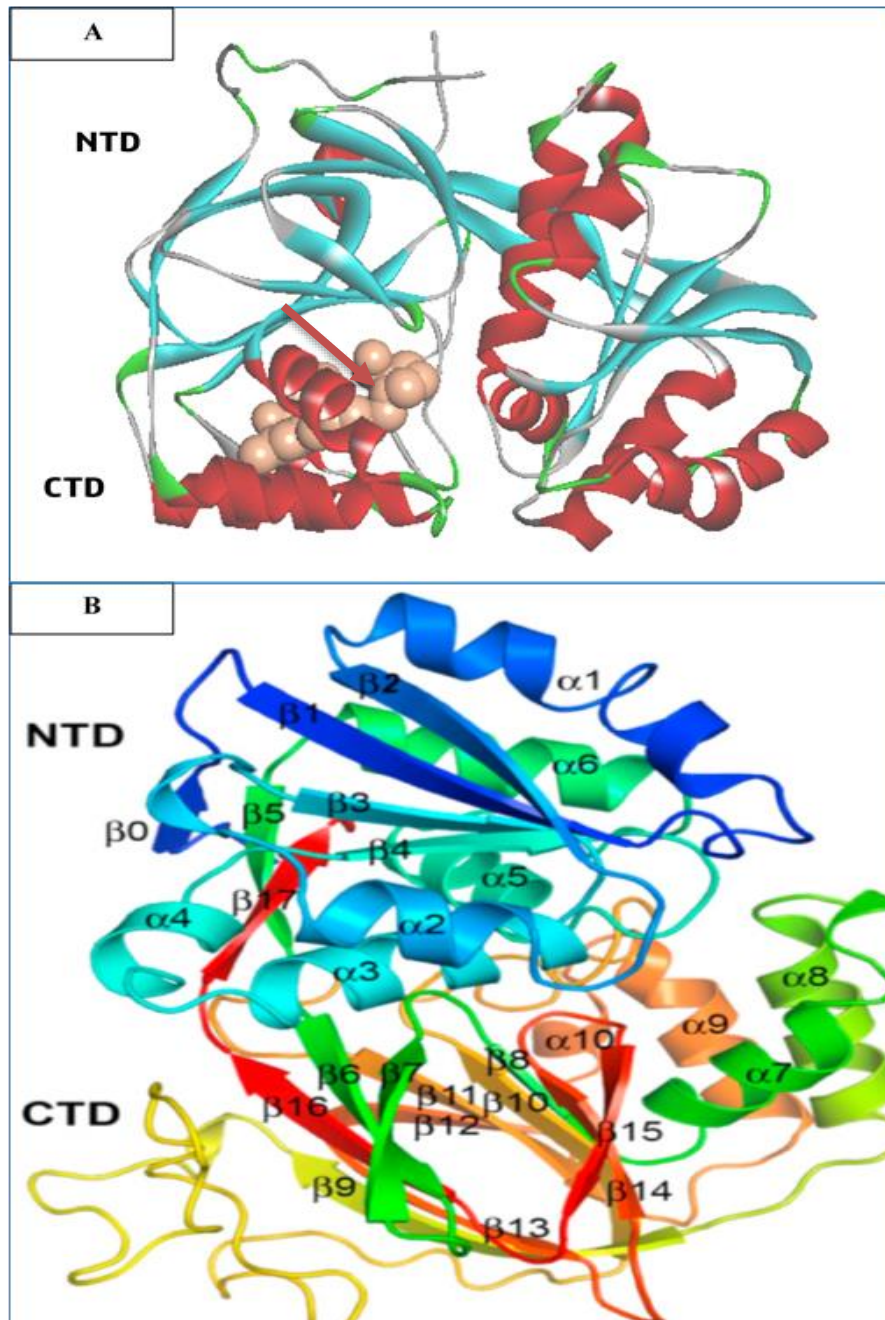
Figure 1.6. Cartoon representations of human SK1 structure. (A) The ribbon coloured in red for the *C* terminus (CTD) contains the lipid binding site and that in cyan for the *N* terminus (NTD) contains the ATP-binding site (Red arrow). Protein data Bank [PDB] code 4v24) [81]. (B) β strands and α helices structure of NTD and CTD of SK1. [81]

Structural similarity was found between SK1 and other lipid-kinases such as Cer kinase (CK) and DGKs, as well as NAD kinases and even 6-phosphofructokinases (PFKs). [75] The overall fold of SK1 contains a two-domain architecture similar to those of NAD kinases [185–187] and DGKs [188–190] (**Figure 1.7**). However, the CTD of SK1 shows substantial structural differences from both NAD kinases and DGKs in particular. Most notable of these is that SK1 possesses a distinct helical arrangement folded on the front sheet of the β sandwich and a coiled loop on the back sheet in the CTD (**Figure 1.7**). According to Labesse *et al.*, there is close sequence homology displayed between the ATP binding domain of SK1[191] and the crystal structure of PFK. [191] Furthermore, a study by Pitson *et al.,* found that the aspartate in the ATP binding site chelates the Mg^{2+} bridging the β- and γ-phosphates of ATP in both PFK and SK1. [75]
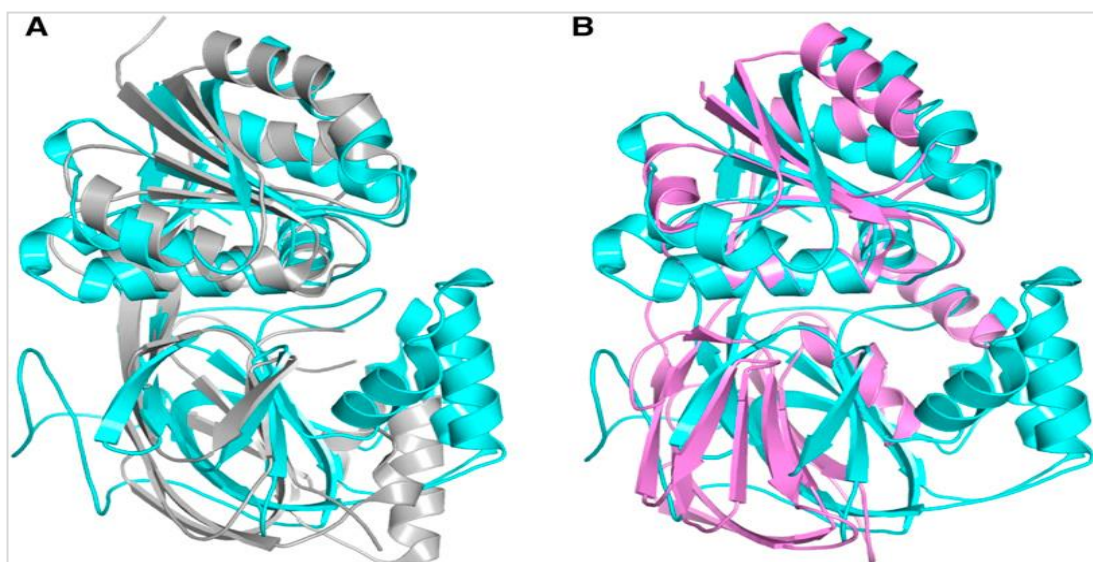
Figure 1.7. Structural Comparison of SK1 with DGK and NAD Kinase. (A) Superimposition of human SphK1 (cyan) and DGK from *Staphylococcus aureus* (DgkB) (gray, Protein data Bank [PDB] code 2QVL).(B) Superposition of human SK1(cyan) and an NAD kinase (pink) from *Archaeoglobus fulgidus* (magenta, PDB code 1ZOZ). [81]

1.8.1 The sphingosine binding site of SK1

Unlike DGKs and NAD kinases, the protein interior of the CTD has characteristic folds and specific lipid-binding pockets, thus offering the substrate specificity for Sph. [81] Sph may access the lipid-binding pocket in the CTD through a tunnel between helices α7-α8 in the C4 domain, which might act as a gate that could open and close for lipid entry. As the Sph enters the pocket, it forms a hydrogen bond with Asp264 of hSK1 (**Figure 1.8**) and this stabilizes its binding within the pocket. [81] The binding of Sph to hSK1 involves anchoring the hydrophilic head group to the protein surface and the accommodation of the long hydrophobic alkyl chain in the interior of a hydrophobic J-shaped tunnel, lined by the side chains of mostly non-polar residues such as Phe287 and 389, and Met392 from the protein. The 2-amino-1,3-diol moiety of the Sph head group is situated at the cleft between the two domains, making hydrogen-bond interactions with Asp167of loop β3-α3 through the 1-hydroxyl and with Asp264 (SK1a) of helix α7and through the 3-hydroxyl (**Figure 1.8**). [81]
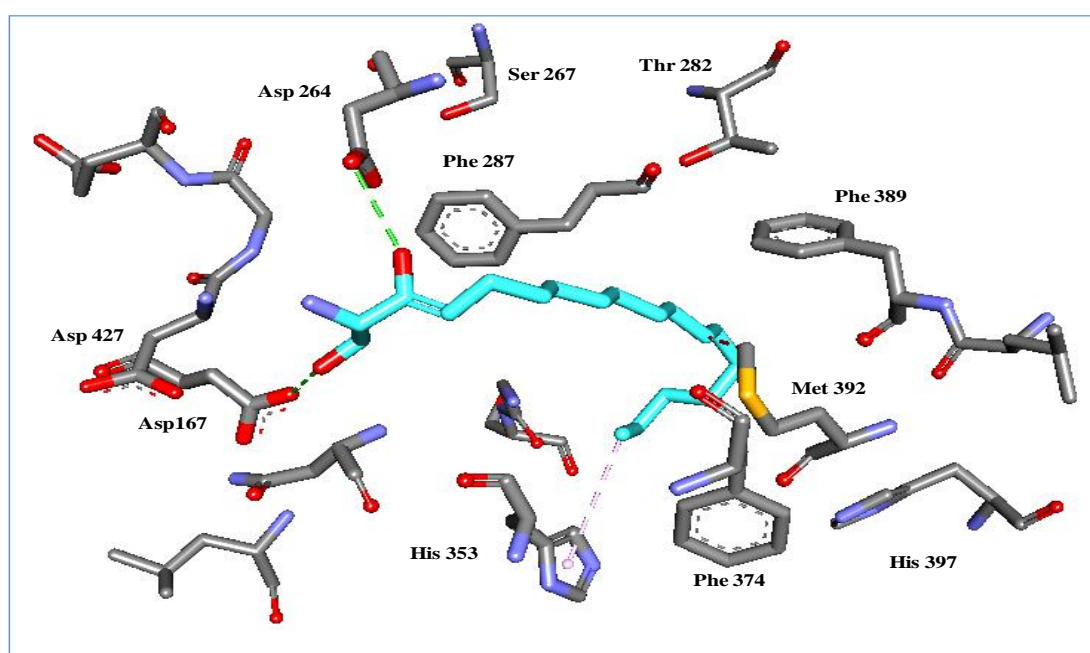
Figure 1.8. Detailed lipid-protein interactions Sph and SK1. Key amino acid residues of hSK1, within a distance of 5 Å from the Sph (cyan), are shown in stick representation with an atomic color scheme of red, blue, and grey for oxygen, nitrogen, and carbon atoms, respectively. Hydrogen-bond interactions and CH-π interactions are denoted by green and pink dashed lines. The figure was drawn using DS Visualizer Protein Data Bank: 4v24). [82]

Although the crystal structure of SK2 has not yet been resolved, there is considerable sequence homology between the two isoforms in the catalytic regions, and only 3 of the 20 residues in the lipid binding site of SK1 are different (**detailed in Chapter 2**).[82]

1.9 SK inhibitors

Extensive studies in many different laboratories have identified a number of SK inhibitors. Based on selectivity for the SK isoforms, they have been classified into three categories: non-selective SK inhibitors, selective SK1 inhibitors and selective SK2 inhibitors.

1.9.1 Non-selective SK inhibitors
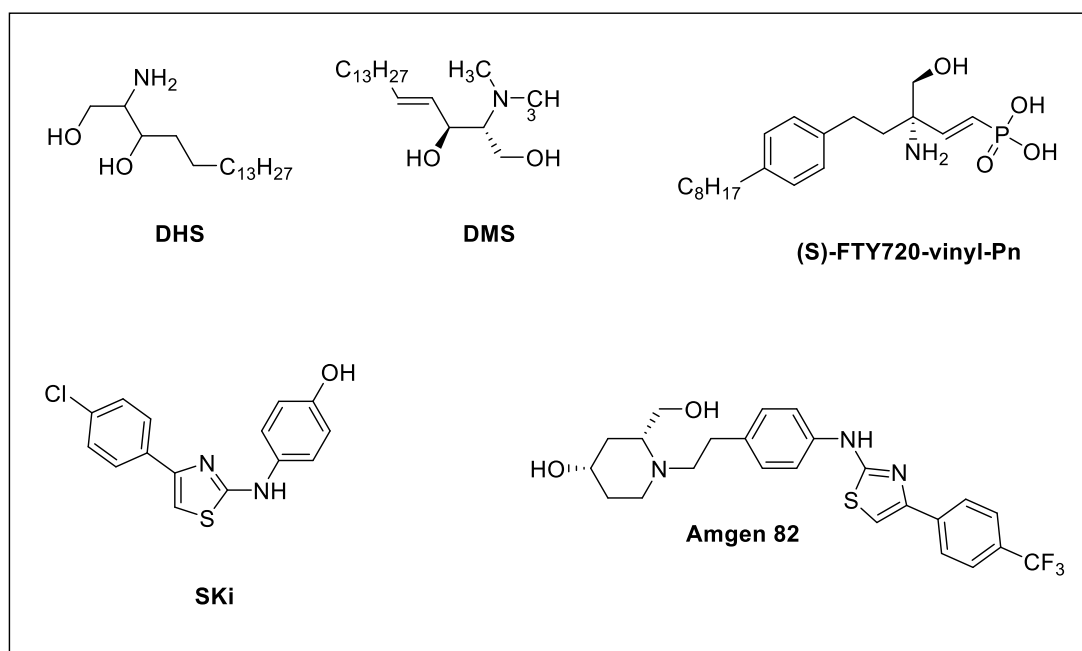
Figure 1.9. Examples of non-selective SK inhibitors.

1.9.1.1 Sphingosine analogues (SK inhibitors)

D, L-*threo*-dihydrosphingosine

D, L-*threo*-dihydrosphingosine (DHS) (**Figure 1.9**) is one of the first developed SK inhibitors. [71,120] Structurally, it is the synthetic *threo* stereoisomer of the naturally occurring D-*erythro*-dihydrosphingosine. DHS competitively inhibits SK1 activity with a K_i of approximately 3-6 μM (~0.2 mol%). DHS acts as a competitive inhibitor of Sph, and as a substrate for SK2 and enters the sphingolipid metabolic pathway.[50,192]

Dimethylsphingosine (DMS)

The *N, N*-dimethyl derivative of Sph, dimethylsphingosine (DMS) (**Figure 1.9**), non-selectively inhibits the activity of both SK isoforms: competitively for SK1 and non-competitively for SK2, with K_i values of 5 μM and 12 μM for SK1 and SK2 respectively. [50,193] DMS also acts as an activator of SK at low concentrations.[194] Although DMS has led to several other SK inhibitors, it has not been further developed itself for therapeutic use because of off- target effects. For example, DHS and DMS inhibit Cer kinase, [195] protein kinase C, [196] 3-phosphoinositide-dependent kinase, [197] SRC kinases [196] and MAPK. [193] DMS is also a stimulator of sphingosine-dependent protein kinase 1 (SDK1)[198] and epidermal growth factor receptor (EGFR).[199]

(S)-FTY720-vinylphosphonate

(*S*)-FTY720-vinylphosphonate (FTY720-vinyl-Pn) is a structural analogue of FTY720-phosphate, and inhibits both SK1 and SK2 (**Figure 1.9**). [128] The (*S*)-enantiomer is a noncompetitive inhibitor with Sph with a K_{iu} of 15 μM and a mixed inhibitor with ATP with a $K_{ic} = 17$ μM and a $K_{iu} = 48$ μM. [128] Upon administration to mice, both enantiomers of FTY720-vinyl-Pn induced transient peripheral lymphopenia and showed dose-dependent inhibition of lysophospholipase D. [200] In addition to inhibiting SK, FTY720-vinyl-Pn antagonises all the five S1P receptors and was a full antagonist at three (S1P$_1$, S1P$_2$, and S1P$_3$) of the five S1P receptors.[200]

1.9.1.2 Small molecules (SK inhibitors)

SKi

One of the first non-lipid, orally bioavailable small molecule inhibitors of SK was SKi; 2-(*p*-hydroxyanilino)-4-(*p*-chlorophenyl) thiazole (**Figure 1.9**). [35,128,201] SKi inhibits both SK isoforms with an IC_{50} of 35 μM for SK1 and 25 μM for SK2. It is a mixed inhibitor of SK1 with a K_i value of 17 μM and a K_{iu} value of 48 μM respectively [128] and does not inhibit PKC, ERK or PI3K. [35] In 2013, an X-ray co-crystal structure of SK1 with SKi was published and showed the inhibitor bound in the Sph binding pocket (**Figure 1.10**). [81] The chlorophenyl ring occupied the interior lipid-binding pocket and a hydrogen bond anchored the phenol hydroxyl group to the side chain of Asp264 of helix α7. [81]
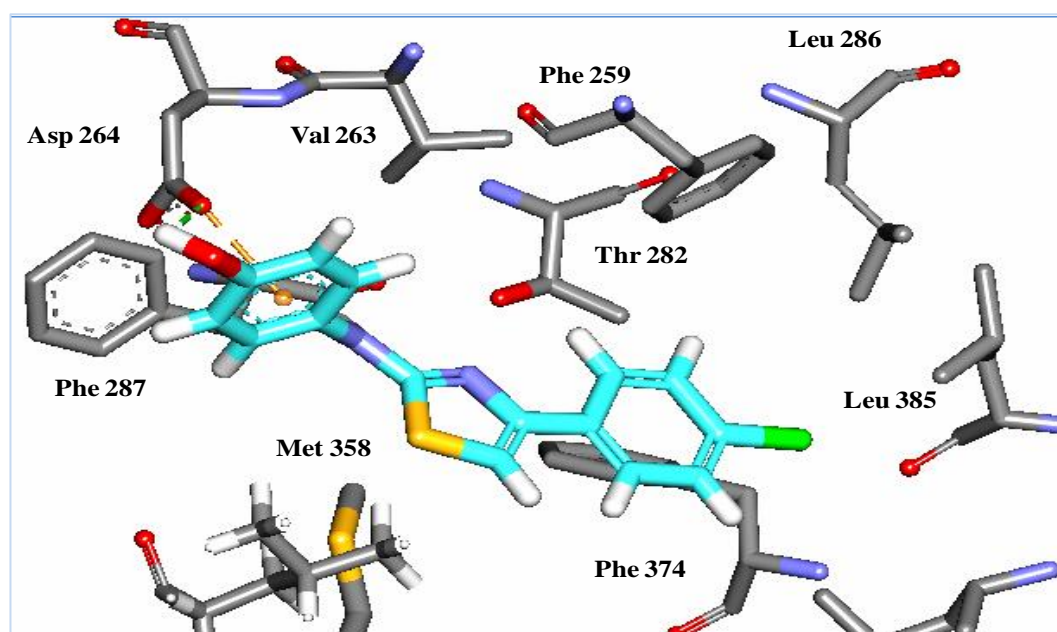
Figure 1.10. Key interactions of SKi with SK1. SKi is shown in stick representation coloured red, blue, yellow, green, and cyan for oxygen, nitrogen, sulfur, chlorine, and carbon atoms, respectively. SK1 is denoted as in the **Figure 1.8**. The hydrogen-bond interaction and CH-π interaction between SKi and Asp 264 is denoted by a green dashed line. The figure was drawn using DS Visualizer (Protein Data Bank: 4v24). [82]

Amgen 82

In 2013, a potent dual SK1/SK2 inhibitor known as Amgen 82 [(2*R*,4*S*)-2-(hydroxymethyl)-1-(4-((4-(4-(trifluoromethyl)phenyl)thiazol-2-yl)amino)phenethyl) piperidin-4-ol] (**Figure 1.9**) was discovered which had IC$_{50}$ values of 0.1 μM and 0.02 μM for SK2 and SK1 respectively. [202] To date, Amgen 82 is the most potent non-selective SK inhibitor reported and was shown to reduce S1P levels in a panel of cancer cell lines. However, when administered at therapeutic concentrations *in vivo*, no appreciable effect on cell viability was observed.[203]

1.9.2 Selective SK1 inhibitors

Recently, major progress has been made towards potent and selective SK1 inhibitors (**Figure 1.11**) with nanomolar potency for SK1 and low micromolar potency for SK2.
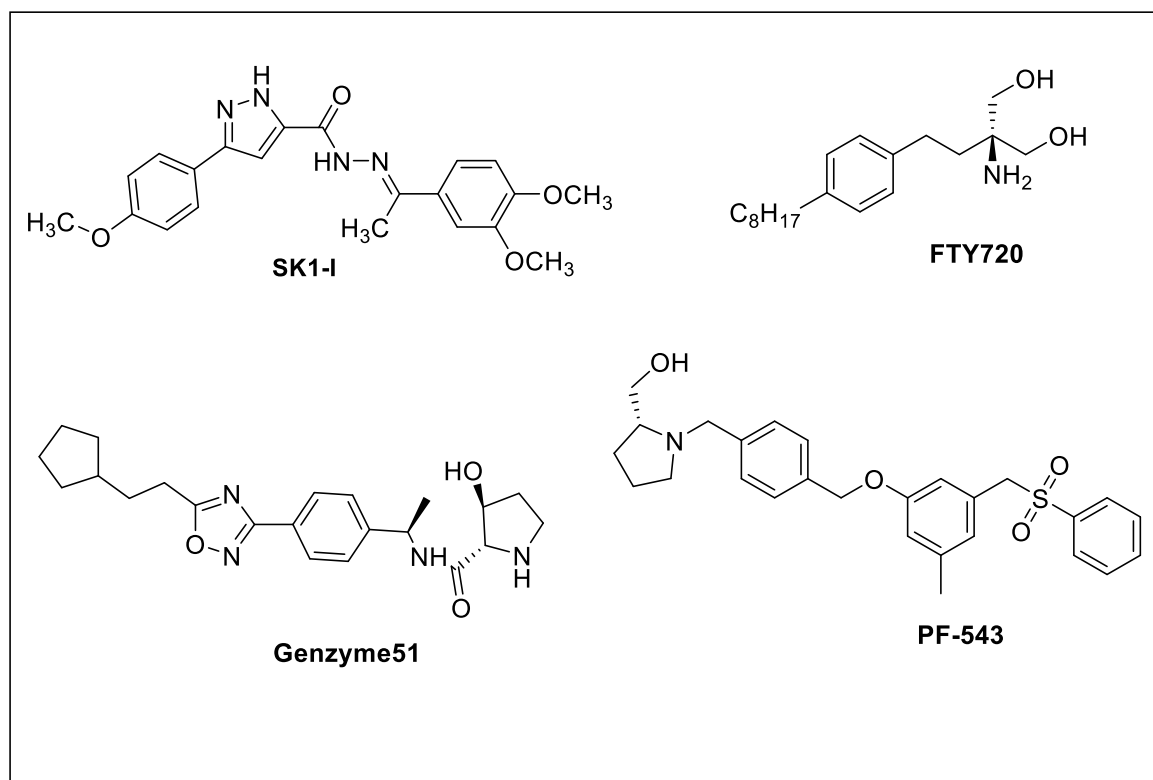
Figure1.11. Examples of selective SK1 inhibitors.

1.9.2.1 Sphingosine analogue (SK1 inhibitors)

FTY720

In 1992, fingolimod (FTY720) was synthesised by chemical modification of an immunosuppressive natural product, ISP-I (myriocin). [204] FTY720 [(2-amino-2-[2-(4-octylphenyl)ethyl]propane-1,3-diol)] is a Sph analogue that competitively inhibits SK1 activity with a K_i of 2 μM **(Figure 1.11)**. [200,204–206] After the discovery of FTY720, several other pharmaceutical companies initiated programmes aimed at the identification of SK inhibitors with increased potency and specificity.

SK1-I

The sphingosine analogue SK1-I (*E*)-N'-(1-(3,4-dimethoxyphenyl)ethylidene)-3-(4-methoxyphenyl)-1H-pyrazole-5-carbohydrazide was the first selective SK1 competitive inhibitor (K_i=10 μM) **(Figure 1.11)**. It blocked the growth of cultured leukaemia cells and inhibited the growth of leukemia xenograph tumours. [207] In addition, it is highly selective toward cancer cells with good bioavailability together with low cytotoxicity and may offer possibilities in the treatment of SK1-mediated diseases. [207]

1.9.2.2 Small molecules (SK1 inhibitors)

Genzyme51

Genzyme51 is a potent inhibitor of SK1, with an IC_{50} value of 58 nM and no inhibition of SK2 at a concentration of 10 μM **(Figure 1.11)**. It exhibited good pharmacokinetic profiling, with a half-life of 7.6 h after oral administration in mice. However, its effect on Sph and S1P levels in blood has not been reported yet. [208,209]

PF-543

Currently, PF-543 **(Figure 1.11)** is the most potent and selective SK1 inhibitor available, with a K_i value of 3.6 nM that is more than 100-fold selective for SK1 over the SK2 isoform.[210] PF-543 decreases the level of endogenous S1P with a proportional increase in the level of Sph in head and neck 1483 carcinoma cells, which are

characterised by high levels of SK1 expression and an unusually high rate of S1P production. Unexpectedly, PF-543 failed to have any effect on the proliferation and survival of these cells.

The X-ray crystal structure of SK1 with PF-543 has been reported [82] and will be discussed in detail in **Chapter 3**. A preliminary *in vivo* study with PF-543 showed that it had a poor pharmacokinetic profile [211] and highlights the need for *in vivo* stable SK1 selective inhibitors.

1.9.3 Selective SK2 inhibitors

In the past few years, potential therapeutic roles for SK2 have begun to emerge through the development of a number of SK2 inhibitors (**Figure 1.12**). [44]
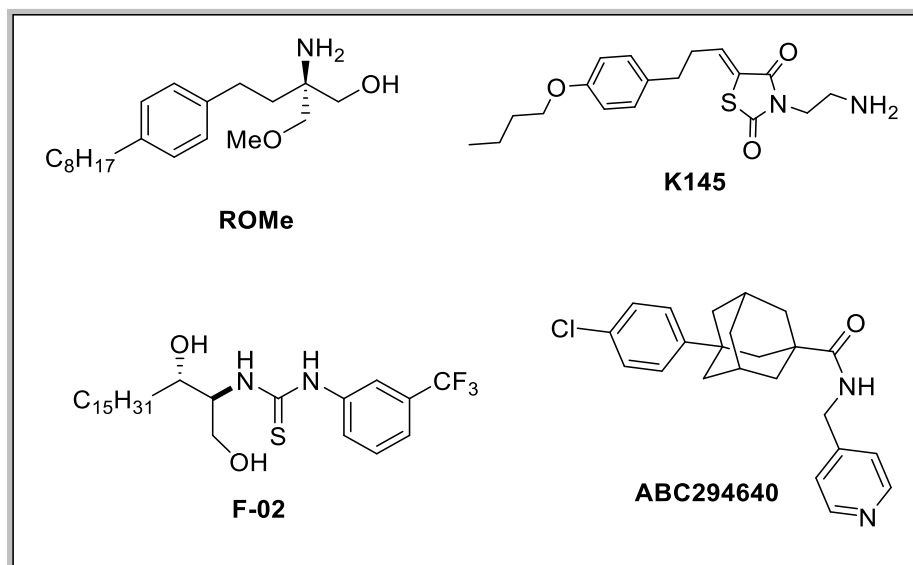
Figure 1.12. Examples of selective SK2 inhibitors.

1.9.3.1 Sphingosine analogues (SK2 inhibitors)

(*R*)-FTY720-OMe (ROMe)

Replacement of the hydroxyl group of FTY720 with a methoxy group to produce (*R*)-FTY720-OMe (ROMe) led to a selective but low potency inhibitor of SK2 (K_i of 16 μM) (**Figure 1.12**). [205] ROMe blocks DNA synthesis, induces apoptosis and stimulates focal adhesion assembly in HEK 293 cells. It also inhibits both growth and S1P-

induced actin rearrangement in MCF-7 breast cancer cells, which prevents the formation of a migratory phenotype and could prevent metastasis. [128,212]

K145

Another sphingosine analogue is K145 [(Z)-3-(2-aminoethyl)-5-(3-(4-butoxyphenyl) propylidene) thiazolidine-2,4-dione] (**Figure 1.12**), which had a Ki of 6.4 μM for SK2 and did not inhibit SK1 and Cer kinase. [213] In contrast to Amgen 82, K145 had an antiproliferative effect on U937 cells via the inhibition of ERK and Akt phosphorylation. It caused a slight decrease in S1P levels similar to FTY720, the SK2 substrate. *In vivo* studies with K145 reduced tumor S1P levels which, was associated with a decrease in tumor volume.[214]

F-02

F-02 (**Figure 1.12**), a thiourea derivative of dihydrosphingosine, is selective SK2 inhibitor with an IC_{50} of 21.8 ± 4.2 μM. Treatment of human pulmonary Artery smooth muscle cells (hPSMAC) with F-02 has no effect on SK1 expression. [215]

1.9.3.2 Small molecules (SK2 inhibitors)

ABC294640

ABC294640 is an analogue of SKi (**Figure 1.12**) [155] but is a selective inhibitor of SK2, with a Ki of 10 μM. [155] It is orally bioavailable with a half life of 4.5 h in mice and it is one of the best characterized *in vivo* inhibitors of SK2 in a number of diseases.[153] ABC294640 has antitumour activity and also inhibits NFκB-mediated chemo-resistance in breast cancer. [159,216] It reduces pro-survival signalling in hepatocellular cancer by acting synergistically with other chemotherapeutics [217] and enhances autophagy in tumour cells, causing non-apopotic cell death. [155]

1.10 Conclusion

There is compelling evidence that SK and S1P are involved in controlling tumour cell proliferation and survival and represent important targets for the development of novel anticancer drugs. Generally, it has been found that the SK/S1P pathway is involved in several physiological processes [218] and identifying the manner in which the SK/S1P pathway participates in health and disease will expand its therapeutic potential.[218] The discovery of several SK inhibitors with antitumor activity *in vivo* provides further support for the hypothesis that SK is an attractive target. Overexpression of SK has been shown to be associated with poor prognosis in several cancers, such as prostatic and breast cancers. Therefore, the development of novel SK inhibitors as a treatment for human cancer has become a major interest.

1.11 Aim of the project

The aim of this project is to design, synthesise and evaluate the effectiveness of SK inhibitors for the treatment of prostate cancer.

The most potent SK1 inhibitor is PF-543, but it fails to have any effect on the proliferation and survival of head and neck squamous-cell carcinoma 1483 cells. [210] One possibility for its lack of anti-proliferative activity is that PF-543 might bind to 'off-target(s)' that neutralise the effect of inhibiting SK1 activity by disturbing the sphingolipid rheostat to promote accumulation of apoptotic Cer. In this regard, it is curious that PF-543 fails to elevate apoptotic Cer levels in 1483 cells. [210]

This project was involved the synthesis analogues of PF-543 to establish if this unexpected inactivity was unique to PF-543 specifically, and to establish whether modifications to its structure could have differential selectivity for SK1 and SK2, improve growth inhibition and induce cancer cell death. New analogues were assessed for SK1/SK2 inhibitory activity and for efficacy in prostate cancer cell lines (LNCaP and LNCaP-AI) and proliferating human pulmonary Artery smooth muscle cells (hPSMAC). These cell lines were selected because they have been extensively used to investigate the role of SK1 and SK2 in regulating cell growth and survival.[129,184,219]

1.11.1 Setting up a drug discovery project

The first aim of the project was to use molecular modelling to design scaffolds related to PF-543 to further explore its structure-activity relationship (SAR) with the ultimate aim of improving selectivity towards one SK isoform over the other. Compounds prepared would be evaluated *in vitro* against the SK isoforms and in cells to explore isoform selectivity with respect to phenotypic outputs in prostatic cancer cells.

Specifically, the objectives were:

1) To design and synthesise potent selective SK1 or SK2 inhibitors as novel anti-cancer agents.

2) To develop a biochemical 96-well plate assay as the primary means of assessment for SK1 and SK2 activity using an ADP-Glo kit (which could be compared with the lower throughput radiometric assay).

3) To develop an SAR profile for the new compounds based on their SK1 and SK2 activity.

4) To use cell-based assays to evaluate their pharmacodynamic and functional effects.

The assay cascade shown in Figure below (**Figure 1.13**) was used to evaluate compounds:
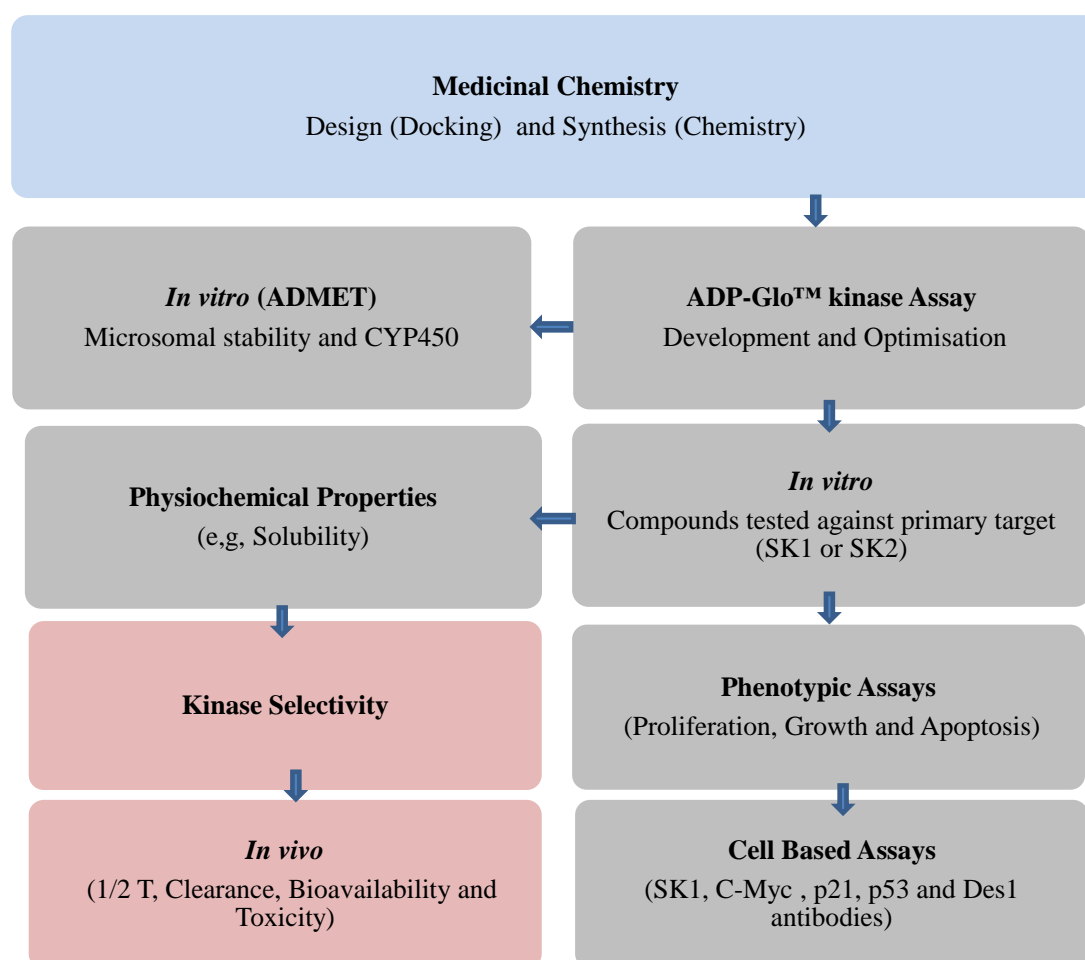
Figure 1.13. Workflow plan for assessment of synthesised compounds.

1.11.2 The assay cascade

Using a pre-defined assay cascade to develop compounds is an essential component of any drug discovery project. Initially, an *in vitro* ADP-Glo assay was developed and optimised to screen all new compounds for specificity and potency against SK1 and SK2, followed by cell-based assays to determine functional effects. Identified active hits against SK1/SK2 were assessed in LNCaP, LNCaP-AI and hPASMC for pharmacodynamic and phenotypic effects on cell growth/proliferation and apoptosis. This included an assessment of whether the compounds were able to induce the proteasomal degradation of SK1 in cells, which enables us to establish whether pharmacodynamic target engagement can be correlated with phenotypic effects. Additional biomarkers for phenotypic changes were assessed including PARP cleavage, p53, p21 and Des1 expression levels. Compounds with on-target and functional activity were assessed for *in vitro* ADMET properties, which included cell permeability and absorption across intestinal epithelial cell (Caco2) and clearance by phase I and phase II metabolising systems. To establish whether compounds had the potential for drug-drug interactions, assessment of CYP450 inhibition was performed.

Chapter 2 Medicinal Chemistry

Synthesis, *in vitro* activity and structure activity relationship of analogues:

toward selective SK1 and SK2 inhibitors.

2.1 Introduction

SKs are potential targets for drug discovery that require an expanded chemical biology tool kit to validate them as drug targets in cancer, which highlights the need for developing more potent and selective isoform inhibitors. The recent determination of the crystal structure of SK1 [81] should aid the development of potent SK1 or SK2 selective inhibitors. In this chapter, how a library of PF-543 analogues was synthesised and profiled for inhibitory SAR against SK1 or SK2 using an optimised ADP-Glo™ assay is described.

2.2 Validation of ADP-Glo™ assay

As discussed in chapter 1, for any drug discovery project there is a need for a primary biochemical assay to screen compounds against a specific target. In the kinase field, high-throughput screening (HTS) has become widely used by drug discovery groups to identify new inhibitors and construct structural activity relationship (SAR) profiles to direct compound optimisation. However, no such assays were available for the sphingosine kinases that we could use in-house. We therefore developed a kinase assay using the ADP-Glo™ reagents from Promega and the SK1 and SK2 inhibitors PF-543 and F-02 for validation. The ADP-Glo™ assay is non-radioactive, robust and can be used in a high-throughput format over a wide range of ATP concentrations. The approach relies on the measuring the amount of ADP formed after the transfer of the γ-phosphate group of ATP to a substrate (e.g. phosphorylation of sphingosine to sphingosine-1-phosphate). [220] Kinase activity is therefore determined indirectly by measuring the formation of ADP using a luminescence approach in three key steps:

1) The kinase-catalysed phosphorylation of substrate is performed, which uses SK, ATP and sphingosine (with or without inhibitors);
2) The remaining ATP that has not been consumed in the process is converted to AMP by a pyrophosphatase; the ADP that was generated in step 1 is then converted to ATP by an adenylate kinase.
3) The newly synthesised ATP is measured by luminescence using a luciferase based reaction (**Figure 2.1**). [220.]
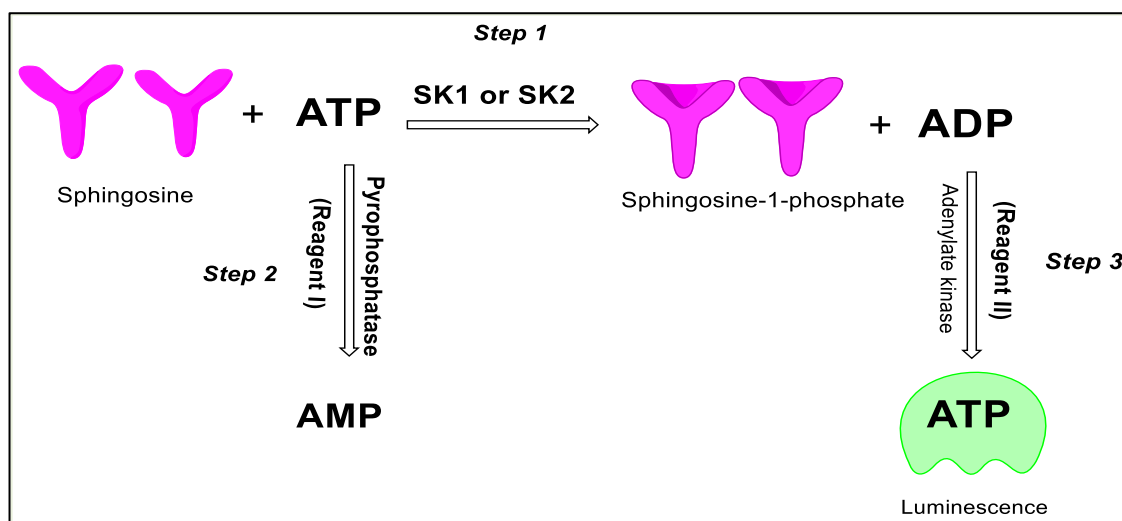
Figure 2.1. The key steps in the ADP-Glo assay. The ADP-Glo assay as 3 key steps: kinase reaction; removal of remaining ATP; conversion of ADP to ATP; detection of luminescence produced by the newly synthesised ATP.

2.2.1 ADP-Glo™ kinase assay optimization

Optimising assay conditions to obtain a robust and reliable signal with a minimal amount of enzyme is an important step in designing high-throughput lipid kinase assays. [220.]Preliminary investigations were performed to determine the optimal kinase reaction time, enzyme and substrate as well as ATP concentrations to obtain the desired screening assay conditions and to evaluate the robustness of the assay. The catalytic properties of the enzyme, such as the number of substrates and subunits of the enzyme participating in each catalytic cycle are important factors in determining the simplicity or complexity of the mathematical models used describe the kinetics of specific enzymes. For example, the mode of inhibition of an inhibitor with respect to substrate needs to be characterised for sphingosine kinase, because it is a two-substrate enzyme with two binding sites catalysing the formation of S1P by utilising sphingosine and ATP. During assay optimization, it is therefore necessary to use a fixed high concentration (usually several fold higher than the K_m) of one substrate with varying concentrations of the other substrate in order to convert the kinetics into an essentially one substrate reaction that obeys Michaelis-Menten kinetics. Initially, the ATP concentration employed was 250 µM (3 x K_m, where the literature-quoted K_m value is 77 µM). [221]. The rationale here was to ensure that the SK ATP binding site was

saturated because our compounds had been designed to be competitive with the sphingosine binding site. D-*erythro*-sphingosine was initially used at the literature-quoted K_m value (3 µM) [128] as a substrate for the sphingosine binding site of the SKs.

2.2.1.1 Determining the optimum kinase reaction time for the SK1 and SK2 assay.

For SK1, an ATP concentration of 250 µM, a substrate concentration of 3 µM [128] and an enzyme concentration of 0.2 µg/ml based on the published values of SK1 [128] were used. For SK2, an ATP concentration of 250 µM, a substrate concentration of 10 µM and an SK2 concentration of 5 µg/ml (optimised data not shown) were used. The optimum kinase reaction time was observed within 90 mins (at 90 mins, there is no evidence of sustained SK activity) (**Figure 2.2: Figure 2.3**) which was identified as the optimum time for use in subsequent SK1 and SK2 assays.
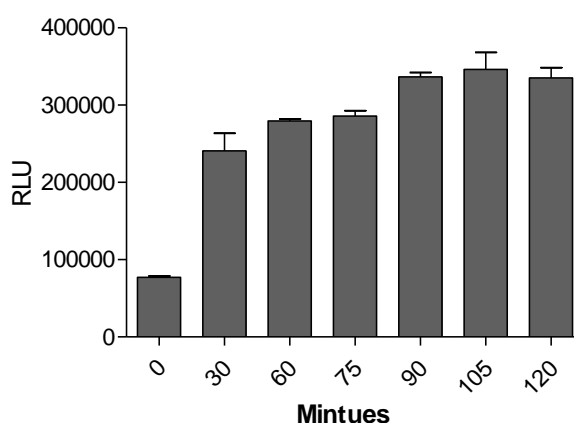
Figure 2.2. Effect of incubation time on detection of SK1 activity. Sph, SK1 and ATP concentrations were fixed at 3 µM, 0.2 µg/ml and 250 µM, respectively. Samples were incubated at different times interval before detection of ADP formed using ADP-Glo. Data are represented as arbitrary luminescence units (mean +/- SEM, n=3) for a single, representative experiment performed three times.
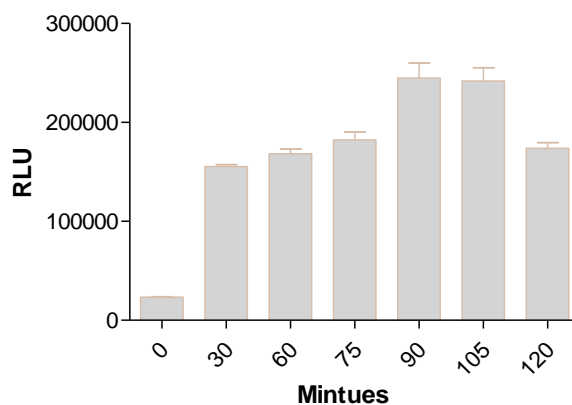
Figure 2.3. Effect of incubation time on detection of SK2 activity. Sph, SK2 and ATP concentrations were fixed at 10 µM, 5 µg/ml and 250 µM, respectively. Samples were incubated at different times interval before detection of ADP formed using ADP-Glo. Data are represented as arbitrary luminescence units (mean +/- SEM, n=3) for a single, representative experiment performed three times.

2.2.1.2 Determining the optimum concentration of the sphingosine substrate for the SK1 assay

Kinetic constants such as the K_m values for both ATP and substrate can be calculated using the Michaelis–Menten equation [$v = V_{max} [S]/(K_m + [S])$], where v is the enzyme reaction rate, V_{max} is the calculated maximal reaction rate at saturation concentration of substrate, [S] is the substrate concentration, and K_m is the substrate concentration that produces a reaction rate that is half of the maximal reaction rate.[128] The kinetic constants including V_{max} and K_m are altered causing a change in steady state in the presence of inhibitor. Using an ATP concentration of 250 µM and an SK1 concentration of 0.2 µg/ml, we determined the specific K_m for sphingosine in our assay. D-*erythro*-sphingosine concentration was varied from 0-400 µM and data collected and fitted to the Michaelis–Menten equation (using Prism Graph Pad software) to calculate the substrate K_m value (**Figure 2.4**: $K_m = 9$ µM). This was three times more than the literature K_m value (3 µM), [128] which is probably due to differences in the assay conditions such as using different substrate and buffer components.
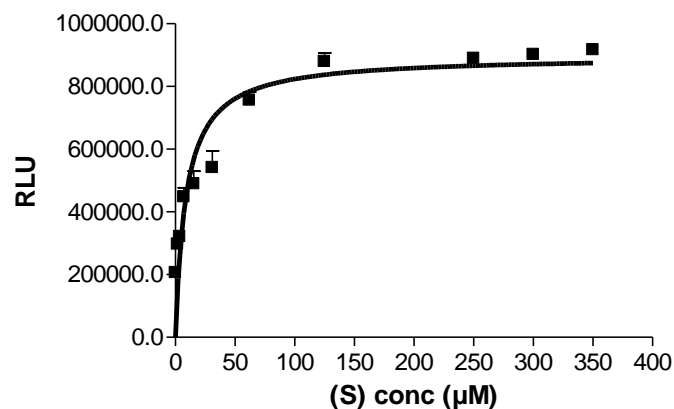
Figure 2.4. Determination of the optimum concentration of the sphingosine (K_m of Sph) in SK1 assay. Sph concentration was varied between 0 and 400 μM whilst SK1 and ATP concentrations were fixed at 0.2 μg/ml and 250 μM, respectively. Samples were incubated for 90 mins before detection of ADP formed using ADP-Glo. Data are represented as arbitrary luminescence units (mean +/- SEM, n=3) for a single, representative experiment performed three times.

2.2.1.3 Determining the optimum concentration of the sphingosine substrate for the SK2 assay

Using an ATP concentration of 250 μM and an SK2 concentration of 5 μg/ml, we determined the specific K_m for sphingosine in our assay. The D-*erythro*-sphingosine concentration was varied from 0-350 μM and data collected and fitted to the Michaelis–Menten equation (using Prism Graph Pad software) to calculate the substrate Km value (**Figure 2.5**: K_m= 19 μM), which was close to the literature K_m value (10 μM). [128]
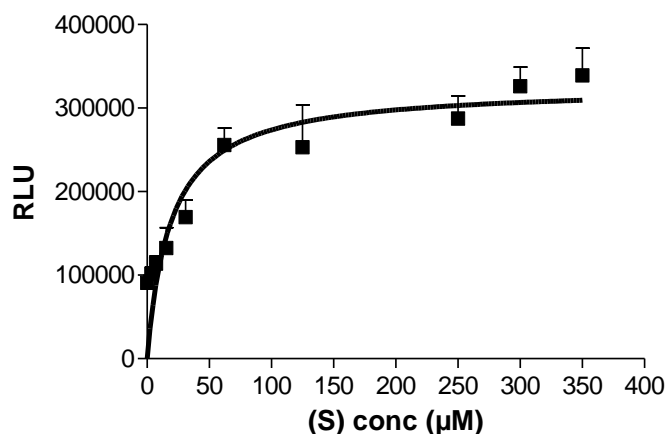
Figure 2.5. Determination of K_m of Sph in the SK2 assay. Sph concentration was varied between 0 and 350 μM whilst SK2 and ATP concentrations were fixed at 10 μg/ml and 250 μM, respectively. Samples were incubated for 90 mins before detection of ADP formed using ADP-Glo. Data are represented as arbitrary luminescence units (mean +/- SEM, n=3) for a single, representative experiment performed three times.

2.2.1.4 Determination the robustness and stability of the ADP-Glo™ assay.

The Z′ factor is a measure of the robustness of the assay. It has been used in high-throughput screening to quantify the effectiveness of an assay after at least three independent experiments to produce a statistically significant data set for evaluation using the equation below, where σ is the standard deviation and μ is the mean; [222]

$$Z′ = 1 - (3(σ+ve + σ-ve)/(μ+ve - μ-ve))$$

Average and SD values were obtained for negative and positive controls. SD-ve and SD+ve represent the standard deviations of data obtained for the negative and positive controls, respectively. Z′ factor value ranges from 0 to 1, and the higher the Z′ factor number, the greater the separation between the positive and negative control. In drug discovery, a single concentration is often performed during the primary screening run and it is critical that "hits" can be distinguished from "noise," which usually requires a Z′ > 0.4. [223]

To evaluate the Z´ factor of the SK assays, the positive control included ATP, Sph and the enzyme, whereas the negative control was performed in the presence of the substrate and ATP but without the enzyme. The Z´ Factors were 0.9 and 0.7 for the SK1 and SK2 assay plates, respectively (**Figure 2.6: Figure 2.7**), suggesting that both SK1 and SK2 ADP-Glo assays have excellent and good separation of data points between the negative and the positive signals respectively and both were robust.
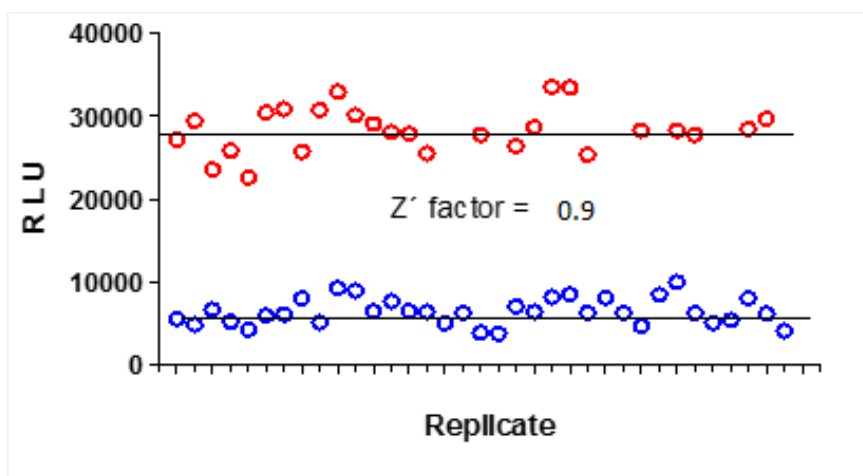
Figure2.6. **Determination of the Z´ factor for SK1**. Red represents the assay in the presence of enzyme, blue represents the assay in the absence of enzyme.
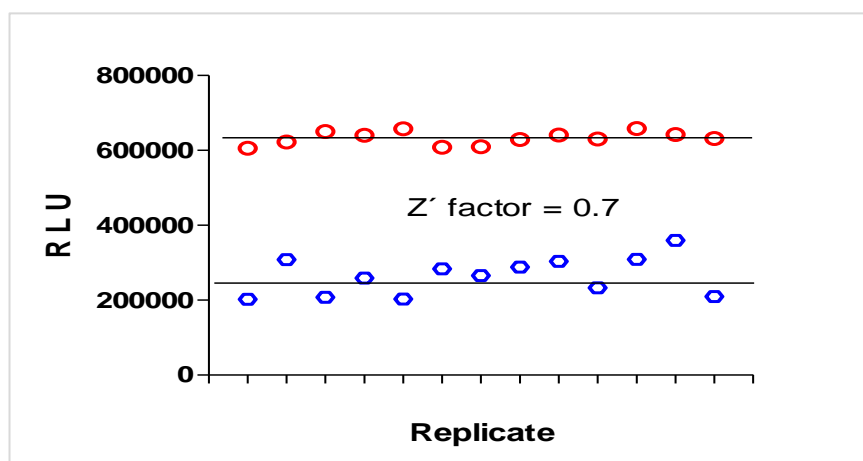
Figure 2.7. **Determination of the Z´ factor for SK2.** Red represents the assay in the presence of SK2, blue represents the assay in the absence of enzyme.

2.2.2 Determination of SK inhibition using the ADP-Glo™ assay

Having optimized conditions for the SK assay, we next validated it as a means to determine inhibitory concentrations with putative inhibitors by assessing PF-543, which is the most potent SK1 inhibitor available. For competitive inhibitors, an inhibition constant (K_i) can be calculated by using the Cheng-Prusoff equation: [K_i= IC$_{50}$/1+ ([s]/K_m)], where [s] is fixed substrate concentration, IC$_{50}$ is the concentration of inhibitor which reduces SK1 activity by 50%, and K_i is a measure of the affinity of the inhibitor for the enzyme and assumes competitive inhibition. These constants, also known as K_{ic} and K_{iu} (competitive and uncompetitive inhibition constants respectively) can be obtained graphically. [224] Using our SK1 assay conditions, the IC$_{50}$ and K_i values determined for **PF-543** against SK1 were 100 nM and 28 nM respectively. Schnute *et al.,* reported a different K_i of 3.6 nM, [210] which is likely to be due to a difference in the ATP concentration and assay system that has been used (**Figure 2.8**).
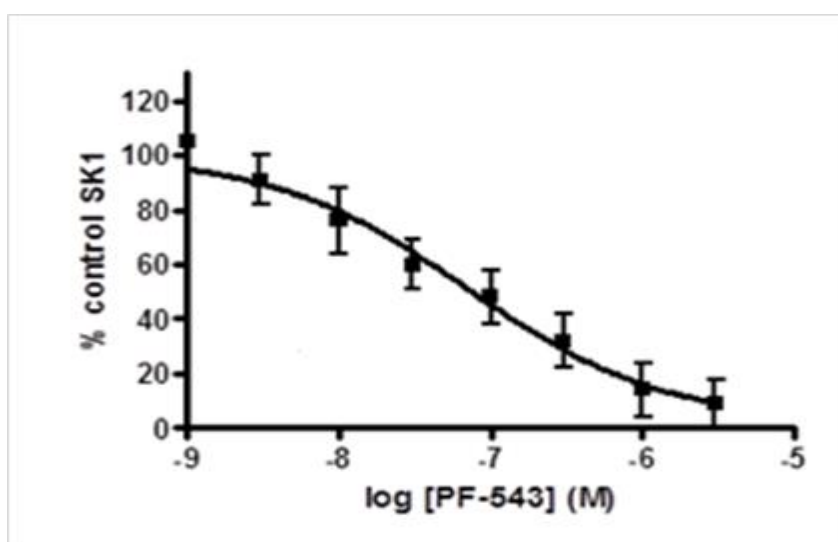
Figure 2.8. **Determination of the IC$_{50}$ value for PF-543 against SK1.** Sph, SK1 and ATP concentrations were fixed at 3 µM, 0.2 µg/ml and 250 µM, respectively. Inhibitor concentrations ranged from 0.001- 3 µM. Samples were incubated at 90 mins before detection of ADP formed using ADP-Glo. Data are represented as percentage of control (mean +/- SEM, n=3) from three separate experiments.

We next validated the optimised SK2 assay as a means to determine inhibitory concentrations with putative inhibitors by assessing F-02, which is a selective inhibitor

of SK2. [215] Using our SK2 assay conditions, the IC_{50} determined for F-02 against SK2 was 109 nM. Byun *et al.*, reported adifferent IC_{50} of 21.8 µM [215] which is likely to be due to a difference in the ATP concentration and assay system that has been used (**Figure 2.9**).
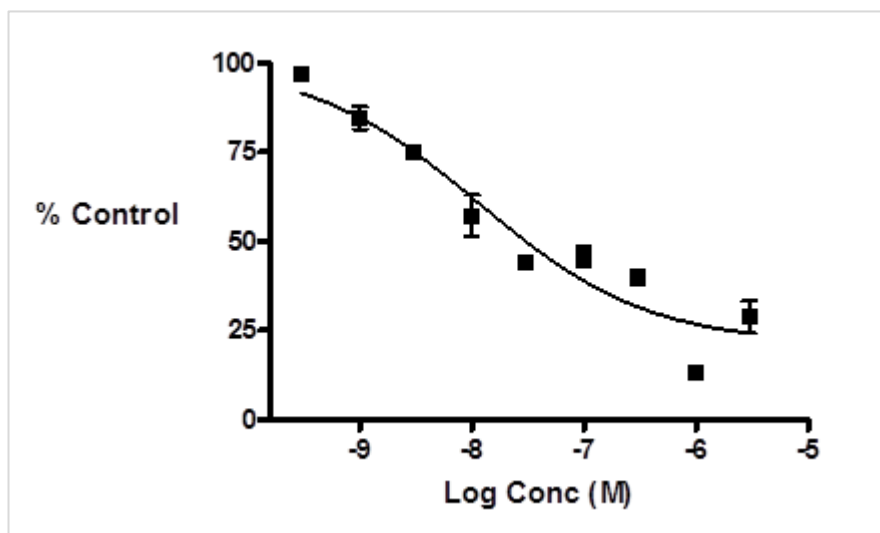
Figure 2.9. Determination of the IC_{50} value for F-02 against SK2. Sph, SK2 and ATP concentrations were fixed at 10 µM, 5 µg/ml and 250 µM, respectively. The inhibitor concentration ranged from 0.001 - 3 µM. Samples were incubated at 90 mins before detection of ADP formed using ADP-Glo. Data are represented as as percentage of control (mean +/- SEM, n=3) for a single, representative experiment performed three times.

Having optimised the ADP-Glo assay and validated it with known SK inhibitors, we used it to determine IC_{50} values for new inhibitors emerging from our synthetic medicinal chemistry program (**see Section 2.3**).

2.3 Results and discussion: modelling, structure-activity relationships of analogues and *in vitro* activity.

To help explain SARs, the crystal structure of SK1 (human) was used for the docking studies, [81] which was downloaded from the Protein Data Bank (PDB4v24). Since the crystal structure of SK2 has not yet been resolved, a simple model of SK2 was generated by mutatiting the three residues in the Sph binding site that are known to differ between the two isoforms. Compounds were docked using GOLD (UPC) Version 4.0 and visualized using Discovery Studio Visualizer (Accerlys) to predict the binding within the active sites of SK1 and SK2.

2.3.1 What was known about PF-543 binding with SK?

The X-ray crystal structure of SK1 complexed with **PF-543** revealed that it bound in a J-shaped hydrophobic pocket normally occupied by the Sph substrate (**Figure 2.1**). This pocket had a toe-like groove at its end and a funnel-like opening that positions the primary alcohol of the Sph substrate close to the ATP binding site to allow phosphate transfer. The inhibitor was well resolved in the lower J pocket region but less so around the pyrrolidine head group, which could be due to it occupying the solvent-exposed region in the ATP binding domain, making it less restrained (**Figure 2.10**). [82] Several hydrophobic interactions were observed between Phe374, Leu405, and ALa360 and the tail phenyl ring of PF-543 within the pocket (toe) (**Figure 2.11**). The middle phenyl ring formed favourable edge-on-face π-π hydrophobic interactions with Phe389, with its methyl group interacting with Phe259, Leu385, and Leu286 (heel). Notably, the hydroxyl in the side-chain of Thr282 does not form a hydrogen bond to the ether oxygen of the **PF-543** because it is too far away (> *5* Å). The phenyl ring proximal to the pyrrolidine head group had CH-π and S-π interactions with the side chains of Ile260 and Met358. H- bonds were only observed between the side chain of Asp460, the pyrrolidine nitrogen and the hydroxyl group of **PF-543** (**Figure 2.11**). Analyses of these interactions were used to design more potent and selective inhibitors of SK1 and SK2.
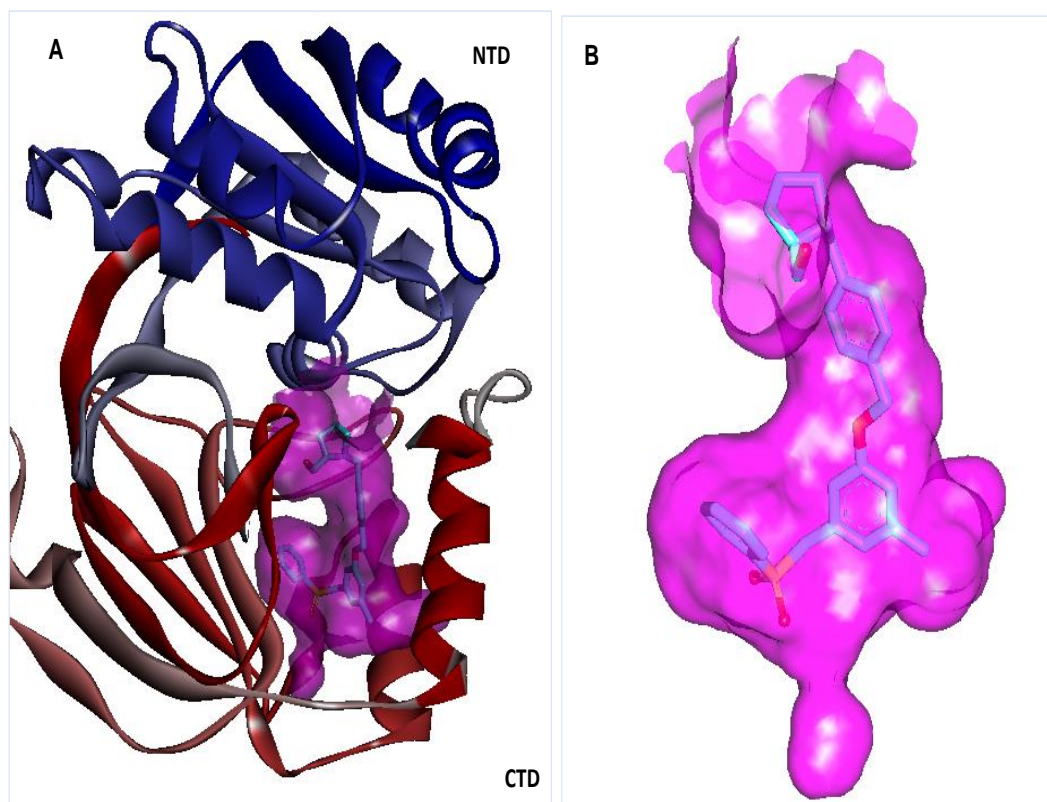
Figure 2.10. Binding of PF-543 to SK1. (A) **PF-543** shown as a cyan stick binds in the J-shaped lipid-binding site, shown in pink, in the C-terminal domain of SK1, shown in red. The *N*-terminal nucleotide binding domain of SK1 is shown in blue. (B) Surface of the J-shaped lipid binding site of SK1 (pink) enclosing **PF-543**. The figure was drawn using DS Visualizer (Protein Data Bank: 4v24).
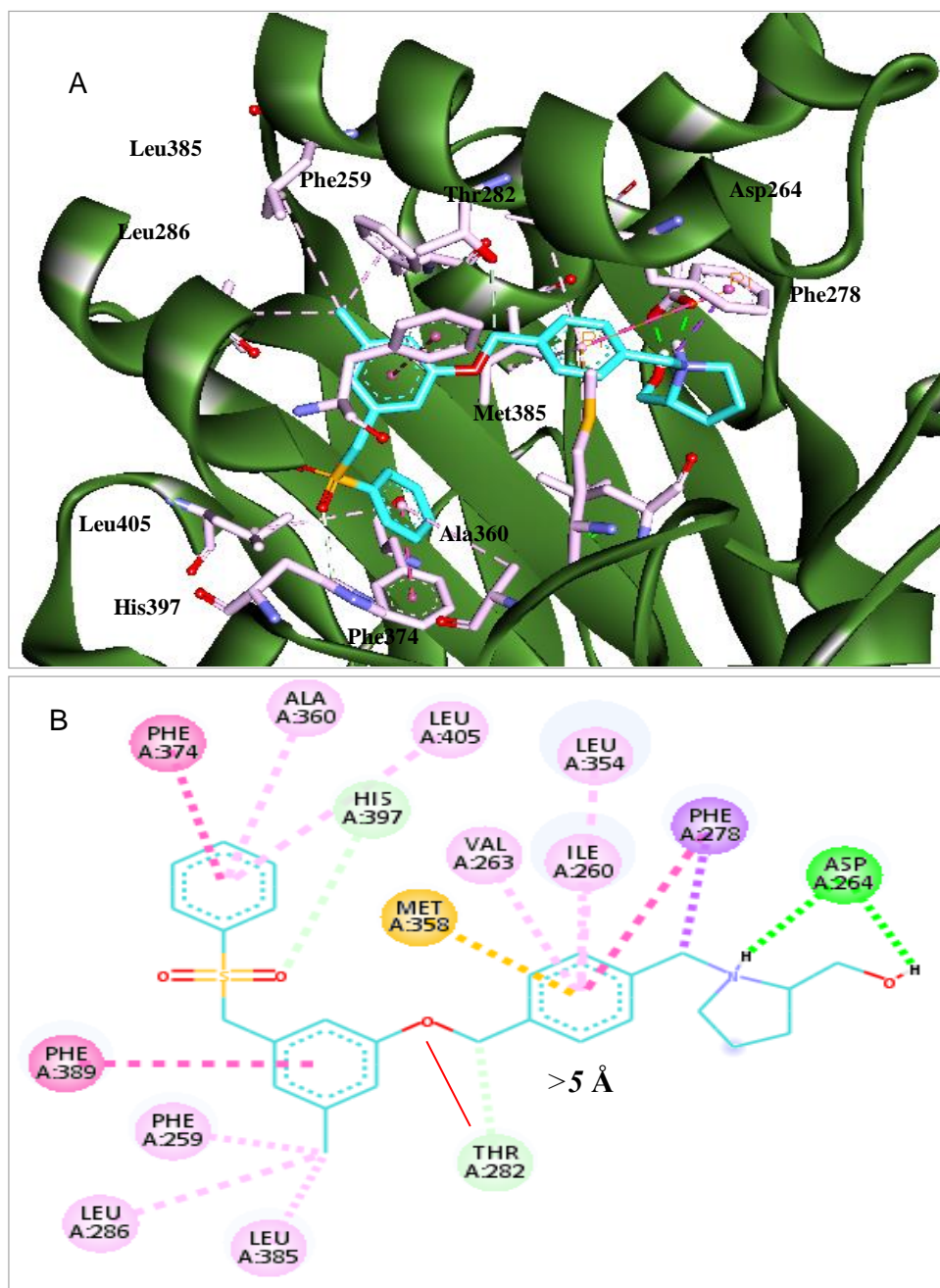
Figure 2.11. Key interactions of PF-543 with SK1. (A) and (B) showing 3D and 2D representations of key amino acid residues of SK1. Residues within a distance of 5 Å from the **PF-543** (cyan) are shown as stick representation with an atomic colour scheme of red, blue, and cyan for oxygen, nitrogen, and carbon atoms, respectively. π-π, CH-π, S-π, and carbon-hydrogen and H -bond interactions are denoted by dark pink, light pink, orange, cyan and green dashed lines, respectively.

2.3.2 Discrimination between SK1 and SK2 structures: key drivers for PF-543 SK1 selectivity.

Although the crystal structures for SK2 have yet to solved, it is well known that this isoform differs in only 3 of the 20 residues in the lipid substrate binding site that form direct contact with PF-543 in SK1. [82] The inner side of the hydrophobic pocket at the toe of the J-region has Phe374 in SK1 replaced by Cys533 in SK2 (**Figure 2.12**), which suggests that the toe is likely to be significantly more spacious in SK2. Moreover, Val304 and Leu517 in SK2 replace Ile260 and Met358 respectively in SK1, which makes the binding site region accommodating the methyl group and sulfone oxygen of PF-543 smaller in SK2 compared with SK1 (**Figure 2.13**). This suggests that selectivity of SK1 for PF-543 is due to encroachment into the heel (the smaller region around the central phenyl) region of the pocket by these residues in SK2. As can be seen in **Figure 2.12: C & D**, the Phe374 side chain is rotated away from the terminal phenyl of PF-543 to form a π-π, stacking interaction (favourable), whereas in SK2, the Cys533 side chain is pointing into the toe and the CH_2 forms a CH-π interaction (lower affinity) with the terminal phenyl group.
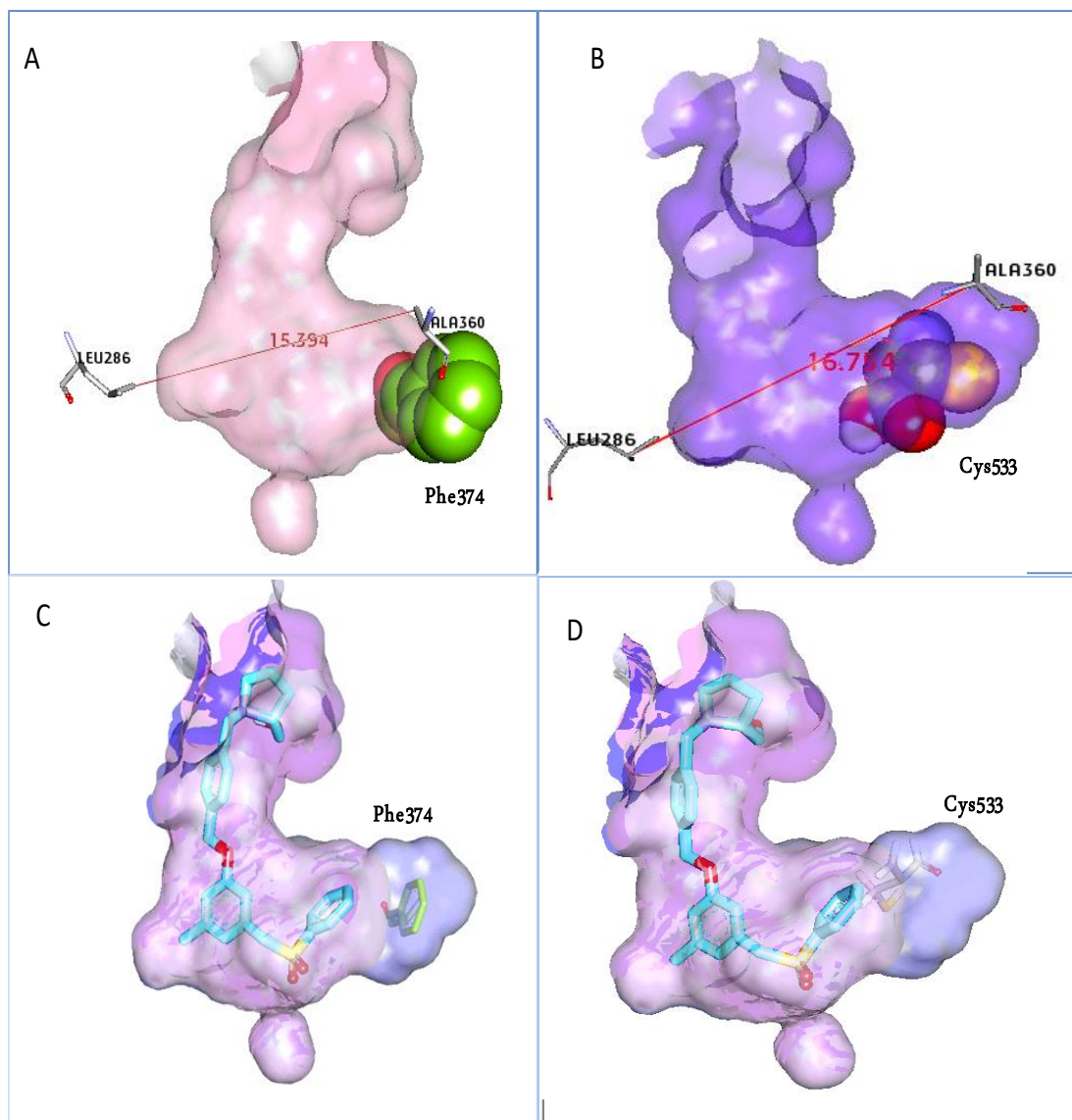
Figure 2.12. Difference in size at the toe of the binding pocket between SK1 and SK2. The toe of the hydrophobic J-shaped pocket in SK1 (coloured in pink (A)) is smaller than in SK2 (coloured in purple (B)) and the docked binding pose of PF-543 in the overlaid SK1 and SK2 (C and D) indicates that the toe of the J-channel is more spacious in SK2 (Cys533) than in SK1 (Phe374).
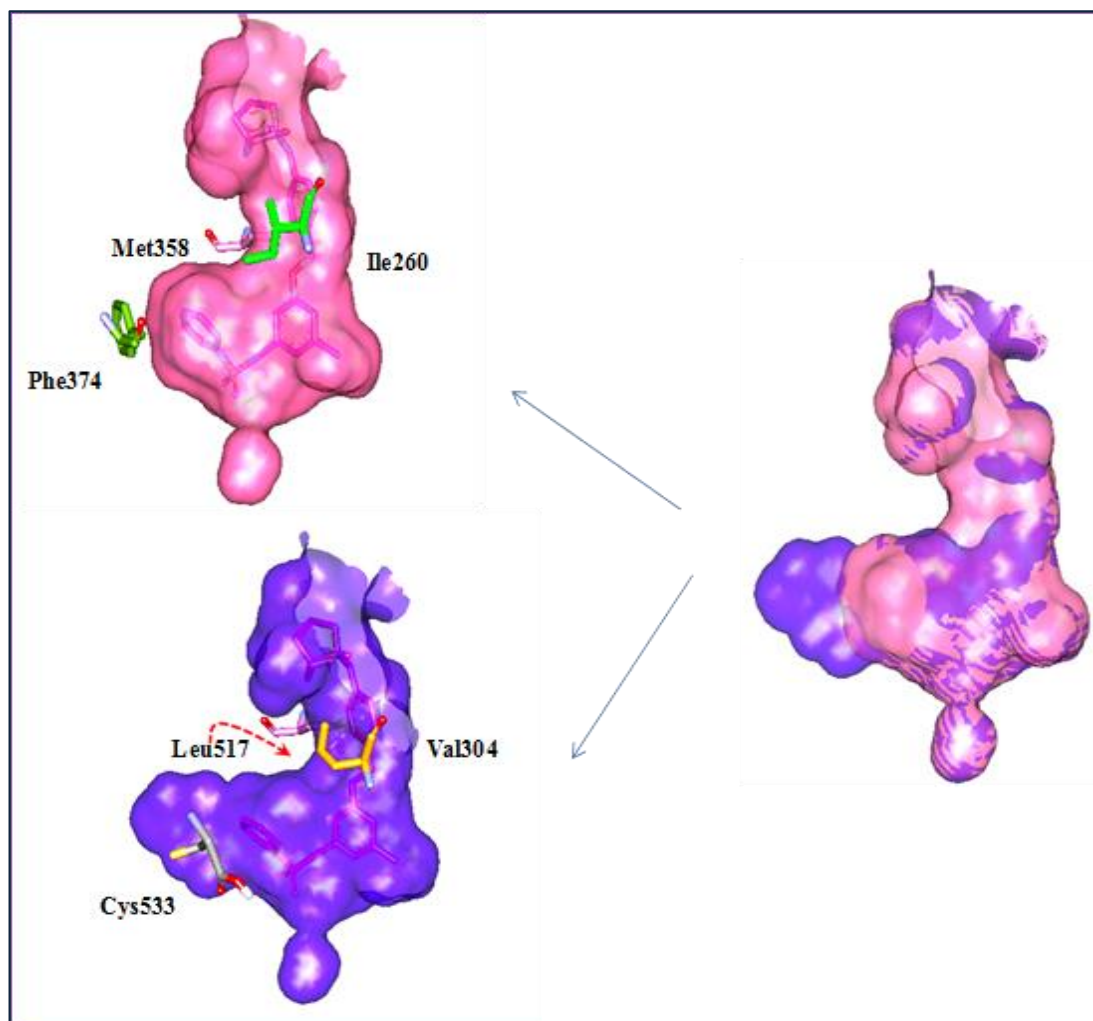
Figure 2.13. Hydrophobic pocket of SK2 differs by 3 residues compared to SK1. Ile260, Met358 and Phe347 (green and pink sticks) in SK1 are mutated to Val304, Leu517 and Cys533 respectively in SK2 (orange, pink and grey sticks). A red arrow indicates that the heel of the J-channel is more compressed in SK2.

2.3.3 Scaffold modifications towards the design of selective SK1 or SK2 inhibitors: key interactions that can be targeted

The initial approach towards the design of selective SK1 or SK2 inhibitors was to exploit the difference in the binding pocket conveyed by these three residues. For example, further enhancement in SK1 selectivity and potency could be achieved by optimising the interactions with Phe374 at the toe, whereas increasing the size of the inhibitor to pack against the equivalent Cys533 could impart selectivity for SK2.
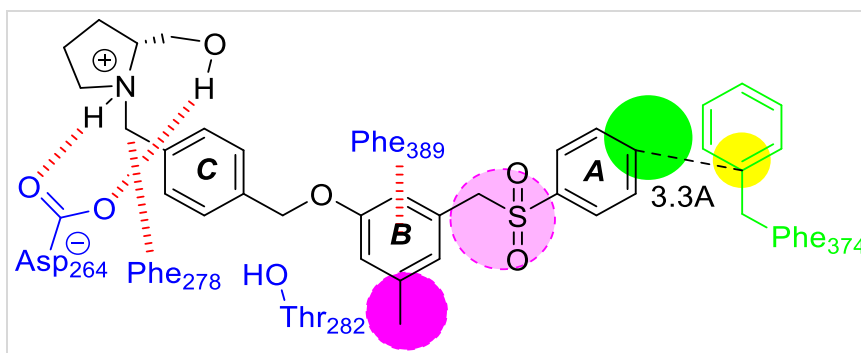
Figure 2.14. Binding mode of PF-543 with SK1 showing the main areas for scaffold modifications. Pink circles represent potential regions of steric intrusion in SK2, the yellow circle represents the location of the sulphur atom of Cys533 in SK2 and the green circle represents the expanded capacity of SK2 compared to SK1.

As shown previously in **Figure 2.12**, the position of Phe374 in SK1 suggested that the addition of any groups to the terminal phenyl ring of PF-543 would preclude accommodation of the compounds in the J-channel of SK1. However, the potentially larger SK2 site, where Cys533 is present, might accommodate these modified versions of PF-543 and therefore define selectivity. The sulfone group and methyl groups in the heel area and just before the toe is a position where SK1-over-SK2 selectivity might be improved (refer to **Figure 2.13**). To characterise the SAR of our SK inhibitors, PF-543 binding was divided into three regions: the terminal phenyl ring (A) and sulfone group as the tail, the phenyl ring (B) and ether as the linker, and the phenyl ring (C) and linked pyrrolidine as the head (**Figure 2.14**).

2.3.4 Design strategies

A. Optimising the linker and the tail to improve potency against SK1

Library 1: Sulfonate instead of sulfone.

The first objective was to introduce an additional hydrogen bond acceptor in the sulfone by replacing it with a sulfonate. The models suggested that this additional oxygen could enable a hydrogen bond to form with the polar residues in the binding pocket and increase affinity for SK1. Sulfonates are not usually found in drugs because of their tendency to hydrolyse, but this approach simplified the synthesis of compounds

as chemical tools to allow exploration of different phenyl substituents (and an isosteric aliphatic ring) to probe the space restrictions at the toe of the pocket.

Library 2: Sulfonamide instead of sulfone.

A small library of compounds was synthesised by replacing the sulfonate with a sulfonamide to explore whether a hydrogen bond donor that targets hydrogen acceptor residues in the binding pocket could convey any potency advantages.

Library 3: Confirming the importance of hydrophobicity in the tail group for SK activity.

Modifications were made to remove the aliphatic or aromatic group from the tail of the scaffold to investigate the importance of a terminal hydrophobic tail moiety for SK inhibitory activity.

B. Optimising the linker and the tail to generate selective SK2 inhibitors

Libraries 4/5: Removal of the sulfone moiety of PF-543

A group of compounds was synthesised based on the replacement of the sulfone moiety with smaller, less polar linker groups (ether, sulphide, methylene) to explore whether selectivity toward the SK2 isoform could be improved. The introduction of *para*-substituents in the terminal phenyl ring was to explore the impact of size on selectivity.

Library 6: Modification of the head to explore how polarity and chirality influence potency and selectivity

Modifications of the hydroxymethylpyrrolidine head included inversion of the chiral centre and replacement of the primary hydroxyl group with other substituents.

2.3.4.1 Optimisation of the hydrophobic tail group towards potent and selective SK1 inhibitors

Library 1: Sulfonate instead of sulfone

The use of a sulfonate functionality was to increase the capacity for hydrogen bonding with the target through the presence of a third oxygen atom as a hydrogen bond acceptor to facilitate an interaction with amino acids in the region as shown in **Figure 2.15.**
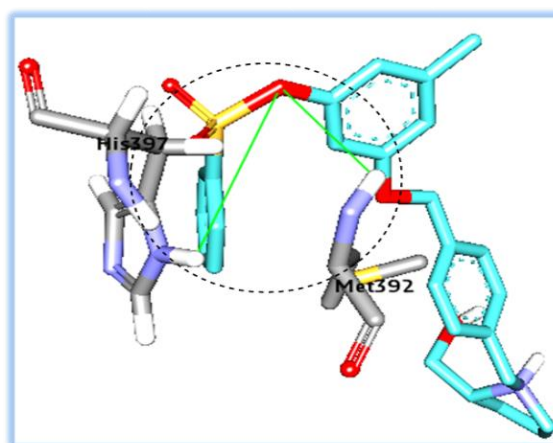
Figure 2.15. The sulfonate analogue bound to SK1. The dashed dark circles indicate the area where H-bonds between the sulfonate and H-donors in residues His397and Met392 could form.

Unexpectedly, the results from the primary ADP-Glo assay revealed that compound **1** with a sulfonate moiety showed a 6-fold decrease in SK1 inhibitor potency compared with **PF-543** (**Figure 2.16**), with only a slight improvement in selectivity towards SK1 over SK2 (**Table 2.1**).

IC50 (nM)* for SK1= 100
IC50 (nM)* for SK2=1130
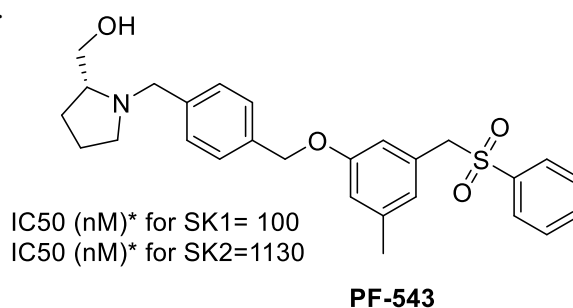
PF-543

Figure 2.16. PF543 with SK1 and SK2 inhibitory activity as determined by our primary assay. *IC_{50} values are an average of three readings.

Table 2.1. SK1 and SK2 inhibitory activity as determined by the ADP-Glo assay for the first library.
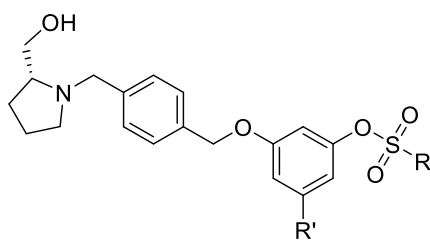
Compounds	R	R´	IC$_{50}$ (nM)* for SK1	IC$_{50}$ (nM)* for SK2
1**		CH$_3$	697	>10000
2**		H	429	>1000
3	OCH$_3$	H	NI	NI
4	Cl	H	NI	NI
5		H	NI	NI
6		H	1000	>10000
7**		H	190	316
8		H	251	>3000
9		H	63	NI

*IC$_{50}$ values are the average of three readings.

**Compound synthesised by a co-worker. NI = No Inhibition.

Docking of compound **1** (**Figure 2.17**) in SK1 clearly showed that it adopts a pose in the active site similar to **PF-543**, with the hydroxylmethylpyrrolidine head group maintaining H-bonding with Asp264 at the mouth of the lipid binding site. There are also π-π stacking interactions and CH-π interaction maintained between the tail phenyl ring and side chains of Phe374 and Ala360, respectively, at the toe end of the site. However, the sulfonate group and the extra H-bond acceptor did not contribute any new key interaction with any surrounding amino acids in the pocket (**Figure 2.17**). The decreased potency against SK1 could be due to removal of the ability of the tail phenyl group and central phenyl ring to make CH-π and π-π interactions with Leu405 and Phe389 respectively, compared with **PF-543**. Moreover, the carbon-hydrogen interactions that were evident with His397 and Thr282 and **PF-543** are no longer available (**Figure 2.17**). Enhanced selectivity for SK1 could be due to SK2 not being able to accommodate the more hydrophilic sulfonate in the narrow heel of the J-channel region because of increased steric hindrance, as all other moieties are the same as **PF-543**.
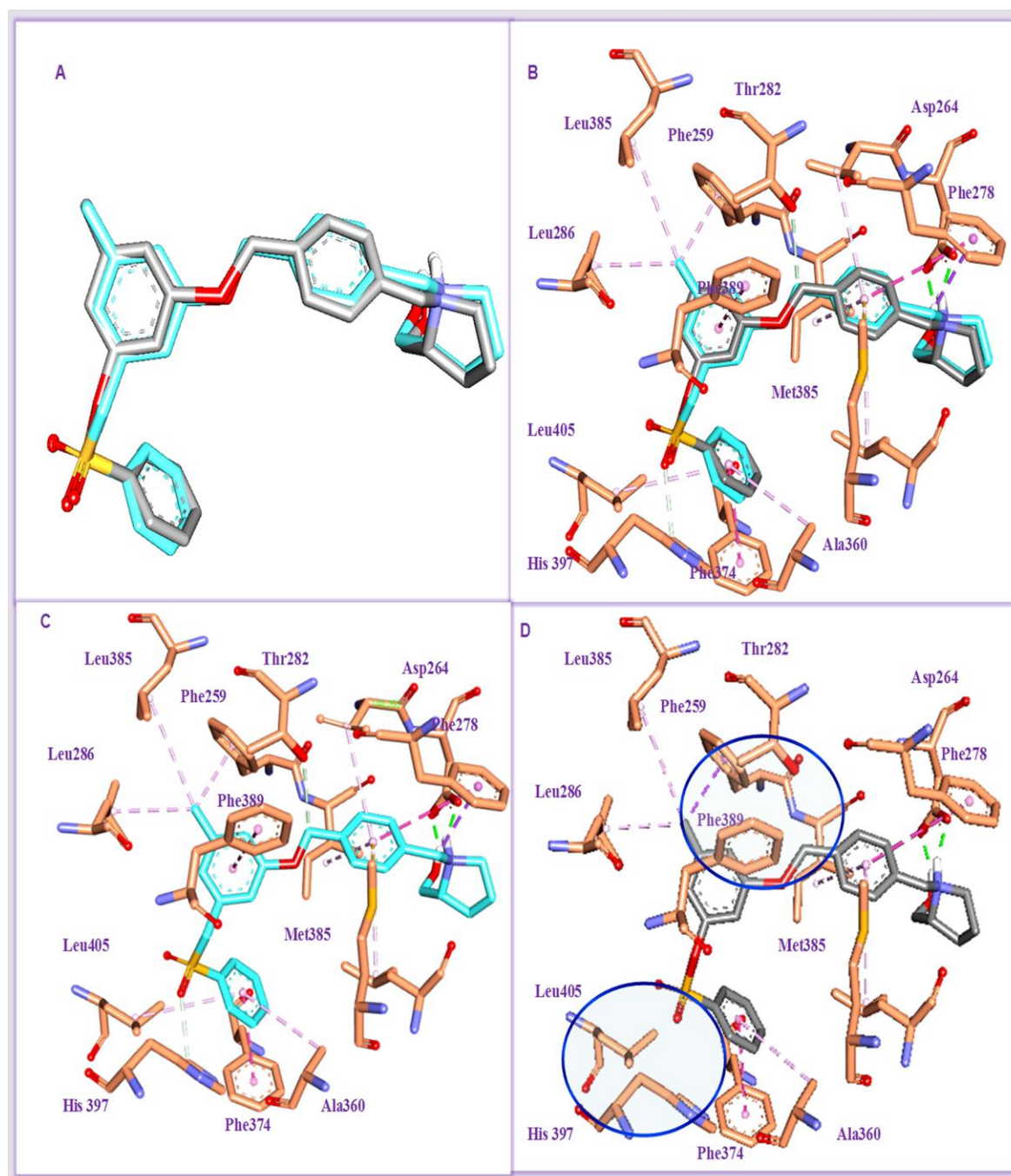
Figure 2.17. Docking binding pose compound 1 into the active site of SK1. 3D structure of overlaid **PF-543** (cyan colour) and compound **1** (grey colour) (A); receptor interactions of overlaid compound **1** and **PF-543**(B); recepror interactions of **PF-543** (C); and receptor interactions of compound **1** (D), blue cricles indicate an area associated with the loss of interactions between compound **1** and SK1 compared to **PF-543**.

To test the importance of the methyl group in the central phenyl moiety, compound **2** was synthesised. Compound **2** had slightly improved SK1 inhibitory activity and selectivity compared with compound **1** (**Table 2.1**) which suggests that the methyl group makes a minimal contribution to binding and is neither essential for the SK activity nor selectivity of our analogues. Binding appears to be more sensitive to changes in the sulfone region.

From the docked pose of compound **2** (**Figure 2.18**), the absence of a methyl group suggests reduced interactions with the three surrounding amino acids Phe259 Leu385, and Leu286 at the base of the ring in the heel of the pocket. The slight improvement in SK1 inhibitory activity for compound **2** over compound **1** could be due to greater flexibility of the molecule within the toe region of the J channel pocket and restoration of π-π, CH-π and the carbon-hydrogen interactions with Phe389, Leu405, Thr282 and His397 respectively. These interactions were observed in the docking pose of PF-543, but were not seen with compound **1** (**Figure 2.18**).

Overall, both compounds showed fewer binding interactions with SK1 compared with **PF-543**, which could explain the increase in IC_{50} from100 nM for **PF-543** to 429 nM for compound **2** and 679 nM for compound **1**. The improvement in selectivity of compound **2** towards SK2 compared with PF-543 and compound **1** could be explained by the removal of a steric clash between the methyl moiety on the central phenyl ring and the heel of the narrower, more hydrophobic J-channelof SK2.
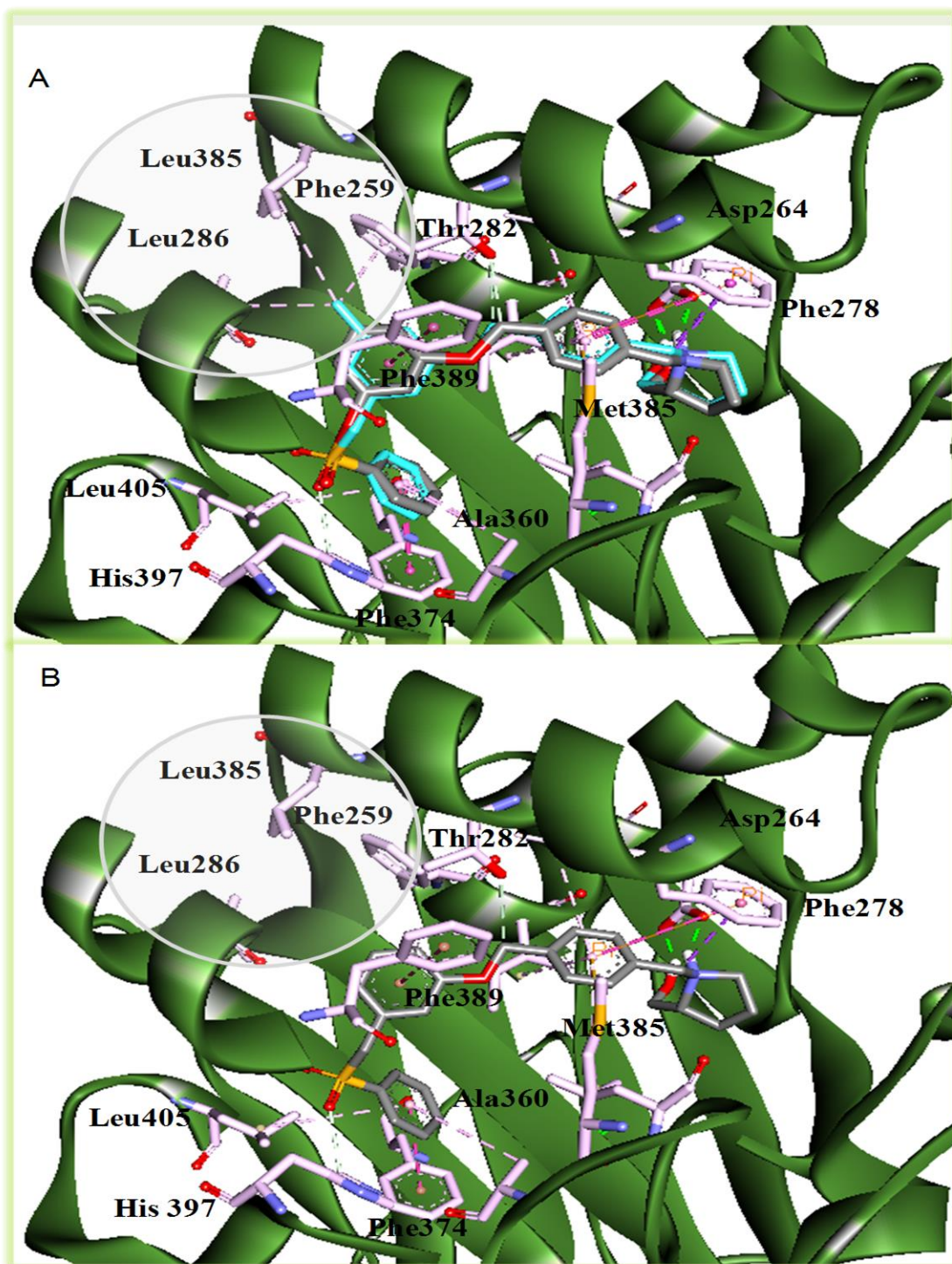
Figure 2.18. Docked compound 2 into active site of SK1. Docked binding pose of overlaid compound **2** (grey colour) and **PF-543** (cyan colour) (A); docked binding pose of compound **2** (B), white cricle indicates an area associated with the loss of interactions between compound **2** and SK1.

Modifications to the tail phenyl ring

The sulfonate modifications to **PF-543** showed promising results in terms of shifting the selectivity for SK1 over SK2. The next step was to explore if *para* substituents in the tail phenyl group could exploit potential size differences between the two isoforms (SK2 was predicted to have a larger toe region) and if additional hydrophobic interactions could improve activity.

Introducing a *para*-methyl group to a phenyl moiety is a common approach in hit optimisation strategies because it could occupy a hydrophobic pocket more tightly. Equally, a halogen atom such as a lipophilic chloro substituent can also have favourable interactions with the hydrophobic pocket. Compound **3** with a methoxy group was synthesised to study whether hydrophilic interactions could be beneficial.

All compounds were inactive (**Table 2.1**), which suggests that there is a severe size restriction at the end of the substrate-binding pocket in both isoforms, and that Phe347 in SK1 and the more spacious Cys533 in SK2 cannot accommodate even small *para*-substituents.

Alkyl groups replacing the phenyl ring

To further investigate the size restrictions in the toe region of the binding site, compounds were prepared with the tail phenyl ring replaced by aliphatic groups of varying lengths and bulkiness (**Table 2.1**).

Reducing the size of the substituent to the smallest hydrophobic group (methyl; compound **6**) reduced activity against SK1 by 2-fold and 10-fold compared with compound **2** and **PF-543**, respectively. Docking studies suggested that the small methyl substituent was unable to interact with the surrounding hydrophobic residues Phe374, Leu347 and Ala360, primarily through a loss of π-π and π-CH interactions with the terminal aromatic moiety (which was seen with **PF-543**) (**Figure 2.19**).

Increasing lipophilicity by expanding the length of the aliphatic substituent (compound **8**) led to a restoration of potency against SK1 activity. The 4-fold increase in potency compared with compound **6** could be due to enhanced hydrophobic alkyl interactions

between the aliphatic *n*-butyl group and the aliphatic side chains of Leu405 and Ala360 and CH-π interactions with Phe374 as discussed above.
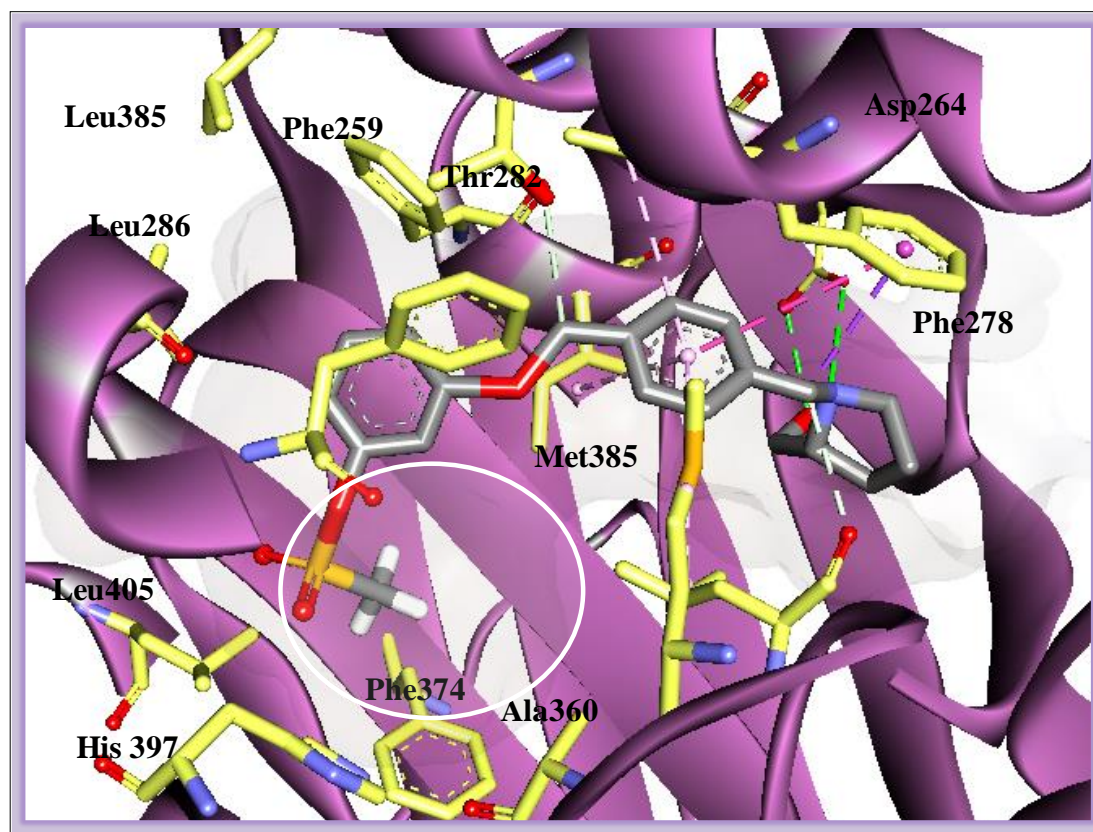
Figure 2.19. Docked compound 6 into the active site of SK1. A white cricle indicates an area associated with the loss of interactions between the methyl group of compound **6** and SK1.

Interestingly, replacement of the phenyl ring by a bulky isobutyl group (compound **7**) improved potency against SK1 compared with other sulfonates, although selectivity towards SK2 was compromised (**Table 2.1**). The docked pose clearly showed that there is a difference in both the orientation (compared with **PF-543**, compound **1** and compound **2**) and interaction with the binding pocket (**Figure 2.20**).
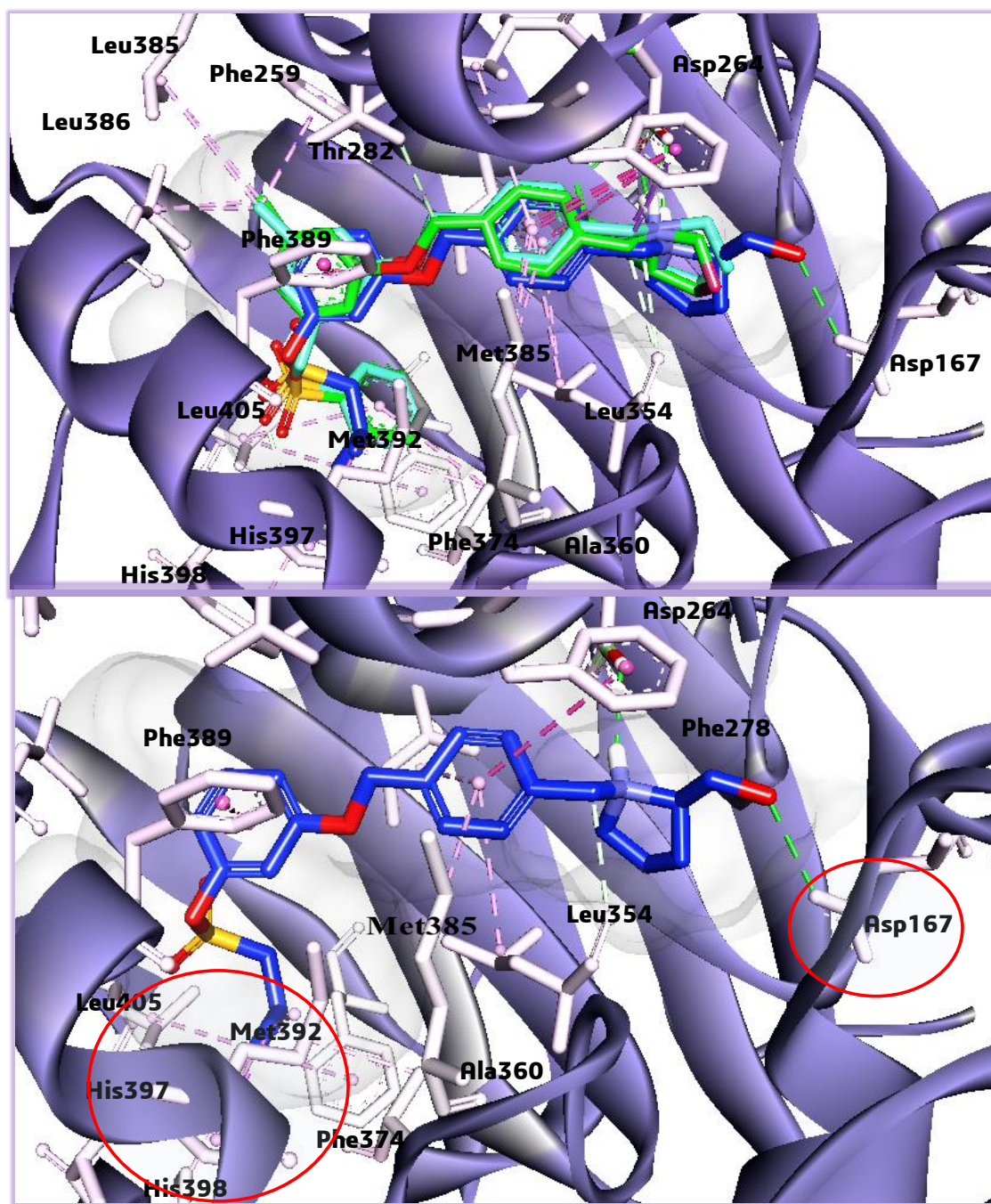
Figure 2.20. Docked compound 7 into the active site of SK1. Red cricles indicate new key interactions introduced by compound **7** to SK1.

The terminal isobutyl group appears to pull the molecule further down into the toe region of the hydrophobic pocket, which causes the hydroxymethylpyrrolidine head of the molecule to flip around and form one new hydrogen bond with Asp167 similar to that observed between Sph and SK1 (**Figure 1.8: section 1.8.1**) but not **PF-543**. The other hydrogen bond with Asp264 (that is seen with **PF-543** and other analogues) is present. The docked pose (**Figure 2.20**) suggests that the improved potency of compound **7** against SK1 (IC_{50} = 190 nM), compared to compound **1** and compound **2**, is likely due to the ability of the branched isobutyl group to increase the number of interactions with residues in the toe. CH-π interactions with Phe374, His397, His398 and alkyl interactions with Leu405, AL360, and Met293 are evident (**Figure 2.20**). Pulling the molecule further down into the pocket to enhance short-range interactions may also be factor.

The reduced selectivity and improved potency against SK2 suggests that the bulky isobutyl group can be more readily accommodated in the larger toe of J-pocket in SK2 which is further favoured by aliphatic interactions with the Cys533 residue in SK2 (**Figure 2.21**).
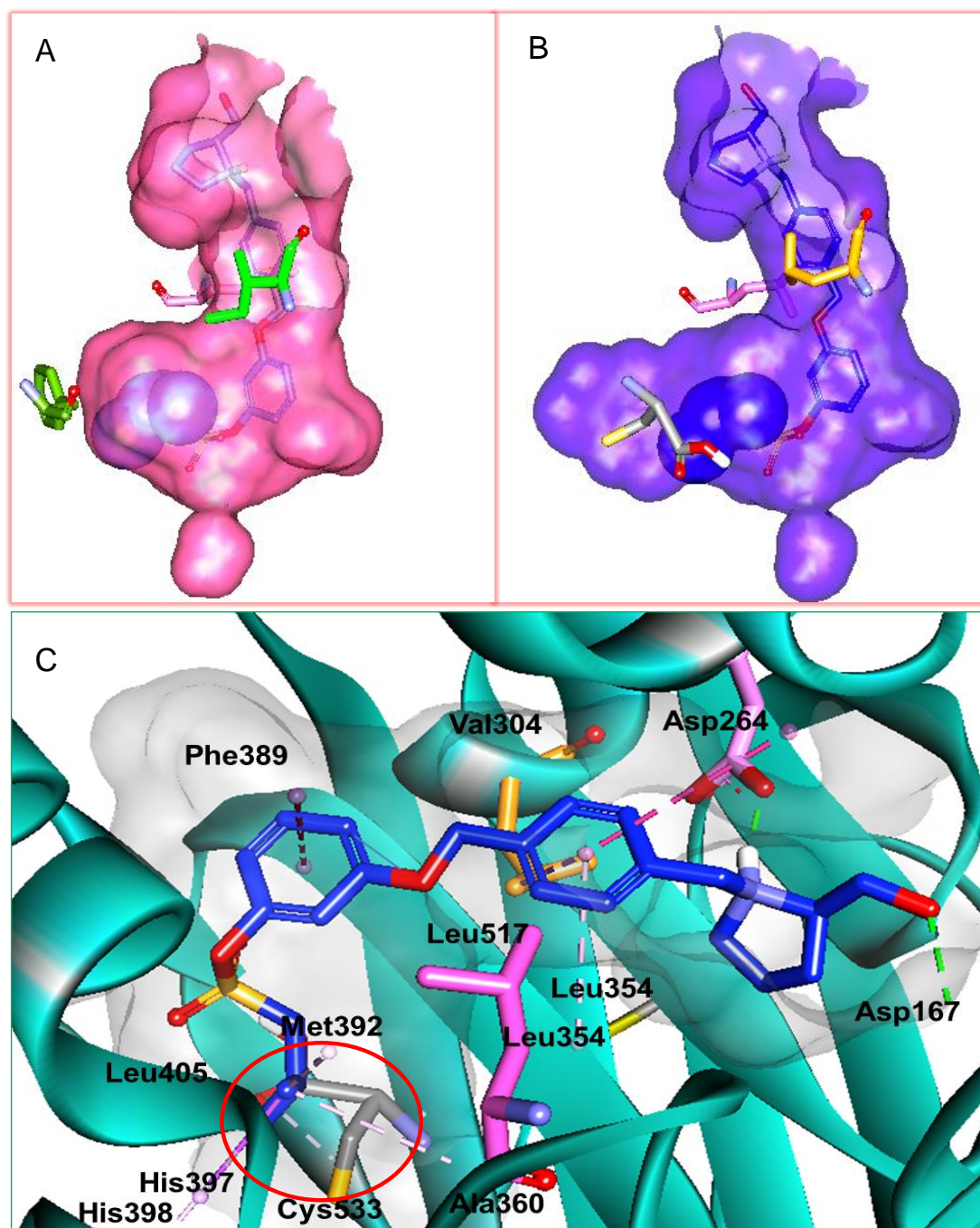
Figure 2.21. Proposed docked pose of compound 7 in SK2. Docked binding pose of compound **7** (blue stick) in the SK1 binding pocket that is shown in pink (A) and in the SK2 binding pocket that is shown in blue (B). The isobutyl chain of compound **7** is in CPK and indicates a tight fit in both pockets. The red circle in (C) indicates the alipatic interaction between Cys533 of SK2 and the isobutyl side chain of compound **7**. Orange, pink and grey sticks are Val304, Leu517, Asp264 and Cys533 respectively.

To further assess the impact of bulk group at the toe of the pocket, the phenyl ring was replaced by a cyclohexyl group (compound **9**), which produced the most potent and selective inhibitor of SK1 (IC_{50} = 63 nM). The narrow pocket in SK1 appeared to accommodate more tightly the flexible and bent cyclohexane ring compared with the planar and flat phenyl ring of **PF-543** and this possibly accounts for the better potency against SK1 (**Figures 2.22)**. Despite the loss of planarity in the tail phenyl group, the cyclohexane ring still maintains CH-π interactions with Phe374 and alkyl interactions with Ala360 and Leu347 with notable new interactions (carbon-hydrogen bond) with Leu345. An additional two new alkyl interactions between the pyrolidine ring and residues Ala201 and Leu253 (**Figure 2.23**), which were not seen with **PF-543** and other analogues, may also be factor.

The loss of planarity in the cyclohexane ring allows the tail of the molecule to occupy the full space of the hydrophobic pocket. This would force the hydrophilic sulfonate towards the narrow channel of SK2. This region is more spacious in SK1 due to presence of the smaller Met358 and Ile260 residues, thereby resulting in increased repulsion in the SK2 pocket (**Figure 2.22**) and consequently to reduced potency for this isoform.
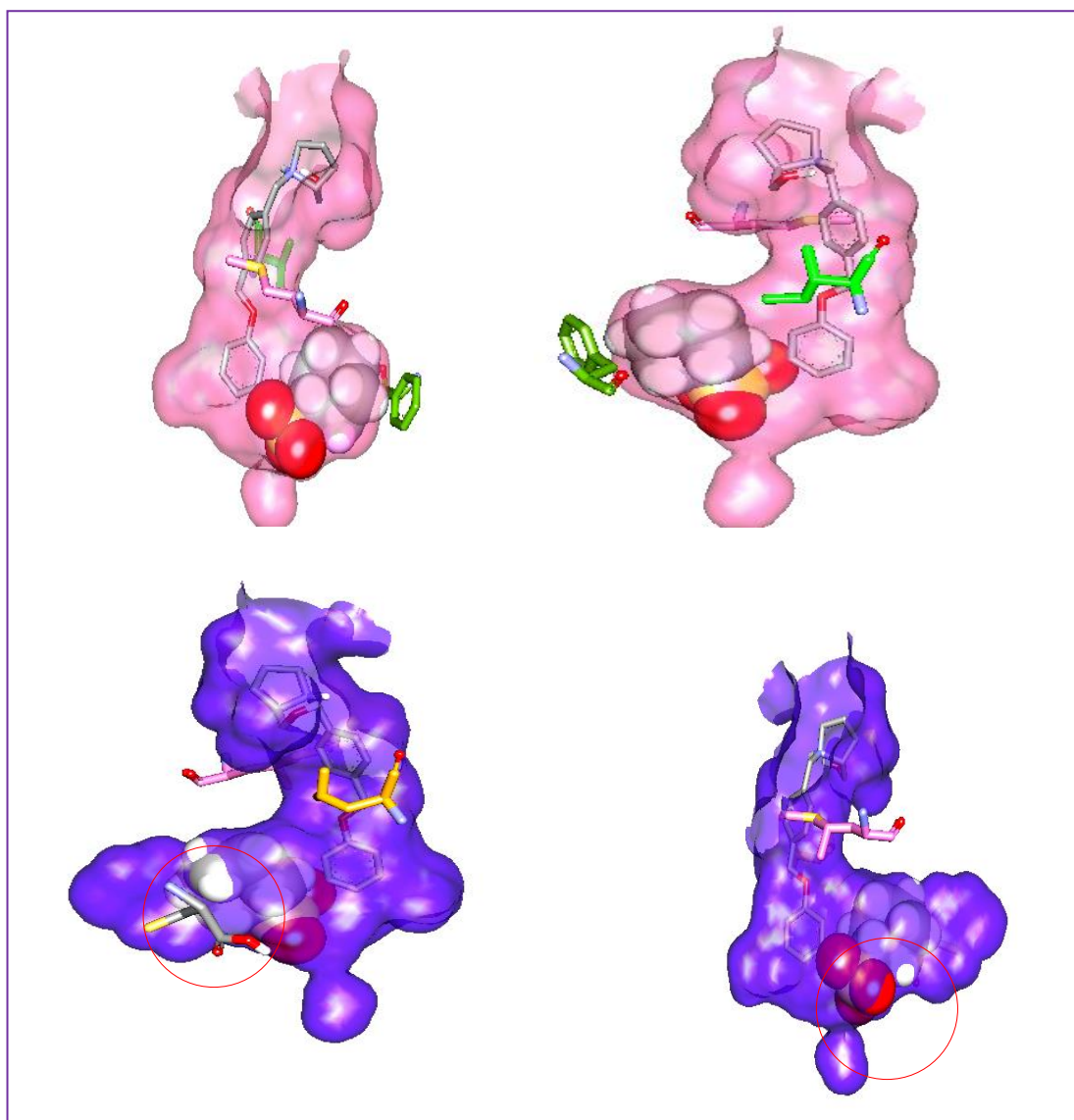
Figure 2.22. Compound 9 binding to SK1 and SK2. Compound **9** (grey stick) in the SK1 binding pocket shown in pink (two sides) and in the SK2 binding pocket shown in blue (two sides). CPK-rendering of the cyclohexyl group shows compound **9** is accommodated closely in the toe of SK1, whereas steric clash is obvious in the SK2 pocket (indiacted by red circles).
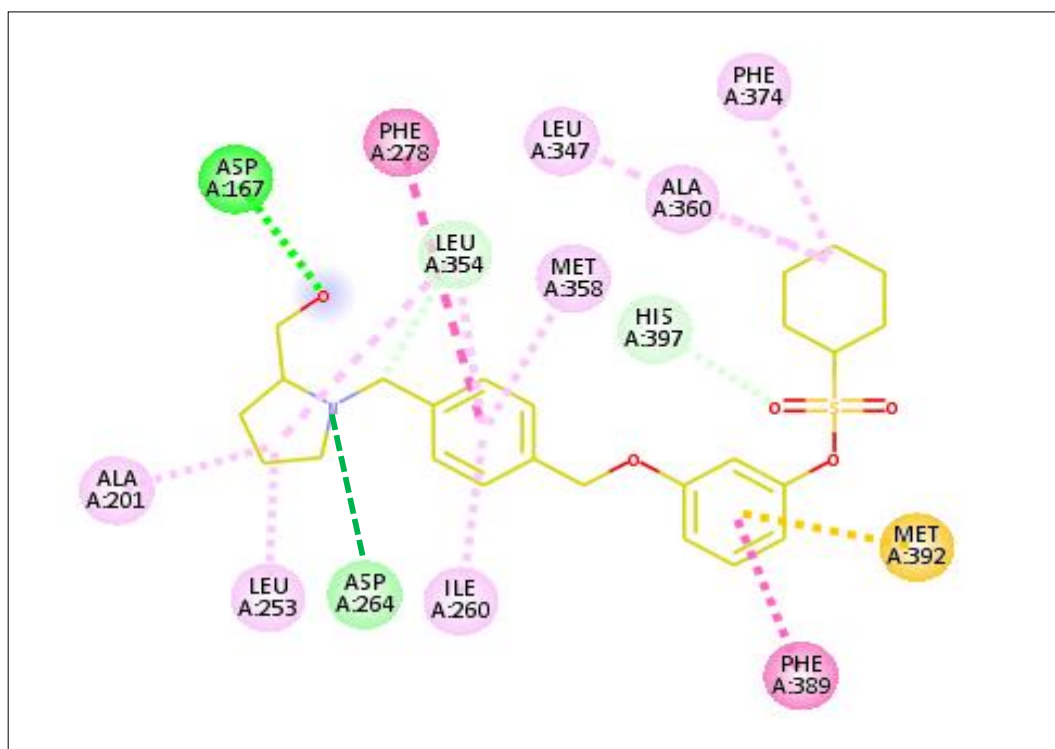
Figure 2.23. Key interactions of compound 9 with the active site of SK1. The 2D diagram for the key interactions of compound **9** (yellow) within the SK1 pocket was generated using DS software. Dashed lines represent the different types of interactions colourerd as follows: green, cyan ,light pink, dark pink and orange for H-bonds, carbon-H-bonds, CH-π, π-π and S –π respectively.

Library 2: Sulfonamide instead of sulfonate

To study the effect of introducing a sulfonamide into the tail of the molecule, compounds containing similar substituents to the sulfonate series were synthesised (**Table 2.2**). The sulfonamide functionality was introduced to explore whether a hydrogen bond donor group could influence activity: the N-H is bulkier than oxygen and could gain closer proximity with hydrogen bond acceptors inside the pocket such as His297 and Met392 (Refer to **Figure 2.15**). Improving stability was another reason for preparing these analogues.

Table 2.2. SK1 and SK2 inhibitory activity as determined by the ADP-Glo assay for the second library.
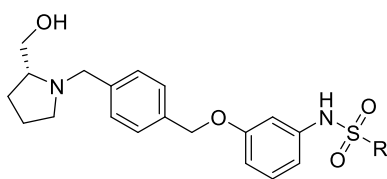
Compounds	R	IC$_{50}$(nM)* for SK1	IC$_{50}$(nM)* for SK2
10		NI	NI
11		NI	NI
12	—OCH$_3$	NI	NI
13	—Cl	NI	NI
14		NI	NI

*IC$_{50}$ values are the average of three readings. NI = No Inhibition.

All compounds containing the sulfonamide moiety were inactive (**Table 2.2**). One possible explanation for the inactivity is that N-H group of sulfonamides increases the polarity and the steric bulk in an area of the binding site that contains various hydrophobic residues, which is incompatible with both isoforms.

Sulfonamides have less conformational flexibility compared to sulfonates and sulfones because of greater resonance stabilisation in the sulphonamide moiety. These more rigid conformations, if less compatible with the shape of the binding site, would not be able to adapt to its topology, and thus prevent binding.

Library 3: Importance of hydrophobicity in the tail group for SK activity

To study if the terminal aromatic group that occupies the toe of the J-region was required at all, two compounds truncated in this region were prepared (compound **15** and compound **16**). The absence of any SK inhibitory activity compared to compound PF-543 and other analogues suggest that a terminal aromatic group that can interact with hydrophobic residues in the toe is essential for activity (**Table 2.3**).

Table 2.3. SK1 and SK2 inhibitory activity as determined by the ADP-Glo assay for the third library
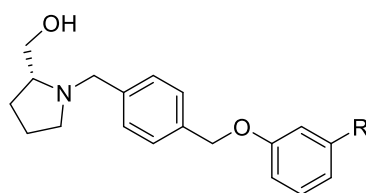
*IC_{50} values are the average of three reading.

Compounds	R	IC_{50} (nM)* for SK1	IC_{50} (nM)* for SK2
15		NI	NI
16**		NI	NI

. **Compound synthesised by a co-worker. NI = No Inhibition.

2.3.4.2 Optimising the linker and the tail to generate selective SK2 inhibitors

Library 4: Removal of the sulfone moiety of PF-543

SAR analysis of the first set of compounds indicated that repulsive interactions in the heel region of the J channel bordered by the bulkier Val304 and Leu517 residues in SK2 could offer an approach towards introducing selectivity. To establish whether size and polarity were important, smaller and less polar functional groups were introduced in place of the sulfone/sulfonate: an ether (**17**), a sulfide (**18**) or a methylene moiety (**19**) (**Table 2.4**). The ether and sulfide-containing compounds were slightly more potent against SK1 than the sulfonate analogue (compound **2**), but notably, all three

were more active against SK2 than any other compounds previously assessed. All were essentially equipotent against both isoforms, confirming our hypothesis that smaller, less polar groups in this region could improve activity against SK2.

Table 2.4. SK1 and SK2 inhibitory activity as determined by the ADP-Glo assay for the fourth library
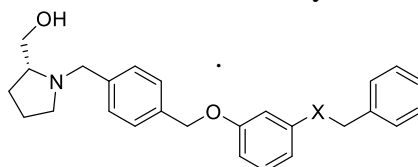
Compounds **	X	IC$_{50}$(nM)* for SK1	IC$_{50}$(nM)* for SK2
17	O	297	408
18	S	244	147
19	CH$_2$	758	654

*IC$_{50}$ values are the average of three readings.

**Compound synthesised by a co-worker.

Docking of **17** and **18** with SK1 suggested a similar binding mode to **PF-543**, with the pyrrolidine head group forming the same two hydrogen bonds with Asp264 (**Figure 2.24: Figure 2.25**). The SK2 inhibitor activity observed for compound **17** and compound **18** is likely due to the removal of the steric and repulsion effects that arise from the sulfone/sulfonate oxygen of **PF-543** and its analogues in the narrower heel of the J-channel (**Figure 2.24: Figure 2.25**). Compound **17** is moderately less potent against SK2 possibly because oxygen is more electronegative, which leads to increased repulsion with Val304 and Leu517. Compound **19** showed a 2-fold and 4-fold decrease in SK1 and SK2 potency respectively compared with compound **18**. In both cases, this is likely due to steric effects resulting from the bulkier methylene group that forces the terminal aromatic ring down into the toe of the pocket of SK1.
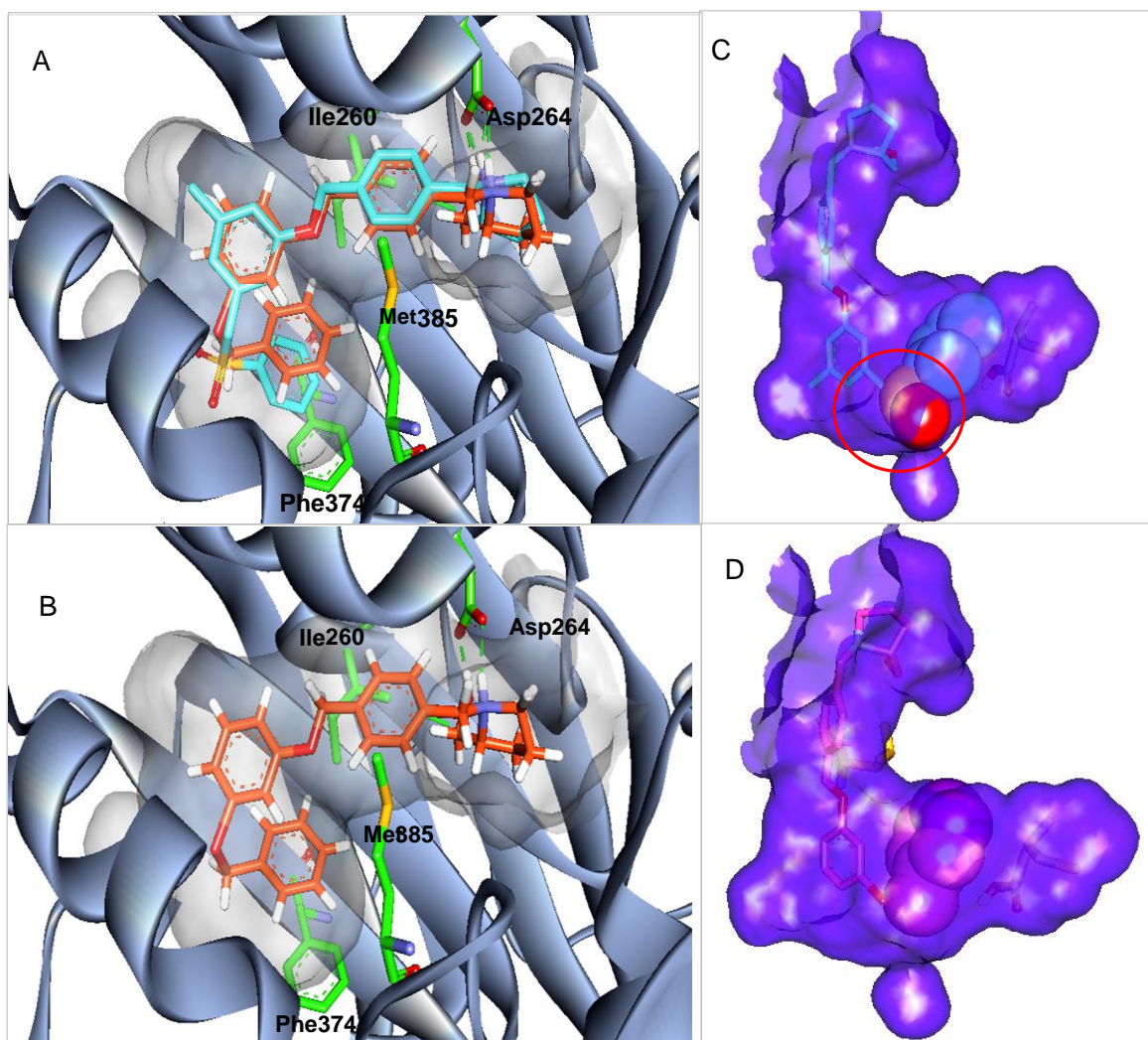
Figure 2.24. Docked pose of compound 17. (A) and (B) show receptor interactions of compound **17** (orange stick) with and without the superimposed **PF-543** (cyan) in SK1. The red circle in (C) indicates a steric clash in the SK2 binding pocket (coloured in blue) caused by the sulfone group of **PF-543** (in CPK); and (D) shows compound **17** accommodated more tighly in SK2 through CPK-redering of the terminal group.
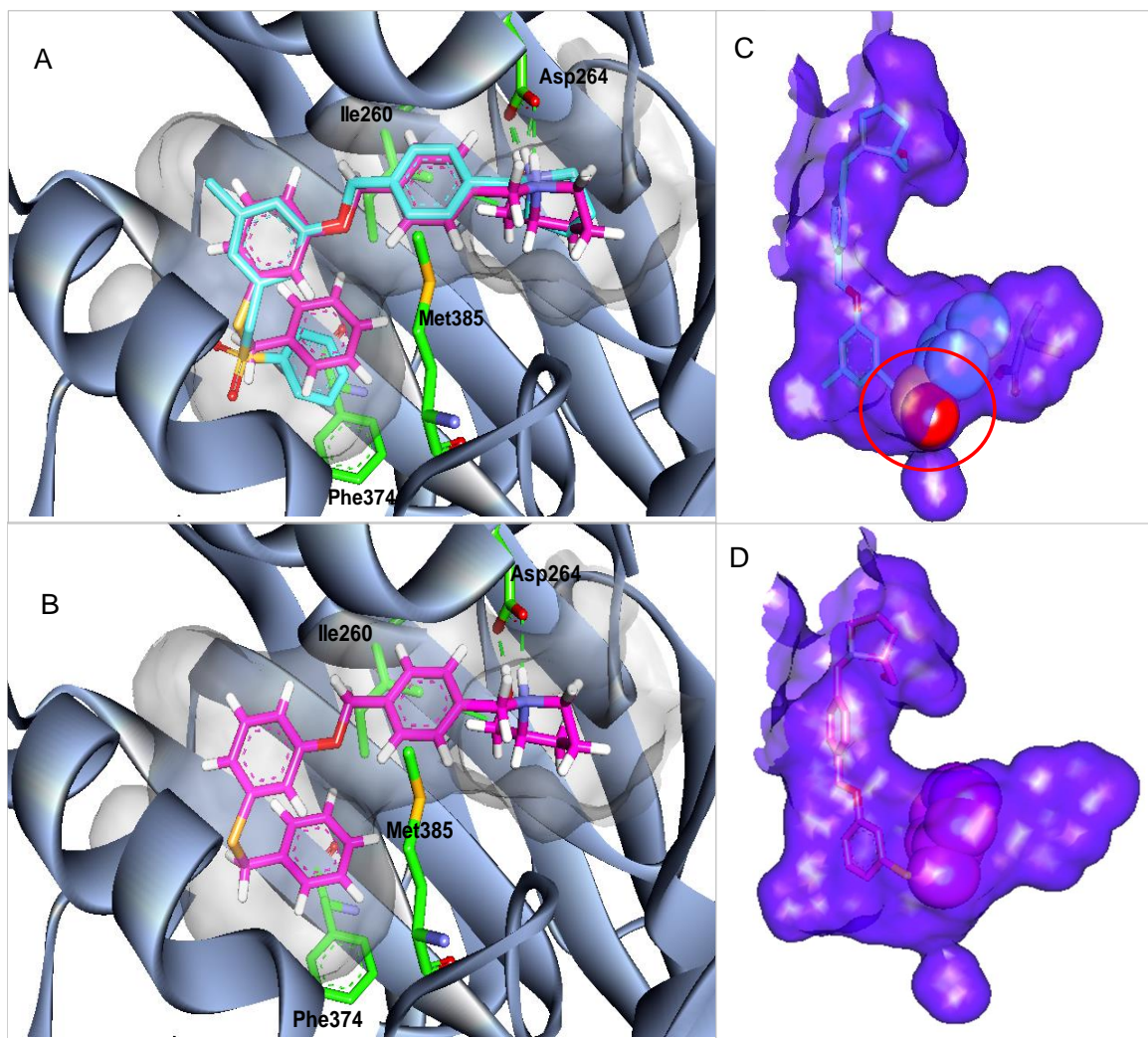
Figure 2.25. Docked pose of compound 18. (A) and (B) show receptor interactions of compound **18** (pink stick) with and without the superimposed **PF-543** (cyan) in the SK1 binding site; red circle in (C) indicates a steric clash in the SK2 binding pocket (coloured in blue) caused by the sulfone group of **PF-543** (in CPK); and (D) shows compound **18** accommodated more tighly in SK2 through CPK-redering of the terminal group.

Library 5: Modifications to the tail phenyl ring of compound 18

As mentioned previously, the toe of the J-channel is likely to be more spacious in SK2 due to the presence of a smaller Cys533 residue at the end of the pocket. The second approach to exploit the differences in size between the SK isoforms in favour of developing selective SK2 inhibition was to increase the size of the terminal group through the introduction of *para*-substituents, or replacement of the phenyl ring itself with a cyclohexyl group (**Table 2.5**). Modifications were performed on the sulfide

analogue because this had the most potent activity against SK2 from the previous series.

Table 2.5. SK1 and SK2 inhibitory activity as determined by the ADP-Glo assay for the fifth library.
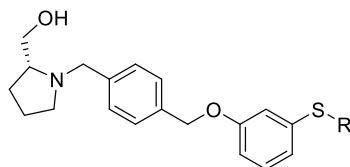
Compounds	R	IC$_{50}$(nM)* for SK1	IC$_{50}$(nM)* for SK2
20		NI	255 nM
21		NI	206 nM
22		NI	NI
23		NI	NI

*IC$_{50}$ values are the average of three readings. NI = No Inhibition.

Inhibitory assays (**Table 2.5**) revealed that the *para*-chloro and *para*-fluoro substituents, compounds **20** and **21**, abrogated SK1 activity and represent the first example of SK2 inhibitors with nanomolar potency and complete selectivity over SK1. The bulkier compounds **22** and **23**, with a *para*-trifluoromethyl substituent and cyclohexyl ring respectively, were inactive against both isoforms, suggesting a crucial role for group size in the toe of the J-pocket in terms of potency and selectivity for SK2.

Similar to the docked pose of ccompound **18** in SK2, the *para*-fluorophenyl ring of compound **21** and *para*-Cl of compound **20** occupied the toe of the J-pocket and the head pyrrolidinium group retained the H-bonds with Asp264 (**Figure 2.26: Figure 2.28**). In SK1 the toe of the J-channel is likely to be smaller than SK2 due to the presence of Phe347, and inactivity against the former isoform by the *para*-substutued analogues and the bulky cyclohexyl derivative could be due to their inability to fit inside this hydrophobic toe region (**Figure 2.27: Figure 2.29)**.

Compounds **20**, **21** and **22** have electron-deficient aromatic rings in the tail group, which could negatively impact hydrophobic interactions in this region of SK1 as shown in **Figures 2.27** and **2.29**. The back of the toe of SK2's J-channel has Cys533 which is likely to create a larger space, providing enough room for compounds **20** and **21** to be accommodated within the pocket (**Figure 2.27: Figure 2.29**). The similar potency of compound **18** against SK2 suggests that the *para*-F and *para*-Cl substituents do not impart any extra favorable interactions with the hydrophobic toe region in this isoform.
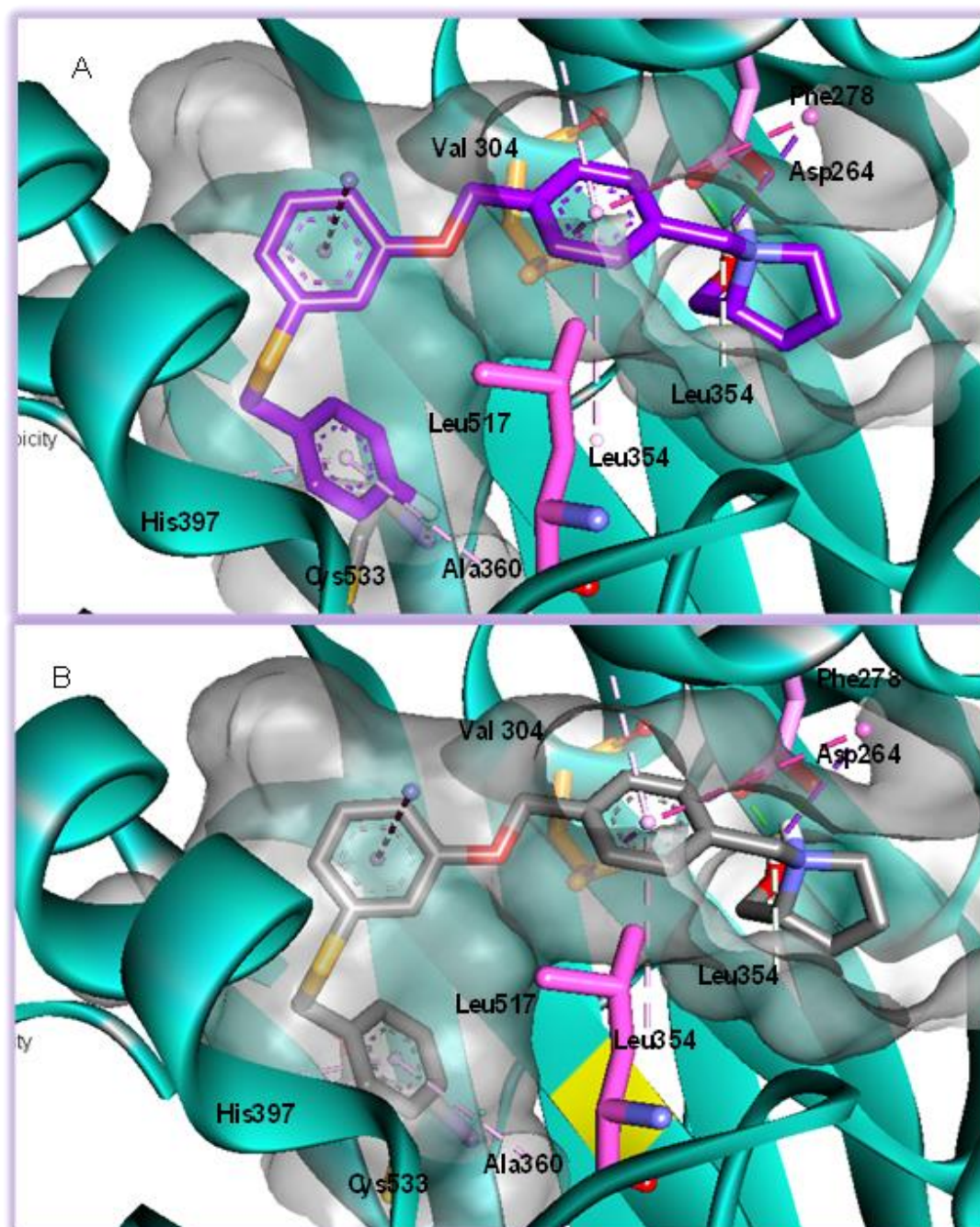
Figure 2.26. Docked pose of compounds 21 and 18. (A) shows compound **21**. (purple) interactions with SK2; (B) shows compound **18** (grey) interactions with SK2. Orange, pink and grey sticks are Val304, Leu517, Asp264 and Cys533 respectively.
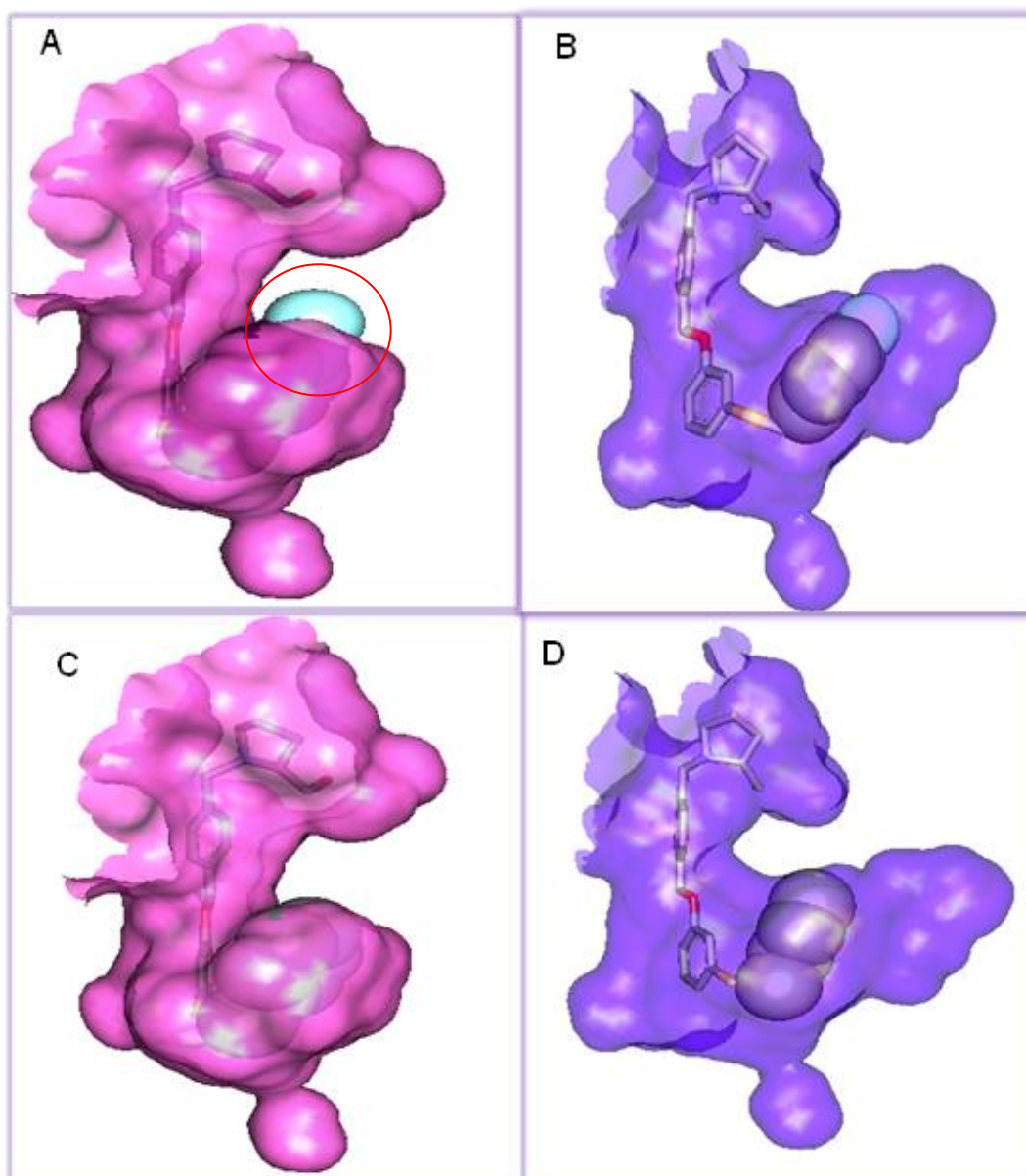
Figure 2.27. Docked poses of compounds 21 and 18. (A) and (B) show compound **21** (the terminal *para-* fluoro phenyl ring in CPK and *para*-F in light blue) accommodates tighly in the toe of SK2 (coloured in blue), while replusion is obvious in the SK1 pocket (in pink and indicated by red circles); (C) and (D) show compound **18** (the terminal phenyl group in CPK) accommodates tighly in the toe of both SK1 and SK2 pockets.
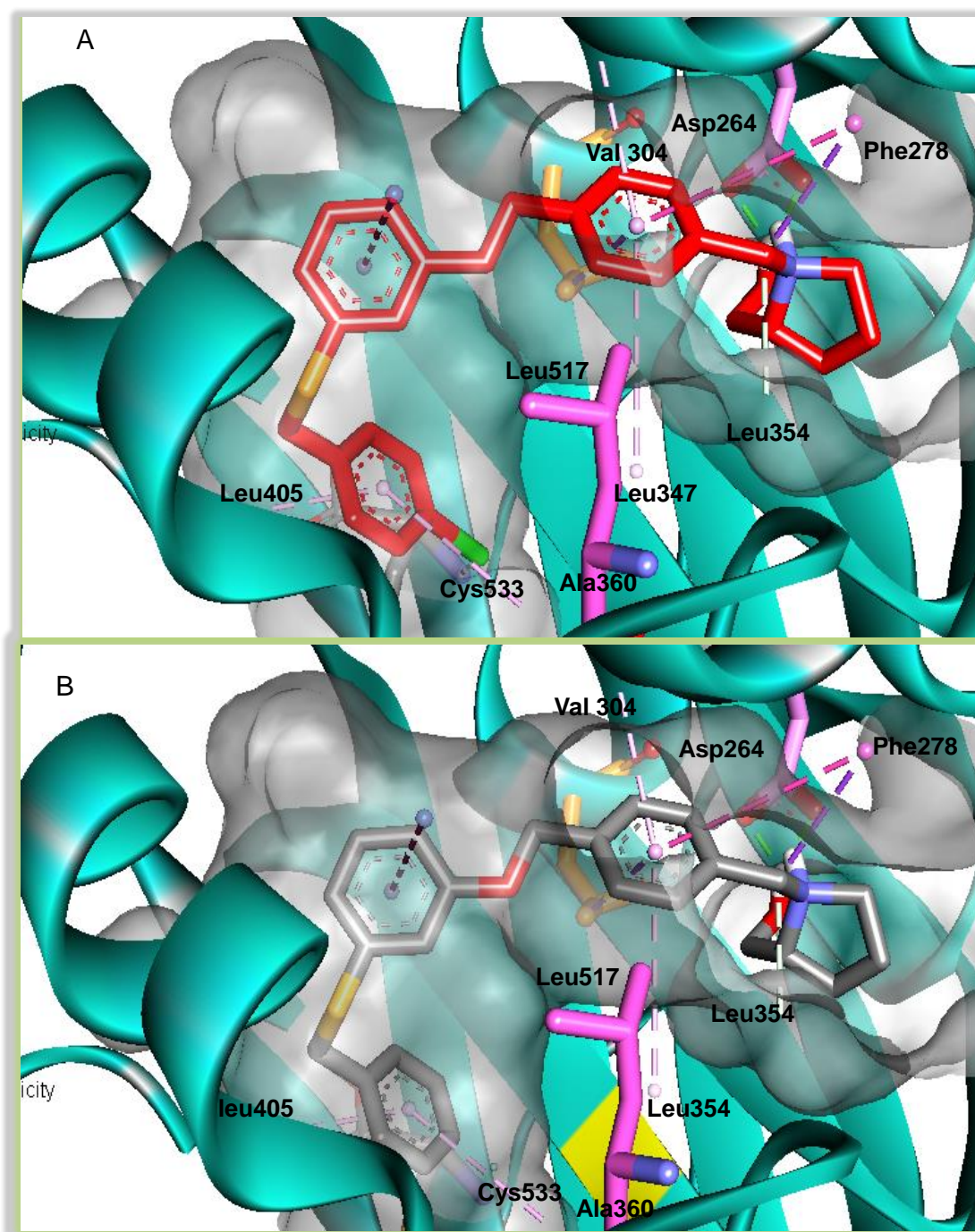
Figure 2.28. Docked poses of compounds 20 and 18 (A) showing compound **20** (red stick) interactions with SK2. (B) showing compound **18** (grey stick) interactions with SK2. Orange, pink and grey sticks are Val304, Leu517, Asp264 and Cys533 respectively.
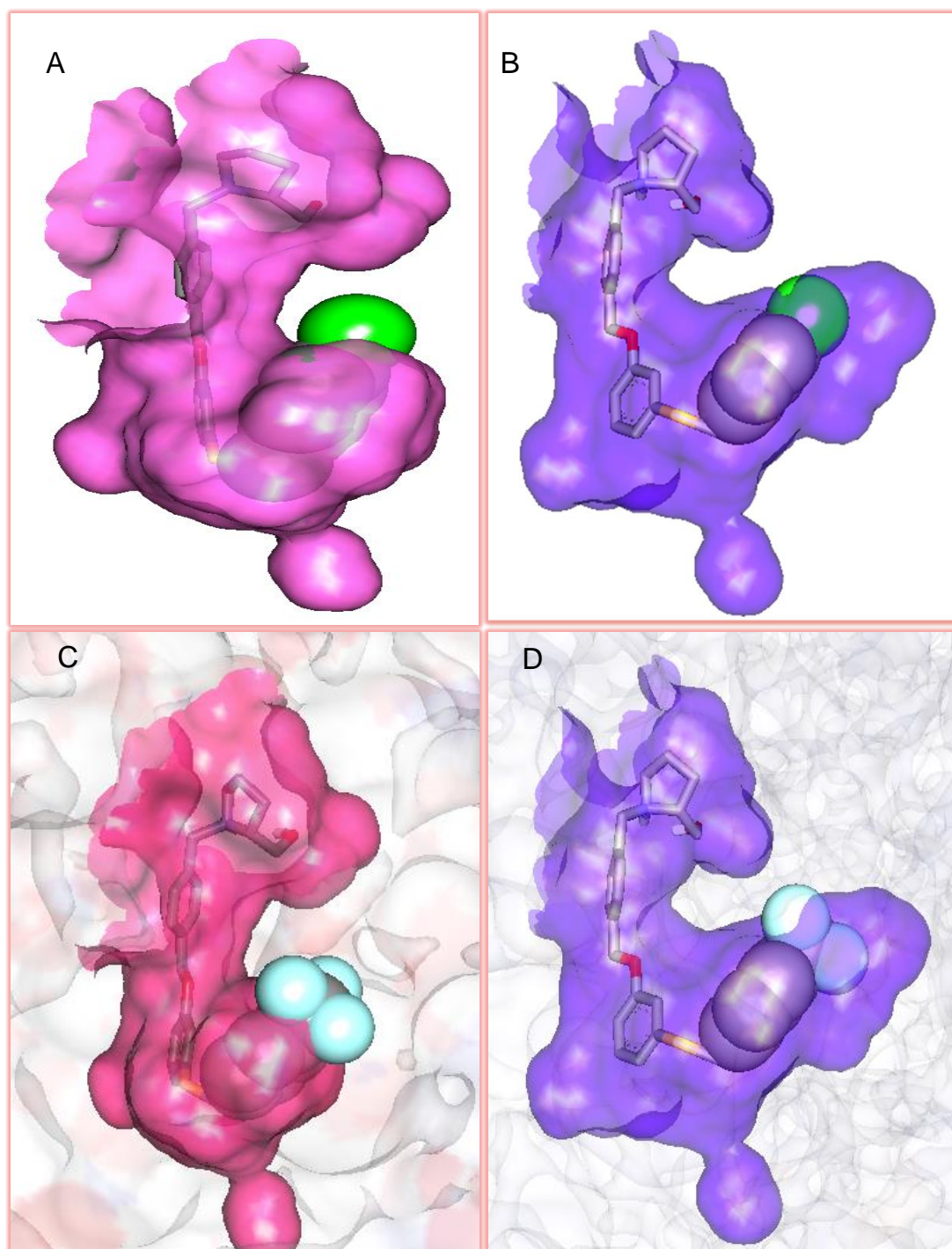
Figure 2.29. Docked poses of compounds 20 and 22. (A) and (B) show compound **20** (*para*-Cl in green) binding in the SK1 pocket (pink) and in the SK2 pocket (in blue); (C) and (D) show compound **22** (*para*-CF$_3$ in light blue) binding in SK1 (pink) and SK2 (blue). C and D clearly show that the CF$_3$ group protrudes out of the toe of the J-pocket, which is unlikely to be accommodated and reflects the inactivity of this compound.

2.3.4.3 Modification of the head to explore how polarity and chirality influence potency and selectivity

Library 6: Crystallographic analysis of the PF-543-SK1 complex and our modelling studies have shown that the hydroxymethylpyrrolidine head group forms essential hydrogen bonds with two Asp residues at the entrance of the sphingosine binding site adjacent to the ATP site where phosphate transfer takes place. Structural modifications to the pyrrolidine tail of the sulfide analogues were made to explore their impact on potency and selectivity

Table 2.6. SK1 and SK2 inhibitory activity as determined by the ADP-Glo assay for the sixth library.
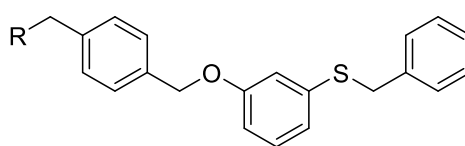
Compounds	R	IC$_{50}$ (nM)* for SK1	IC$_{50}$ (nM)* for SK2
24		NI	NI
25		NI	NI
26		NI	NI
27		NI	NI
28		NI	NI

IC$_{50}$ values are the average of three readings. NI = No Inhibition.

Compound **24** (**Table 2.6**) was synthesised to explore the impact of an isosteric replacement of the primary hydroxyl group with a primary amine. The rationale for this replacement was to introduce an ionic group that was capable of forming salts to improve water solubility and reduce lipophilicity. The primary amine was of similar size to the hydroxyl and able to form a similar hydrogen-bond network. Potentially, it could improve binding affinity by introducing ionic interactions with the Asp residues in the site. Unexpectedly, **Table 2.6** shows this modification completely abrogated inhibitor activity against both isoforms: this is more likely due to the presence of positively charged residues in the vicinity of the amine group, causing its inactivity through mutual repulsion.

The absence of activity for the (*S*)-enantiomer (**25**) is possibly due to an increase in the distance between the -OH of the hydroxmethylypyrrolidine moiety, which may not be sufficiently close to interact with Asp264. The importance of distance and directionality to an optimal hydrogen network in this region was confirmed by **27** and **26**, which also lack any inhibitory activity. The more flexible hydroxyethyl moiety of **27** appears to have a negative impact on hydrogen bonding with the aspartate residues, leading to a loss of SK inhibitory activity in both isoforms. Docking the piperidine analogue (**26**) in the active site of SK1 and the model of SK2 (**Figure 2.30**) showed that the key interactions between Asp264 and the head group were no longer present. This again confirms the importance of distance and directionality for optimal hydrogen bonding, which is lost with the larger ring scaffold (**Figure 2.30**).

To further investigate whether the hydroxyl group and chirality are essential for activity, compound **28**, which lacks any polar groups was prepared. It was inactive, which highlights the importance of hydrogen bonding with Asp264 in this region, which was confirmed by the docked pose that lacked the key hydrogen bonds with Asp264 (**Figure 2.31**).
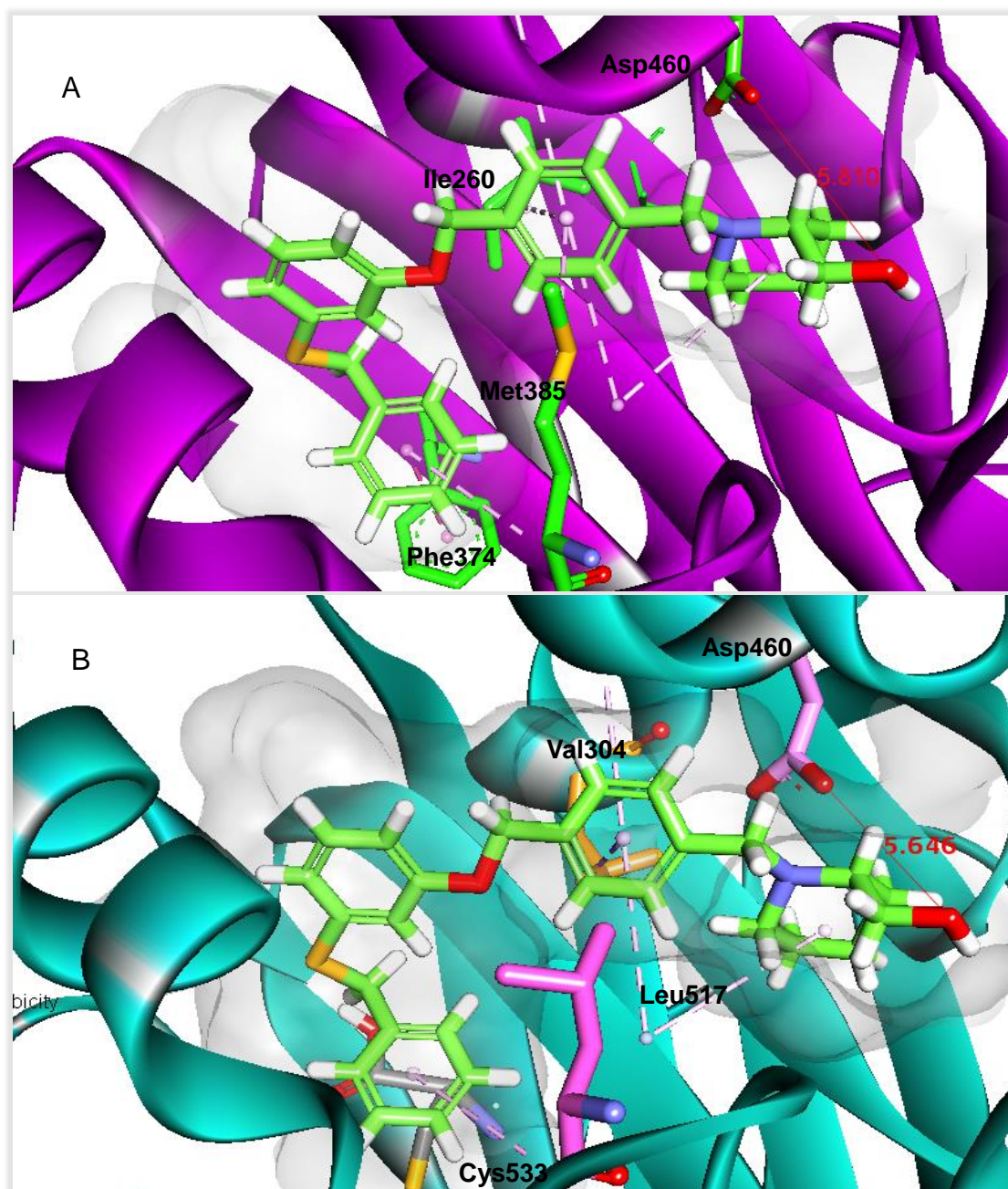
Figure 2.30. Docked pose of compound 26. Key interactions of compound **26** (green stick) with active sites of SK1 (A) and SK2 (B). Red lines indicate a distance of > 5Å (with actual distances shown) observed between Asp264 and the hydroxyl group of the pyrrolidine head group. Pink and grey sticks areVal304, Leu517, Asp264 and Cys533 respectively.
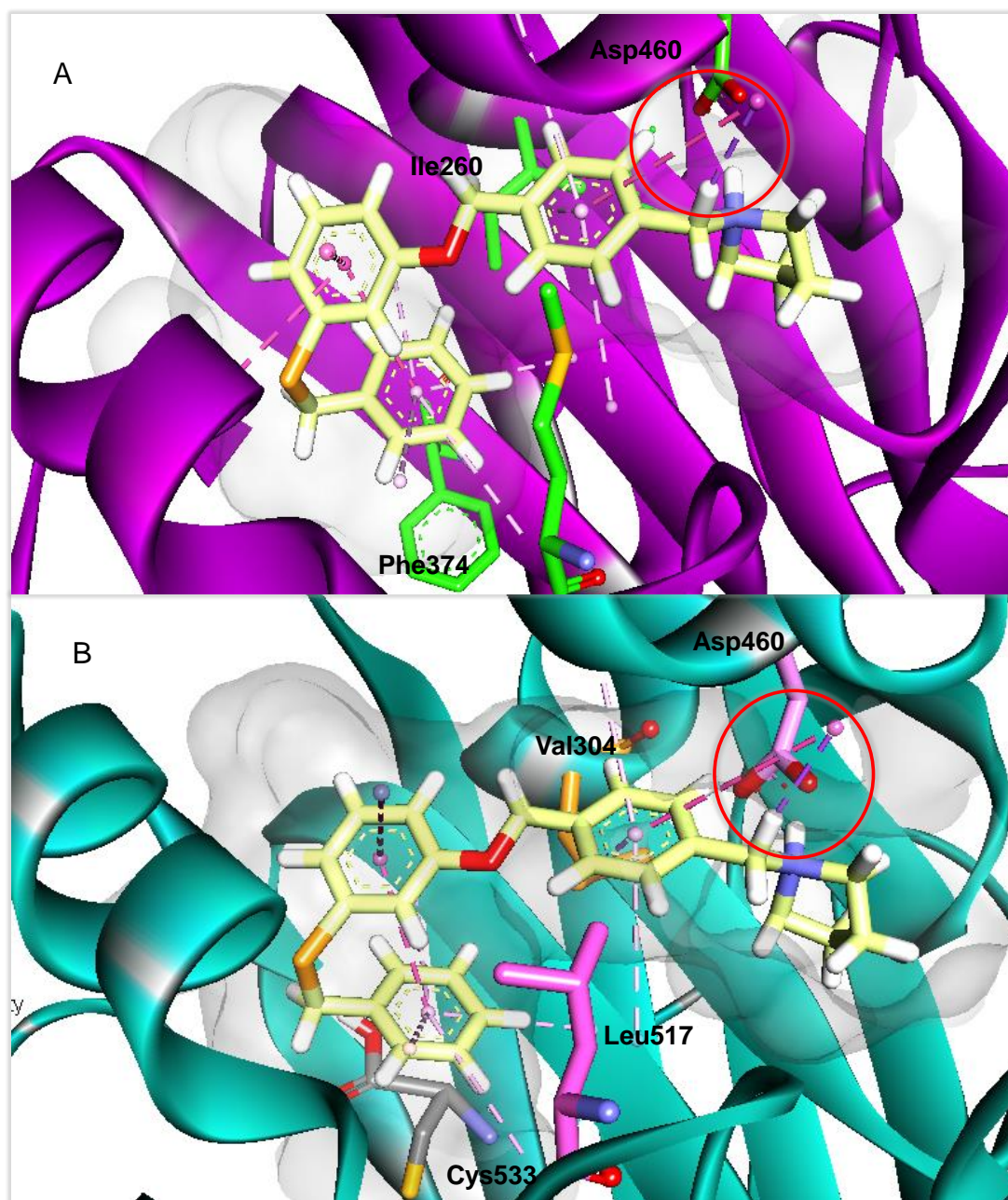
Figure 2.31. Docked poses of compound 28. Key interactions of compound **28** (yellow stick) with active sites of SK1 (A) and SK2 (B). Red circles indicate loss of H-bonds between Asp264 and the head pyrrolidine moiety that lacks a hydroxyl group. Pink and grey sticks areVal304, Leu517, Asp264 and Cys533 respectively.

2.4 Synthetic strategies

Compounds were synthesised by adapting the method used to prepare **PF-543** as described by Schunte *et al*, in which the 3-(bromomethyl)-5-methylphenyl acetate was treated with sodium benzene sulfonate, followed by hydrolysis of the resulting ester (compound I) to afford the phenol (compound II). This was then alkylated in acetonitrile at 60ºC to afford the aldehyde (compound III), which was then subjected to reductive amination to produce **PF-543** in good yield (95%) after column chromatography (**Scheme 2.1**).[210]
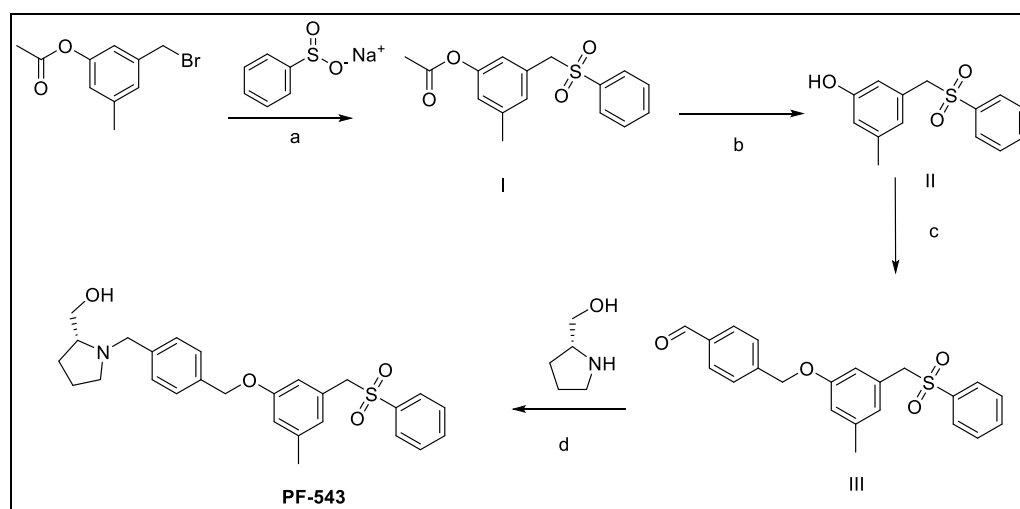
Scheme 2.1. Method for preparing PF-543. Reagents and conditions: (a) Aliquat, 85 °C, 18 h in EtOAc (b) NaHCO$_3$, rt, 36 h. (c) MeCN, 60 °C, 2 h. (d) NaBHAc$_3$, DCE, 24 h.

2.4.1 Synthesis of sulfonates and sulfonamide analogues

The synthetic approach to the sulfonate and sulfonamide analogues involved three key steps (**Scheme 2.2**). The first step was to sulfonylate a hydroxyl or amino group of resorcinol or 3-aminophenol with an alkyl or aryl sulfonyl chloride under mild basic conditions to produce the mono-substituted phenols **29-38**. In the second step, the remaining phenolic groups of compounds **29-38** were alkylated with the *p*-bromomethyl benzaldehyde (**39**) under basic conditions to afford the benzylic ether benzaldehydes **40-49**. The final step involved the reductive amination of compounds **40-49** with (R)-pyrrolidin-2-yl methanol to give the corresponding tertiary amines **3-14** in reasonable overall yields.
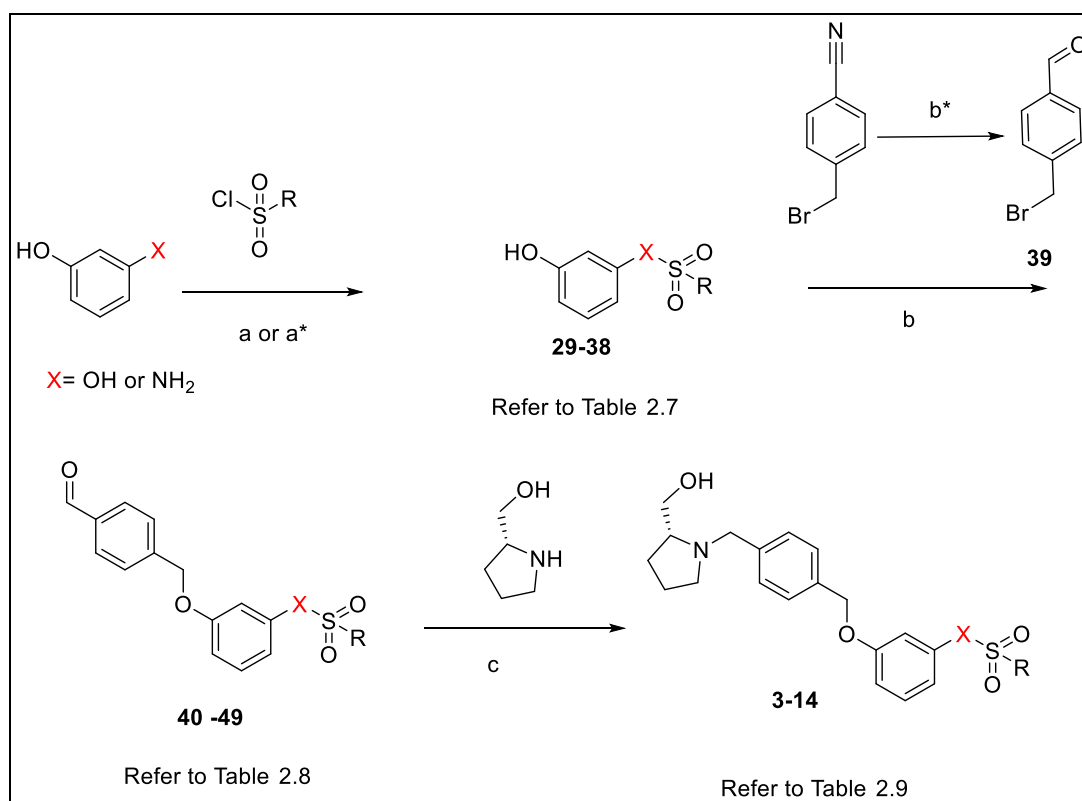
Scheme 2.2. Method for synthesis of sulfonate and sulfonamide analogues. Reagents and conditions: (a) Sat. aqueous $NaHCO_3/Et_2O$ (a*) pyridine (1.57 eq) in CH_2Cl_2 (b) K_2CO_3 (2.75 eq), MeCN, 60 °C, 3 h. (b*) DIBAL-H, 25 °C toluene, 1 h (c) NaBHAc$_3$ (1.5 eq), DCE, 24 h.

2.4.1.1 Step 1: Regioselective sulfonylation of resorcinol and 3-aminophenol (29-38)

The first step in the synthetic pathway involved the regioselective sulfonylation of resorcinol or aminophenol to produce the mono-susbstituted phenols **29-38** (**Scheme 2.3**). [225]
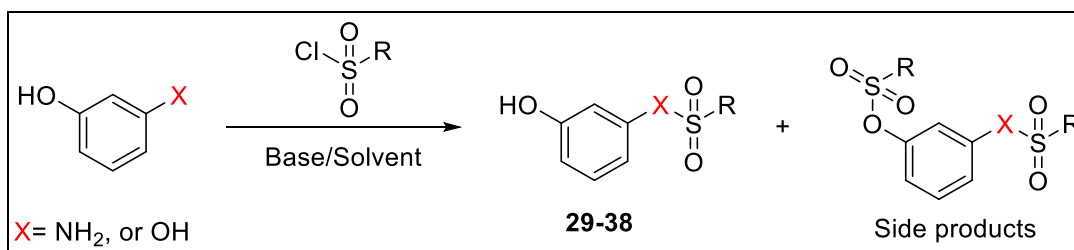
Scheme 2.3. Regioselective sulfonylation of resorcinol and 3-aminophenol.

Compounds **29-38** were generated in moderate yields (**Table 2.7**) due to the production of side-products that are formed through the double sulfonylation of either both OH /or NH_2 groups of the starting material (**Scheme 2.3**).

Table 2.7. Mono substituted phenols (**29-38**) and their yields produced by sulfonylation with sulfonyl chloride.
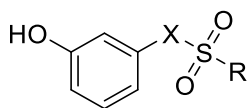
29-38

Compounds	X	R	Yield (%)
29	O	—⟨benzene⟩—OCH$_3$	34
30	O	(butyl chain)	36
31	O	—⟨benzene⟩—Cl	29
32	O	—⟨benzene⟩—	15
33	O	(cyclohexyl)	13
34	NH	—⟨benzene⟩—OCH$_3$	56
35	NH	(butyl chain)	55
36	NH	—⟨benzene⟩—Cl	51
37	NH	—⟨benzene⟩—	29
38	NH	(cyclohexyl)	88

The challenging step in this reaction was to separate the desired product from the unreacted starting material and the side-product, which had both functional groups sulfonylated. The reproducible and robust method achieved was based on the differences in the *pKa* values of the various derivatives produced during the reaction as follows (**Figure 2.32**). The organic layer was separated and washed with saturated aqueous potassium carbonate solution (pH>12) to remove the starting material with two phenolic groups (*pKa* =9.07 and 10.5). [226] For aminophenol, the organic layer was washed with 0.01 M HCl to remove any compound with a free amino group (*pKa~* 4). The organic layer was then washed with 1 M NaOH to extract the product with the remaining free phenolic group to leave the disulfonylated side-product in the organic layer. Neutralisation of the water layer with 0.1 M HCl followed by extraction with organic solvent isolated the pure desired products (**Figure 2.32**). As an example of how mono-sulfonylation of the desired phenol product was confirmed, the ^{1}H NMR spectrum of compound **29** is shown in **Figure 2.33**. The singlet at 9.89 ppm corresponds to the hydroxyl proton. The singlet at δ 3.86 ppm integrating to 3H represents the methoxy group. The formation of the sulfonamide with a free hydroxyl rather than a sulfonate with a free amino group was confirmed by the appearance of two singlet peaks in the ^{1}H NMR spectrum of compound **34**: the singlet at 10.00 ppm corresponds to the phenolic proton and the singlet at 9.40 ppm corresponds to the NH proton (**Figure 2.33**). The ^{1}H NMR spectrum of the desired compound **31** (**Figure 2.34**) has one singlet for the hydroxyl proton, whereas the ^{1}H NMR spectrum of the bis-sulfonylated side-product shows loss of the -OH peak at 10.01 ppm (**Figure 2.34**). The appearance of one *p*-disubstituted 4 H proton signature in the aromatic region in **Figure 2.34** indicate the introduction of one new aromatic ring into the structure, whereas two *p*-disubstituted signatures suggest that sulfonylation has occurred twice to generate the unwanted side-product (**Figure 2.34**).
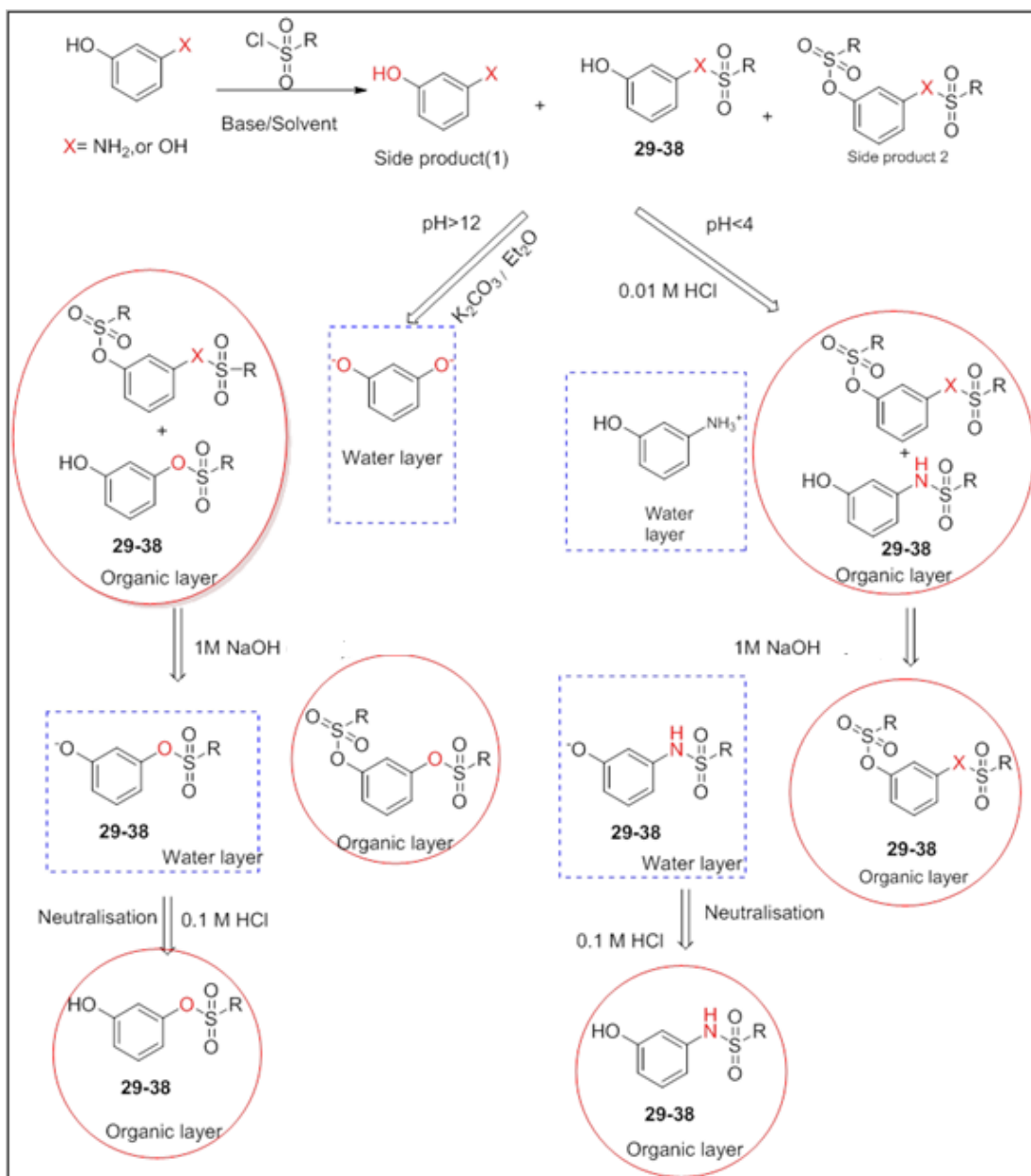
Figure 2.32. Workflow for the isolation of compounds 29-38 from unreacted starting material and bis- sulfonylated side products.
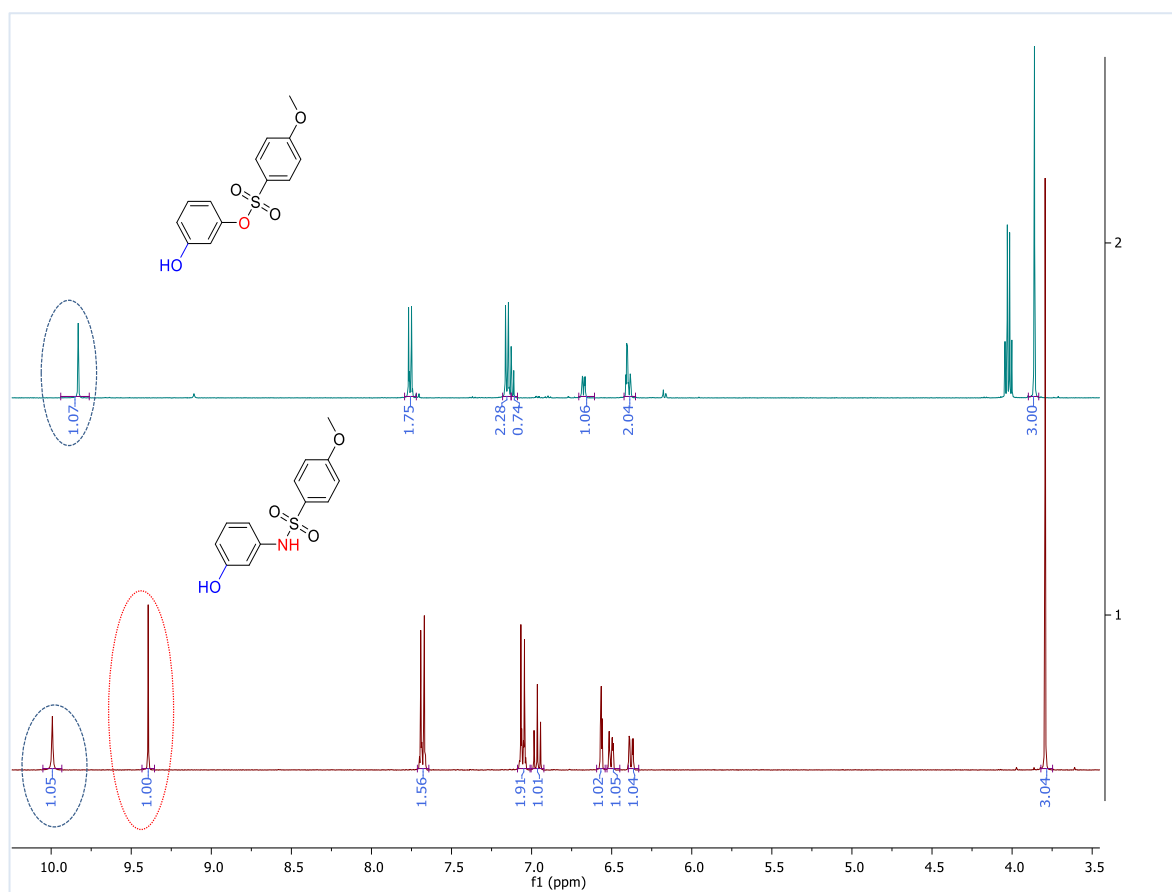
Figure 2.33. ¹H NMR (DMSO-d₆) of compounds 29 and compound 34. Circled peaks colored blue and red correspond to OH and NH₂ respectively. Circled peaks indicate key differences in signals used to identify which were sulfonates or sulfonamides.
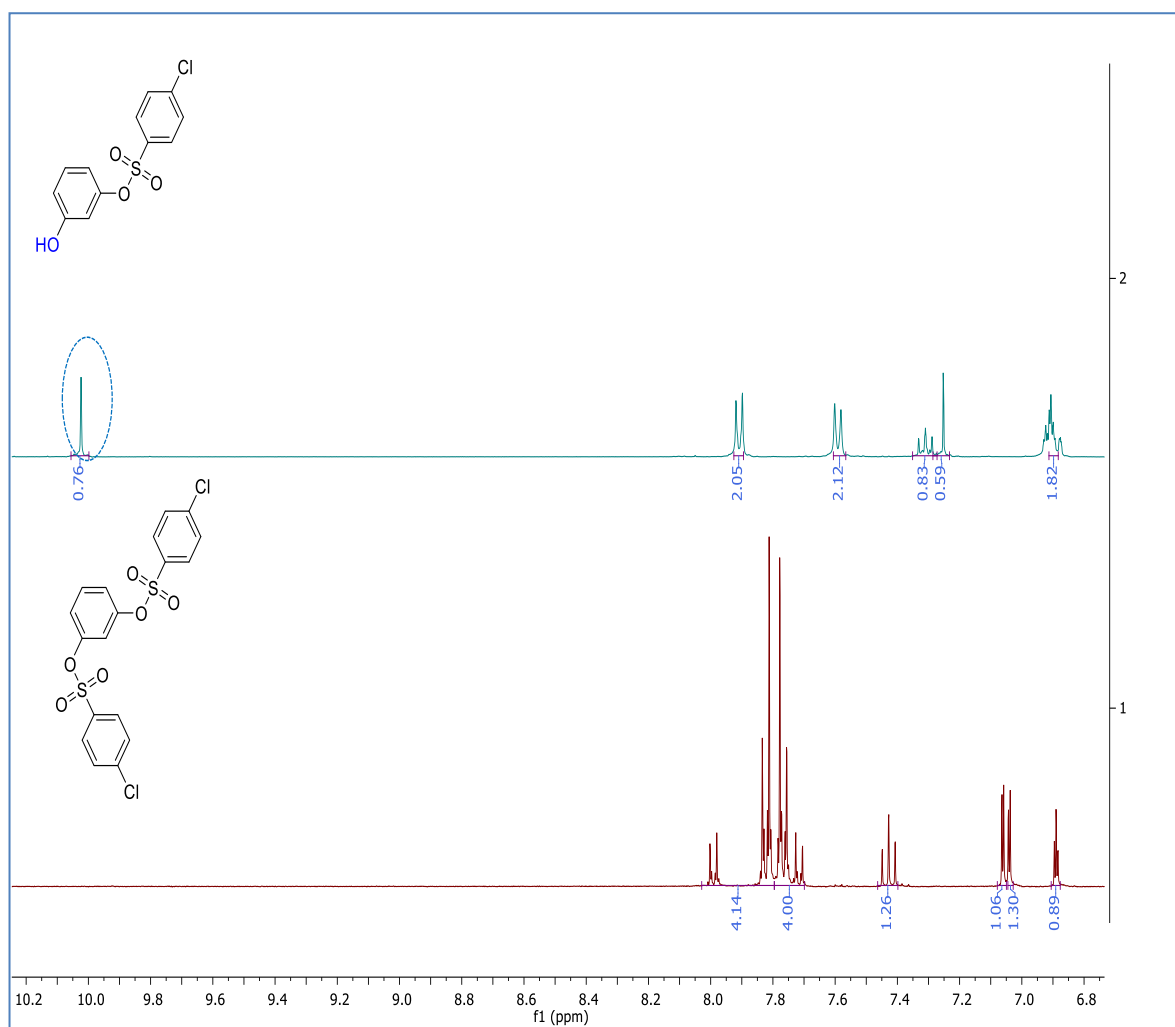
Figure 2.34. **^{1}H NMR (DMSO-d$_6$) of compound 31 and its side product.** Circled peak indicates key difference in signals used to identify which were target compounds or side products.

The mechanism for the first sulfonylation step proceed via an S_N2 process in which the phenolic group of resorcinol is deprotonated by base to give the corresponding anion, which acts as a nucleophile to displace the Cl^- of alkyl or aryl sulfonyl chlorides to form the desired compounds via an associative transition state (**Scheme 2.4**). Synthesis of the sulfonamides uses pyridine and not bicarbonate as the catalyst, where pyridine possibly displaces the chloride to generate a reactive pyridinium intermediate that has a better leaving group. The displaced pyridine following the nucleophilic attack by the amine acts as the base to deprotonate the sulfonamide.
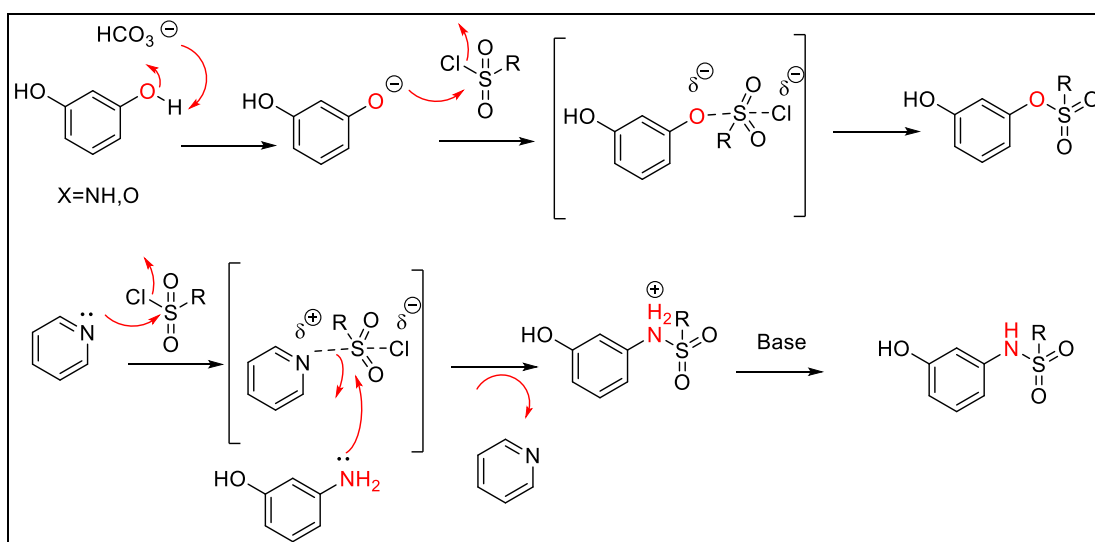
Scheme 2.4. Suggested S_N2 mechanism of the mono-sulfonylation of resorcinol or 3-aminophenol.

An S_N1 mechanism is also possible, in which the chloride anion dissociates from the sulfonyl group to form the electrophilic intermediate (**Scheme 2.5**), which is the rate determining step and not the attack by the nucleophile.
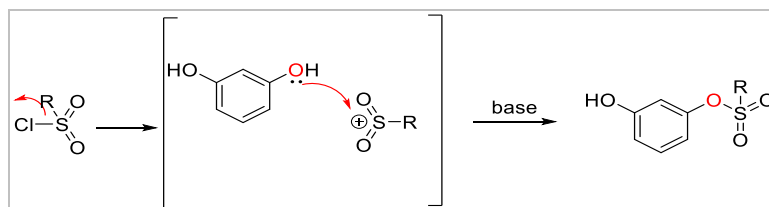
Scheme 2.5. S_N1 mechanism for the mono-sulfonylation of resorcinol.

The phenoxide anion is a strong nucleophile and is likely to attack rapidly before the sulfonyl chloride dissociates, which favours the S_N2 mechanism, particularly as the reaction was carried out in diethyl ether, an aprotic, nonpolar solvent that promotes S_N2.

2.4.1.2 Step 2: Formation of benzylic ether benzaldehydes (40-49)

The second step involved the preparation of the alkylating reagent p–bromomethylbenzadehyde (**39**) (Step A; **Scheme 2.6**) which was used to alkylate compounds **29-38** under basic conditions to give the desired compounds **40-49** in varying yields (Step B; **Scheme 2.7**) **Table 2.8.**

2.4.1.2.1 Step 2 (A): Synthesis of p–bromomethylbenzadehyde

The reagent p–bromomethylbenzadehyde is commercially expensive, so it was prepared by the reduction of p-(bromomethyl) benzonitrile to the corresponding aldehyde (**39**) using the selective reducing agent diisobutylaluminium hydride (DIBAL-H) (**Scheme 2.6**).
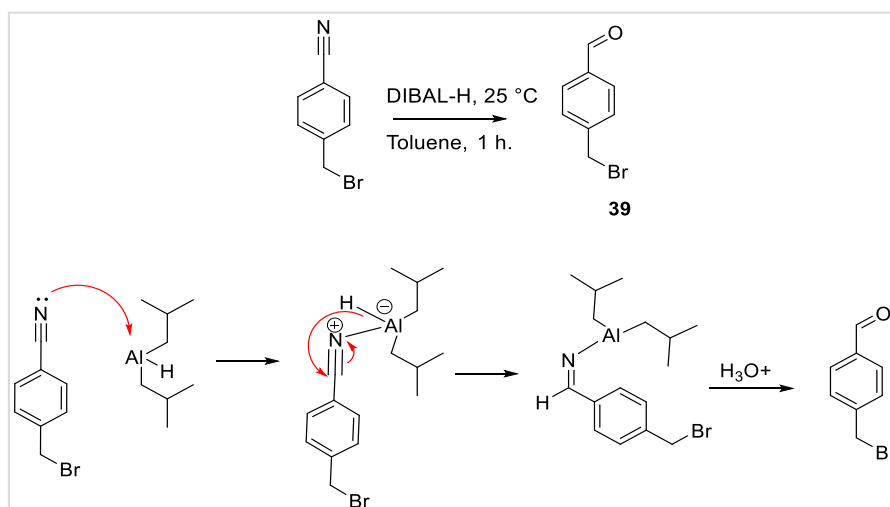
Scheme 2.6. Synthesis of p–bromomethylbenzadehyde showing the mechanism for reduction with DIBAL-H.

The mechanism for this reaction proceeds via an acid-base catalysed reaction between an unshared electron pair on the nitrile nitrogen with the aluminium of the DIBAL—H. This is followed by the transfer of a hydride ion from the DIBAL—H to the carbon of the nitrile, with subsequent hydrolysis of the aluminium complex to form the aldehyde (**Scheme 2.6**). Reduction to the aldehyde was confirmed by the presence of a downfield singlet corresponding to the formyl H at 10.01 ppm (**Figure 2.35**).
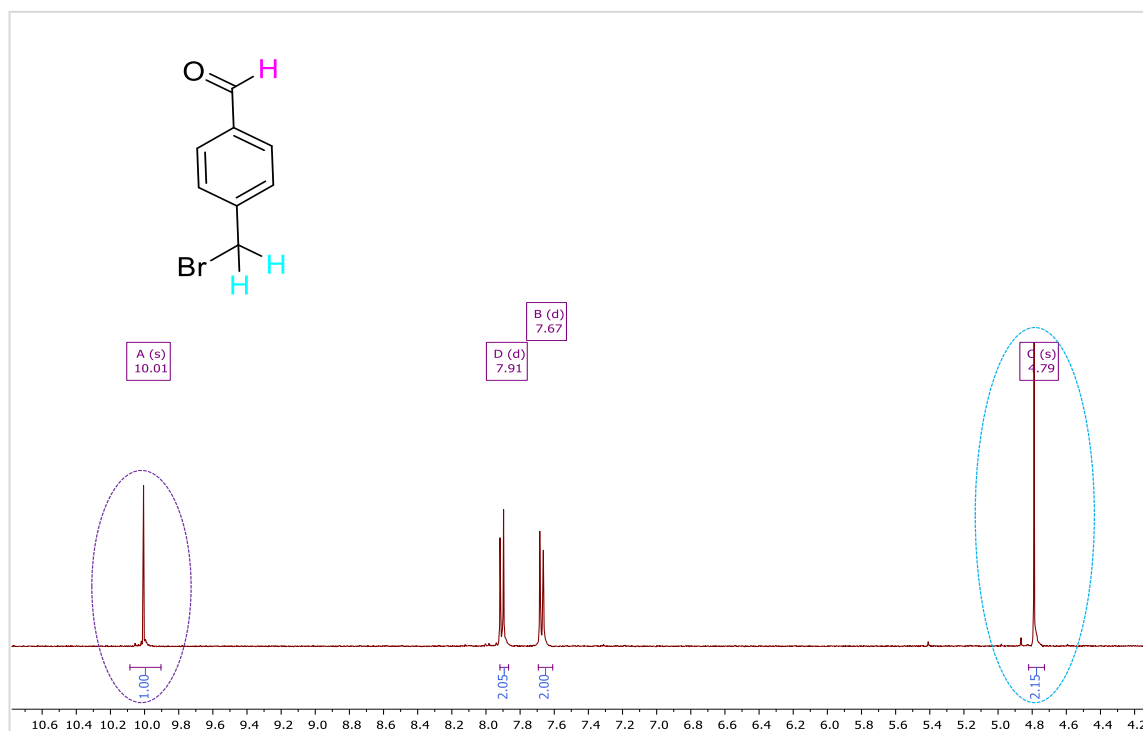
Figure 2.35. ^{1}H NMR (DMSO-d$_6$) of compound 39. Circled peaks coloured cyan corresponds to CH$_2$ and purple corresponds to CHO.

2.4.1.2.2 Step 2 (B): Alkylation of compounds (40-49)

In this step, monosulfonated phenols **29-38** were alkylated with **39** to give the desired bifunctional compounds **40-49** in moderate to good yields (**Table 2.8**). As an example of structural elucidation, the ^{1}H NMR spectrum of **41** is shown below (**Figure 2.36**). Successful alkylation was characterised by a downfield shift at 5.46 ppm of the benzylic singlet indicating that the protons were adjacent to the more electronegative oxygen in the ether moiety, while the aromatic region contained a *p*-disubstituted and *m*-disubstituted signature integrating to 8 protons showed that two phenyl rings were in the structure. The downfield singlet at 10.34 ppm confirmed that the aldehyde was still present, and in this specific example, the coupling pattern in the aliphatic region showed that an *n*-butyl group was in the structure.
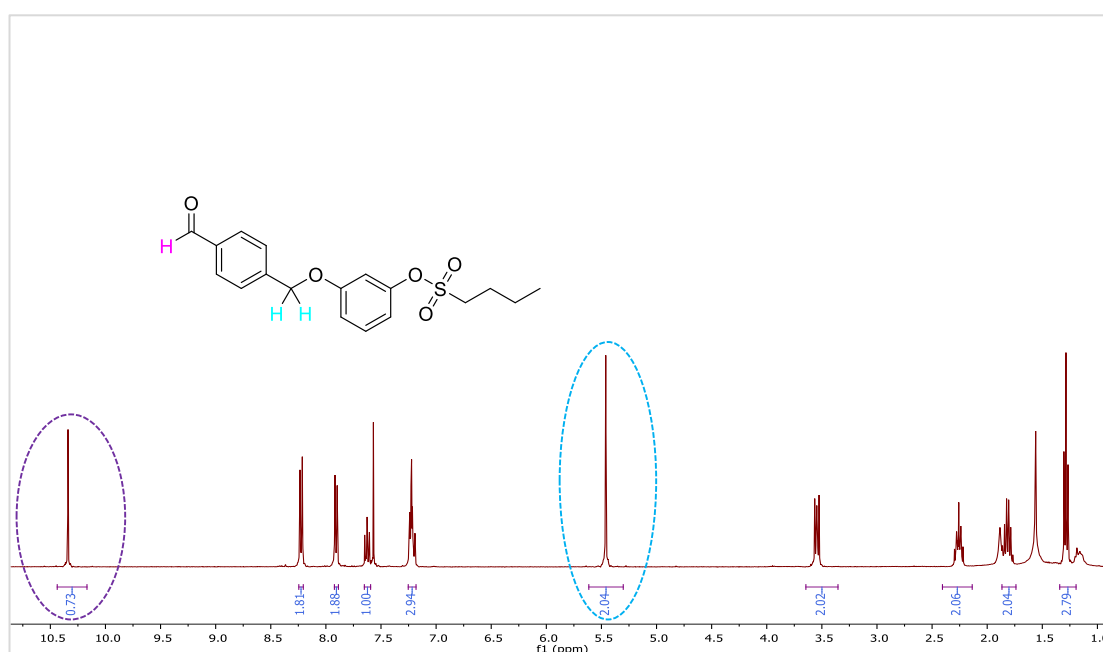
Figure 2.36. ^{1}H NMR (Chloroform-d) spectrum of compound 41. Circled peaks coloured cyan corresponds to CH$_2$ and purple corresponds to CHO.

Similar to the previous sulfonylation step, alkylation is likely to proceed via an S_N2 mechanism, in which phenolic group of intermediates **29-38** is deprotonated by base to the nucleophilic phenoxide anion that acts to displace bromide via the associated transition state (**Scheme 2.7**).
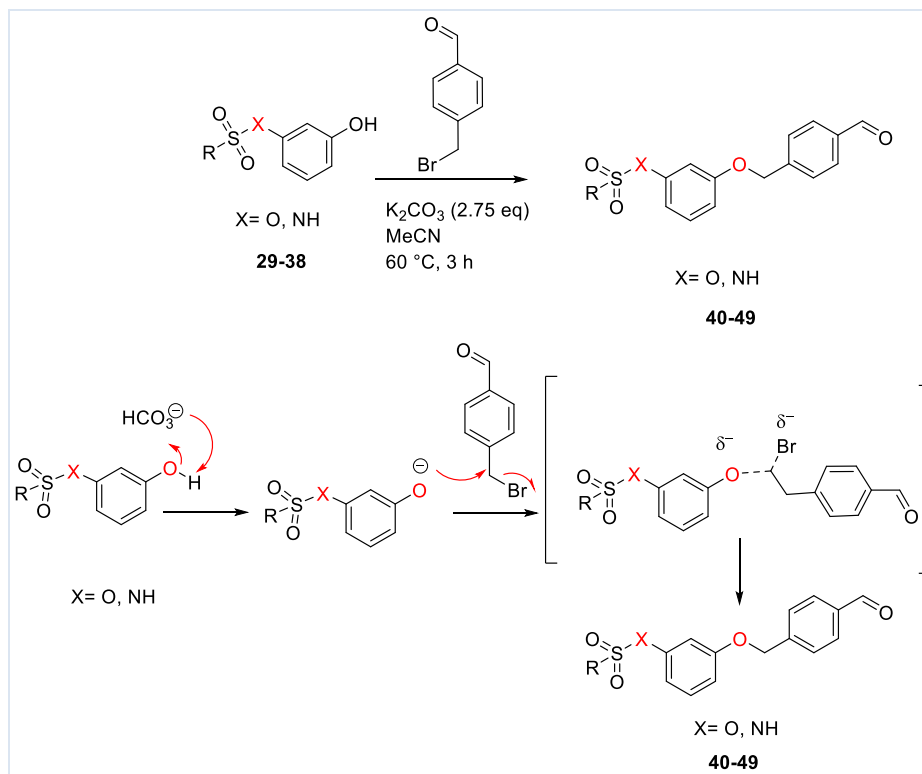
Scheme 2.7. Synthesis of 40-49 and the associated mechanism for their formation.

Table 2.8. Benzylic ether benzaldehydes (**40-49**) and their yields produced by alkylation with compound **39**
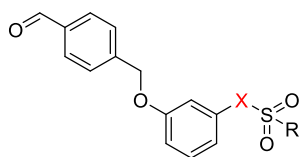
X= O, NH

40-49

Compounds	X	R	Yield (%)
40	O	⟨p-C6H4–OCH3⟩	85
41	O	⟨butyl chain⟩	70
42	O	⟨p-C6H4–Cl⟩	88
43	O	⟨p-C6H4–CH3⟩	78
44	O	⟨cyclohexyl⟩	95
45	NH	⟨p-C6H4–OCH3⟩	28
46	NH	⟨butyl chain⟩	36
47	NH	⟨p-C6H4–Cl⟩	35
48	NH	⟨p-C6H4–CH3⟩	26
49	NH	⟨cyclohexyl⟩	34

The yields for the sulfonamide derivatives (26-36%) were lower than the sulfonates (70-95%) because a second alkylation of **45-49** with **39** formed the bis-alkylated side-products (**Scheme 2.8**). This arose because the primary sulfonamide, like the phenol, is a weak acid with a pKa of around 10, [227] and can also be deprotonated by potassium carbonate to react with the bromomethylbenzadehyde. **Figure 2.37** illustrates the ^{1}H NMR spectra of the desired product (**47**) and its bis-alkylated side-product, the formation of which was suggested by the appearance of two singlets at 9.98 and 10.03 ppm indicating the presence of two aldehyde groups in the structure. The peaks at 4.98 and 5.12 ppm correspond to two benzylic proton singlets adjacent to atoms of different electronegativity (*O* and *N*), whilst an aromatic region corresponding to 12 protons that contains two *p*-disubstituted signatures also suggests double alkylation by **39**.
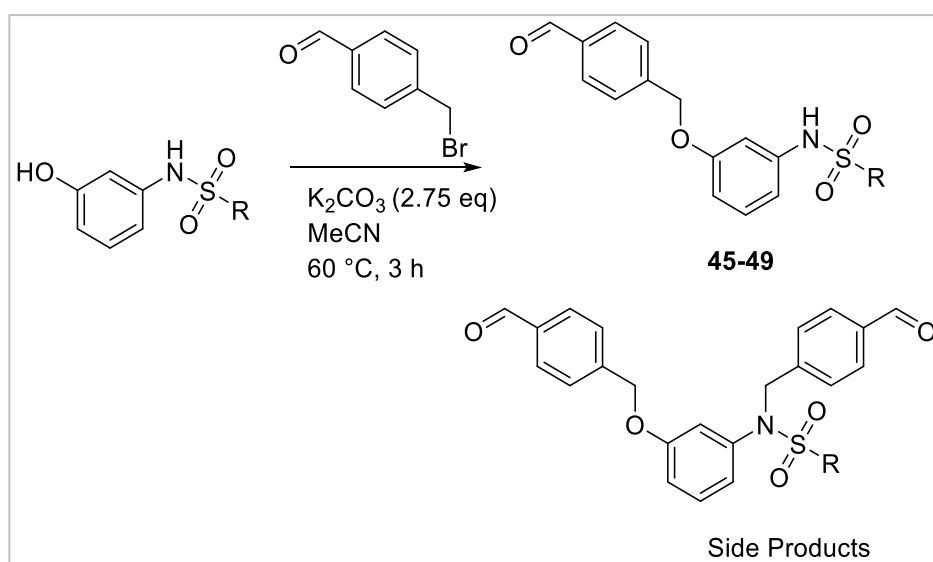
Scheme 2.8. Alkylation of the sulfonamides with 39 can yield mono- and bis-alkylated products.
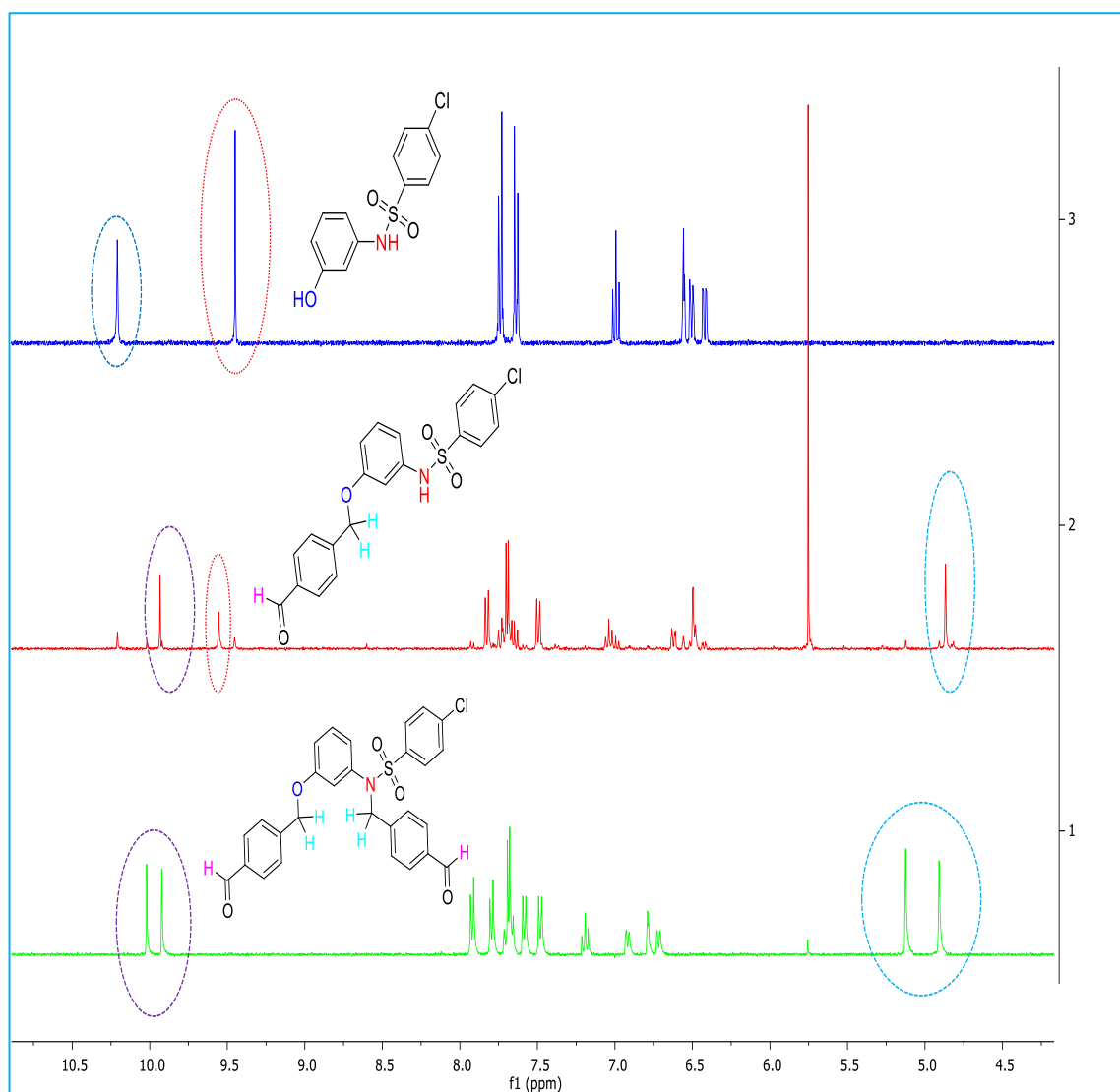
Figure 2.37. ^{1}H NMR (DMSO-d${}_6$) of compounds 36 (upper) and 47 (middle) and its side-product (lower) formed by bis-alkylation. Circled peaks indicate key differences in signals used to identify which were target compounds or side products

2.4.1.3 Step 3: Reductive amination (3-14)

The final reaction in this synthetic pathway involved the reductive amination of the aldehydes **40-49** with (*R*)-pyrrolidin-2-yl methanol in the presence of the reducing agent sodium triacetoxyborohydride to generate the final library of amines (**3-14**) that were used for SAR profiling of the sulfonate and sulfonamide analogues of **PF-543** (**Scheme 2.9**). The yields of the amines are shown in **Table 2.9**.
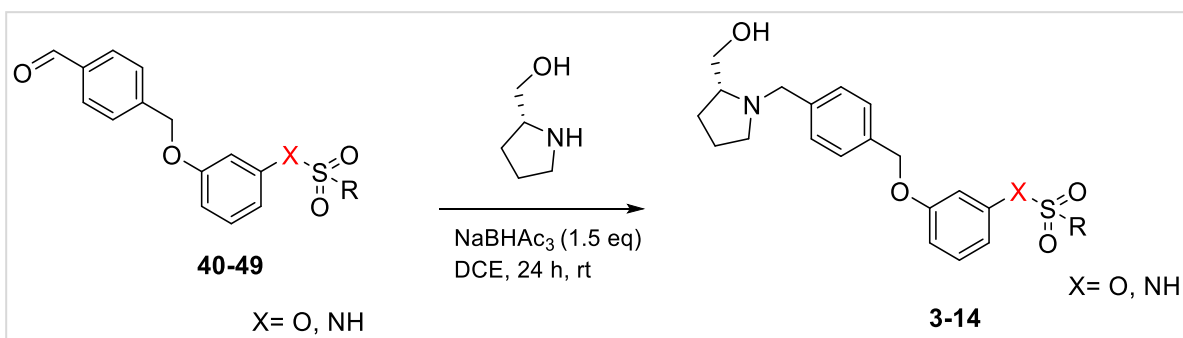
Scheme 2.9. Synthesis of amines 3-14.

Table 2.9. Sulfonate and sulfonamide analogues (**3-14**) and their yields formed by reductive amination with 2-(hydroxymethyl)pyrrolidine.
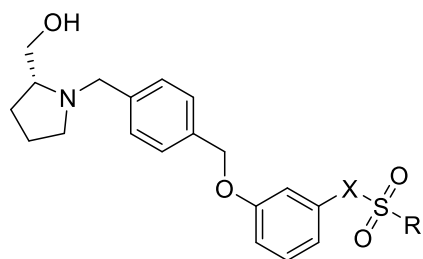
3-14

Compounds	X	R	Yield (%)
3	O	⊢〈 〉—OCH₃	35
4	O	⊢〈 〉—Cl	37
5	O	⊢〈 〉—	45
8	O	⊢∿	54
9	O	⊢〈 〉	74
10	NH	⊢∿	65
11	NH	⊢〈 〉—	51
12	NH	⊢〈 〉—OCH₃	57
13	NH	⊢〈 〉—Cl	55
14	NH	⊢〈 〉	60

The mechanism for reductive amination is shown in **Scheme 2.10**. The first step involves the formation of the carbinolamine intermediate through the nucleophilic attack of the secondary amine on the aldehyde (**Scheme 2.10**), which is followed by formation of the imine (Schiff base) via the loss of water. [228] The imine and aldehyde are in equilibrium, and anhydrous conditions are required to promote the reaction. In the case of our compounds, a phenyl group adjacent to the iminium group helped stabilise the intermediate by resonance. There are many reducing agents that could be used in this reductive amination: the selection of sodium triacetoxyborohydride (NaBH(OAc)$_3$), was because it shows selectivity toward the imine over the aldehyde. This is due to the stabilisation of the boron-hydrogen bond by the steric and the electron-withdrawing effects of the three acetoxy groups, which gives it milder reducing properties. [229] Presumably, a more powerful reducing reagent will reduce the aldehyde through to the alcohol before the amine can form the imine which is then reduced.

Scheme 2.10. Mechanism for the reductive amination reaction.

As an example of how target compounds were identified, the ^{1}H NMR spectrum of **4** in shown in **Figure 2.38**. The loss of the characteristic aldehyde peak at ~10 ppm and the appearance of the non-equivalent benzylic protons next to the chiral pyrrolidine ring as two asymmetric peaks (one doublet at 4.03 ppm and one multiplet at 3.45 ppm) was taken as indicative of successful coupling between the reagents. The two non-equivalent methylene protons between the hydroxyl group and chiral centre also appear as two multiplets at 3.30 and 3.37 ppm, whilst the singlet at 4.42 ppm represents the hydroxyl proton. The singlet at 5.00 ppm represents the deshielded ether benzylic protons. The coupling in the aromatic region is consistent with the substitution pattern seen for the precursors in this series.
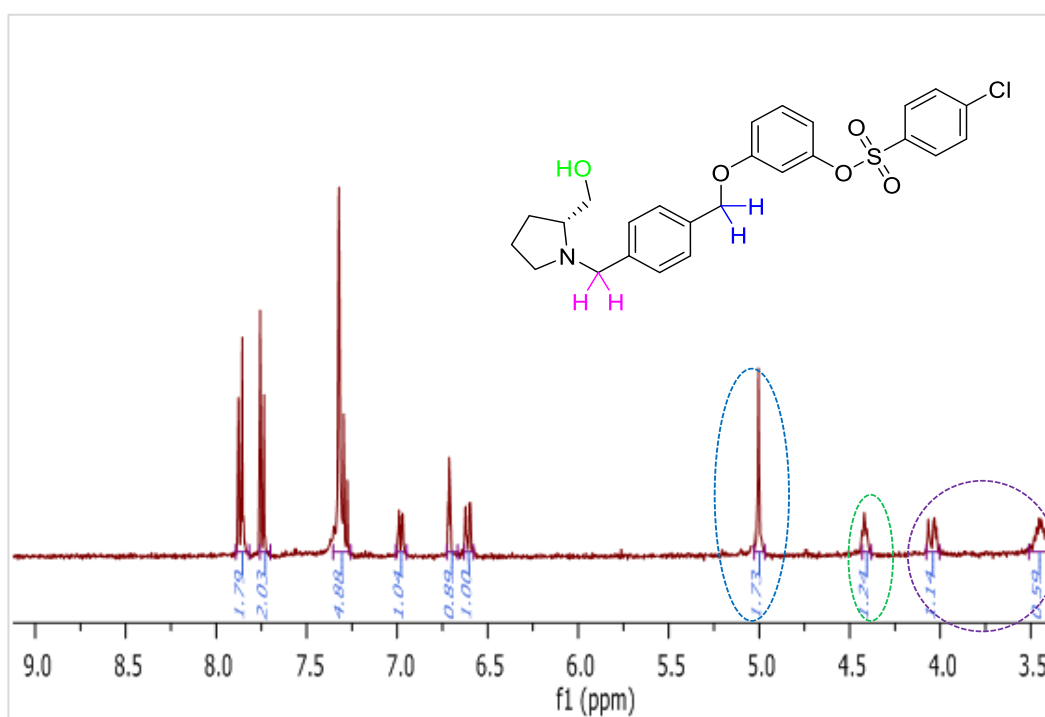
Figure 2.38. ^{1}H NMR (DMSO-d$_6$) of compound 4. Circled peaks indicate the key signals used to identify the target compound.

2.4.2 Synthesis of sulfide containing analogues of PF-543

A library of analogues was synthesised using the approach shown in **Scheme 2.11**. This involved two alkylation steps followed by a reductive amination to produce the desired compounds **50-54** (**Scheme 2.11**).
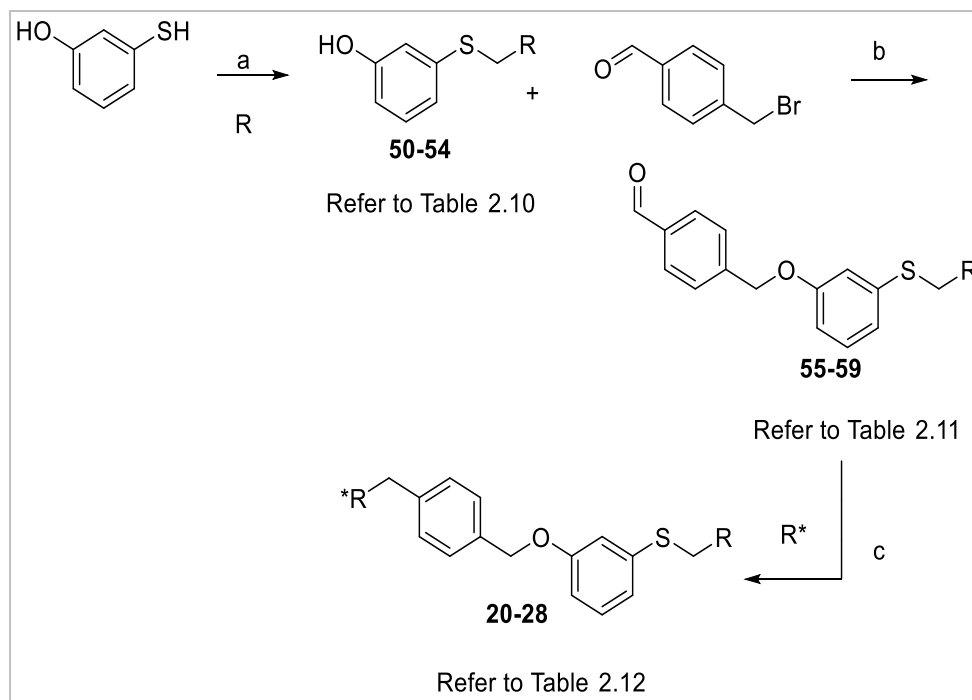
Scheme 2.11. Synthesis of sulfide-containing analogues of PF-543. Reagents and conditions: (a) Sat. K_2CO_3/ MeCN, N_2,3 h(b) K_2CO_3 (2.75 eq), MeCN, 60 °C, N_2, 3 h.(c) $NaBHAc_3$ (1.5 eq), DCE, N_2, 24 h.

The commercially available 3-mercaptophenol was treated with aryl or alkyl bromides to give the corresponding sulfides (**Scheme 2.12**). Alkylation occurred exclusively on the more acidic thiol group (pKa= 6) rather than on the phenol to yield predominantly monoalkylated products **50-54** (**Table 2.10**). Compounds were extracted and isolated as previously described in **Section 5.1.2.3** to remove both unreacted starting material and disubstituted products.
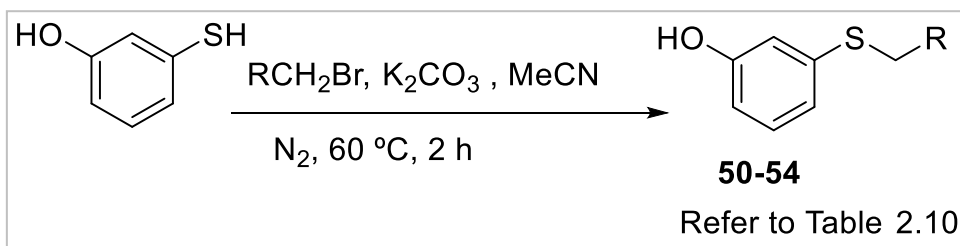
Scheme 2.12. Synthesis of compounds 50-54.

Table 2.10. Alkylated sulfides (**50-54)** and their yields produced by alkylation with benzyl /cyclohexyl methyl bromide.

50-54
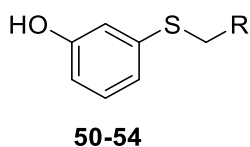
Compounds	R	Yield (%)
50		95
51		44
52		96
53		53
54		65

As an example to show how the successful *S*-substituted thiophenols were characterised, the ^{1}H NMR spectrum of **50** is shown in **Figure 2.39**. The appearance of the characteristic singlet of the hydroxyl proton at 9.58 ppm in combination with the benzylic proton singlet at a higher field (4.24 ppm) than we would expect with a benzyl ether (e.g. 5.46 pm in **41**) demonstrated that the monoalkylated benzyl sulfide had formed.
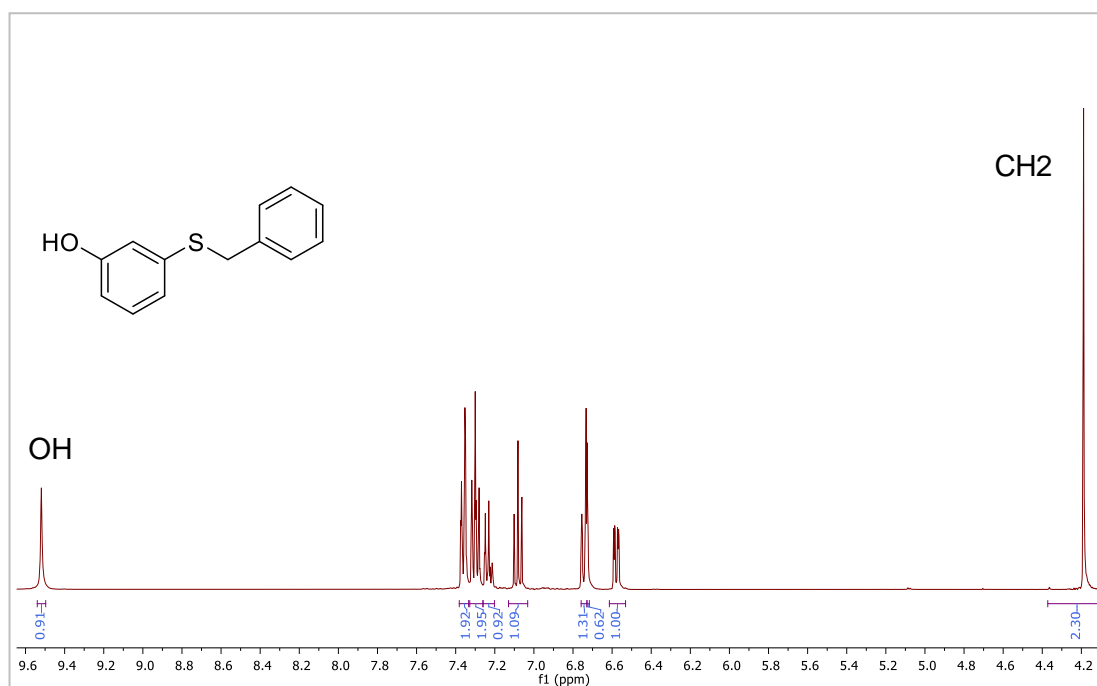
Figure 2.39. ^{1}H NMR (DMSO-d$_6$) of compound 50.

The phenols were then alkylated with **39** using the conditions and procedure previously described (**Table 2.11**). As can be seen in the ^{1}H NMR spectrum of **55** (**Figure 2.40**), the coupled product was confirmed by the presence of a downfield singlet corresponding to the formyl proton at 9.98 ppm in combination with two benzylic proton singlets at different fields corresponding to chemical shifts expected for an ether and a sulfide (5.18 and 4.22 ppm respectively).

Table 2.11. Benzylthio)phenoxy)methyl)benzaldehyde **55-59** and their yields produced by alkylation with **39**.
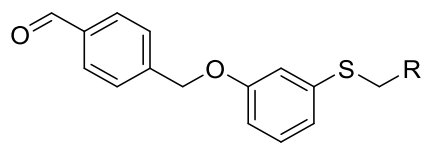
55-59

Compounds	R	Yield%
55		75
56	Cl	86
57	F	89
58	C–F (F, F)	99
59		37
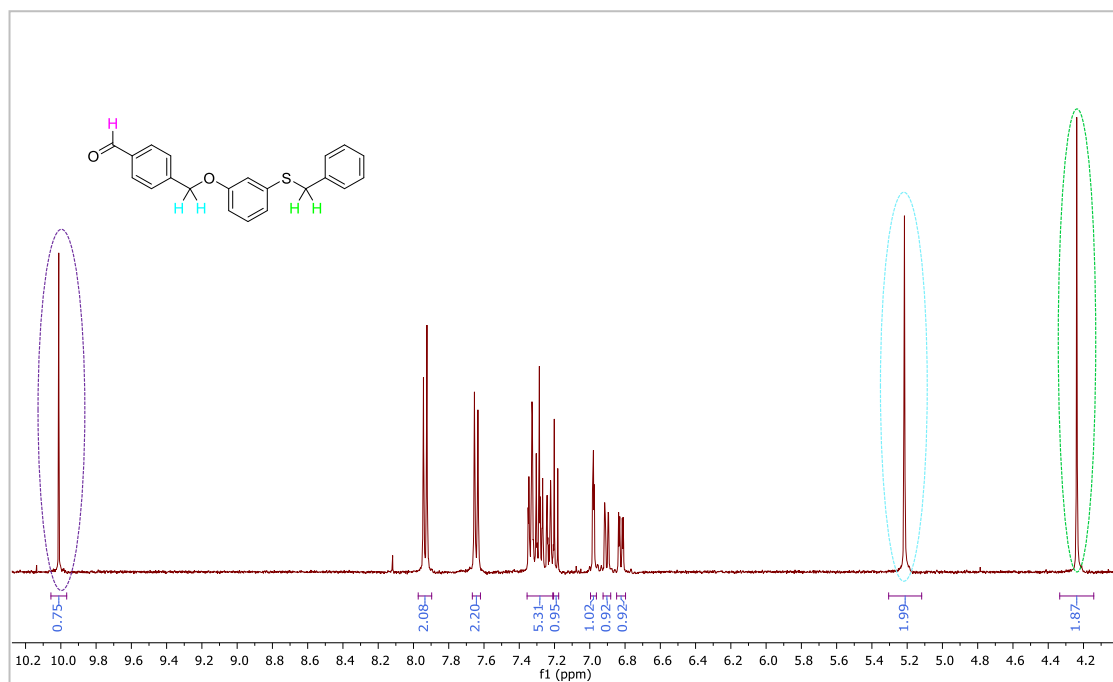
Figure 2.40. ^{1}H NMR (DMSO-d$_6$) of 55. Circled peaks coloured cyan correspond to CH$_2$ of the ether benzylic group, green corresponds to CH$_2$ of the benzyl group and purple corresponds to CHO.

The corresponding benzaldehydes were then treated with different amines using the reductive amination conditions described previously (**see Section 5.1.2.7**) to afford compounds **20-28** (**Table 2.12**)**.** To generate the anisosteric primary amino analogue of the (*R*)-pyrrolidin-2-ylmethanol series, compound **24** was prepared via the Boc-protected compound **60** followed by deprotection with trifluoroacetic acid (TFA) in dichloromethane (**Scheme 2.13**).
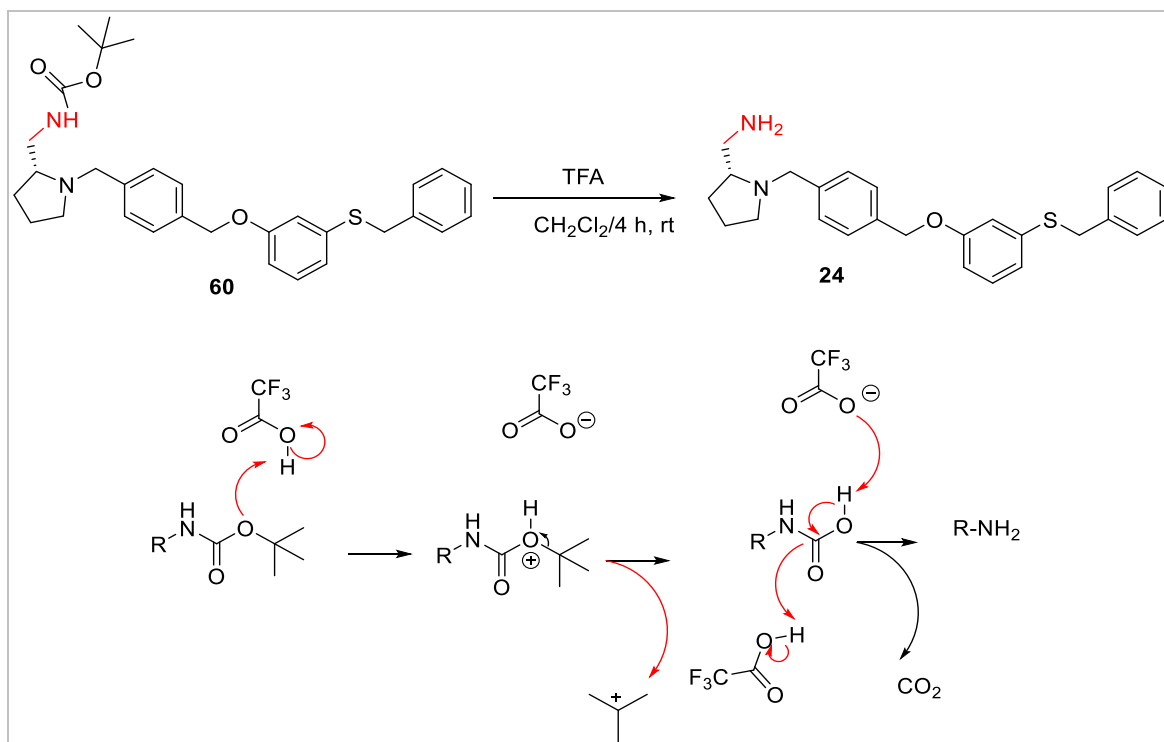
Scheme 2.13. Synthesis and mechanism for the preparation of compound 24.

The deprotection mechanism is initiated via protonation f the *t*-butyl carbamate by TFA which results in the loss of the *t*-butyl cation to then form 2,2-dimethylethene and the carbamic acid. This unstable intermediate decarboxylates to generate the free amine. [230]

Table 2.12. Sulfide containing analogues **20-28** and their yields formed by reductive amination with 2-(hydroxymethyl) pyrrolidine

20-28

Compounds	R	R*	Yield%
20	(4-Cl-phenyl)	(pyrrolidin-2-yl)methanol OH	99
21	(4-F-phenyl)	(pyrrolidin-2-yl)methanol OH	36
22	(4-CF₃-phenyl)	(pyrrolidin-2-yl)methanol OH	52
23	cyclohexyl	(pyrrolidin-2-yl)methanol OH	61
24	phenyl	(pyrrolidin-2-yl)methanamine NH₂	36
25	phenyl	(pyrrolidin-2-yl)methanol OH	36
26	phenyl	(piperidin-2-yl)methanol OH	24
27	phenyl	HO–ethyl–NH	53
28	phenyl	pyrrolidine	99

110
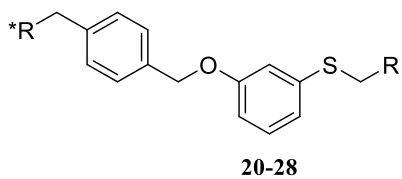
2.4.3 Synthesis of the truncated 3-(methoxymethyl)phenoxy analogue of PF-543.

Resorcinol was treated with chloromethyl methyl ether under basic conditions in acetone to afford a regio-selective alkylated phenol (**61**). Formation of **61** was confirmed by the appearance of the hydroxyl peak at 9.41 ppm in the ^{1}H NMR spectrum and two new singlets at 3.36 ppm and 5.11 ppm that correspond to CH_3 and CH_2 groups respectively are indicative of a successful mono-alkylation (**Figure 2.41**). The phenol was then alkylated with **39** using previously described conditions to form **62**, followed by reductive amination to afford **15** in a good overall yield (43%) (**Scheme 2.14**).
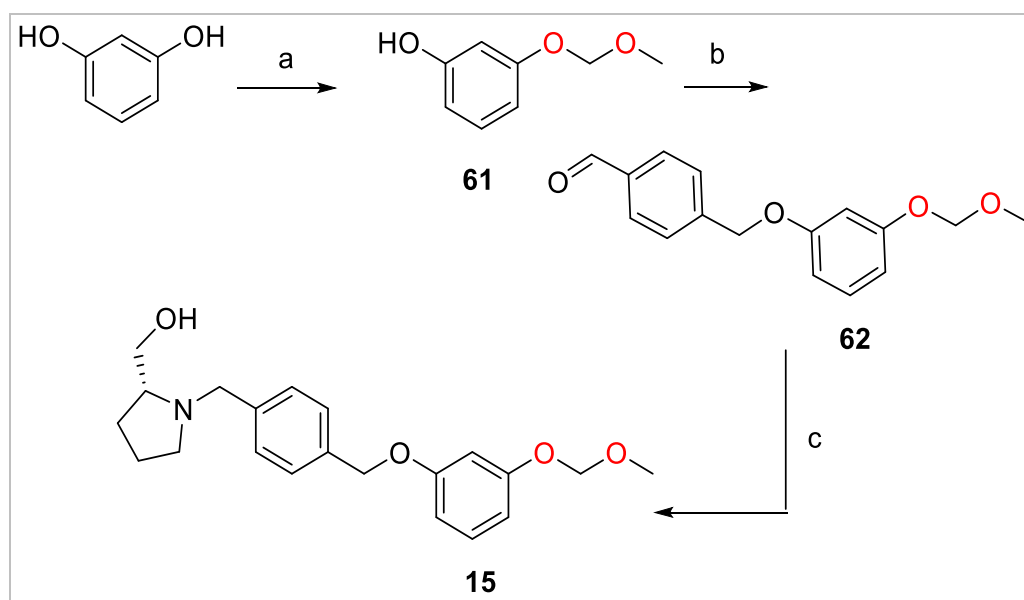
Scheme 2.14. Synthesis of the (methoxy)phenoxy) methyl analogue. Reagents and conditions: (a) chloromethyl methyl ether, caesium carbonate, acetone, N_2, 0 °C, 1.5 h (b) K_2CO_3 (2.75 eq), MeCN, 60 °C, N_2, 3 h. (c) ((*R*)-pyrrolidin-2-yl) methanol, NaBHAc$_3$ (1.5 eq), DCE, N_2, 24 h.
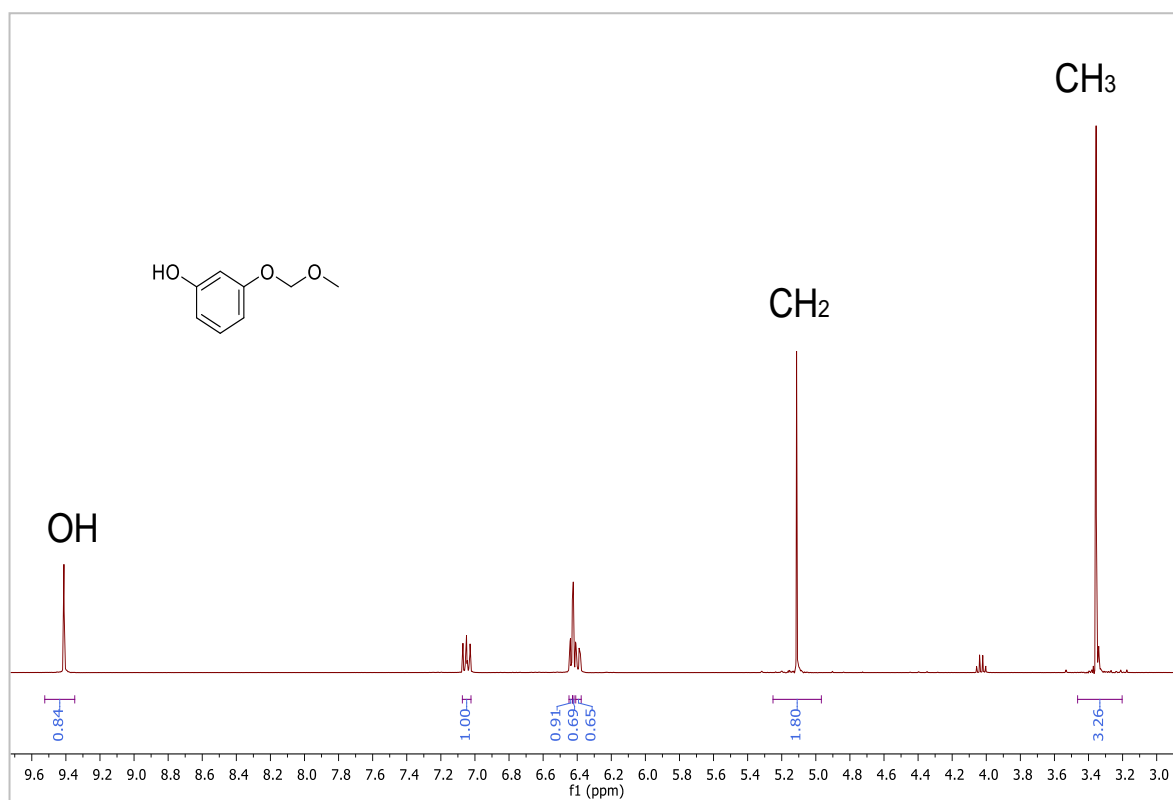
Figure 2.41. ^{1}H NMR (DMSO-d$_6$) of compound 61.

2.5 *In vitro* assessment of biophysicochemical and pharmacokinetic properties

Whilst improving potency against a specific target during the design phase of a new compound, substantial efforts should also be focused on the optimization of its biophysicochemical properties (e.g. solubility, permeability and metabolic stability) and pharmacokinetic (ADMET) properties (e.g. absorption, distribution, metabolism, excretion and toxicity) [231] before progressing to *in vivo* pharmacokinetic (PK) profiling. *In vitro* ADMET property assessments, including permeability, metabolic stability, and CYP450 inhibition properties, were performed with **PF-543** and compounds **17**, **18** and **21** to establish whether improvements had been made with the new compounds. All assays were performed and evaluated by Cyprotex Discovery Ltd (Macclesfield, UK).

2.5.1 Absorption and permeability

In the early stage of compound development, aqueous solubility and permeability are crucial parameters that need to be measured. Regardless of potency in the primary assay, compounds that have good oral bioavailability are needed if they are to become a preclinical candidate. Furthermore, optimised solubility, absorption and permeability are essential to deliver compounds across cell membrane to show activity in cells. [232]

To predict the *in vivo* human intestinal absorption and estimate the permeability of **PF-543** across the intestinal epithelia, the apparent permeability coefficients (P_{app}) were measured using the Caco-2 cell line model. Caco-2 cells have characteristics that resemble intestinal epithelial cells, such as the formation of a polarized monolayer, a well-defined brush border on the apical surface and intercellular junctions. Assessing transport in both directions (apical to baso-lateral (A−B) and baso-lateral to apical (B−A) across the cell monolayer enables an efflux ratio to be determined that indicates whether a compound undergoes active efflux by P-glycoprotein transporters. **PF-543** was found to have a high permeability like propranolol (**Table 2.13**) suggesting good intestinal absorption is likely. The efflux ratio (ER) of **PF-543** was 1.72, indicating little active efflux, which is normally apparent when the ER value is < 5. [233]

Table 2.13. Apparent permeability of compound **PF-543**.

Permeability	PF-543	Propranolol
Compartment A to B Mean P_{app} (x10^{-6} cm s^{-1})	19.4	30.0
Compartment B to A Mean P_{app} (x10^{-6} cm s^{-1})	33.4	32.8
Efflux Ratio	1.72	1.09

ADMET properties for any new compound can be predicted to some extent based on physiochemical properties. [234] Indeed, physiochemical properties have been widely used to predict permeability and absorption based on calculating the predicted cLogP, and a total polar surface area (tPSA). tPSA$\leq$ 120 Å^2 and cLogP $\leq$ 5 are considered acceptable progression criteria for any new compound for oral admininistration. [235] Our analogues are structurally similar to **PF-543** and have cLogP and tPSA values that suggest that they are more lipophilic. We would therefore expect compounds **17**, **18** and **21** to have good permeability and absorption (**Figure 2.41**).
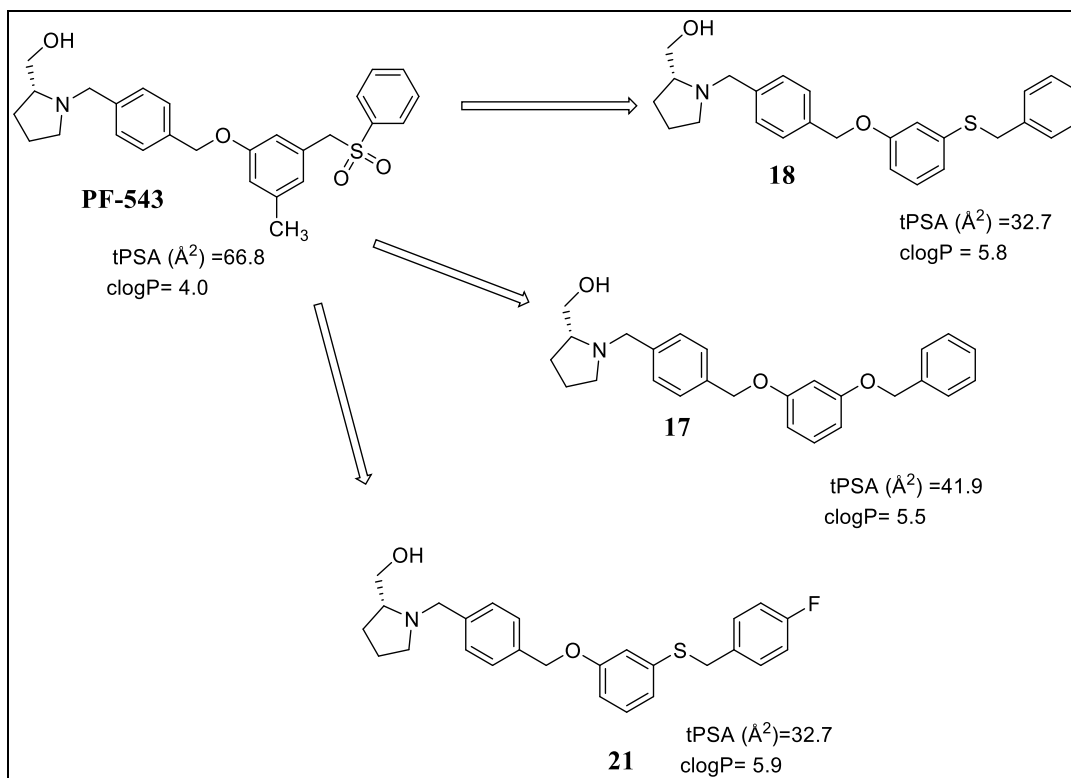
Figure 2.42. cLogP and tPSA ($\mathring{A}^2$) of PF-543 and compounds 17, 18 and 21.

2.5.2 Solubility

The solubility of a compound is a parameter that determines its absorption from the gastrointestinal tract and its oral bioavailability. It is also essential to assess solubility at an early stage in drug discovery because poor solubility can limit the quality of the data generated in other *in vitro* assays. Compounds with solubilities less than 1 µM are considered to be a highly insoluble, between 1 and 100 µM to be partially soluble and > 100 µM to be highly soluble. As can be seen from **Table 2.14**, the solubility of compounds **17**, **18** and **21** are correlated with their predicted lipophilicity values: the most lipophilic, compound **21** with the *para*-fluorophenyl group, has low solubility compared to **18**. Relative to compounds **18** and **21**, compound **17** has lower lipophilicity and improved solubility (111 µM) due to the presence of oxygen in place of sulfur.

Table 2.14. Solubility and lipophilicity values for **17**, **18** and **21**

Compounds	Solubility (μM)	cLogP	tPSA (Å^2)
21	10	5.96	32.7
17	111	5.5	41.9
18	30	5.8	32.7

2.5.3 Hepatocyte stability of PF-543

In vitro hepatocyte stability assays were conducted to determine the *in vitro* intrinsic clearance and half-life. As can be seen from **Table 2.15**, **PF-543** was cleared more rapidly with a half-life of 2.21 mins and a high intrinsic clearance of 628 μL/min/10^6 cells (where low and high CL_{int} are defined as <3.3 and > 17.8 μL/min/10^6 cells respectively). [236] The fact that **PF 543** is a lipophilic compound makes it a good substrate for liver metabolising enzymes via CYP450-catalysed oxidations. Such high clearance could be due to a combination of phase I and phase II metabolic processes, as intact liver cells contain both sets of metabolising enzymes. **PF-543** possesses many structural features that make it highly susceptible to phase I metabolism, including *O*-dealkylation of the ether, deamination of the pyrrolidine moiety and aromatic hydroxylation, particularly of the electron rich head aromatic group. In addition, the central toluyl group is a target for phase I aliphatic hydroxylation (**Figure 2.43**). The most likely site for phase II metabolism is the primary alcohol, which could undergo conjugation with glucuronic acid.

Table 2.15. Hepatocyte stability of compound PF-543

Hepatocyte Stability Species=Mouse	PF-543
$t_{1/2}$ (min)	2.21
CL_{int} (µL/min/10^6 cells)	628
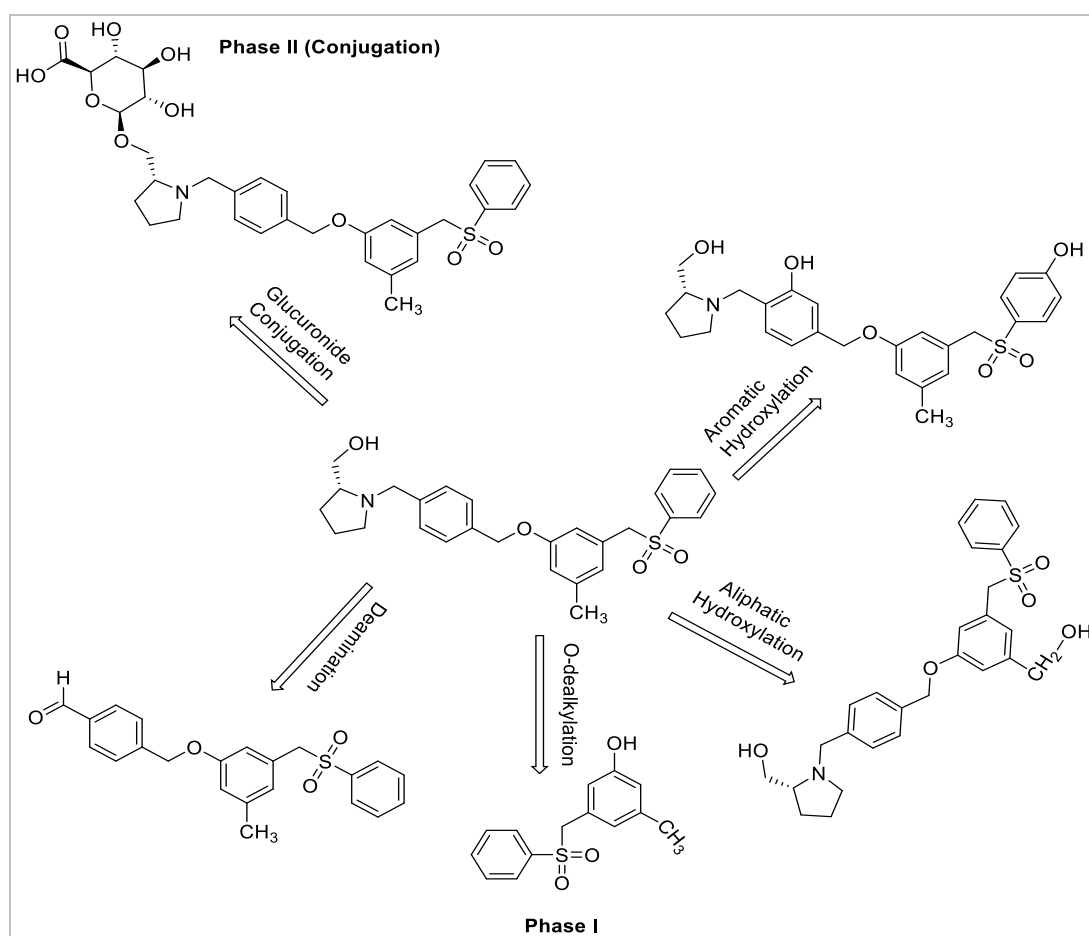
Figure 2.43. Possible sites of Phase I and Phase II metabolism of PF-543 and its possible metabolites. Note; the aldehyde group generated by deamination will be further oxidised to a carboxylic acid by liver dehydrogenases.

2.5.4 . Microsomal stability of compounds 17, 18 and 21

The liver constitutes the principal site of drug metabolism, and the main aim of the microsomal stability *in vitro* study is to measure the predictable compound clearance by phase I and phase II. [237] Phase I metabolism involves numerous processes that alter compound structure, predominantly via oxidation utilizing the cytochrome P450 complex of enzymes. Phase II reactions involve conjugations with endogenous polar molecules, the most common being glucuronic acid via glucuronyl transferases. [237]

The advantage of using the S9 mouse liver fraction preparation for *in vitro* screening of microsomal stability is that it contains a wide variety of both phase I and phase II enzymes. [237] Microsomal stability studies can be performed to investigate phase I oxidations using NADPH only as the enzyme co-factor or to investigate combined phase I and II metabolism, using NADPH + uridine 5'-diphospho-glucuronic acid (UDPGA) cofactors in the preparation. The microsomal stability assay has several advantages over the hepatocyte stability assay: it can be adjusted to a high throughput screening format that enables large numbers of compounds to be screened inexpensively.

The data from **Table 2.16** suggests that all compounds underwent significant phase I metabolism, with high clearance rates similar to **PF-543**. This finding was related to a short half-life and high intrinsic clearance seen for compounds in the presence of NADPH compared to only a slightly longer half-life in the presence of NADPH and UDPGA and for phase II, which suggests phase I is the rate-determining step (**Table 2.16**).

Table 2.16. Microsomal stability of compounds **PF-543**, **17**, **18** and **21**.

Compounds	Microsomal Stability (Species=Mouse) Cofactor=NADPH only Phase I			S9 Stability (ProteinType=S9, ProteinConc=1mg/ml, Species=Mouse Cofactor=NADPH + UDPGA) Phase II		
	$CL_{int}(\mu L/min/mg$ protein)		$t_{1/2}(min)$	$CL_{int}(\mu L/min/mg$ protein)		$t_{1/2}(min)$
PF-543	441		3.14	ND		ND
17	174		7.96	28.4		24.4
18	440		3.15	60.7		11.4
21	335		4.14	118		5.88
Control	diazepam	302	4.59	Midazolam	25.5	27.1

From the similar phase I clearance rates in the above table, it appears compounds undergo similar transformations, because different functionalities do not alter metabolism rates. For example, compounds **18** and **21** differ only in **site A** (**Figure 2.44**), which suggests that the *para*-fluoro substituent is not preventing aromatic hydroxylation in this ring, otherwise the half-life would have been increased. Unlike the other analogues, **PF-543** has a benzylic group, yet has a similar clearance rate, which suggests that aliphatic hydroxylation is not responsible for the high clearance seen across the series. Compounds **17**, **18** and **21** could each undergo *O*- or *S*-debenzylation in **site A**, but **PF-543** cannot, which implies that dealkylation here is not the primary phase 1 metabolic route. The feature that is common to **PF-543**, **17, 18** and **21** is the central benzylic ether moiety between **sites C** and **B**, suggesting that *O*-dealkylation at this junction is the most likely metabolic route. Alternatively, deamination of the common pyrrolidine could be the primary route (**Figure 2.44**).

Generally, highly lipophilic molecules can have low oral bioavailability through a combination of poor solubility and rapid metabolism because they are good substrates

for CYP450. Potentially, the phase I metabolic rate of these compounds could be reduced by modification of the benzylic ether in **site B** (e.g. replace O with CH_2 – compound **63; Figure 2.44**), but this would increase lipophilicity and reduce solubility. If deamination in **site C** is the primary phase I metabolic route, then replacement of the methylene hydrogens with atom (s) that cannot be abstracted by CYP450 to initiate oxidation could address this issue. An amide link would prevent deamination (compound **64; Figure 2.44**), but this would alter the relative orientation of the pyrrolidine ring with respect to the phenyl group and reduce binding with the target SK. A difluoromethylene group (compound **65; Figure 2.44**) should retain the molecular conformation, but would significantly lower the pKa of the pyrrolidine, reducing its ability to form salts, which could have consequences for both its water solubility and its binding with SK. Such suggested modifications illustrate the difficulties of balancing pharmacodynamic and pharmacokinetic considerations when developing preclinical drug molecules.
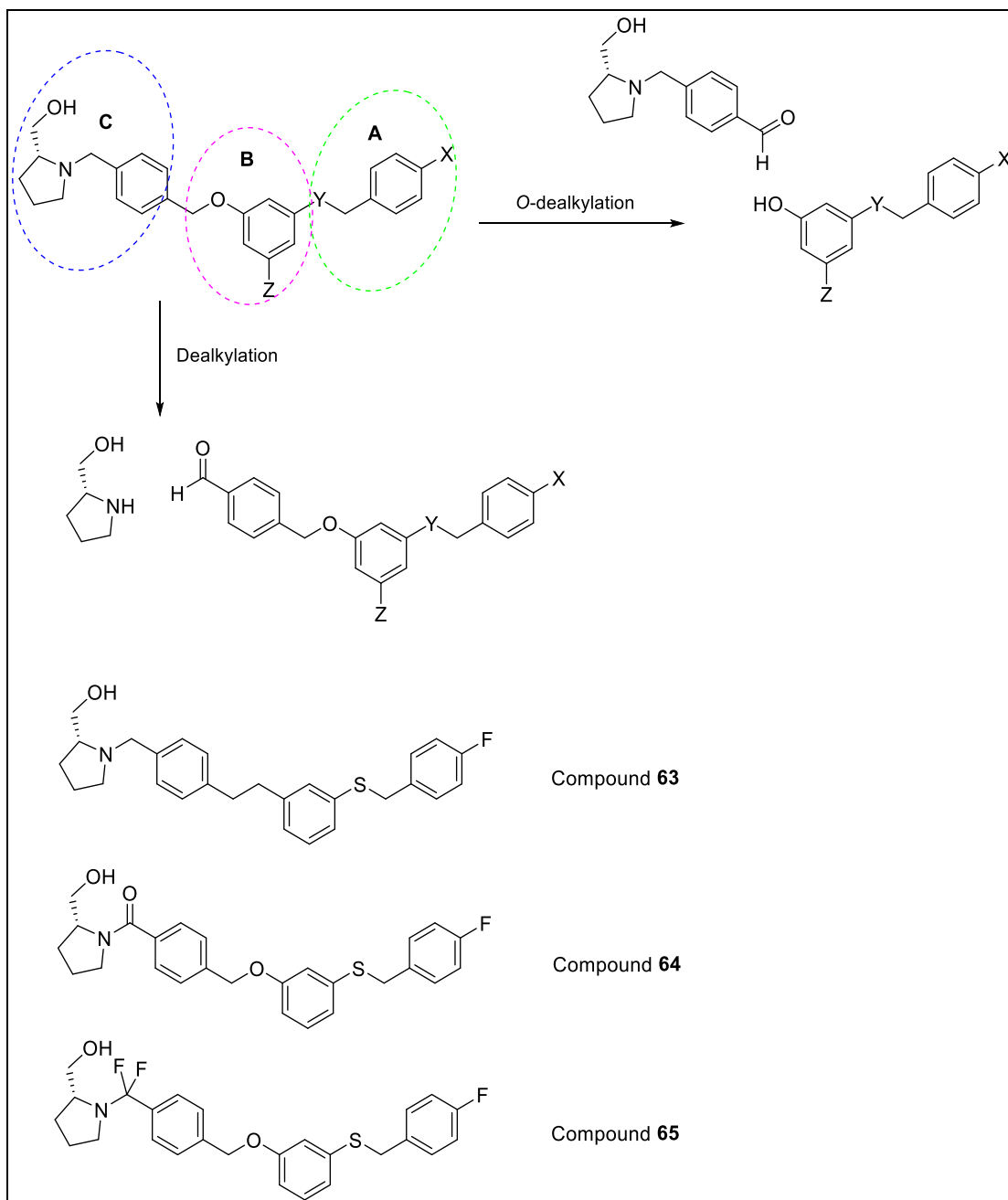
Figure 2.44. Top: most likely phase I metabolites across the series based on similar phase I clearance rates. Bottom: possible modifications that could be made to address the high phase I clearance rates

2.5.5 . Cytochrome P450 inhibition

Cytochrome P450 is a family of enzymes that plays a crucial role in the metabolism of drugs and represents the main complex likely to involve possible drug-drug interactions via common substrate binding. Screening against CYP450 isoforms is now well established as a component of any drug discovery programme to alert for possible drug interactions in the clinic. [238]

Evaluating the cytochrome P450 inhibition of a new investigational drug is recommended in the draft FDA guidance for drug interaction studies. [239] Usually a drug is metabolized by more than one CYP isozyme, but different CYP isozymes themselves have different substrate specificities. For example, CYP1A2 tends to metabolize planar amines and amides, CYP2D6 candidates are medium sized basic amines, substrates for CYP2C9 are aromatic, lipophilic, neutral and acidic molecules, whereas CYP2C18 oxidizes both hydrophobic and hydrophilic molecules. CYP3A4 is considered the major contributor to CYP450-mediated metabolism and its substrates are large lipophilic, positively charged or neutral molecules. [235,240] CYP3A4 is also found in the intestinal gut epithelia and can impact bioavailability directly through the absorbing surface. Alterations in CYP3A4 activity through drug interactions can therefore significantly alter systemic drug concentrations at the site of absorption through a first-pass effect. When tested against these five CYP450 isoforms (CYP1A, CYP2C18, CYP2D6, CYP2C9 and CYP3A4) and compared with known inhibitors of each isoform (potent inhibitor: $IC_{50} < 1\,\mu M$; moderate inhibitor: IC_{50}: $1\,\mu M$ to $10\,\mu M$; weak or non-inhibitor: $IC_{50} > 10\,\mu M$ [235,240]), our compounds had no effect on any enzyme at the concentrations used (**Table 2.17**). Combined with the metabolic stability studies, these data suggest that compounds **17** and **21** are good substrates for CYP450, but do not inhibit the enzymes activity itself.

Table 2.17. Cytochrome P450 inhibition of compounds **17** and **21**.

Isoforms	CYP1A IC$_{50}$ (μM)	CYP2C18 IC$_{50}$ (μM)	CYP2D6 IC$_{50}$ (μM)	CYP2C9 IC$_{50}$ (μM)	CYP3A4 IC$_{50}$ (μM)
Substrate	Alphanaphthoflavone 0.0675	Quinidine 0.0511	Tranylcypromin 7.3	Sulfaphenazole 0.513	Ketoconazole 0.0533
Compounds					
17	>25	>25	>25	>25	>25
21	>25	>25	>25	>25	>25

2.6 Conclusions

To conclude this chapter, a number of new analogues of compound **PF-543** were synthesized, screened against SK1 and SK2 in an ADP-Glo™ assay developed in-house, and an SAR profile constructed. The co-crystal structure of SK1 with **PF-543** provided a useful tool to understand the binding properties of the compounds with the Sph binding site of SK1 itself and a related SK2 model based on simple mutations in the binding site. Understanding the key differences between the SK1 and SK2 structures in the Sph binding site provided guidance in terms of designing selective SK2 over SK1 inhibitors. Compound **9** was the most selective SK1 inhibitor with IC_{50} of 63 nM, while compound **21** was the most potent and selective SK2 inhibitor with an IC_{50} of 206 nM. However, ADMET properties of these new analogues still need to be improved. **PF-543** and compound **21** have good Caco2 permeability and do not inhibit cytochrome P450. However, metabolic studies revealed that these inhibitors are cleared rapidly and more stable analogues are needed if we are to progress to *in vivo* studies. Compound **21** also has only moderate solubility (10 µM), which also needs to be addressed.

In **Chapter 3**, we report on cell-based investigations into whether the selectivity profiles seen in the ADP- Glo™ assay were translated into the cellular setting using pharmacodynamic markers of target engagement with SK1 and SK2, and what phenotypic response was observed.

Chapter 3. Biology

Differential dose dependent effect of novel SK inhibitors in LNCaP and LNCaP-AI cells: mechanisms and functional relevance.

3.1 Introduction

The human prostate cancer cell lines LNCaP (androgen-dependent) and LNCaP-AI (androgen-independent) cells have been used as examples of *in vitro* models of human prostate carcinoma. Both have been established from a lymph node metastasis of human prostate carcinoma. [241] These cells proliferate *in vitro* in the presence of androgens in the culture medium and maintain the characteristics of human prostate cancer, such as stimulation and secretion of organ-specific proteins, expression of the androgen receptor and responsiveness to hormones. [242]

Culturing LNCaP cells under conditions of androgen deprivation for lengthy periods of time produces LNCaP AI cells, which subsequently grow independently of androgen, although androgen receptors are still expressed and can be stimulated in response to various stimuli. [242] Therefore, LNCaP-AI cells provide a recapitulated model of poor prognosis and resistance to anti-androgen therapy in advanced stage prostate cancer. Human pulmonary artery smooth muscle cells (hPASMC) were used in this study as a model for non-cancerous proliferating cells.

As discussed in **Chapter 2**, **PF-543** was chemically modified to produce selective SK1, SK2 and dual SK1/SK2 inhibitors with nanomolar potency assessed using an *in vitro* kinase ADP-Glo-Assay. This chapter describes the pharmacodynamic and phenotypic effects of **PF-543** and exemplars from these novel SK inhibitors in prostate cancer cells.

3.2 Results

3.2.1 PF-543 induces the proteasomal degradation of SK1 and this can be reversed by MG132.

PF-543 has previously been reported to induce the proteasomal degradation of SK1 in hPASMC cells.[215,219] Therefore, a preliminary study was undertaken to investigate the effect of **PF-543** on SK1 degradation in hPASMC, LNCaP and LNCaP-AI cells. In this regard, **PF-543** induced a marked reduction in SK1 expression in these cells (**Figure 3.1**). The reduction in SK1 levels was noticeable within 24 h of treatment with the inhibitor and it was reversed by MG132, a specific reversible proteasome inhibitor. However, treatment of these cells with the cathepsin B inhibitor CA074Me (lysosomal inhibitor) did not reverse the effect, which confirmed that lysosomal degradation was not involved in the degradation of SK1 induced by **PF-543** (**Figure 3.2**). This finding is in agreement with the published studies. [39,215,219]
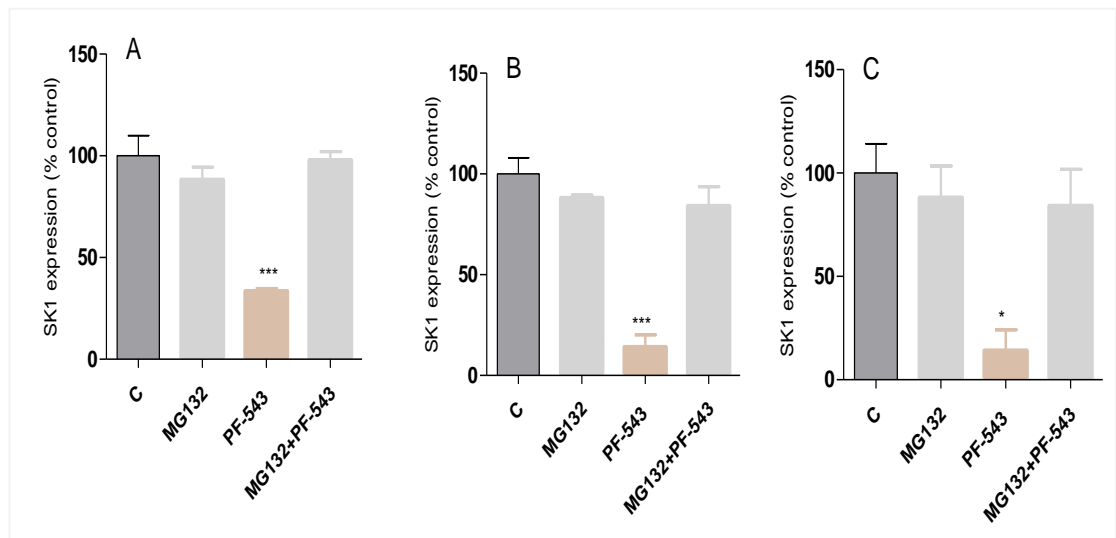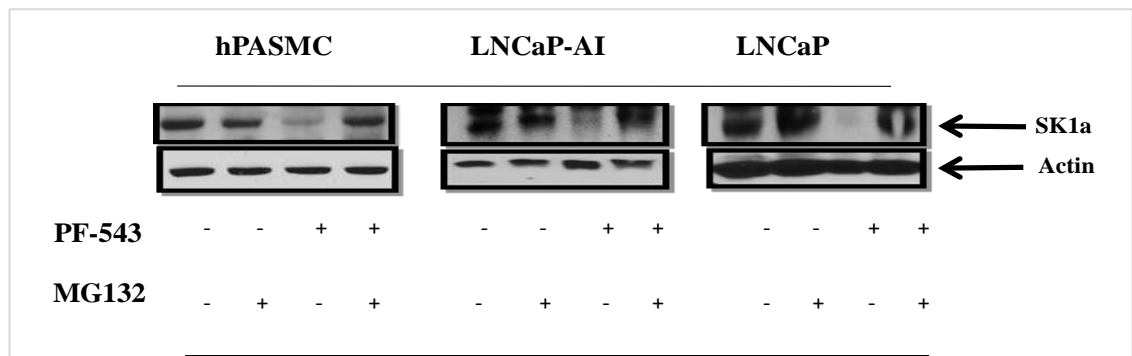
Figure 3.1. Effect of PF-543 on SK1a protein expression in hPASMC (A), LNCaP-AI (B) and LNCaP (C) cells. Cells were treated for 24 h with **PF-543** (100 nM) or with the vehicle alone (DMSO, 0.1% v/v) in the absence or presence of MG132 (10 μM, 30 mins pre-treatment). The SK1 (42 kDa) protein level was measured by western blotting analysis using anti-SK1 antibody. Blots were stripped and re-probed with anti-actin antibody to ensure comparable protein loading between samples. Results are representative of at least three separate experiments. Also shown are bar graphs as blots were quantified by densitometry and expressed as a percentage of the control (DMSO, 24 h) (control=100%). Results are expressed as means +/− SEM for n = 3 experiments. The data was analysed by Dunnett post-test, *p < 0.05, ***p < 0.001 versus control (C).
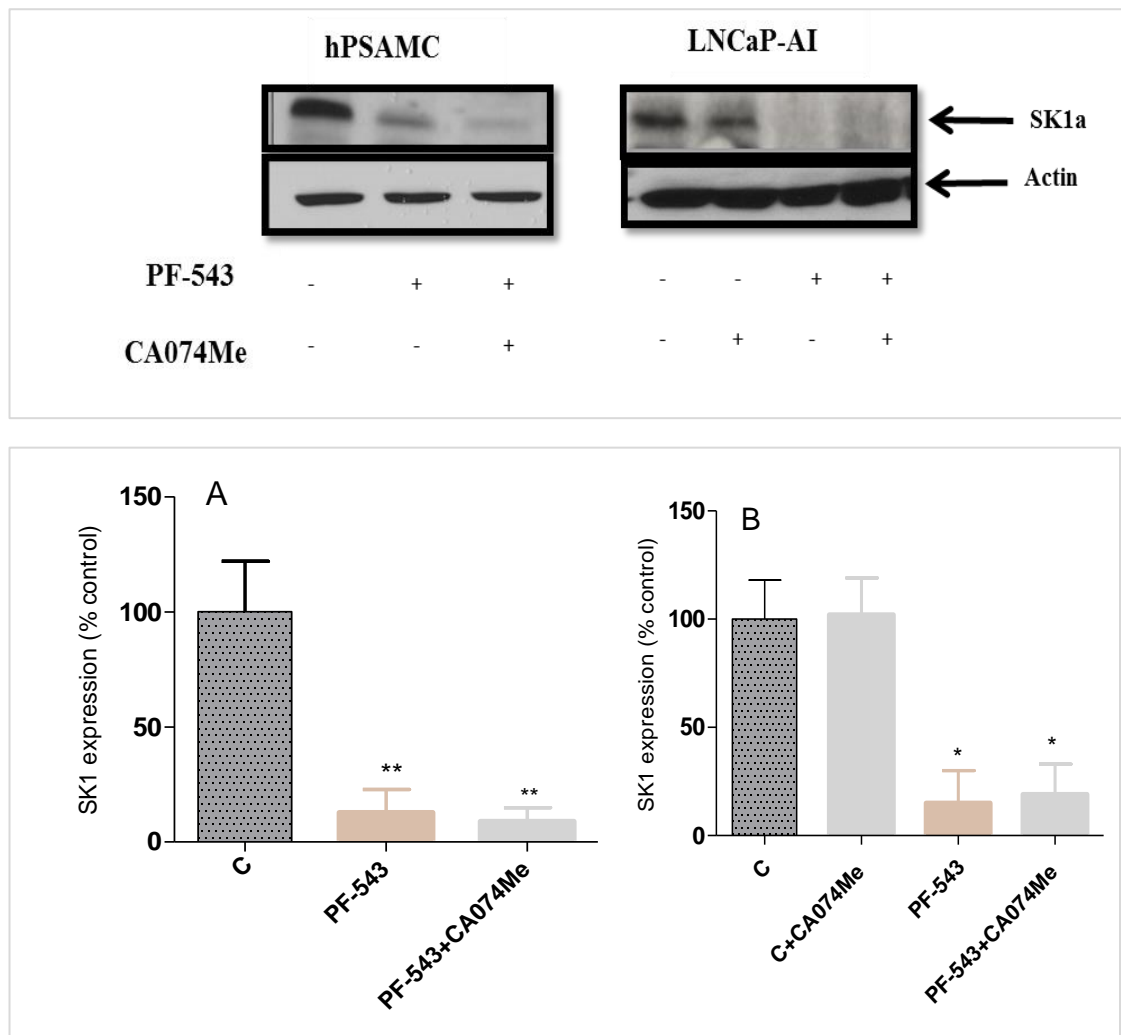
Figure 3.2. Lack of a role for the lysosomal pathway in the PF-543 induced down-regulation of SK1a expression in hPASMC (A) and LNCaP-AI (B) cells. Cells were pre-treated with the cathepsin B inhibitor CA074Me (10 μM, 30 mins) before being treated for 24 h with **PF-543** (100 nM) or with the vehicle alone (DMSO, 0.1% v/v). The SK1 (42 kDa) protein level was measured by western blotting analysis using specific anti-SK1 antibody. Blots were stripped and re-probed with anti-actin antibody to ensure comparable protein loading between samples. Results are representative of at least three separate experiments. Also shown are bar graphs as blots were quantified by densitometry and expressed as a percentage of the control (DMSO, 24 h) (control=100%). Results are expressed as means $+/-$ SEM for n = 3 experiments. The data was analysed by Dunnett post-test, *p < 0.05 versus control (C).

To further investigate whether **PF-543** activates the proteasomal pathway in a similar way to the SK1/2 inhibitor, SKi, we evaluated the effect of **PF-543** on c-Myc expression levels, which has a very short half-life and is removed in response to SKi in LNCaP-AI cells, [243] due to activation of the proteasome. Pre-treatment of LNCaP-AI cells with **PF-543** did not induce down-regulation of c-Myc protein levels **(Figure 3.3)** indicating that it does not directly activate the proteasome in these cells. There is correlation with the K_i for inhibition of SK1 catalytic activity by **PF-543**, suggesting that **PF-543** binds directly to SK1 to induce a conformational change that allows enhanced ubiquitination and proteasomal degradation of SK1 (discussed in detail in **section 3.3.1**).
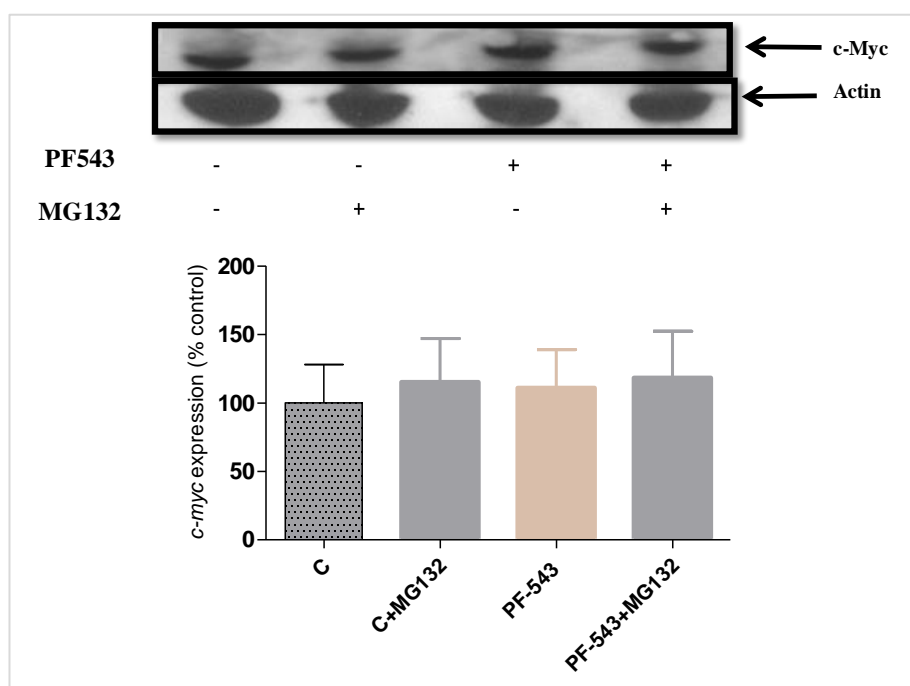
Figure 3.3. Effect of PF-543 on c-Myc protein expression in LNCaP-AI cells. Cells were treated for 24 h with PF-543 (100 nM) or with the vehicle alone (DMSO, 0.1% v/v). The c-Myc (57 kDa) protein level was measured by western blotting analysis using anti-c-Myc antibody. Blots were then stripped and re-probed with anti-actin antibody to ensure comparable protein loading between samples. Results are representative of at least three separate experiments. Also shown are bar graphs as blots were quantified by densitometry and expressed as a percentage of the control (DMSO, 24 h) (control=100%). Results are expressed as means +/− SEM for n = 3 experiments. The data was analysed by Dunnett post-test, *p> 0.05 versus control (C).

3.2.2 Effect of new SK inhibitors on SK1 expression

In **Figures 3.1** and **3.2**, the SK1 selective inhibitor **PF-543** was shown to induce the proteasomal degradation of SK1 in mammalian cells, and previous studies have established that the dual SK1/SK2 inhibitors (e.g. SKi) induce proteasomal degradation of SK1 in LNCaP-AI cells. [129] In contrast, SK2 selective inhibitors such as **ROMe** failed to reduce SK1 expression in these cells. [128] However, the selective SK2 inhibitor ABC294640 was shown to induce the proteasomal degradation of SK1 in LNCaP-AI cells,[39] which was accounted for by also inhibiting Des1, which regulates the activity of the proteasome. Our new SK inhibitors were therefore examined for their effect on proteasomal degradation of SK1 in both prostate cancer cells and hPASMC cells at 100 nM for 24 h. In agreement with the *in vitro* SK1 ADP-Glo activity assay, compounds **1**, **2**, **6**, **7**, **8**, **17**, and **18** (SK1/SK2 inhibitors) and **9** (selective SK1 inhibitor) induced marked reductions in the level of SK1 expression in these cell lines after 24 h treatment. This finding was consistent with the effect of the parent compound **PF-543** on SK1 in these cell types (**Figure 3.4 A, B: Figure 3.5**). Compounds **20** and **21**, which are SK2 selective inhibitors, did not reduce SK1 expression levels in hPASMC cells (**Figure 3.4 C**).
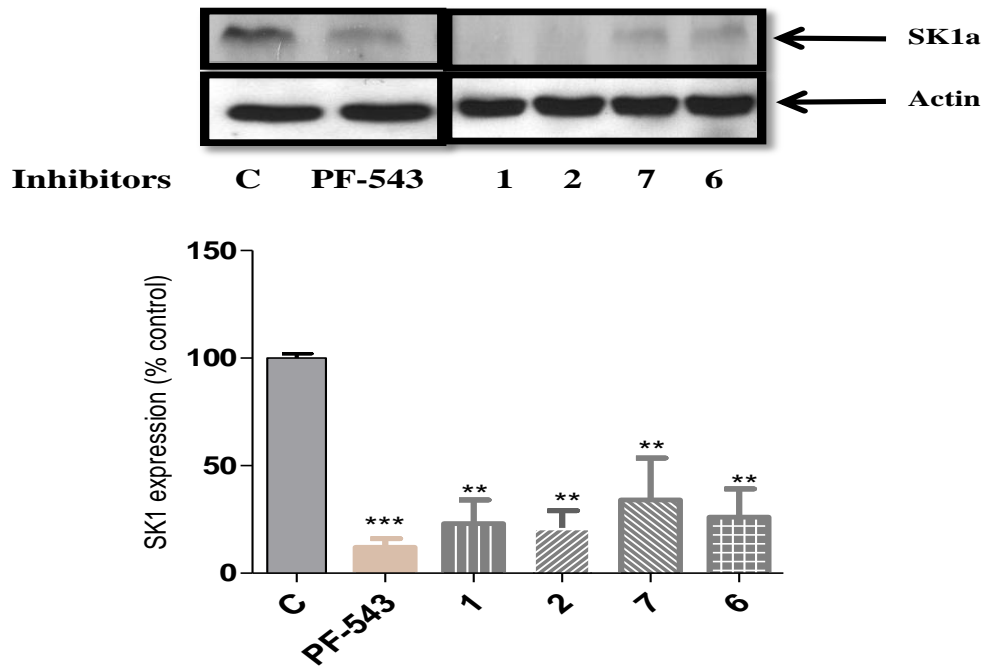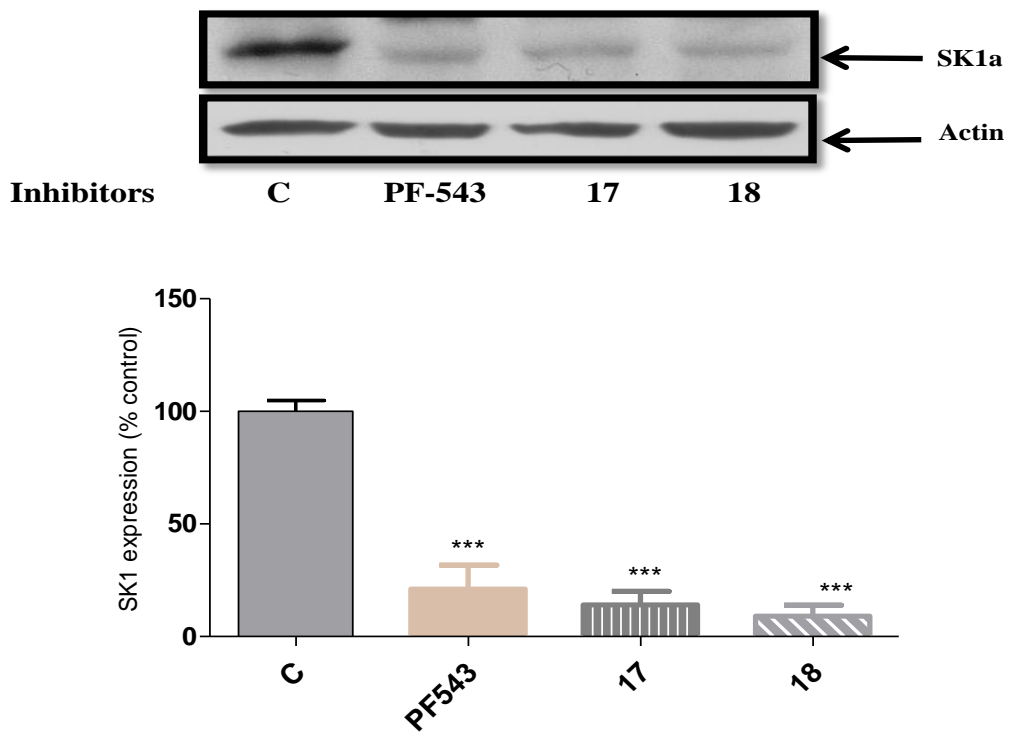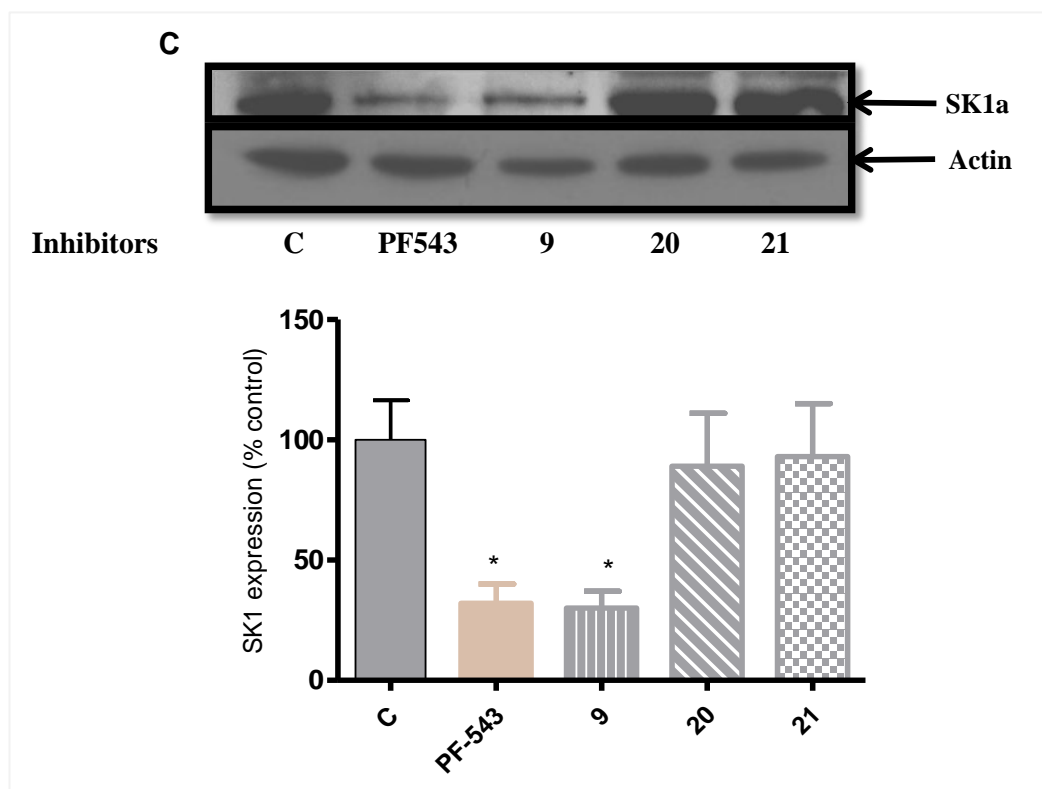
Figure 3.4. Effect of compounds (PF-543, 1, 2, 7, 6, 17, 18, 9, 20 or 21) on SK1a protein expression in hPASMC cells. Cells were treated for 24 h with **PF-543** and **1, 2, 7, 6, 17, 18, 9, 20** or **21** (100 nM) or with the vehicle alone (DMSO, 0.1% v/v). SK1 protein levels were then measured by western blotting analysis using specific anti-SK1 antibody. Blots were stripped and re-probed with anti-actin antibody to ensure comparable protein loading between samples. Results are representative of three separate experiments. Also shown are bar graphs as blots were quantified by densitometry and expressed as a percentage of the control (DMSO, 24 h) (control=100%). Results are expressed as means +/− SEM for n = 3 experiments. The data was analysed by Dunnett post-test, *p < 0.05, **p < 0.01, ***p < 0.001 versus control (C).
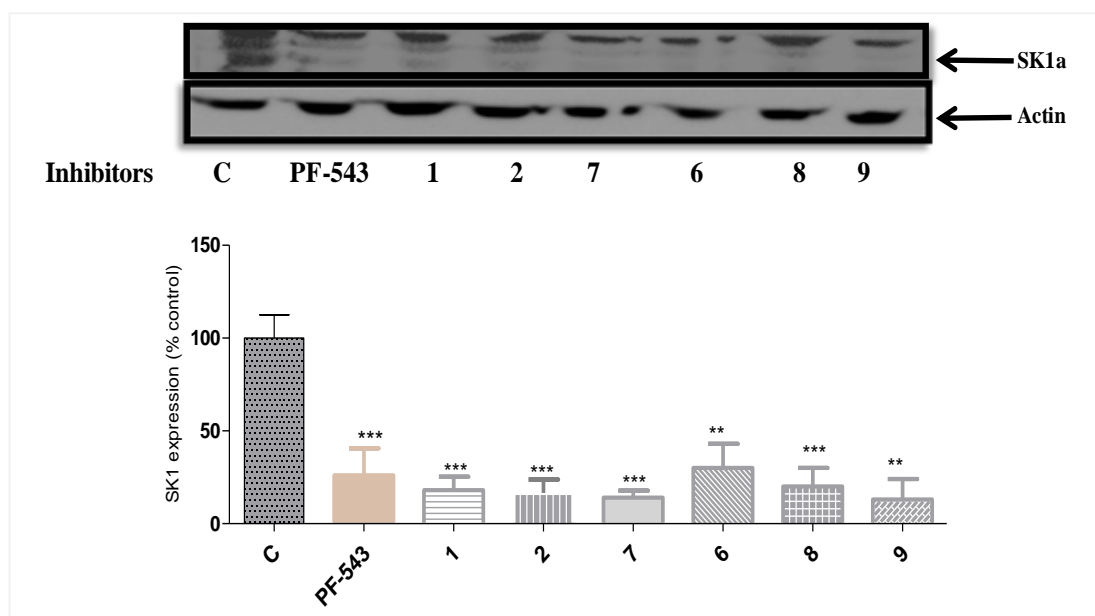
Figure 3.5. Effect of compounds (1, 2, 7, 6, 8, and 9) on SK1a protein expression in LNCaP cells. Cells were treated for 24 h with **PF-543** and **1**, **2**, **7**, **6**, **8** or **9** (100 nM) or with the vehicle alone (DMSO, 0.1% v/v). SK1 protein levels were the measured by western blotting analysis using specific anti-SK1 antibody. Blots were stripped and re-probed with anti-Actin antibody to ensure comparable protein loading between samples. Results are representative of three separate experiments. Also shown are bar graphs as blots were quantified by densitometry and expressed as a percentage of the control (DMSO, 24 h) (control=100%). Results are expressed as means $+/-$ SEM for n = 3 experiments. The data was analysed by Dunnett post-test, **p < 0.01, ***p < 0.001 versus control (C).

3.2.3 Effect of new SK inhibitors on the proteasomal degradation of SK1 in LNCaP and LNCaP-AI cells.

The effect of the new SK inhibitors (100 nM, 24 h) on SK1 expression was assessed in hPASMC or LNCaP-AI cells in the presence and absence of the cell permeable proteasome inhibitor, MG132. All the inhibitors reduced the expression of SK1 in both cell types and pretreatment of the cells with the proteasome inhibitor MG132 reversed the effect of the SK inhibitors on SK1 protein levels (**Figures 3.6: Figure 3.7**), indicating that dual SK1/SK2 and SK1 selective inhibitors reduce SK1expression via the proteasomal degradation pathway.

Figure 3.6. Effect of proteasomal degradative pathway inhibition on SK inhibitor-induced down-regulation of SK1a expression by compounds 1, 7, 8 and 9 in LNCaP-AI cells. LNCaP- AI cells were pre-treated with the proteasome inhibitor MG132 (10 μM, 30 mins) before being treated with for 24 h with SKi (10 μM), **PF-543**, 1, **7**, **8** or **9** (100 nM) or with the vehicle (DMSO, 0.1% v/v). The levels of SK1 in cells were then measured by western blotting analysis with anti-SK1 antibody. Blots were stripped and re-probed with anti-actin antibody to ensure comparable protein loading. Results are representative of two separate experiments.
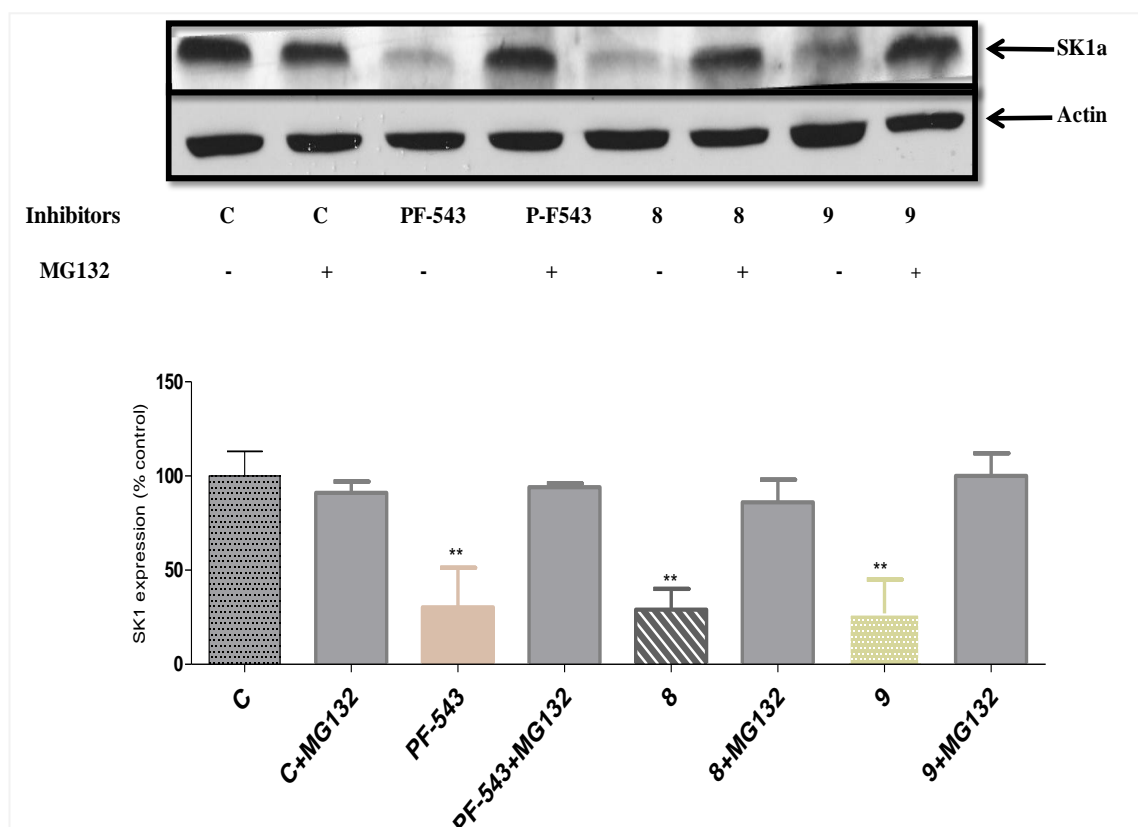
Figure 3.7. Effect of proteasomal degradative pathway inhibition on SK inhibitor-induced down- regulation of SK1a expression by PF-543 and compounds 8 and 9 in hPASMC cells. Cells were pre-treated with the proteasome inhibitor MG132 (10 μM, 30 mins) before being treated for 24 h with SKi (10 µM), **PF-543** and (**8** or **9**) (100 nM) or with the vehicle (DMSO, 0.1% v/v). The levels of SK1 in cells were then measured by western blotting analysis with anti-SK1 antibody. Blots were stripped and re-probed with anti-actin antibody to ensure comparable protein loading. Results are representative of three separate experiments. Also shown are bar graphs as blots were quantified by densitometry and expressed as a percentage of the control (DMSO, 24 h) (control=100%). Results are expressed as means +/− SEM for n = 3 experiments. The data was analysed by Dunnett post-test, **p < 0.01 versus control (C).

In contrast, the treatment with a specific inhibitor of the lysosomal protease cathepsin B (CA074Me) did not prevent SK1 down-regulation in response to the inhibitors in hPSMACcells or LNCaP-AI cells (**Figure 3.8: Figure 3.9**), indicating that the lysosomal proteolytic pathway is not involved.
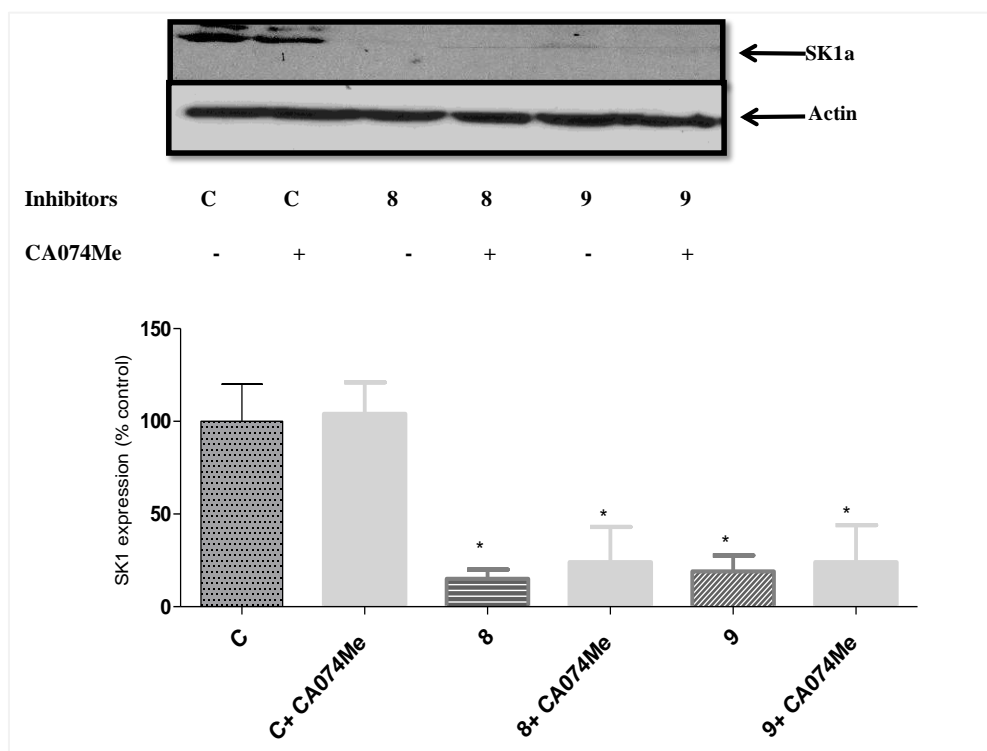
Figure 3.8. Effect of lysosomal degradative pathway inhibition on SK inhibitor-induced down-regulation of SK1 expression by compounds 8 and 9 in hPSMAC cells. Cells were pre-treated with the cathepsin B inhibitor CA074Me (10 μM, 30 mins) before being treated for 24 h with **8** or **9** (100 nM), or with the vehicle (DMSO, 0.1% v/v). SK1 protein levels were measured by western blotting analysis using anti-SK1 antibody. Blots were stripped and re-probed with anti-actin antibody to ensure comparable protein loading. Results are representative of three separate experiments. Also shown are bar graphs as blots were quantified by densitometry and expressed as a percentage of the control (DMSO, 24h) (control=100%). Results are expressed as means +/− SEM for n = 3 experiments. The data was analysed by Dunnett post-test, *p < 0.05, versus control (C).

Inhibitors	C	C	PF-543	PF-543	1	1	7	7	6	6
CA074Me	-	+	-	+	-	+	-	+	-	+
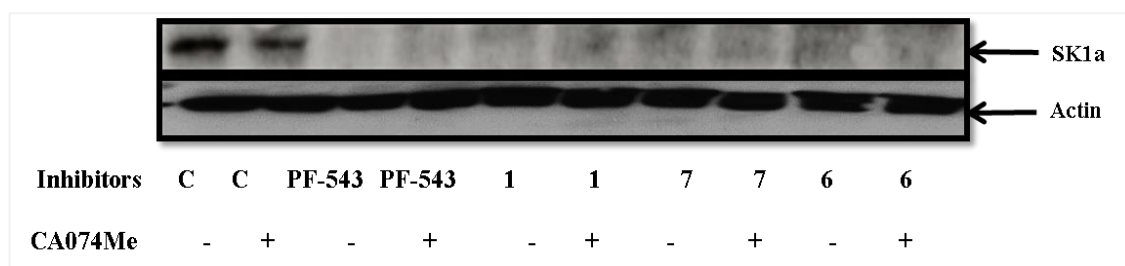
Figure 3.9. Effect of lysosomal degradative pathway inhibition on SK1 inhibitor-induced down-regulation of SK1 expression by PF-543 and compounds 1, 7 and 6 in LNCaP-AI Cells. Cells were pre-treated with the cathepsin B inhibitor CA074Me (10 μM, 30 mins) before being treated for 24 h with **PF-543**, **1**, **7** or **6** (100 nM) or with the vehicle (DMSO, 0.1% v/v). SK1 protein levels were measured by western blotting analysis using anti-SK1 antibody. Blots were stripped and re-probed with anti-actin antibody to ensure comparable protein loading. Results are representative of two separate experiments.

To assess whether these inhibitors were activating the ubiquitin-proteasomal pathway in a similar way to the SK1/SK2 dual inhibitor SKi, their effect on the protein levels of c-Myc, was also measured. Treatment of LNCaP-AI cells with these inhibitors (100 nM) did not promote the degradation of c-Myc (Mr=57 kDa). Therefore, unlike SKi, these compounds do not appear to be directly activating the proteasome (**Figure 3.10**), but are more likely inducing the proteasomal degradation of SK1 by directly binding to it as seen with **PF-543**.
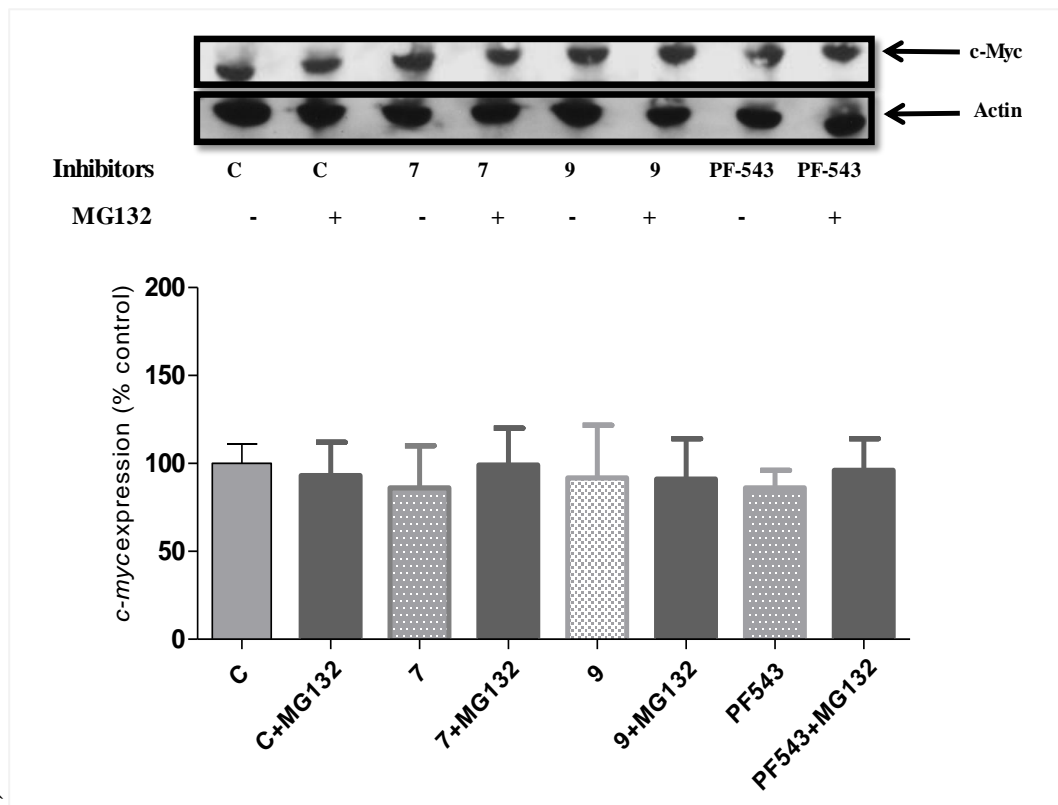
Figure 3.10. Effect of SK inhibitors on c-Myc protein expression in LNCaP-AI cells. Cells were pre-treated with the proteasome inhibitor MG132 (10 μM, 30 mins) before being treated for 24 h with **PF-543**, **7** or **9** (100 nM) or with the vehicle (DMSO, 0.1% v/v). C-Myc protein levels were then examined by western blotting analysis using specific antibodies for c-Myc (57 kDa). Blots were stripped and re-probed with anti-actin antibody to ensure comparable protein loading between samples. Results are representative of three separate experiments. Also shown are bar graphs as blots were quantified by densitometry and expressed as a percentage of the control (DMSO, 24 h) (control=100%). Results areexpressed as means +/− SEM for n = 3 experiments. The data was analysed by Dunnett post-test, p> 0.05, ***p < 0.001 versus control (C).

3.2.4 Effect of PF-543 on LNCaP-AI and LNCaP Cell Survival

A) Morphology

SKi, a potent SK1/SK2 inhibitor, induced morphological changes in LNCaP cells that involved retraction of cell processes. In contrast, **PF-543**, a selective SK1 inhibitor,-treated LNCaP cells did not exhibit these morphological features and resembled untreated cells (**Figure 3.11**).

Control

SKi
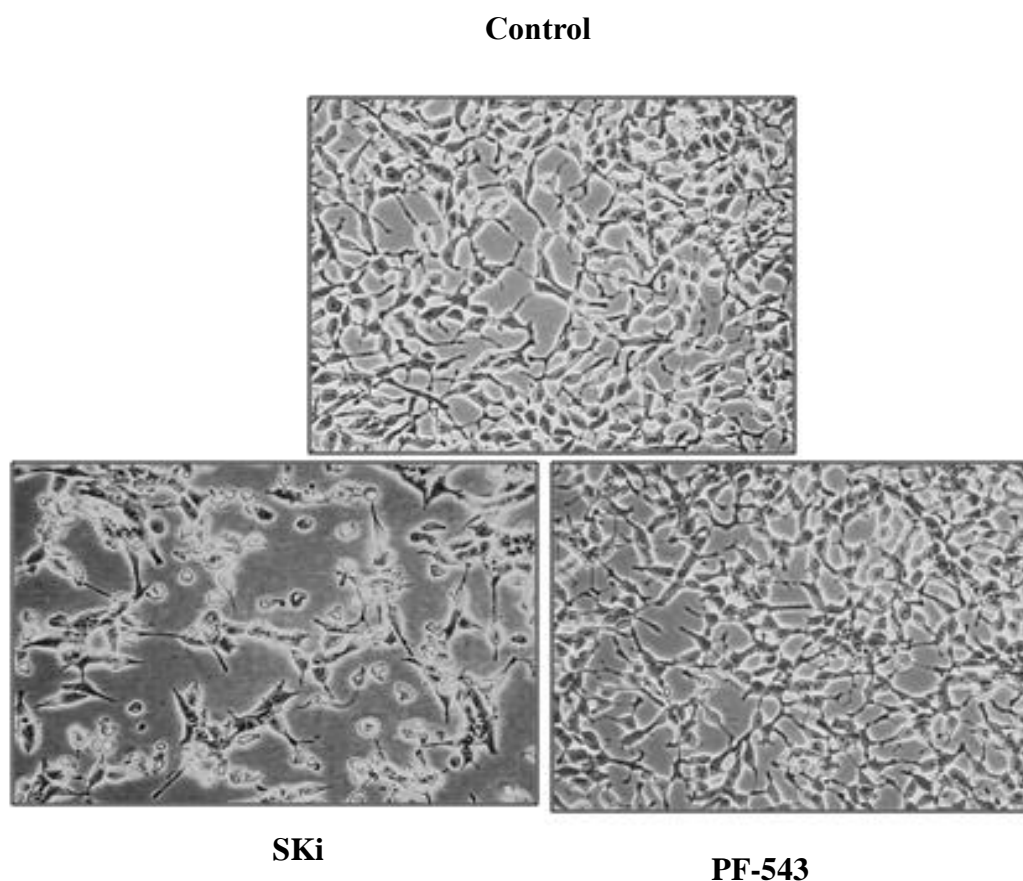
PF-543

Figure 3.11. Effect of SKi (10 µM) or PF-543 (100 nM) on the morphology of LNCaP cells after 24 h. Cells were seeded at 1×10^6 cells per well in a 96 well plate and incubated with SKi (10 µM) and PF-543 (100 nM) for 24 h. Images were taken using a Nikon TMS inverted phase contrast microscope. Objective lens x20. Results are representative of at least three separate experiments.

B) Cell Viability

To evaluate whether **PF-543** induces a cytotoxic effect on LNCaP-AI and LNCaP cells, an MTT assay (which measures total mitochondrial activity, directly comparable to the total number of viable cells) and a DNA synthesis assay ($[^3H]$-thymidine uptake into newly synthesised DNA) were employed as described in the materials and methods (**Chapter 5, section 5.3.1; section 5.3.2**). Staurosporine, which is known to induce apoptotic cell death through a caspase-dependent mechanism [244] was used as a positive control. LNCaP and LNCaP-AI cells were treated for 24 h with three different concentrations of staurosporine, (5, 10 and 30 µM) and **PF-543** at 100 nM, a concentration which severely reduces SK1 expression levels in LNCaP and LNCaP-AI cells. Cell viability was calculated by comparing to the mean cell viability for staurosporine or **PF-543** as the % of the mean viability of the untreated cells (control). **Figure 3.12** shows that treating LNCaP and LNCaP-AI cells with 100 nM **PF-543** for 24 h did not significantly affect viability of these cells. In contrast, cells treated with staurosporine (5-30 µM) showed a significant reduction in viability compared to the untreated control group.
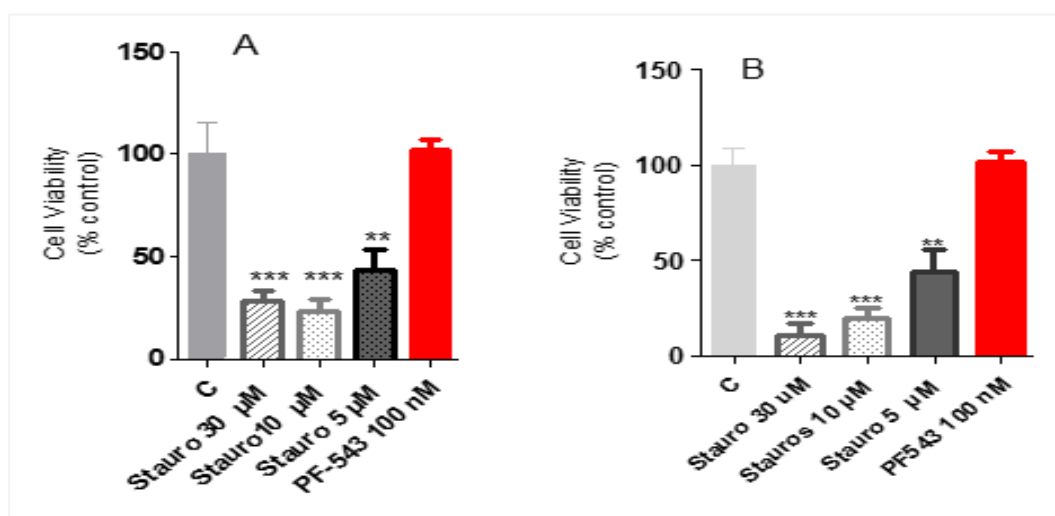
Figure 3.12 Effect of staurosporine on viability of LNCaP (A) and LNCaP AI (B) cells (MTT Assay). Cells were plated at 10000 cells/well in a 96-well plate. After overnight incubation, the cells were treated for 24 h with Staurosporine (5, 10, 30 µM) or PF-543 (100 nM) or with the vehicle alone (DMSO, 0.1% v/v). Results are expressed as means $+/-$ SEM for n = 3 experiments. The data was analysed by Dunnett post-test, **p < 0.01, ***p < 0.001, versus control (C).

SKi (10 µM) reduced DNA synthesis in LNCaP AI and LNCaP cells, whereas **PF-543** did not (**Figure 3.13**), which is consistent with previous studies where PF-543 did not inhibit proliferation of hPASMC or 1483 head and neck carcinoma cells. [210,215]
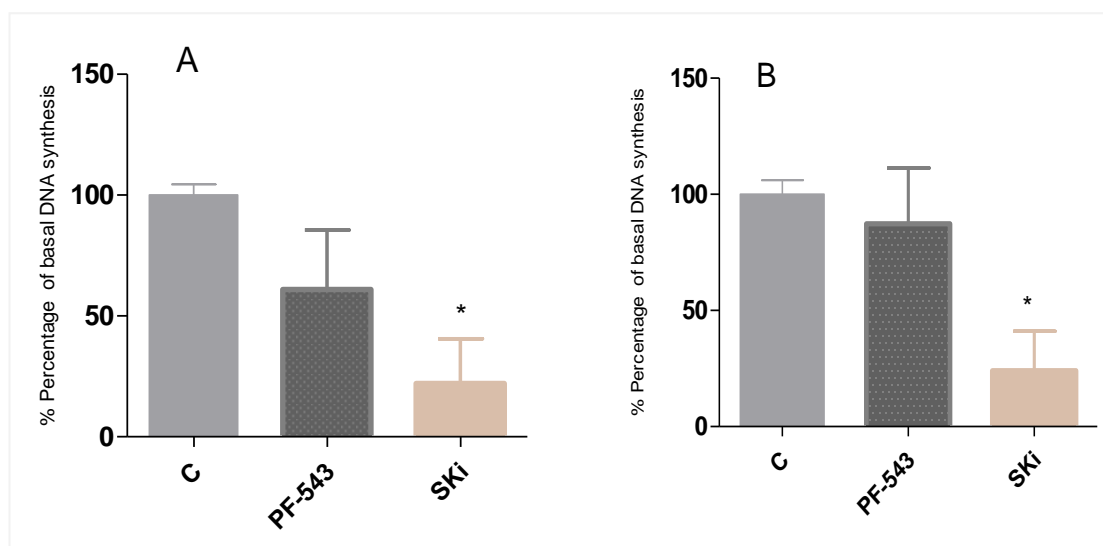
Figure 3.13. Effect of PF-543 on DNA synthesis in LNCaP (A) and LNCaP AI (B) cells. Cells were plated at 10000 cells/well in a 96-well plate. After overnight incubation, the cells were treated for 24 h with SKi (10 µM) or **PF-543** (100 nM) or with the vehicle alone (DMSO, 0.1% v/v) then incubated at 37°C in 5% CO_2. Results are expressed as means +/− SEM for n = 3 experiments. The data was analysed by Dunnett post-test, $*p < 0.05$ versus control (C).

C) Apoptosis

The effect of **PF-543** on apoptosis was investigated in comparison with SKi. As shown in **Figure 3.14**, the marker of the apoptotic process, cleaved PARP (89 kDa) was present in LNCaP cells treated with SKi (5-10 µM) for 48 h, whereas **PF-543** had no effect, indicating that it fails to induce apoptosis in these cells at 100 nM, the concentration that effectively removes SK1 from these cells.
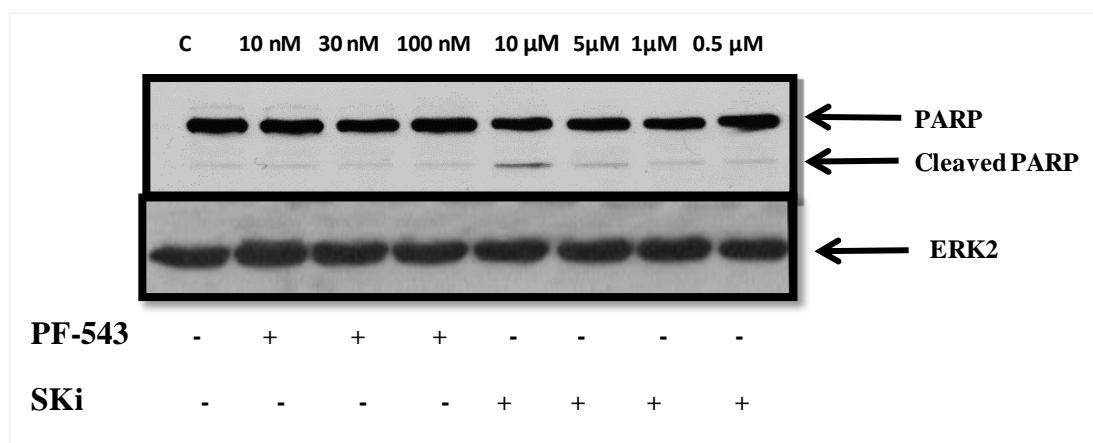
Figure 3.14. Effect of PF-543 and SKi on PARP cleavage in LNCaP cells. Cells were treated for 48 h with SKi (0.5-10 µM) and **PF-543** (30-100 nM) or with the vehicle alone (DMSO, 0.1% v/v). PARP cleavage was then evaluated by western blotting analysis using an antibody detecting both full-length (116 kDa) and cleaved (89 kDa) PARP. Blots were stripped and re-probed with anti-ERK-2 antibody to ensure comparable protein loading between samples. Results are representative of two separate experiments.

To further assess whether **PF-543** induces apoptosis of LNCaP and LNCaP-AI, a one-step cellular caspase-3/7 assay was used (**Chapter 5, section 5.3.3**). This assay is very quick, simple and amenable to high throughput cell-based screening of compounds in a 96-well plate format. To validate this assay in terms of specificity for the caspase 3/7 apoptotic pathway, a specific caspase-3/7 inhibitor, Ac-DEVD-CHO was used. Compared with control cells, treatment of LNCaP cells with staurosporine (5-30 µM) resulted in a statistically significant increase in activated caspase-3/7 levels (13, 28 and 20-fold respectively). In addition, treatment of LNCaP-AI cells with staurosporine (5-30 µM) resulted in a statistically significant increase in activated caspase-3/7 levels (31, 34 and 47) folds respectively. The caspase-3/7 inhibitor, Ac-DEVD-CHO (100 µM for 24 h) alone had no effect on caspase-3/7 activity on both prostatic cell lines, but did reduce the effect of staurosporine on caspase-3/7 activity in both cell types (**Figure 3.15**).
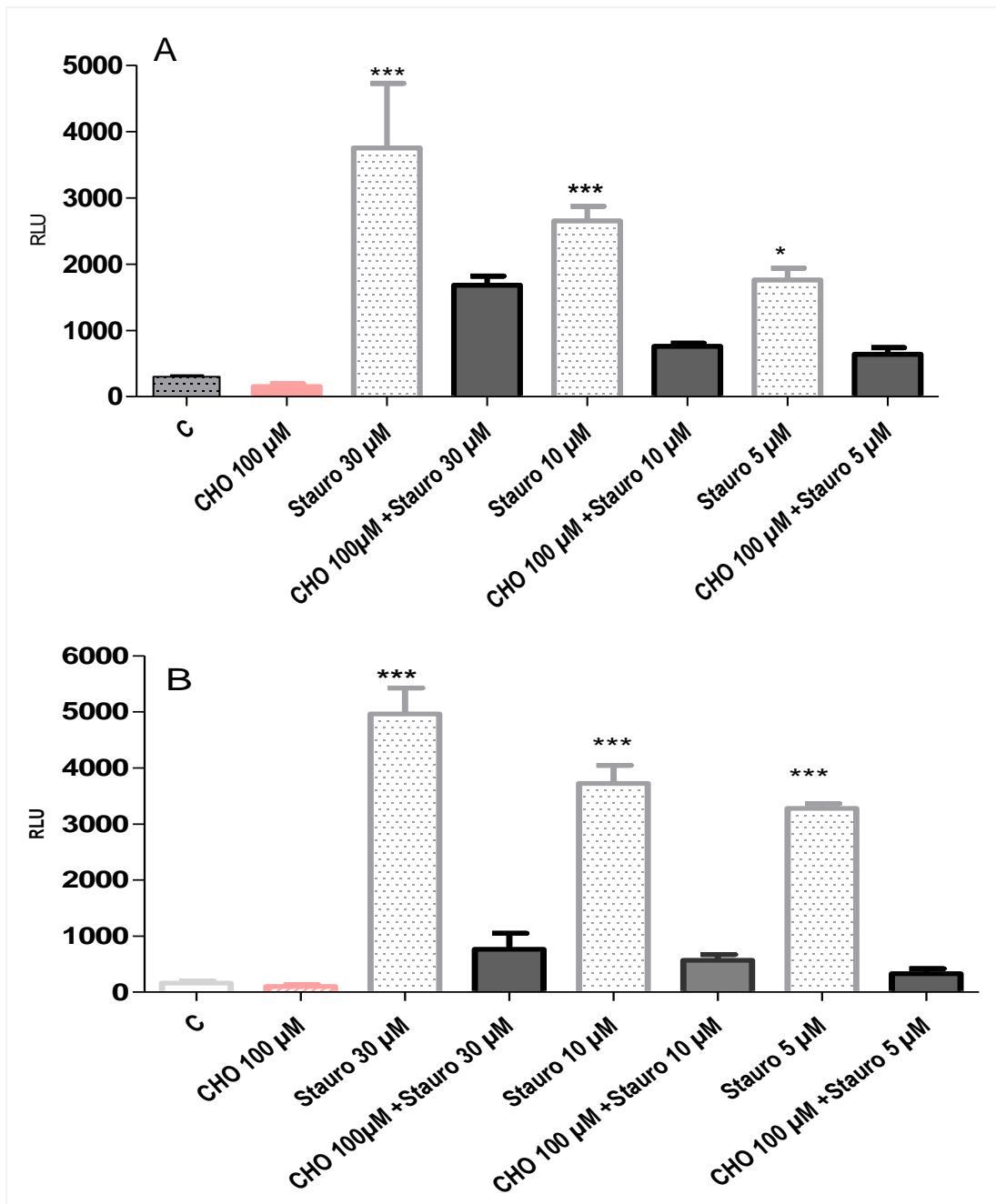
Figure 3.15. Validation of the caspase 3/7 assay in LNCaP (A) and LNCaP AI (B) cells.
Cells were plated at 10000 cells/well in a 96-well plate. After overnight incubation, cells were
treated for 24 h with staurosporine (5, 10 and 30μM) in the absence or presence of the protein
Ac-DEVD-CHO (CHO, 100 μM, 30 mins pre-treatment) or with the vehicle alone (DMSO,
0.1% v/v) then incubated at 37°C in 5% CO_2. Results are expressed as means +/− SEM for n
= 3 experiments. Results are expressed as means +/− SEM for n = 3 experiments. The data was
analysed by Dunnett post-test, *p < 0.05, ***p < 0.001 versus control (C).

Unlike the positive control staurospaurine, **PF-543** failed to increase caspase-3/7 activity in LNCaP and LNCaP-AI cells, indicating that apoptosis had not been induced **(Figure 3.16)**.
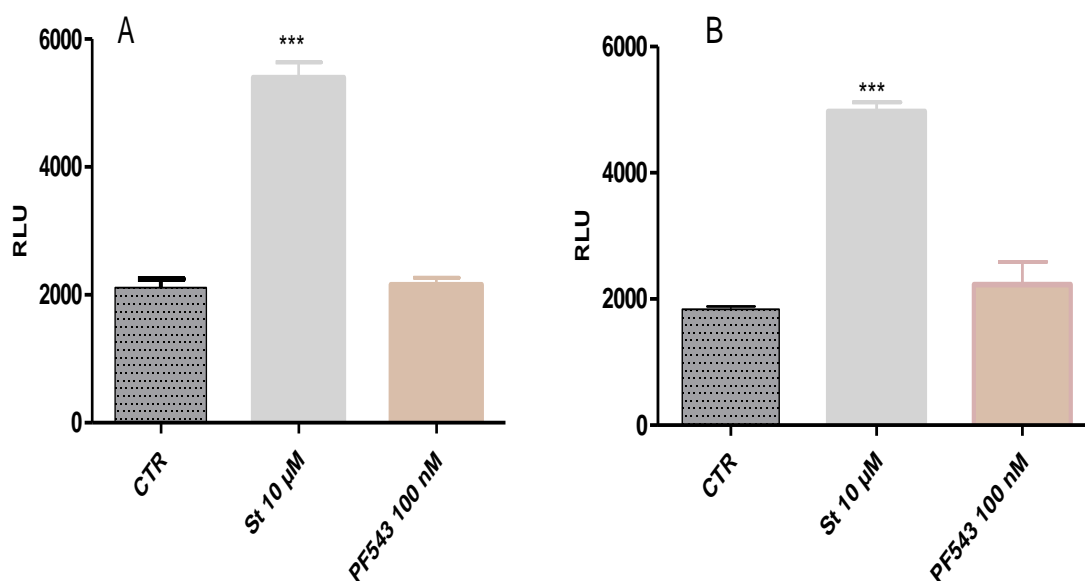
Figure 3.16. Lack of effect of PF-543 on caspase3/7 activity in LNCaP (A) and LNCaP AI (B) cells. Cells were plated at 10000 cells/well in a 96-well plate. After overnight incubation, the cells were treated for 24h with staurosporine (Stauro, 10 µM) and PF-543 (100 nM) or with the vehicle alone (DMSO, 0.1% v/v), then incubated at 37°C in 5% CO_2. Results are expressed as means +/− SEM for n = 3 experiments. The data was analysed by Dunnett post-test, ***$p < 0.001$ versus control (C).

3.2.5 Effects of new SK inhibitors in LNCaP and LNCaP-AI cell survival

It has been established that the removal of SK1 by SKi (10 µM over 48 h) was associated with apoptosis of LNCaP via the activation of executioner caspase-3 and caspase-7 [129] and the induction of PARP cleavage. [129] The apoptotic status of LNCaP and LNCaP-AI cells was next evaluated following treatment with our novel inhibitors.

The first step was to assess whether treatment with these inhibitors (100 nM for 24 h) induced any morphological changes in LNCaP-AI cells. At 100 nM, these inhibitors (e.g. **17** and **7**) did not induce any shrinkage of LNCaP-AI cells (**Figure 3.17A**), but did so at 10 µM for 24 h (**Figure 3.17 B**). The activation of apoptosis in LNCaP-AI cells treated with compounds **1**, **2**, **6** and **7** (10 µM) occurred within 24 hours, as assessed by the appearance of cleaved PARP (**Figure 3.18**).
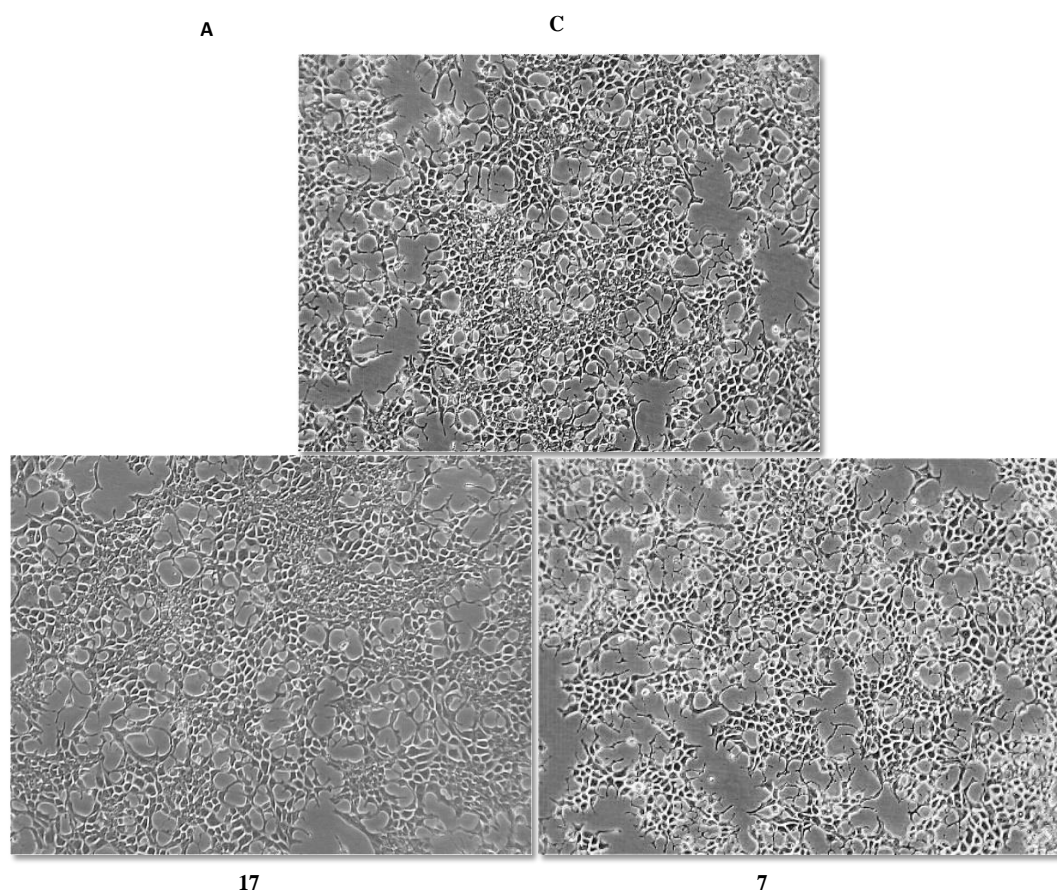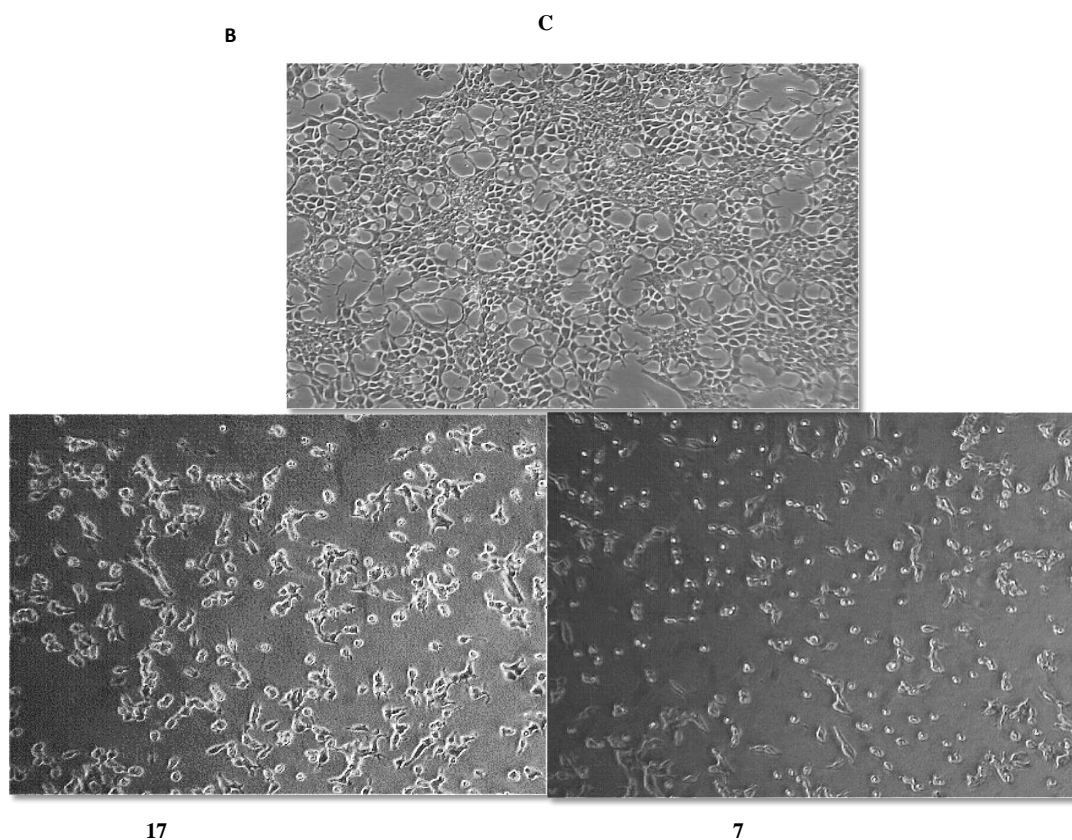
Figure 3.17. Effect of compounds (17 and 7) on the morphology of LNCaP AI cells at 100 nM (A) and 10 μM (B) after 24 h. Cells were seeded at $1\text{x}10^6$ cells per well in a 96 well plate and incubated with compounds (**17** and **7**) (100 nM or 10 μM) for 24 h. Images were taken using a Nikon TMS inverted phase contrast microscope. Objective lens x20. Results are representative of three separate experiments.
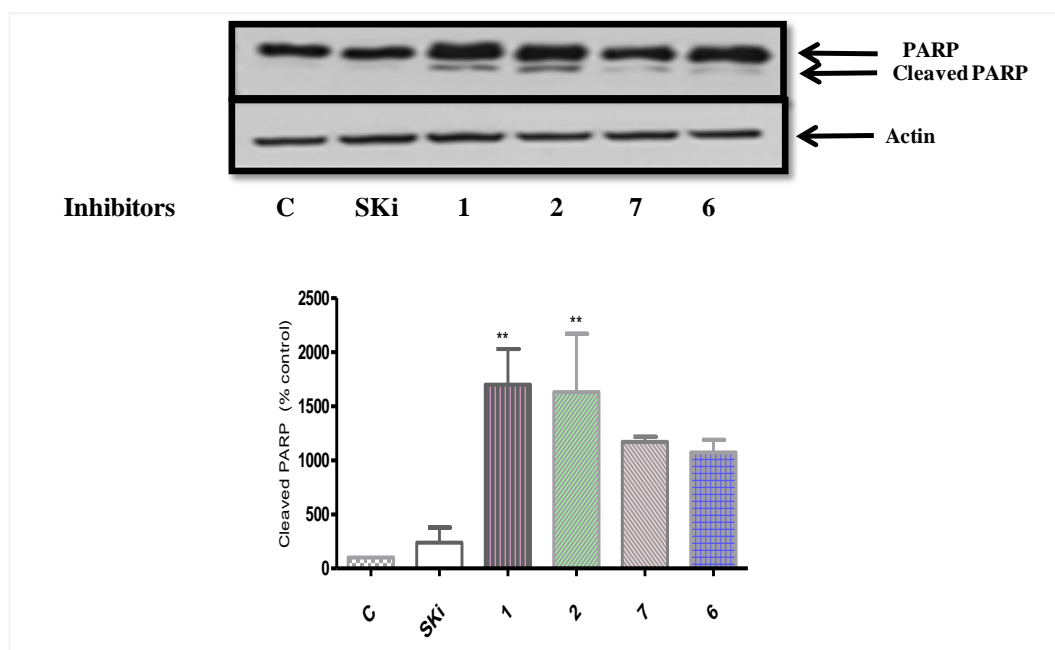
Figure 3.18. Effect of new SK inhibitors on PARP cleavage in LNCaP AI (A) cells. Cells were treated for 24 h with SKi and **1**, **2**, **7**, or **6** (10 μM) or with the vehicle alone (DMSO, 0.1% v/v). Apoptosis was then evaluated by western blotting analysis of the expression of apoptosis-related markers: PARP cleavage using an antibody detecting both full-length (116 kDa) and cleaved (89 kDa) PARP. Blots were stripped and re-probed with anti-actin-antibody to ensure comparable protein loading. Results are representative of three separate experiments. Also shown are bar graphs as blots were quantified by densitometry and expressed as a percentage of the control (DMSO, 24 h) (control=100%). Results are expressed as means +/− SEM for n = 3 experiments. The data was analysed by Dunnett post-test, **p < 0.01 versus control.

3.2.6 Effect of novel SK inhibitors on cell viability of LNCaP and LNCaP-AI cell line

To examine the effect of our SK inhibitors in LNCaP, LNCaP-AI cancer cells, cytotoxicity was assessed by a MTT viability assay (**Chapter 5, section 5.3.2**).

3.2.6.1 Effect of the new SK inhibitors on LNCaP and LNCaP-AI cells viability after 24 h

Since the selectivity profile against the SK1 (observed in the ADP-Glo assay was largely translated into the cellular setting, an MTT assay (**Chapter 5, section 5.3.2**) was carried out to investigate what phenotypic response the observed target engagement led to.

Firstly, prostate cancer cells were incubated with 100 nM SK inhibitors for 24 h. **Figure 3.19** shows that these inhibitors did not significantly affect prostate cancer cell viability during the period of treatment compared to the untreated control. However, the percentage of viable cells was decreased in the LNCaP and LNCaP-AI following exposure with 10 µM of these inhibitors (**Figure 3.20**). In contrast, treatment with our selective SK2 inhibitors (compounds **20** and **21**) did not significantly decrease cell viability in the LNCaP and LNCaP-AI following exposure at 10 µM.
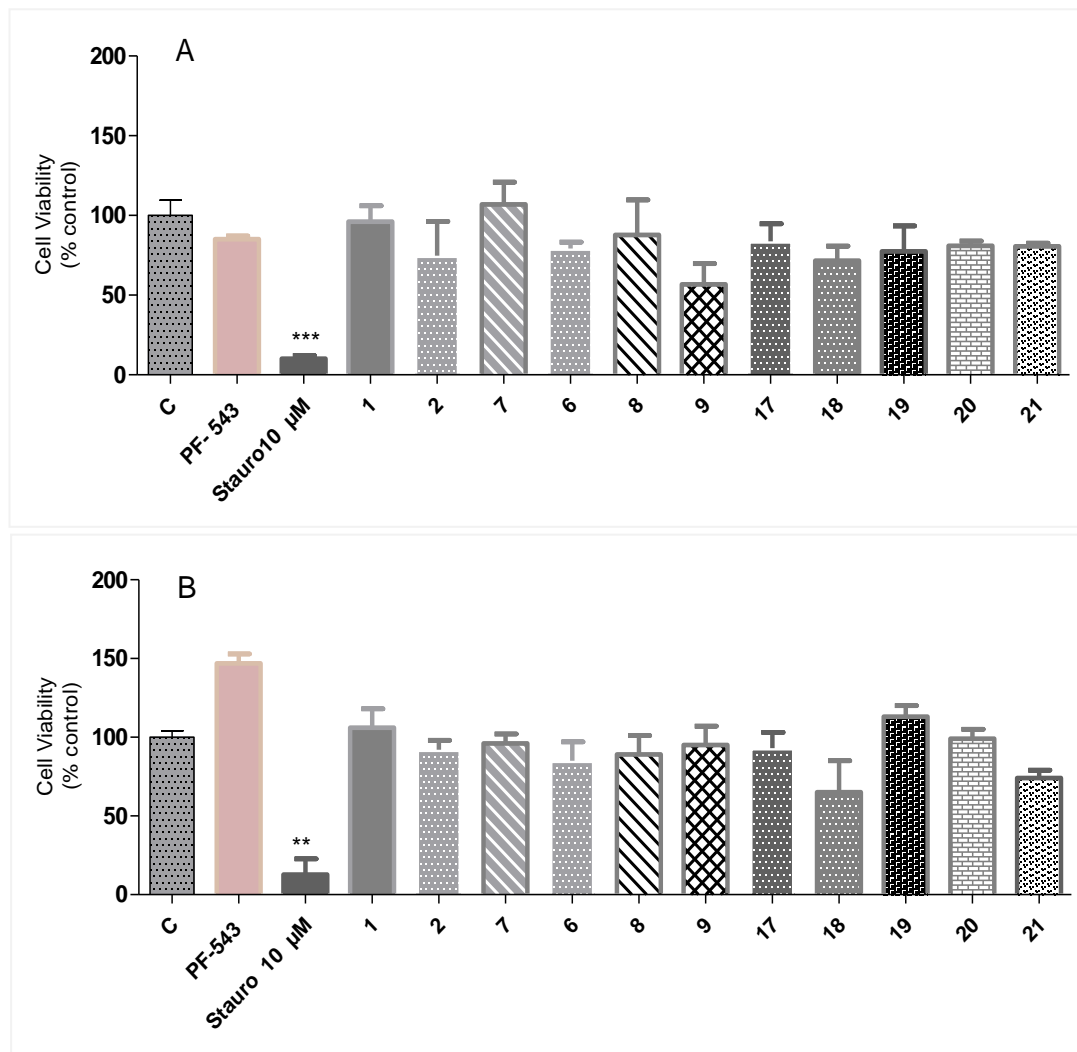
Figure 3.19. Effect of SK inhibitors (100 nM) on viability of LNCaP (A) and LNCaP AI (B) cells after 24 h. Cells were plated at 10000 cells/well in a 96-well plate. After overnight incubation, the cells were treated for 24 h with 100 nM of the SK inhibitors and staurosporine (10 µM) or with the vehicle alone (DMSO, 0.1% v/v), then the plate was incubated at (37°C in 5% CO_2). Results are expressed as means +/− SEM for n = 3 experiments. The data was analysed by Dunnett post-test, $p > 0.05$, ***$p < 0.001$ versus control (C).
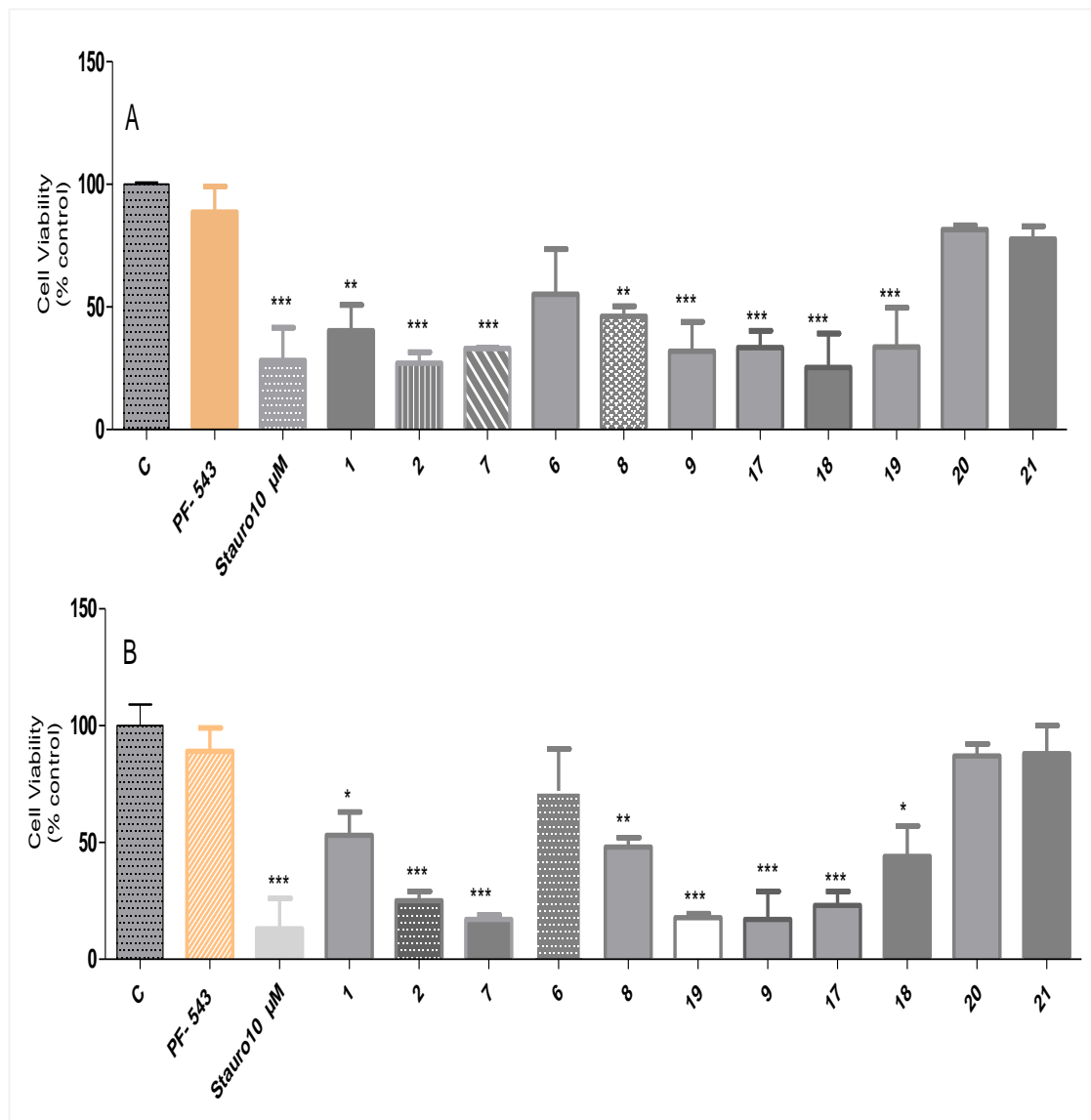
Figure 3.20. Effect SK inhibitors (10 µM) on viability of LNCaP (A) and LNCaP AI (B) cells after 24 h. Cells were plated at 10000 cells/well in a 96-well plate. After overnight incubation, the cells were treated for 24 h with the SK inhibitors and staurosporine (10µM) or with the vehicle alone (DMSO, 0.1% v/v), then the plate was incubated at 37°C in 5% CO_2. Results are expressed as means +/− SEM for n = 3 experiments. The data was analysed by Dunnett post-test, *p < 0.05, **p < 0.01, ***p < 0.001 versus control (C).

The cell viability IC_{50} of the selective SK1 inhibitor compound **9** (**Figure 3.21 A**) against LNCaP and LNCaP-AI was 8.9 and 6.9 µM, respectively, whilst compound **18** (SK1/SK2 inhibitor), (**Figure 3.21 B**) had comparable IC_{50} values of 7.6 and 6.2 µM, respectively. The cell viability IC_{50} values are higher than the effects seen in cells at the pharmacodynamic SK1 level (100 nM), which suggests that these inhibitors could be targeting other enzymes in S1P/SK pathway in order to affect phenotypic outputs such as viability. This is also reflected by the higher concentrations required to induce apoptosis. The absence of any effect on viability by compounds **20** and **21** at 10 µM suggests that SK2 is not involved in invoking this phenotype.
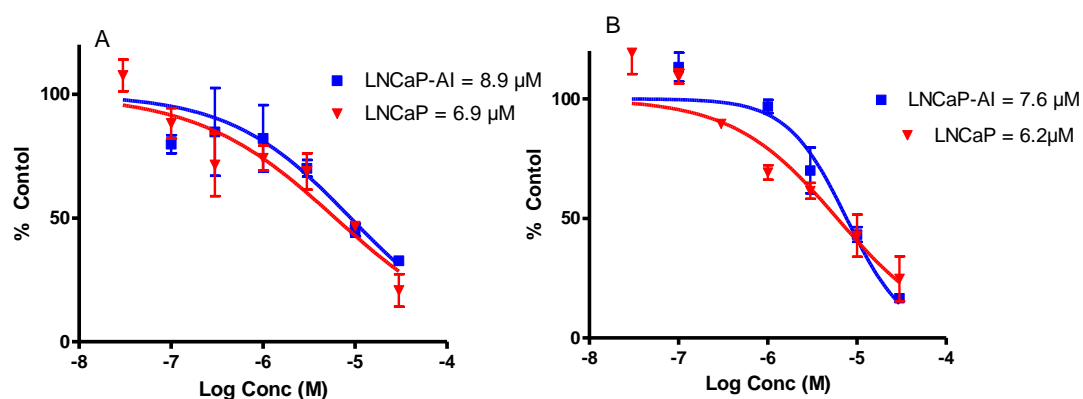
Figure 3.21. Cell viability IC_{50} for compounds 9 (A) and 18 (B) in LNCaP and LNCaP-AI cells after 24h. Cells were plated at 10000 cells/well in a 96-well plate. After overnight incubation, the cells were treated for 24 h with **9** or **18** (30µM-0.3nM) or with the vehicle alone (DMSO, 0.1% v/v), then the plate was incubated at 37°C in 5% CO_2. Results are expressed as means +/− SEM for n = 3 experiments. The data was analysed by Dunnett post-test, * *p < 0.05, **p < 0.01, ***p < 0.001 versus control.

3.2.6.2 Human cell line cell viability screening

Cytotoxicity against human normal prostatic cells (PNT2A) was then determined using the MTT assay method. This was conducted to determine whether the SK inhibitors reduced cell viability in a non-cancer cell line. For this purpose, two different concentrations of the SK inhibitors (100 nM and 10 µM for 24 h) were assessed against PNT2A cells. No reduction in cell viability was observed across the series, although compound **18** (**Figure 3.22**) did have an effect at 10 µM. These data demonstrated that there is a therapeutic window for compounds such as 9 and 18, which can reduce the viability of LNCaP and LNCap-AI cells with IC_{50}'s lower than 10 µM without affecting normal prostate cells.
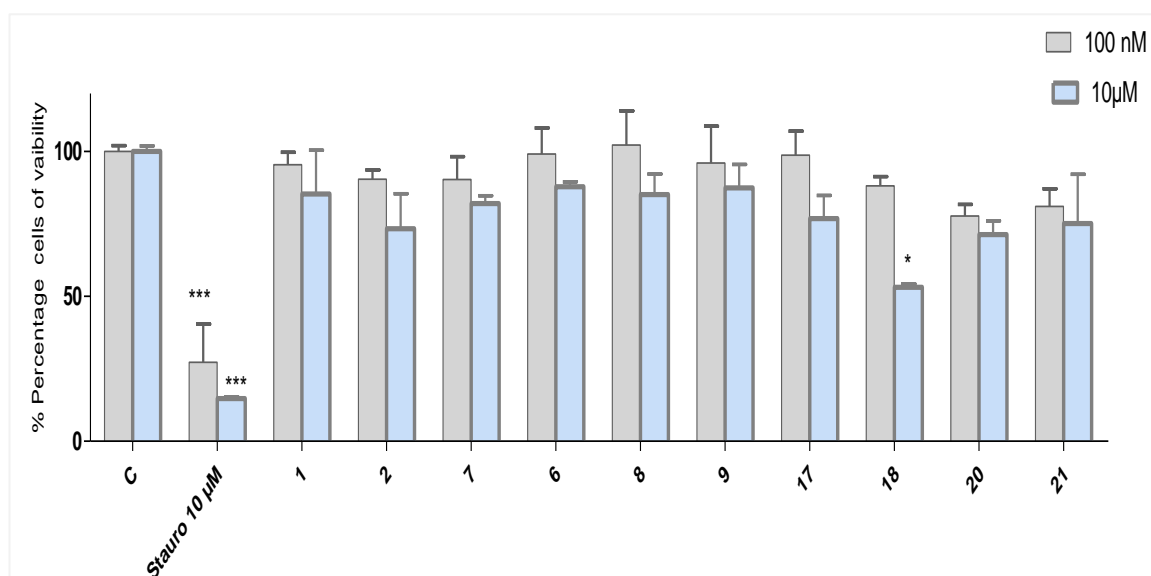
Figure 3.22. **Effect of SK inhibitors on viability of PNT2A cells.** Cells were plated at 10000 cells/well in a 96-well plate. After overnight incubation, the cells were treated for 24 h with SK inhibitors (100 nM or 10 µM) and staurosporine (10µM) or with the vehicle alone (DMSO, 0.1% v/v), then the plate was incubated at 37°C in 5% CO_2. Results are expressed as means +/− SEM for n = .3 experiments. The data was analysed by Dunnett post-test, ***p < 0.001 versus control (C).

3.2.7 Effect of new SK inhibitors on DNA synthesis in LNCaP and LNCaP-AI cells

A previous study by our group provided evidence of a link between SK1 inhibition in LNCaP-AI cells and growth arrest. [39] We therefore examined whether our new SK inhibitors had a similar effect. The effect of compounds on LNCaP and LNCaP-AI cell proliferation was investigated by measuring [^{3}H] thymidine uptake into newly synthesised DNA (**Chapter 5 section 5.3.1**). Cells were exposed to 100 nM or 10 µM of SK inhibitors for 24 h (**Figures 3.23** and **3.24**, respectively), with no reduction in DNA synthesis evident at 100 nM. Conversely, a reduction in proliferation for SKi and compounds **1**, **2**, **7**, **8** and **9** compared with control cells occurred at 10 µM, but not for the selective SK2 inhibitors **20** and **21** (**Figure 3.24**).
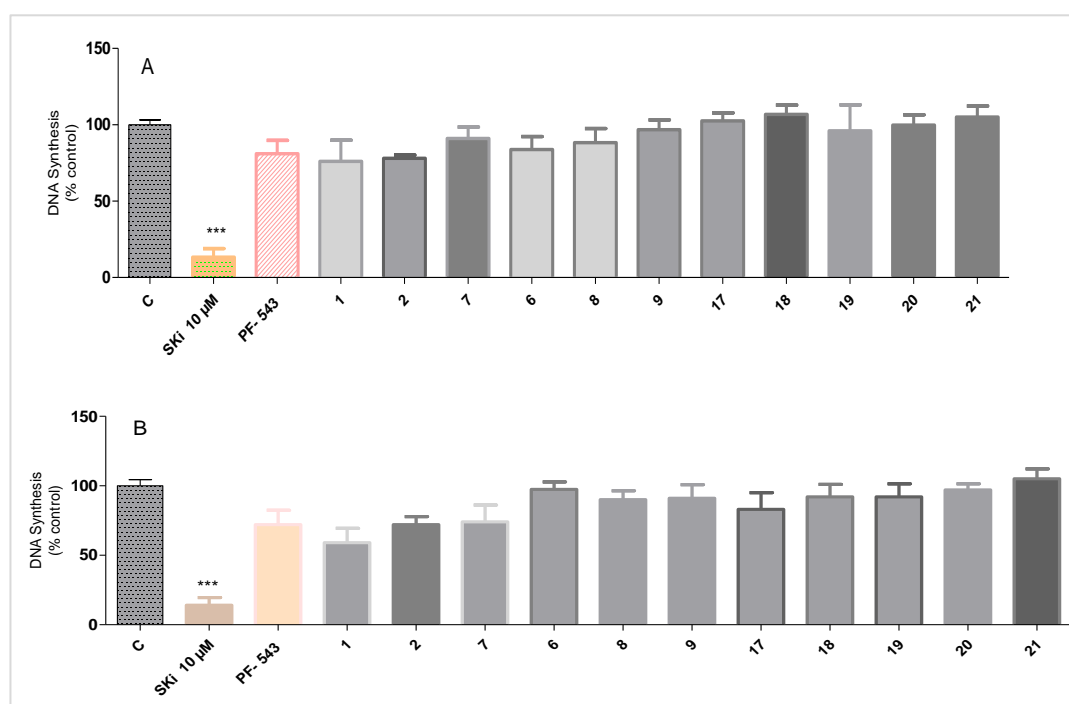
Figure 3.23. Effect of SK inhibitors on DNA synthesis of LNCaP (A) and LNCaP AI (B) cells after 24 h. Cells were seeded in a 96 well plate at 10000 cells per well in complete medium and incubated for 24 h. After overnight incubation, the cells were treated for 24 h with SKi (10M, positive control) and SK inhibitors (100 nM) or with the vehicle alone (DMSO, 0.1% v/v), then the plate was incubated at 37°C in 5% CO_2. Results are expressed as means +/− SEM for n = 3 experiments. The data was analysed by Dunnett post-test p > 0.05, ***p < 0.001 versus control (C).
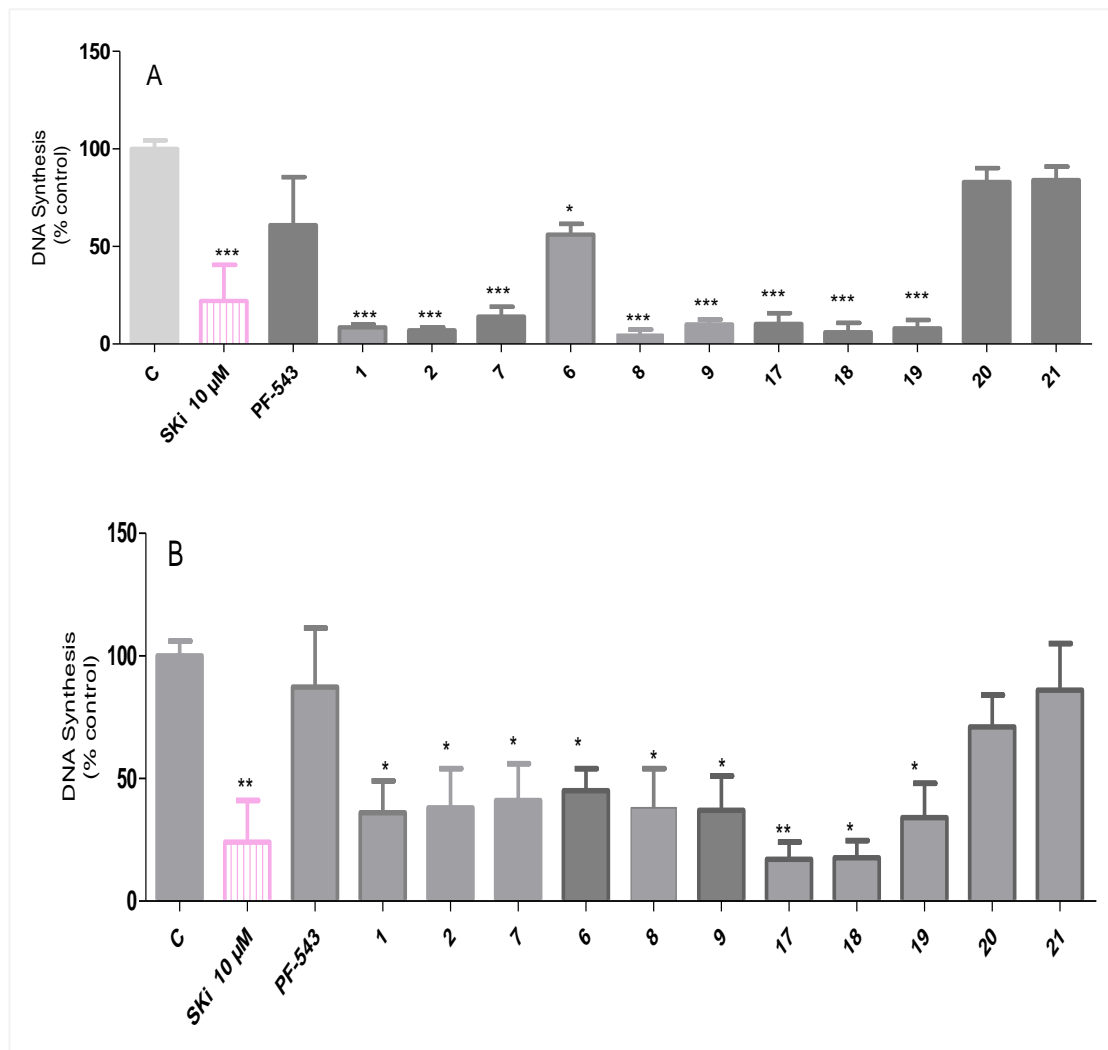
Figure 3.24. Effect of SK inhibitors on DNA synthesis of LNCaP (A) and LNCaP AI (B) cells after 24 h. Cells were seeded in a 96 well plate at 1x104 cells per well in complete medium and incubated for 24 h. After overnight incubation, the cells were treated for 24 h with SKi (10 µM) and SK inhibitors (10 µM) or with the vehicle alone (DMSO, 0.1% v/v), then the plate was incubated at 37°C in 5% CO_2. Results are expressed as means +/− SEM for n = 3 experiments. The data was analysed by Dunnett post-test, *p < 0.05, **p < 0.01 versus control (C).

3.2.8 Effect of SK inhibitors on Caspase-3/7 activity in LNCaP and LNCaP-AI cells

Further experiments were performed to investigate the mechanism underlying the reduction in cell viability of LNCaP and LNCaP-AI induced by our SK inhibitors. When cells were incubated at 100 nM and 10 µM concentrations for 24h, our compounds did not induce any activation of caspase 3/7 (**Figure 3.25: Figure 3.26**). This finding excludes any role for caspase-3/7-related apoptotic signaling for our SK inhibitors in prostate cancer cell viability.
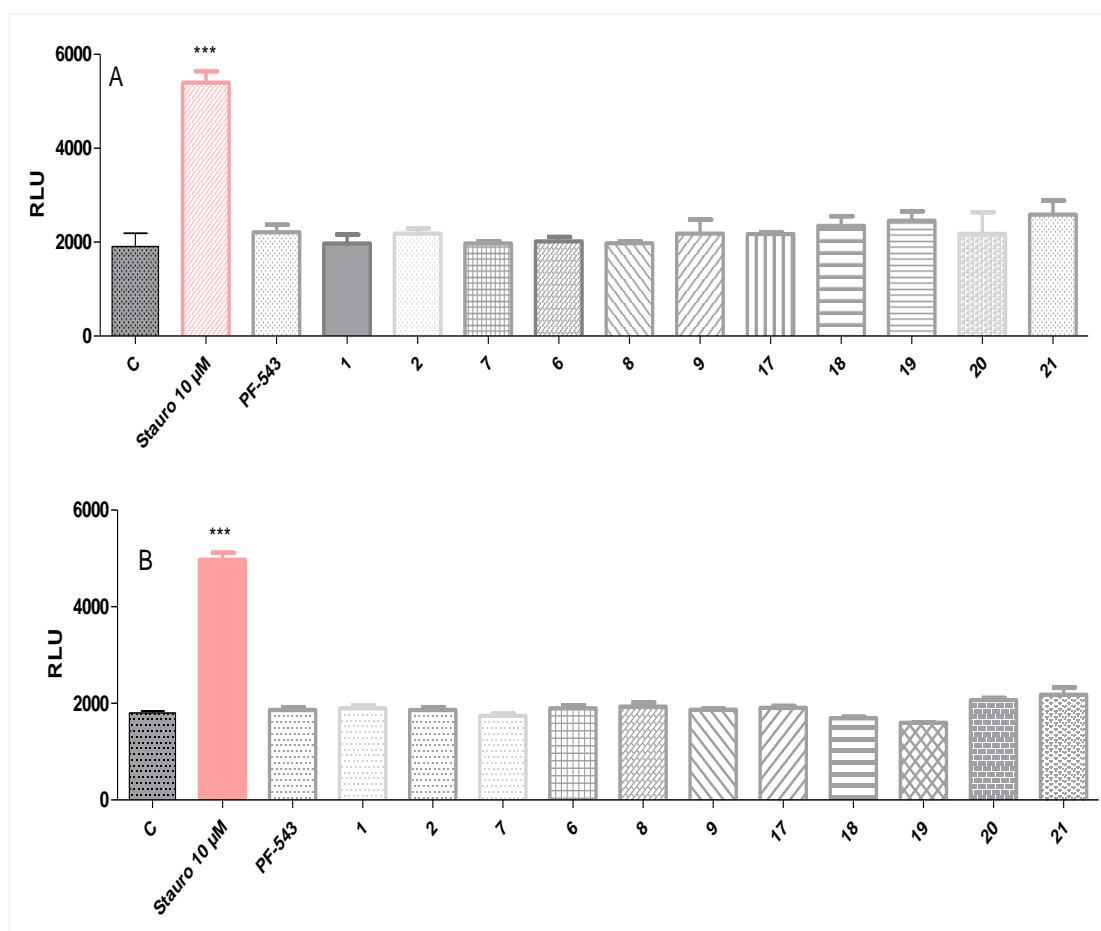
Figure 3.25. **Effect of SK inhibitors on caspase-3/7 activity in LNCaP (A) and LNCaP AI (B) cells.** Cells were plated at 10000 cells/well in a 96-well plate. After overnight incubation, the cells were treated for 24 h with SK inhibitors (100 nM) and staurosporine (Stau, 10 µM), or with the vehicle alone (DMSO, 0.1% v/v) then the plate was incubated at 37°C in 5% CO_2. Results are expressed as means $+/-$ SEM for n = 3 experiments. The data was analysed by Dunnett post-test, $p > 0.05$, ***$p < 0.001$ versus control (C)
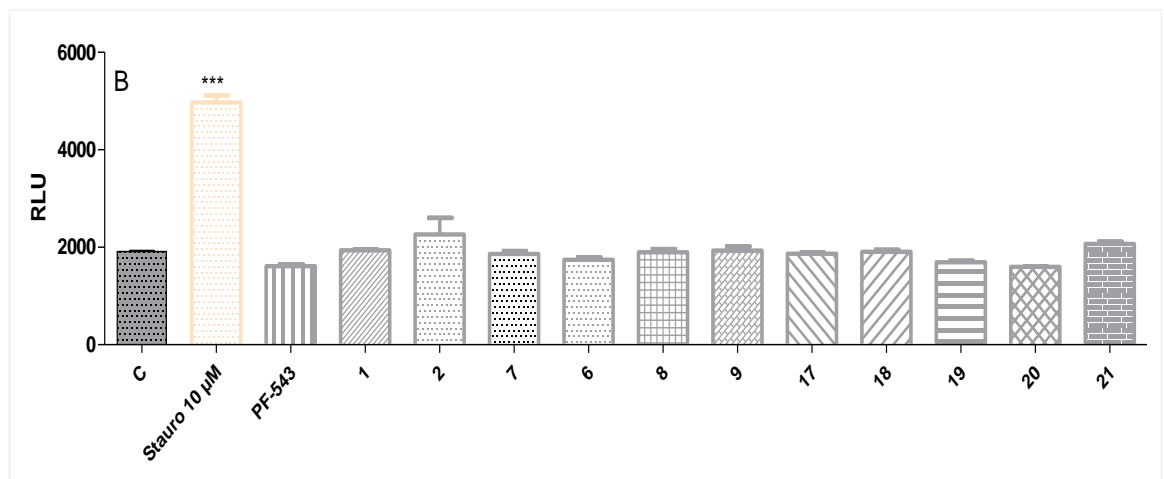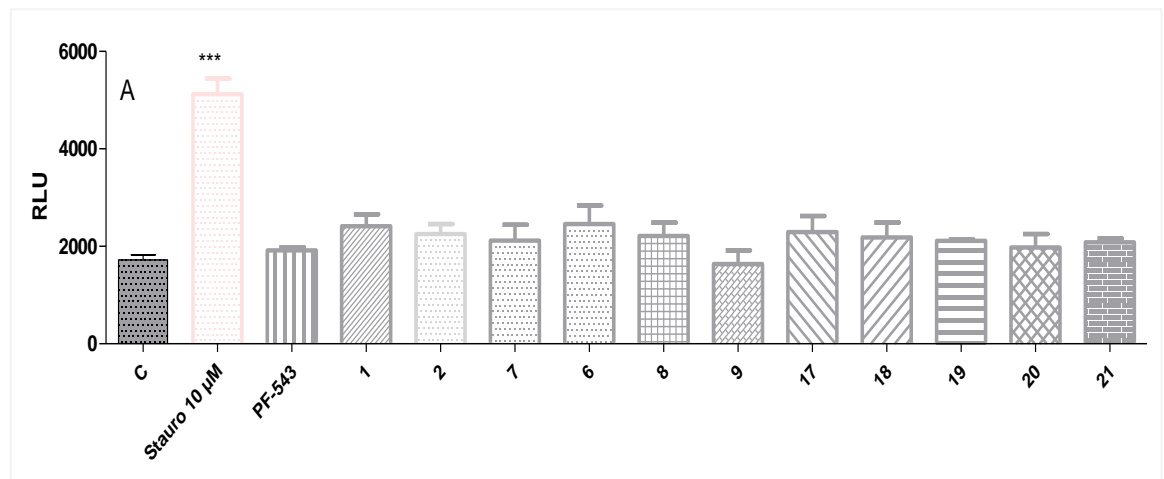
Figure 3.26. Effect of SK inhibitors on caspase-3/7 activity in LNCaP (A) and LNCaP AI (B) cells. Cells were plated at 10000 cells/well in a 96-well plate. After overnight incubation, the cells were treated for 24 h with SK inhibitors (10 µM) and staurosporine (stau, 10 µM), or with the vehicle alone (DMSO, 0.1% v/v), then the plate was incubated at 37°C in 5% CO_2. Results are expressed as means +/− SEM for n = 3 experiments. The data was analysed by Dunnett post-test, $p > 0.05$, ***$p < 0.001$ versus control (C).

3.2.9 Effect of novel SK inhibitors on autophagy in LNCaP and LNCaP-AI cells

Autophagy is highly regulated process that involves the degradation of cytoplasmic components within lysosomes. [246] Nutrient insufficiency commonly develops in actively growing solid tumors and nutrient starvation has been shown to stimulate SK1 in breast cancer cells and trigger autophagy to maintain cell growth in the absence of extracellular nutrients. [247] Hence, autophagy induced by SK1 may represent a momentary adaptive response that allows cancers cells to persist and proliferate in the absence of nutrients until neovascularization of the tumour mass occurs. SK2 appears to inhibit autophagy in LNCaP and LNCaP-AI cells. [184] Previous studies have shown that the ceramide/S1P rheostat is also involved in regulating autophagy. [247–249] Moreover, a previous study showed that treatment with the dual SK1/2 inhibitor SKi inhibits the autophagic pathway in both LNCaP and LNCaP-AI cell lines. However, the SK2-specific inhibitor ROMe induced an autophagy response in LNCaP and LNCaP-AI cells.[243]

We next assessed whether our SK inhibitors induced a reduction in cell viability by modulation of the autophagic process in LNCaP cells. Initially, we assessed the effect of SK inhibitors on LNCaP cell viability in the absence or presence of bafilomycin A1 (baf-A1), a known inhibitor of autophagy. [250] Studies by Daniel *et al.,* found that treatment with 100 nM baf-A1 for 1 h blocks the fusion of autophagosomes with lysosomes in the rat hematoma H-4-II-E cell line. [251] As shown in **Figure 3.27**, MTT assays showed that Baf-A1 reversed the reduction in cell viability induced by ROMe in LNCaP cells. However, it did not have any effect on reversal of the reduction in cell viability induced by our new SK inhibitors (**Figure 3.27**). These data indicated that our inhibitors do not have their effect on cell viability through the autophagy pathway.
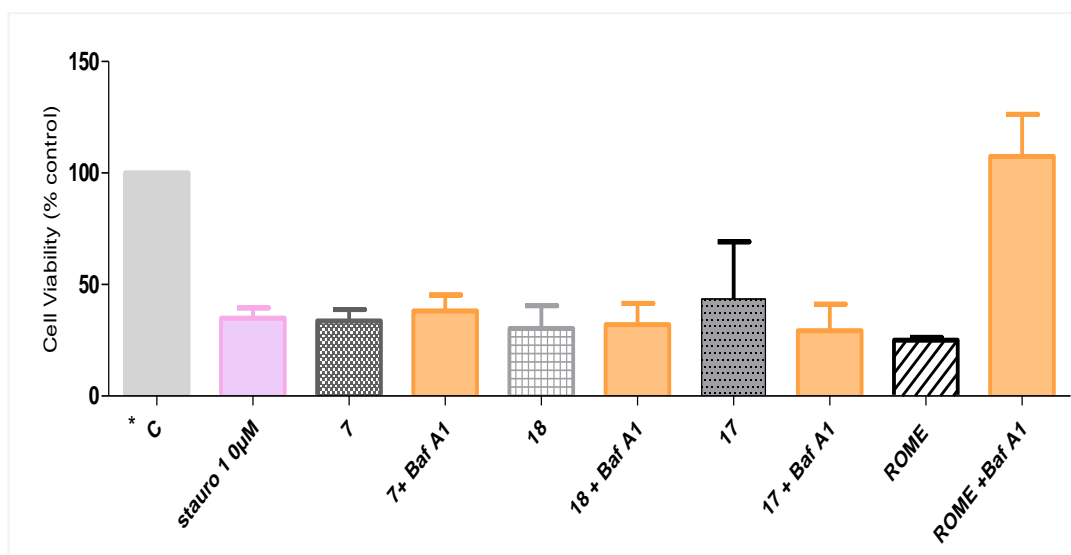
Figure 3.27. Effect of SK inhibitors on cell viability in the presence and absence of autophagy inhibitor, Bafilomycin A1 of LNCaP cells. Cells were seeded in a 96 well plate at 10000 cells per well in complete medium and incubated for 24 h. After overnight incubation, the cells were treated with 100 nM bafilomycin A1 for 1 h before being treated for 24 h with staurosporine (10 µM) and SK inhibitors (10 µM) or with the vehicle alone (DMSO, 0.1% v/v), then the plate was incubated at 37°C in 5% CO_2. Results are representative of two separate experiments.

3.2.10 Effect of SK inhibitors on p53 and p21 expression in LNCaP and LNCaP-AI cells

Previous studies have shown that inhibition of SK2 activity and down-regulation of SK1 expression with ABC294640 or dual inhibition of SK1/2 by SKi induce p53, a tumor suppressor gene active in the cellular response to DNA damage and cell cycle arrest,[39] and p21, an anticancer protein specific to senescence [252] in LNCaP AI cells. In common with SKi, treatment of LNCaP-AI cells for 24 h with exemplars from our new series induced a substantial increase in p53 expression at 10 µM (**Figure 3.28**).

Furthermore, the induction of p21 was also observed when LNCaP-AI cells were treated with 10 µM concentrations for 24 h (**Figure 3.29**). Our new SK inhibitors may therfore be inducing senescent death of LNCaP AI cells at 10 µM via the induction of p53 and p21.
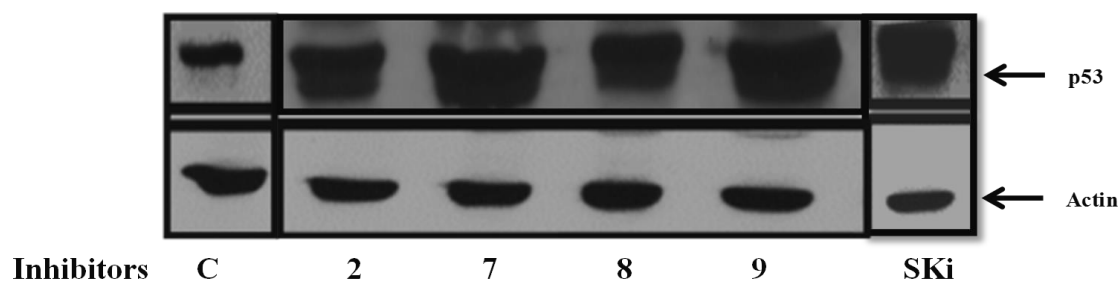
Figure 3.28. Effect of SK inhibitors on p53 expression in LNCaP-AI cells. Cells were treated for 24 h with SK inhibitors (10 μM) or vehicle (DMSO, 0.1% v/v) as indicated. p53 protein levels were then examined by western blotting analysis using specific antibodies for p53 (53 kDa). Blots were stripped and re-probed with anti-actin antibody to ensure comparable protein loading between samples. Results are representative of two separate experiments.
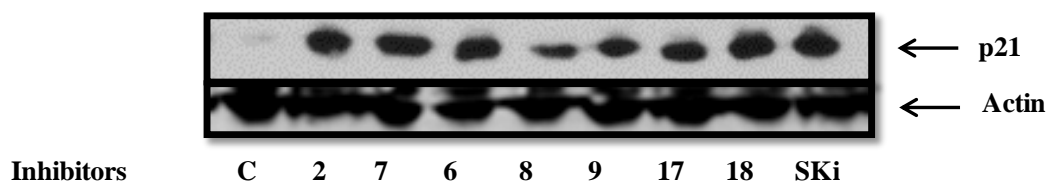
Figure 3.29. Effect of SK inhibitors on p21 expression in LNCaP-AI cells. Cells were treated for 24 h with SK inhibitors (10 μM) and SKi (10 μM) or with the vehicle alone (DMSO, 0.1% v/v) as indicated. Levels of p21 protein were then examined by western blotting analysis using specific antibodies for p21. Blots were stripped and re-probed with anti-actin antibody to ensure comparable protein loading between samples. Results are representative of two separate experiments.

3.2.11 Effect of our new SK inhibitors on Des1 expression in LNCaP AI cells

It has already been established that SKi reduces S1P levels and markedly increases sphingosine in prostate cancer cells and increases dihydroceramide levels in these cells by inhibition of dihydroceramide desaturase, Des1. [149] A recent study showed that ABC294640 and SKi induce the proteosomal degradation of Des1 (38 kDa) in LNCaP-AI cells. [39] To investigate whether our new SK inhibitors had a similar a role in regulating Des1 expression, LNCaP-AI cells were treated with SK inhibitors at 100 and 300 nM for 24 h before immunoblotting cell lysates with an anti-Des1 antibody. Des1 was not downregulated after exposure to 100 nM (data not shown), although an

effect was seen at 300 nM for our SK1 and SK1/SK2 inhibitors. No effect was seen with our selective SK2 inhibitor compound **21** at this concentration.
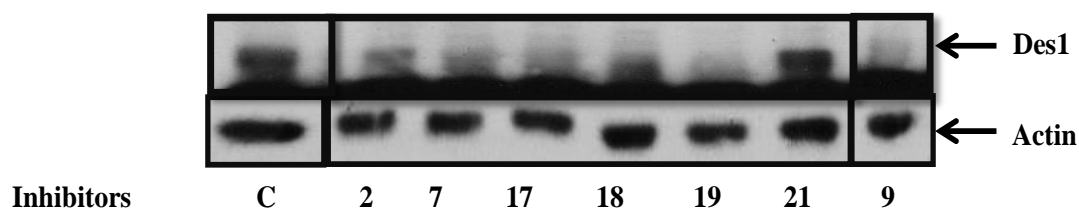
Figure 3.30. Effect of SK inhibitors on Des1 expression in androgen-independent LNCaP-AI cells. LNCaP-AI cells were treated for 24 h with SK inhibitors (300 nM) for 24 h with the vehicle alone (DMSO 0.1% v/v). Blots were stripped and re-probed with anti-actin antibody to ensure comparable protein loading between samples. Results are representative of one separate experiment. Note: blot was run by co-worker.

3.2.12 Effect of novel SK inhibitors at 10 μM on c-Myc expression levels.

Previous studies have shown that for SKi and ABC294640 to ablate SK1, direct activation of the proteasome is necessary; this in turn results in degradation of proteins such as Des1, SK1 and c-Myc, which are generally turned over rapidly through this route. The ability of our compounds to activate the proteasome was also measured at the protein level of c-Myc. A high concentration of these compounds (10 µM) decreased c-Myc expression levels in LNCaP-AI cells (**Figure 3.31**), which suggests that similar to SKi, these compounds are an activator of the proteasome at this concentration.
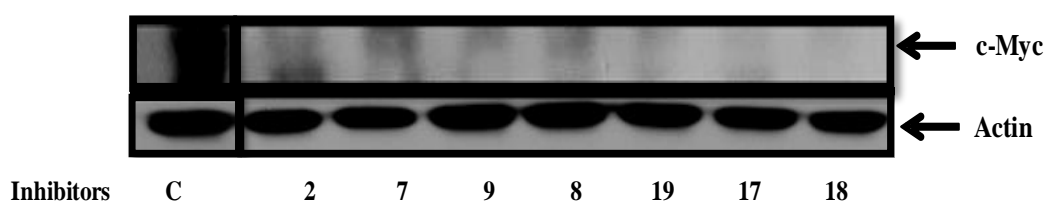
Figure 3.31. Effect of SK inhibitors on c-Myc expression in LNCaP-AI cells. Cells were treated for 24 h with **2**, **7**, **9**, **8**, **17** or **18** (10 M) or with the vehicle alone (DMSO, 0.1% v/v.). c-Myc protein levels were then examined by western blotting analysis using specific antibodies for c-Myc (57 kDa). Blots were stripped and re-probed with anti-actin antibody to ensure comparable protein loading between samples. This experiment was performed once.

3.3 Discussion

3.3.1 Proteasomal degradation of SK1

The data presented in the current chapter demonstrates that **PF-543** or the selective SK1 inhibitor, compound **9** and SK1/SK2 inhibitors, compounds **1**, **2**, **7**, **8**, **17** and **18** but not the SK2 selective inhibitors, compounds **21** and **20**, induced degradation of SK1 in LNCaP and LNCaP-AI and hPSMAC cells that could be reversed by the proteasome inhibitor, MG132 (**Figure 3.6: Figure 3.7**). Unfortunately, due to lack of commercial antibodies sufficiently sensitive to detect SK2 protein, attempts to determine whether SK2 was subject to the same regulation by the proteasome were unsuccessful (data not shown). The role for the lysosome in the degradation of SK1 in response to **PF-543** and the SK inhibitors (**Figure 3.8; Figure 3.9**) is excluded because SK1 degradation was not reversed with the specific lysosomal cathepsin B inhibitor, CA074Me. Our group has previously shown that the SK1/2 inhibitor, SKi, induces proteasome activation and subsequent degradation of SK1, cyclin D1 and c-Myc in LNCaP-AI and LNCaP cells. [129,243] However, the selective SK1 inhibitors, **PF-543** and RB005 [39] or SK2 inhibitor ROMe, failed to modulate c-Myc or cyclin D expression in these cells.[128] In line with previous findings, our new SK2 selective inhibitors (compounds **20** and **21**), as well as the selective SK1 inhibitors **PF-543** and compound **9**, failed to modulate c-Myc expression in LNCaP-AI cells at 100 nM concentration. In contrast with SKi, the dual SK1/SK2 inhibitor compound **7** (100 nM) showed no effect on c-Myc expression levels in these cells, suggesting that the inhibition of both SK1 and SK2 together is not solely responsible for the removal of c-Myc. Instead inhibition of Des1 is necessary to activate the proteasome (see later) and compound **7** has no effect on Des1 at 100 nM. The findings in this study suggest that the new SK inhibitors cannot be considered as direct proteasomal activators at 100 nM because of their failure to induce down-regulation of c-Myc. Previous reports have demonstrated that SK1 can be polyubiquitinated and degraded by the proteasome, [129,253] which is consistent with the suggestion that these inhibitors at 100 nM could simply bind directly to SK1, leading to a conformational change in SK1,targeting it for polyubiquitination and degradation by the proteasome.

3.3.2 Elucidation of mechanisms underlying the concentration dependent (100 nM or 10 µM) effect of novel SK1, SK1/2 inhibitors on the survival LNCaP and LNCaP-AI

This study demonstrates that the new SK inhibitors have a dose-dependent effect on the survival of LNCaP and LNCaP-AI cells, which is due to their differential effects on SK1 and Des1 expression. Thus, low concentrations of these inhibitors (100 nM) reduce the expression of SK1 via direct binding without affecting the expression of Des1 (NJP and SP, unpublished). However, high concentrations of these inhibitors (10 µM) induce a reduction in Des1 expression via a mechanism that involves proteasome activation (detailed below). Thus, the effect of SK1 inhibitors on proteasomal degradation is a direct effect whereas the Des1 and c-Myc response occurs at a higher concentration through an indirect effect on the proteasome. The results in our study showed that the new SK inhibitors at 10 µM modulate proliferation and growth of LNCaP and LNCaP-AI cells, possibly via a combined action on Des1 and SK1 (**Figure 3.20: Figure 3.24**). To elucidate the possible mechanisms of the inhibitors' effects on cell survival in relation to SK1/Des1 inhibition and removal from these cells, a wide range of cell death mechanisms such as apoptosis, autophagy and growth arrest were investigated.

3.3.3 Effect of the new SK inhibitors on growth arrest of LNCaP and LNCaP-AI cells

There are two models proposed that might explain induction of the growth arrest observed with the new SK inhibitors at high concentrations (10 µM). These are as follows:

A) SK1 and Des1 inhibition and the accumulation of dihydroceramide

Both SKs and Des1, the last enzyme in the *de novo* synthesis of ceramide (Cer), are of interest as therapeutic targets. The concept of targeting Des1 to promote growth arrest in cancer cells is supported by several studies. [39,173,254] For example, Kraveka *et al.* showed that in SMS-KCNR neuroblastoma cancer cells, siRNA knockdown of Des1increased dihydroceramide levels and inhibited cell growth, promoting cell cycle arrest at G0/G1. [173] Consistent with this study, others have shown that the dual

SK1/SK2 inhibitor, SKi, results in a substantial increase in dihydroceramide levels and that SKi is a non-competitive inhibitor ($Ki = 0.3$ μM) of Des1.[129,184,254] It has been established that inhibition was indirect and could result from inhibition of NADH-cytochrome b5 reductase. [254,255] Cingolani *et al.,* also demonstrated that SKi reduced cell proliferation that was linked to inhibition of Des1 and subsequent accumulation of dihydroceramide.[254]

Venant *et al.* also found that the SK2 inhibitor ABC294640 decreases the growth of prostate cancer cells via inhibition of Des1 activity and a subsequent accumulation of dihydroceramide levels in these cells.[256] In addition, a study by our group proposed that Des1 has a role in restricting protein degradation via the proteasome. Therefore, an increase in the proteasomal degradation of SK1a and Des1 was associated with Des1 inhibition by SKi or ABC294640. [39] A recent study suggested that Des1 inhibition was responsible for growth arrest rather than SK1; however, our group has suggested that both SK1 and Des1 inhibition were responsible for growth arrest. This is an indirect effect of SK inhibitors on the proteasomal degradation (by activation of the proteasome) of SK1a and which can be differentiated for direct inducers of proteasomal degradation (e.g. **PF-543**).

Consistent with these reports, the current study demonstrated that our novel SK1 inhibitors at high 10 µM concentrations might induce growth arrest and non-apoptotic death by a mechanism that involves proteasomal degradation of both SK1 and Des1. Indeed, 300 nM of the SK inhibitors removed Des1 from LNCaP-AI cell (**Figure 3.30**), and therefore, it follows that Des1 will be inhibited at the higher concentration of 10 µM used in this study. The proposed mechanism by which the new SK inhibitors induce LNCaP and LNCaP-AI cell growth arrest may involve accumulation of dihydroceramide and subsequent activation of the proteasome via modulation of the *de novo* ceramide pathway, which may affect the balance between dihydroceramides and Cer species. [254] The activation of the proteasome using 10 µM of the new SK inhibitors was confirmed by removal of c-Myc (**Figure 3.31**). Taken together, the findings provide strong evidence that the potential mechanisms by which the new SK inhibitors (10 µM) arrest cell growth include reduced expression of SK1, Des1 and c-Myc. Nonetheless, further investigation is required to confirm this possibility.

In contrast, our results showed that the SK1 selective inhibitor, **PF-543** (10 µM) and the SK2 selective inhibitor, compound **21** (10 µM), failed to remove Des1 (**Figure 3.30**) and to inhibit proliferation of LNCaP-AI or LNCaP cells (**Figure 3.20**). These findings are entirely consistent with previous studies showing that SK2 inhibition in isolation does not have any growth inhibitory effects on PC3 cells. However, removal of Des1 either by Des1 only inhibitors, the dual SK1/SK2 inhibitor, SKi or its analogues that are SK1 inhibitors was considered as the primarily cause of induced-antiproliferative effects on prostate cancer (PC3) cells. [257]

The cell proliferation, cell growth, and apoptosis assays demonstrated that the new SK inhibitors (SK1 selective, SK2 selective and non-selective SK1/2 inhibitors) do not produce an anti-proliferative effect or induce growth arrest of LNCaP and LNCaP-AI cells at 100 nM; a concentration which induces proteasome degradation of SK1 by direct binding and has no effect on Des1 in LNCaP-AI cells.

B) Growth arrest in LNCaP-AI via the p53/p21-dependent pathway

This study provides strong evidence that the SK1 and SK1/SK2 inhibitors, compounds **1**, **2**, **6**, 7, **8**, **9**, **17**, **18**, and **19** (10 µM) induce inhibition of DNA synthesis (**Figure 3.24**) and promoted the expression of senescent markers p53/p21 at 10 µM (**Figures 3.28: Figure 3.29**), which is associated with modulation of both Des1 and SK1.

In support of this, a previous study by our group showed that proteasomal degradation of SK1 and inhibition of Des1 by SKi or ABC294640 induced growth arrest in LNCaP-AI via the p53/p21-dependent pathway. [39] Thus, SKi and ABC294640 induced an increase in p53 and p21 expression. The same study suggested that the effects of SKi and ABC294640 on p53 expression was mediated by Des1 inhibition, whereas the increase in p21 expression induced by SKi or ABC294640 might involve regulation by both Des1 and SK. [39] This was based on the finding that siRNA knockdown of Des1 induced an increase in p53 expression, while siRNA knockdown of both SK1 and Des1 was required to increase p21 expression. [39] Therefore, when both SK1 and Des1 are removed, it is possible that LNCaP-AI cells undergo growth arrest or senescent death. [39] Senescence is a tumour suppression mechanism that involve permanent growth arrest and it can be triggered by any cellular stresses or unrepaired DNA damage. [258,259]

Recently, the role of senescence, in cancer cell death has been widely investigated; it has been found that senescence induction is associated with activation of p21 and p53 as well as ablation of c-Myc abrogation. [252]

In contrast, our results showed that the the SK2 selective inhibitor, compound **21** (10 μM), failed to ablate Des1 (**Figure 3.30**), to induce accumulation p53/p21 (data not shown), and to inhibit DNA synthesis of LNCaP-AI (**Figure 3.24**). These findings are entirely consistent with previous studies showing that the SK2 selective inhibitor, ROMe, failed to to induce an increase in p53/p21 level and subsequent growth arrest of LNCaP-AI. [39] In terms of the concentration dependent effects on growth arrest, 100 nM of the panel of new SK inhibitors can only remove SK1 by a direct binding mechanism, but not Des1 (data not shown), hence, these inhibitors failed to induce accumulation of p53 and p21 (data not shown), markers of cells undergoing growth arrest or senesence.

3.3.4 Exclusion of caspase-3/7-dependent apoptosis and autophagy pathways

This study demonstrated that the new SK inhibitors (at 100 nM or 10 μM) lacked the ability to induce caspase 3/7 activation in LNCaP and LNCaP-AI. Well-known mechanisms of cell death, such as apoptosis, were considered as potential mechanisms by which inhibition of SK1 induce cell death. Previous studies have shown that SK1 and SK1/SK2 inhibitors, such as SKI-178 and SKi induce apoptosis in a variety of cancer cell lines, including human acute myeloid leukaemia and LNCaP cells. [129,260]However, the SK2-specific inhibitor, ROMe, does not affect Cer levels nor does it induce apoptosis in LNCaP cells. [184,201,260] Moreover, the mechanism by which SKi or SKI-178 induce apoptosis in NKLGL cells is associated with increased Cer and decreased S1P levels, consistent with inhibition of SK1 and in line with the predicted outcome of modulating the sphingolipid rheostat via elevation of the Cer level, which in turn activates caspase-3/7-mediated apoptosis. [22] A number of studies supporting this concept have shown that siRNA knockdown of SK1 or treatment with SK1 inhibitors reduces the viability of prostate cancer cells; an effect that was linked to an increased ceramide/S1P ratio. [144,145,149,183] SKi induces apoptosis of LNCaP cells via

modulation of Cer (C22:0) levels. However, these ceramides do not change in LNCaP-AI cells which are resistant to SKi-induced apoptosis. [129]

It has been demonstrated in LNCaP cells that both SK1a and SK1b are degraded by the proteasome in response to SKi [129] and this leads to an increase in C22:0 Cer levels. However, in LNCaP-AI cells, SK1a is degraded but SK1b is resistant to SKi. Consequently, there is no increase in C22:0 Cer because SK1b is still present to remove it and LNCaP-AI cells do not undergo apoptosis because SK1b is still present and can exert a protective effect by removing C22:0 Cer. [129] Nonetheless, SKi (10 µM) inhibits Des1 and induces proteasomal degradation of SK1a in LNCaP-AI cells and together this appears to be responsible for the increase in p53/p21 expression and subsequent growth arrest and possibly senescent cell death.

The mechanism outlined above might account for the resistance of LNCaP and LNCaP-AI cells to the new SK inhibitor-induced activation of caspase-3/7, which might be linked to the inability of these inhibitors to remove SK1b. However, this needs to be tested. The inhibitor SKi induces a compensatory mechanism that increases SK1b mRNA expression in cells to negate its removal by proteasomal degradation.[129] Therefore, resistance to apoptotic cell death can be overcome using a combination of siRNA to reduce the expression of SK1a and SK1b and SKi to activate the proteasome in LNCaP-AI cells. Under these conditions LNCaP-AI cells undergo apoptosis. [129]

The role of autophagy was suggested based on previous studies showing that inhibition of SK2 with ROMe induced autophagic cancer cell death. [212] For instance, ROMe inhibits DNA synthesis in breast cancer cells and induces the autophagic death of leukemic T-ALL cell lines. [212] In support, the reduction of cancer cell viability by another SK2 inhibitor, ABC294640 was associated with the activation of autophagy-mediated death. [261] The preliminary data presented in this study excluded the role of autophagy in SK2 or SK1/2-induced prostate cancer cell death. As shown in **Section 3.2.9**, the reduction in cell viability induced by ROMe in LNCaP cells was reversed by Baf-A1 (an inhibitor of the autophagy process), but not for the new SK inhibitors (**Figure 3.27**). Thus, these data indicated that the autophagy pathway is not modulated

by these inhibitors to affect cell viability, although further measurements are required to definitively exclude autophagy as a possibility.

3.3.5 Caspase-independent PARP cleavage is mediated by dihydroceramide accumulation in a dose-dependent manner

In this study, the role of caspase-dependent apoptosis has been excluded. Although the nature of the inhibitor-induced, caspase-independent apoptosis is not clear, it is suggested that PARP cleavage, an enzyme that plays a major role in the repair of damaged DNA, mediated by the dual SK1/SK2 inhibitors **1**, **2**, **7** and **6** (10 µM; **figure 3.18**) could occur by means of a caspase-independent mechanism.

Caspase-independent PARP cleavage can be induced by dihydroceramide and dihydrosphingosine and subsequent DNA fragmentation. Indeed, γ-tocopherol has been shown to interrupt *de novo* synthesis of sphingolipids and induce caspase-independent cell death.[262] Consistent with this study, the new SK inhibitor (10 µM)-induced PARP cleavage might contribute to a caspase-independent cell death, which may be triggered by accumulation of dihydroceramide because of inhibition of Des1 activity and the modulation of the *de novo* ceramide pathway. Indeed, Holliday and collaborators have shown that sphinganine, a specific inhibitor of Des1 (GT11), increases the level of the endogenous specific subset of dihydroceramide (C22:0 and C24:0) and induce cytotoxicity via a caspase-independent mechanism, increasing DNA damage and mixed cell death. [263] DNA damage is associated with sphingolipid metabolism.[264] It has been reported that in response to DNA damage, SK1 is down-regulated by p53 and the subsequent loss of SK1 is crucial for p53-mediated initiation of apoptosis (caspase 2 activation) or cell senescence. [37,265]

There is evidence to show that fenretinide, another Des1 inhibitor, represses cell proliferation (cell cycle) and induces caspase-independent apoptosis in multiple cancer types including via modulation of Bcl-2 family members. [266] Shen *et al*. also reported that fenretinide resulted in a 50% reduction in anti-apoptotic Bcl-2 mRNA expression in the LNCaP prostate cancer cells. [267] As discussed earlier, the inability of these inhibitors (100 nM) to be a direct activator of the proteasome and to remove Des1

could be linked to the absence of down-stream accumulation of dihydroceramide, which is a well-established regulator of caspase-independent apoptosis. [266,267]

3.4 Conclusion

The research reported in Chapter 3 has established that our new SK inhibitors at high concentrations induce growth arrest of LNCaP and LNCaP-AI cancer cells through activation of proteasome and p53/p21-dependent pathways (senescence) that requires removal of Des1. SK1 is removed by these inhibitors, possible through direct binding, and together at high concentrations induce a p21/p53-dependent growth arrest of prostate cancer cells. These results provide strong evidence that besides SK, Des1 may play a part in the cellular response to certain chemical treatments, which requires further investigation.

Chapter 4. **General Discussion**

Prostate cancer is one of the major diagnosed cancers in men and the second leading cause of cancer-related deaths in the UK, with 30 deaths every day.[268] In its early stages, there are some therapeutic approaches such as surgical prostatectomy, radiotherapy, hormonal and chemotherapeutic agents. Nonetheless, the vast majority of prostate cancer patients become resistant to these therapeutic treatments, due to the development of the incurable castration-resistant prostate cancer responsible for the high mortality rate amongst prostate cancer patients. [269] Currently, only palliative options are available for treatment of patients with advanced-resistant prostate cancer. [269] The development of effective therapeutic agents for prostate cancer has become a major goal for researchers in both academia and industry. This requires the identification of novel and valid targets, an understanding of the molecular mechanisms underlying prostate cancer and the discovery of new compounds for this target that can be developed into effective new drug therapies. Early drug discovery projects involve target validation and lead optimisation, followed by the establishment of *in vitro* (biopharmaceutical and pharmacokinetic properties) and *in vivo* efficacy before being approved for clinical trials.

Sphingosine kinase (SK1 and SK2) has become a major target for the treatment of prostate cancer (**Chapter 1, section 1.7**), with several SK inhibitors in preclinical studies or early stage clinical trials. One such inhibitor, ABC294640, is in clinical trials for the treatment of KSHV-associated lymphoma. [157] Consequently, there is a demand to develop compounds that can act on SK/S1P signalling pathway such as SK inhibitors. There are numerous studies establishing the role of SK1 and/or SK2 in prostate cancer (**Chapter 1, section 1.7**) and there is compelling evidence that SK participates in cancer progression. For example, it is involved in the positive selection of cancer cells with a survival and growth advantage as a result of its over-expression. [28,33,106] SK inhibitors may therefore represent a novel class of anti-cancer therapeutic agents. The aim of the project was to discover and characterise novel compounds that could be eventually developed into effective anti-cancer drugs by targeting the SK/S1P pathway.

An important step in any drug discovery research is the lead optimisation that aims to enhance the potency, selectivity and physicochemical properties to develop effective

drug leads. Effective lead optimisation depends mainly on chemical synthesis, computer-assisted modelling and robust functional assays.

The current study identified entirely new potent SK inhibitors using simple synthetic approaches that led to the discovery of the potent SK1 inhibitor, compound **9**, and shifted the selectivity toward SK2 as exemplified by compound **21**. Significantly, this study contributed toward the exploration of the SK2 structure via utilisation of computer modelling (**Chapter 2: section 2.3: Table 4.1**), which can be used to develop more potent SK2 inhibitors. Moreover, the current study revealed the role of SK1 and Des1 in the cellular mechanism of action of SK1 inhibitors (**Chapter 3: section 3.3**).

In chapter 2, a simple synthetic approach was developed to produce a library of compounds that has been screened for SK1 and/or SK2 activity using an in-house optimised ADP-Glo assay and the SAR of these compounds was extensively studied via computer modelling. The major SAR findings were as follows:

Modifications of the tail and linker regions of the molecules were critical for selectivity toward SK1 *versus* SK2. Furthermore, modifications of this tail-group were crucial for modulating the SK inhibitor activity. In addition, compounds with a sulfonate group (e.g. compounds **1** and **2**) provide better inhibitor potency against SK1 compared with SK2 (the smaller channel in SK2 results in compression, therefore steric hindrance might prevent high affinity binding of **1** and **2** to SK2). The introduction of a bulky substituent at the *para* position of the tail phenyl ring of library containing the sulfonate group caused a significant decrease in SK1 potency (e.g. compounds **3**, **4** and **5**), possibly through negative steric influences in the active site. However, the replacement of the phenyl ring with a bulk isobutyl group (e.g. compound **7**) restored the SK1 inhibitor activity. Furthermore, maintaining the bulkiness and reducing planarity by incorporating cyclohexane into the tail of molecule (instead of phenyl group) provided optimal activity and selectivity for SK1 (e.g. compound **9: Table 4.1**). Thus, compound **9** was the most potent and selective SK1 compound within the group, with compounds **10-14**, in which the sulfonate moiety was replaced by sulphonamide resulting in loss of SK inhibitor activity.

The replacement of the sulfone or sulfonate groups with the equivalent ethers resulted in compounds with SK2-over-SK1 selectivity. For example, compounds **17**, **18**, and **19** showed promising SK2-over-SK1 selectivity. Unlike the sulfonates library, the introduction of the *para* substituent at the tail phenyl ring of this library promoted the SK2-over-SK1 selectivity (e.g. compounds **20** and **21 Table: 4.1**). However, the isosteric replacement of the tail phenyl ring with a cyclohexane group decreased inhibitor selectivity and activity towards SK2 (compound **23**). Modification of the head group highlighted the importance of the chiral centre, the *R* stereochemistry, and the methyl hydroxyl group and pyrrolidine size of the ring for retaining SK inhibitor activity. This was confirmed by the lack of SK inhibitor activity for any compounds with an altered head group (compounds **24-28**).

The integral element of drug discovery projects is drug-like properties (e.g. solubility, stability, permeability, ADMET). One of the biggest challenges in drug discovery is to identify compounds that are "drug-like" i.e those with high potency combined with good physicochemical and ADMET properties. [237] This project revealed that the SK inhibitors **17**, **18** and **21** were lipophilic and like PF543, were predicted to have good Caco2 permeability and absorption (no efflux), which is essential for target binding and engagement. However, the solubility of these molecules requires improvement (**Chapter 2; section 2.5: Table 4.1**). Compounds **17** and **21** had promising properties in terms of drug-drug interactions suggested by the lack of effect on cytochrome P450 activity. However, metabolic studies revealed that these inhibitors were cleared rapidly, emphasising the need for more stable analogues if *in vivo* studies to progress (**Chapter 2; section 2.5**).

Research conducted in Chapter 3 explored the effect of the new SK inhibitors on SK1 expression in LNCaP, LNCaP-AI and hPSMAC cells. In addition, they were used to characterise the role of SK1 in regulating cell growth and death. The data demonstrated that some of the SK inhibitors induced proteasomal degradation of SK1 in LNCaP, LNcaP-AI cells and hPSMAC cells. It is known that SK inhibitors such as SKi can activate the proteasome to accelerate the degradation of SK1[129] and it has been proposed that this occurs via a Des1-dependent mechanism. [39] However, this study demonstrated that SK1 inhibitors at low nM concentration (e.g, compounds **7**, **8**, and

9) did not activate the proteasome as evidenced by their lack of effect on c-Myc levels (**Chapter 3: sections 3.2.3: Table 4.1**). Instead, it is proposed that these inhibitors bind directly to SK1 (in agreement with the K_i for inhibition of SK1 catalytic activity) to enhance its degradation by the proteasome. These inhibitors bind strongly to SK1 due to their chemical structure and lipophilic properties that might enhance their interaction with the target. The mechanisms of SK1 removal (direct binding or proteasomal activation) could be distinguished by effects on c-Myc, which are removed by SK inhibitors that activate the proteasome and not by SK1 inhibitors that promote degradation of SK1 by direct binding.
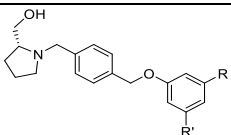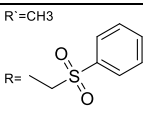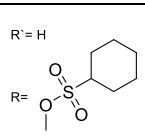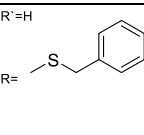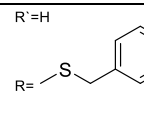
Data presented in Chapter 3 revealed that inhibitors modulate proliferation and growth of LNCaP and LNCaP-AI cells in a dose-dependent manner. Treatment with 100 nM concentrations of the new inhibitors only removed SK1 by a direct binding mechanism, but not Des1 or c-Myc. Hence, at this concentration these SK inhibitors failed to activate the proteasome and consequently to induce growth arrest, caspase3/7 activation and cell death (**Chapter 3: section 3.2.8**). However, at 10 µM concentrations, the inhibitors induced growth arrest via a p21/p53-dependent pathway in LNCaP and LNCaP-AI cells, possibly due to the combined SK1 and Des1 ablation. This is supported by the fact that the inhibition of both SK1 and Des1 has been shown to be associated with the accumulation of p53 and p21, markers of cells undergoing growth arrest and senescence. [39] The research also demonstrated that the new SK inhibitors induced caspase-independent cell death, possibly mediated by Des1 inhibition. Thus, the new SK inhibitors at 10 µM, but not 100 nM, induced PARP cleavage. This finding is in line with a previous report that interruption of *de novo* synthesis of sphingolipids after treatment of LNCaP cells with γ-tocopherol induced a caspase-independent PARP cleavage that has been linked to a high level of dihydroceramide and dihydrosphingosine accumulation and subsequent DNA fragmentation in these cells. [262]

Of note is that the current study revealed an entirely new mechanism of action of SK1 inhibitors. The results suggested that SK1 and Des1 may function together to modulate cancer cell survival and revealed the importance of other metabolites in the SK/S1P

pathway, such as dihydroceramide and dihydrosphingosine, in maintaining prostate cancer cell survival.

Table 4.1 Full profile of hit compounds **9**, **18** and **21** vs **PF-543**.

Property	PF543	9	18	21
	R`=CH3 	R`= H 	R`=H 	R`=H
Pharmacological data				
SK1 (IC_{50})	100 nM	63 nM	244 nM	No Effect
SK2 (IC_{50})	1000 nM	No Effect	147 nM	206 nM
SK1 degradation: lNCaP	100 nM	100 nM	100 nM	No Effect
SK2 degradation LNCaP-AI	100 nM	100 nM	No effect	No Effect
Cell-viability (IC_{50}): LNCaP	No effect	8.9 μM	6.9 μM	No effect
Cell-viability (IC_{50}): LNCaP-AI	No effect	7.6 μM	6.2μM	No effect
Caspase 3/7 LNCaP	No effect	10 μM	10 μM	No effect
Caspase 3/7 LNCaP-AI	No effect	10 μM	10 μM	No effect
P21/P53	No effect	10 μM	10 μM	No effect
C-Myc degredation	No effect	10 μM	10 μM	No effect
Des1 degredation	No effect	10 μM	10 μM	No effect
Molecular properties				
Clog P	3.75	5.1	5.8	5.69
tPSA($Å^2$)	69	76	33	33
***In vitro* PK studies**				
Mouse microsomal clearance $t_{1/2}$ (min)	3.14	41.0	3.15	4.14
Mouse S9 clearance $t_{1/2}$ (min)	2.21	19.1	11.4	5.8
Caco2 permeability (cms-1) and efflux ratio		4.97	5.4	1.07
CYP450 inhibition (μM)	>25	>25	>25	>25

4.1 General conclusion and future directions

With a focus on the early stages in drug discovery, this project contributes to analogue optimisation, compound profiling and target validation. This drug discovery project produced new SK1 and SK2 inhibitors utilising a simple synthetic approach and computer modelling that have good target engagement in cells. In addition, the findings presented in the SAR study of the new inhibitors could assist in the design of more effective compounds. The current work provides important information about the function of the SK/S1P pathway in prostate cancer cells. In addition, the current work highlighted that combined targeting of SK1/Des1 might represent a successful therapeutic approach for the treatment of prostate cancer to help overcome some of the major issues related to anti-cancer therapies (i.e. lack of efficacy and development of resistance to current therapies). Indeed, inhibition of these enzymes has multiple effects that are anticipated to reduce prostate cancer growth and progression. Further investigation is required to assess the effect of the new SK inhibitors on SK1b expression, S1P, Cer and dihydroceramide levels in cancer cells. In addition, a further compound optimisation is highly recommended to improve microsomal stability and the physiochemical properties of these new inhibitors.

4.1.1 Future directions for chemistry

Analogues of compound 9 to improve SK1 potency and selectivity

Previous observations indicate that the *heel* area in SK1 is more spacious than in SK2 and a steric effect can be used to increase the selectivity for SK1 over SK2. Therefore, compounds with a bulkier group such as Br, CF_3 or isopropyl instead of the CH_3 substituent in the central phenyl ring should be synthesised and assessed (e.g compound **66**) (**Figure 4.1**).
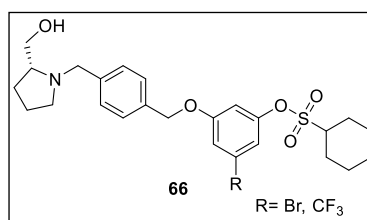
Figure 4.1 . Suggested analogues of compound 9.

Analogues of compound 21 to improve potency and selectivity for SK2

Preliminary findings in this study indicate that a repulsive steric interaction between SK2 and the central phenyl linker, and that a smaller group could be preferred in this position to improve potency. Modelling studies have suggested that replacement of the central phenyl group with an aliphatic linker that retains the same distance could be used as a tool to increase the selectivity for SK2-over SK1 (compound **67**) (**Figure 4.2**). Modelling studies have also suggested that moving the central ether position to be adjacent to the head phenyl ring (**Figure 4.2**) could provide further interactions with the hydrogen bond acceptors of Thr282 in SK2 that was not involved any interaction with previous analogues due to distance limitation (compound **68**).
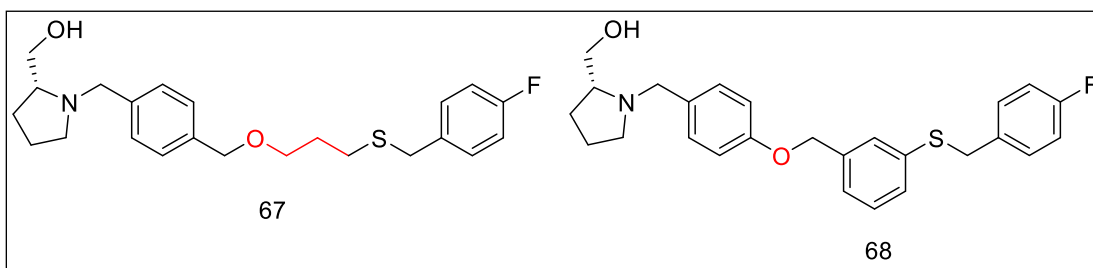
Figure 4.2. Suggested analogues of compound 21.

Molecular modelling studies have identified a deep pocket in the toe of the J-channel in SK2 which is absent in SK1, which can be occupied by the *para* fluorine moiety of compound **21**. However, this compound had poor microsomal stability and low solubility. In addition to the suggested changes made in **Section 2.5.4** to address metabolic stability, replacement of the central phenyl group with a pyridine or pyrimidine ring would reduce its clogP 5.9 to 4.6 for compound **69**, which would lower lipophilicity whilst enhancing solubility and reducing affinity for CYP450 isoforms (**Figure 4.3**).
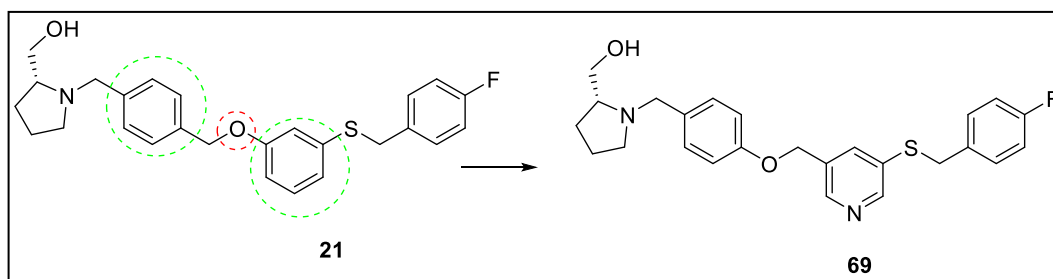
 Figure 4.3. Proposed analogues of compound 21 to address lipophilicity issues.

Chapter 5. Materials and Methods

5.1 Chemistry

5.1.1 General experimental details

Reagents and solvents: All commercially available reagents and solvents used were obtained (and used without further purification) from Sigma-Aldrich, Alfa-Aesar or Fisher Scientific unless otherwise stated.

Nuclear Magnetic Resonance (NMR) spectroscopy: Proton (^{1}H NMR) and carbon (^{13}C NMR) nuclear magnetic resonance spectra were run either on JEOL Lambda Delta 400 (400 MHz) or Bruker AMX-400 (400 MHz) spectrometers at 400.0 and 100.6 MHz respectively. The deuterated solvent used for each of the compounds is specified in the text. Chemical shifts are stated in parts per million (ppm) and multiplicity indicated as singlet (s), doublet (d), doublet of doublet (dd), triplet (t), quartet (q), pentet (p), and multiplet (m). Coupling constants (J) are quoted in hertz (Hz).

Mass spectrometry: High-resolution mass spectroscopy (HRMS) was obtained using electron impact ionisation (ESI) in a Fourier transform analyser by Exactive® Thermo Scientific. Mass to charge ratio (m/z) molecular ion radical is given as [M+].

Purification of products: Reactions were monitored by thin layer chromatography (TLC) using silica gel plates 60 F254 aluminium sheets (Merck, Feltham, United kingdom) using UV light for detection at 254 nm and 366 nm. Flash column chromatography was performed in a SP4 Biotage MPLC apparatus using silica gel 0.040-0.063 mm as a particle size (Fisher Scientific, Loughborough, United Kingdom) with a cartridge size of 10 g or 50 g depending on the scale of the reaction to purify. The conditions and the solvents for purification are showed in every compound. LC-MS purity was determined using an Agilent Technologies 1220 series LC system with Agilent 6100 series single quadrupole mass spectrometer. Separation was achieved with anAgilent Eclipse C18 4.6 x 50 mm column; flow rate: 1 mL/min; Detection: 254 nm; sample volume: 0 µL; mobile phase: acetonitrile/5mM ammonium acetate: water/5mM ammonium acetate; 5%, 1.48 mins; 5-100%, 8 mins; 100%, 13.5 mins; 100-5%, 16.5 mins; 5%, 18 mins. All compounds were ≥ 95% pure as determined by LC-MS.

5.1.2 Chemical synthesis of target compounds

5.1.2.1 General procedure A (Monosulfonylation of resorcinol) [225]
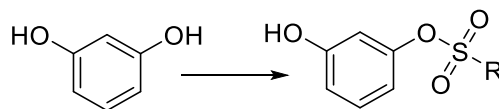
To a suspension of resorcinol (1.5 eq) in saturated sodium hydrogen carbonate (12 mL) and diethyl ether (14 mL), sulfonyl chloride (1.0 eq) was added at room temperature. After the reaction mixture was stirred overnight, the mixture was diluted with diethyl ether and water, the organic layer was separated and washed with saturated aqueous potassium carbonate solution, then extracted with 1M aqueous NaOH. The aqueous layer was then acidified with 3 M aqueous HCl, and then extracted with diethyl ether (**see Figure 2.32**). The resultant organic layer which contained the desired product was dried over anhydrous MgSO₄ and concentrated to afford the desired sulfonate derivatives. Products were purified as explained previousely in section 2.4.1.1.

3-Hydroxyphenyl 4-methoxybenzenesulfonate (29)
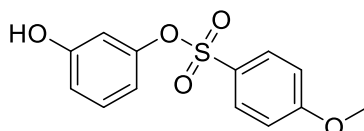
The reaction was carried out according to general procedure **A** using 4-methoxybenzenesulfonyl chloride (800 mg, 3.87 mmol. 1 eq) and resorcinol (638 mg, 5.80 mmol, 1.5 eq) to afford the title compound (375 mg, 34% yield) as a red brown oil. ^{1}H NMR (400 MHz, DMSO-d_6) δ 3.86 (s, 3H), 6.38 (m, 1H), 6.39 – 6.41 (m, 1H), 6.68 (ddd, J = 1.0, 2.3, 8.2 Hz, 1H), 7.12 (d, J = 8.1 Hz, 1H), 7.13 – 7.17 (m, 2H), 7.74 – 7.77 (m, 2H), 9.89 (s, 1H). ^{13}C NMR (100MHz, DMSO-d_6) 58.1, 106.3, 114.5, 115.6,

115.9, 128.3, 131.1, 132.6, 154.7, 159.3, 161.2. ESI-HRMS calculated for $C_{13}H_{11}O_5S$ (M-H) $^-$: 279.0442, found: 279.0448.

3-Hydroxyphenyl butane-1-sulfonate (30)
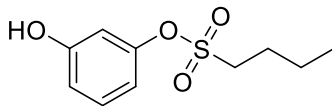
The reaction was carried out according to general procedure **A** using butanesulfonyl chloride (675 µL, 5.11 mmol, 1.0 eq) and resorcinol (842 mg, 7.66 mmol, 1.5 eq) to afford the title compound (431 mg, 36% yield) as a brown oil. ^{1}H NMR (400 MHz, DMSO-d_6) δ 0.93 (t, J = 7.4 Hz, 3H), 1.43 (dt, J = 7.4, 14.7 Hz, 2H), 1.70 – 1.83 (m, 2H), 3.41 – 3.52 (m, 2H), 6.70 (t, J = 2.2 Hz, 1H), 6.71 – 6.78 (m, 2H), 7.25 (t, J = 8.1 Hz, 1H), 9.94 (s, 1H). ^{13}C NMR (100 MHz, CDCl$_3$) δ 13.0, 20.9, 24.9, 49.8, 109.1, 113.5, 113.9, 130.1, 149.4, 156.3. ESI-HRMS calculated for $C_{10}H_{13}O_4S$ (M-H)$^-$: 229.0543, found: 229.0540.

3-Hydroxyphenyl 4-chlorobenzenesulfonate (31)
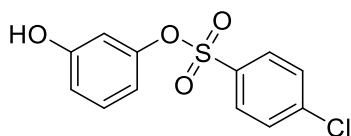
The reaction was carried out according to general procedure **A** using 4-chlorobenzenesulfonyl chloride (800 mg, 2.82 mmol, 1.0 eq) and resorcinol (462 mg, 4.24 mmol, 1.5 eq) to afford the title compound (232 mg, 29% yield) as a yellow oil. ^{1}H NMR (400 MHz, DMSO-d_6) δ 6.40-6.47 (m, 1H), 6.57 (dd, J = 8.0, 2.1, 0.8, 1H), 6.87 (m, 1H), 7.05 (m, 1H), 7.75 (d, J = 8.1 Hz, 2H), 7.88 (d, J =8.1 Hz, 2H), 9.88 (s, 1H). ^{13}C NMR (100 MHz, DMSO-d_6) 108.3, 113.5, 115.9, 129.3, 130.1, 131.2, 133.5, 138.1, 152.3, 158.3. ESI-HRMS calculated for $C_{12}H_8O_4ClS$ (M+H)$^-$: 282.7105, found, 282.7101.

3-Hydroxyphenyl 4-methylbenzenesulfonate (32)
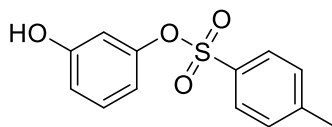
The reaction was carried out according to general procedure **A** using 4- toluenesulfonyl chloride (800 mg, 4.19 mmol, 1.0 eq) and resorcinol (692 mg, 6.29 mmol, 1.5 eq) to afford the title compound (162 mg, 15% yield) as a brown oil. ^{1}H NMR (400 MHz, DMSO-d_6) δ 2.42 (s, 3H), 6.51 (m, 1H), 6.90 (m, 1H), 6.92 (dd, J = 6.8, 2.4 Hz, 2H), 7.59 (d, J= 8.2, 2H), 7.77 (d, J= 8.2, 2H), 10.02 (s, 1H). ^{13}C NMR (100 MHz, DMSO-d_6) 20.9, 101.3, 106.4, 115.6, 126.9, 130.4, 131.4, 132.7, 138.2, 152.1, 158. ESI-HRMS calculated for $C_{12}H_{11}O_4S$ (M-H)$^-$: 263.0382, found: 263.0380.

3-Hydroxyphenyl cyclohexanesulfonate (33)
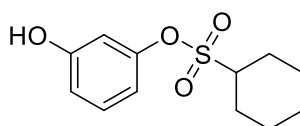
The reaction was carried out according to general procedure **A** using cyclohexanesulfonyl chloride (500 mg, 2.52 mmol, 1.0 eq) and resorcinol (416 mg, 3.78 mmol, 1.5 eq) to afford the title compound (80 mg, 13% yield) as a colourless oil. ^{1}H NMR (400 MHz, DMSO-d_6) δ 1.30 – 1.35 (m, 2H), 1.46 – 1.55 (m, 2H), 1.58-1.69 (m, 2H), 1.83 (dt, J = 3.4, 13.2 Hz, 2H), 2.10 – 2.23 (m, 2H), 3.49 (tt, J = 3.5, 11.8 Hz, 1H), 6.69 (t, J = 2.2 Hz, 1H), 6.71 (m, 1H), 6.75 (ddd, J = 1.0, 2.3, 8.3 Hz, 1H), 7.25 (t, J = 8.1 Hz, 1H), 9.90 (s, 1H). ^{13}C NMR (100 MHz, DMSO-d_6) δ 24.3, 24.7, 25.9, 58.6, 106.0, 109.7, 110.5, 129.9, 139.6, 158.0. ^{1}ESI-HRMS calculated for $C_{12}H_{15}O_4S$ (M-H)$^-$: 255.0696, found: 255.0697.

5.1.2.2 General procedure B (selective sulfonylation of 3-aminophenol) [270]
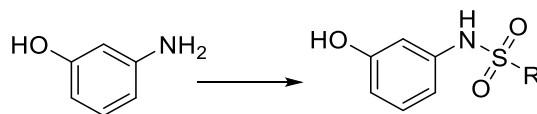
To a solution of 3-aminophenol (1.5 eq) and pyridine (1.6 eq) in CH_2Cl_2 (20 mL) was added drop-wise a solution of sulfonyl chloride (1.0 eq) in CH_2Cl_2 (20 mL) at room temperature. After the reaction was stirred at room temperature overnight, 0.01 M HCl was added (30 mL), the organic layer was separated, washed with 1 M NaOH, then the aqueous layer was acidified with 3 M HCl to pH 4 before being extracted with CH_2Cl_2. The resultant organic layer, which contained the desired product, was then dried over anhydrous $MgSO_4$ and concentrated to afford the desired sulphonamides derivatives.

N-(3-Hydroxyphenyl)-4-methoxybenzenesulfonamide (34)
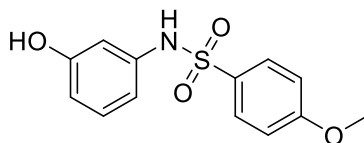
The reaction was carried out according to general procedure **B** using 4-methoxybenzenesulfonyl chloride (800 mg, 3.87 mmol, 1.0 eq) and 3- aminophenol (639 mg, 5.80 mmol, 1.5 eq) to afford the title compound (600 mg, 56% yield) as a brown oil. ^{1}H NMR (400 MHz, DMSO-d_6) δ 3.80 (s, 3H), 6.39 (ddd, J = 0.9, 2.4, 8.2 Hz, 1H), 6.51 (ddd, J = 1.0, 2.0, 8.0 Hz, 1H), 6.57 (t, J = 2.2 Hz, 1H), 6.97 (t, J = 8.1 Hz, 1H), 7.07 (d, J = 8.9 Hz, 2H), 7.69 (d, J = 9.0 Hz, 2H), 9.40 (s, 1H), 10.00 (s, 1H). ^{13}C NMR (100 MHz, DMSO-d_6) 55.6, 106.7, 110.3, 110.8, 114.3, 128.8, 129.7, 131.3, 139.0, 157.8, 162.3. ESI-HRMS calculated for $C_{13}H_{14}NO_4S$ (M+H)$^+$: 280.0638, found: 280.0638.

N-(3-Hydroxyphenyl)butane-1-sulfonamide (35)
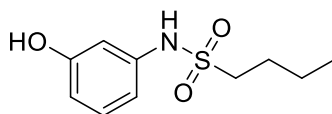
The reaction was carried out according to general procedure **B** using butanesulfonyl chloride (800 mg, 5.10 mmol, 1.0 eq) and aminophenol (842 mg, 7.66 mmol, 1.5 eq) to afford the title compound (630 mg, 55% yield) as a brown oil. ^{1}H NMR (400 MHz, DMSO-d_6) δ 0.87 (t, J = 8.0 Hz, 3H), 1.39 (m, 2H), 1.61 (m, 2H), 3.00-3.08 (m, 2H), 6.14 (dd, J = 8.2, 2.3, 0.8 Hz, 1H), 6.19 (m,1H), 6.31 (dd, J = 8.0, 2.0, 0.8 Hz,, 1H), 7.03 – 7.05 (m, 1H), 9.80 (s, 1H), 10.00 (s, 1H).^{13}C NMR (100 MHz, CDCl$_3$) δ 13.0, 20.9, 24.9, 49.8, 109.1, 113.5, 117.9, 130.1, 139.4, 159.1. ESI-HRMS calculated for C$_{10}$H$_{14}$O$_3$NS (M-H)$^-$: 228.0701, found: 228.0702.

4-Chloro-*N-*(3-hydroxyphenyl)benzenesulfonamide (36)
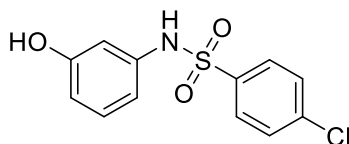
The reaction was carried out according to general procedure **B** using 4-chlorobenzenesulfonyl chloride (800 mg, 3.79 mmol, 1.0 eq) and 3-aminophenol (619 mg, 5.67 mmol, 1.5 eq) to afford the title compound (550 mg, 51% yield) as a yellow oil. ^{1}H NMR (400 MHz, DMSO-d_6) δ 6.43 (ddd, J = 1.0, 2.3, 8.1 Hz, 1H), 6.51 (ddd, J = 1.0, 2.0, 8.0 Hz, 1H), 6.57 (t, J = 2.2 Hz, 1H), 7.00 (t, J = 8.0 Hz, 1H), 7.65 (d, J = 8.7 Hz, 2H), 7.75 (d, J = 8.7 Hz, 2H), 9.47 (s, 1H), 10.22 (s, 1H).^{13}C NMR (100 MHz, DMSO-d_6) 104.7, 110.0, 111.5, 129.2, 130.4, 130.8, 137.4, 138.1, 140.1, 159.4. ESI-HRMS calculated for C$_{12}$H$_9$NO$_3$ClS (M-H)$^-$: 282.9997 found: 282.9999.

N-(3-Hydroxyphenyl)-4-methylbenzenesulfonamide (37)
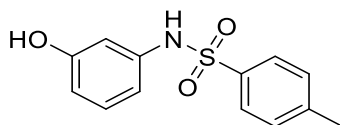
The reaction was carried out according to general procedure **B** using 4- toluenesulfonyl chloride (500 mg, 2.62 mmol, 1.0 eq) and 3-aminophenol (432 mg, 3.93 mmol, 1.5 eq). The residue was purified by flash column chromatography using a gradient from 0 to 4% MeOH in CH_2Cl_2 to afford the title compound as a white solid (200 mg, 29% yield). ^{1}H NMR (400 MHz, DMSO-d_6) δ 2.34 (s, 3H), 6.29 (ddd, J = 8.1, 2.3, 0.8 Hz, 1H), 6.36 (ddd, J = 8.0, 2.0, 0.8 Hz, 1H), 6.42 - 6.59 (m, 1H), 6.60 – 6.93 (m, 1H), 7.51 – 7.58 (m, 2H), 7.69 – 7.80 (m, 2H), 9.41 (s, 1H), 10.14 (br. s, 1H). ^{13}C NMR (100 MHz, DMSO-d_6) δ 21.3, 106.9, 110.4, 111.1, 129.2, 129.8, 130.9, 137.2, 138.8, 139.6, 157.8. ESI-HRMS calculated for $C_{13}H_{14}NO_3S$ (M+H)$^+$: 264.0612, found: 264.0623.

N-(3-Hydroxyphenyl) cyclohexanesulfonamide (38)
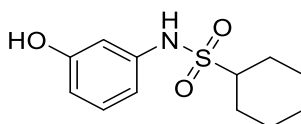
The reaction was carried out according to general procedure **B** using cyclohexanesulfonyl chloride (500 mg, 2.73 mmol, 1.0 eq) and 3-aminophenol (451 mg, 4.10 mmol, 1.5 eq) to afford the title compound (607 mg, 88% yield) as a pale yellow crystals. ^{1}H NMR (400 MHz, DMSO-d_6) δ 1.27-1.36 (m, 2H), 1.40-1.54 (m, 2 H), 1.60-1.70 (m, 2 H), 1.83-1.90 (m, 2 H), 2.22 - 2.40 (m, 2 H), 3.60 (m, 1 H), 6.64 - 6.69 (dd, J = 8.2, 2.3, 0.8 Hz, 1H), 6.70-6.80 (m, 1H), 6.88-6.90 (m, 1H), 7.30 (m, J=8.13 Hz, 1 H) 9.93 (s, 1 H), 10.03 (s, 1H). ^{13}C NMR (100 MHz, DMSO-d_6) δ 24.1, 24.5, 25.9, 65.6, 101.5, 109.1, 116.5, 130.1, 139.2, 159.0. ESI-HRMS calculated for $C_{12}H_{16}NO_3S$ (M-H)$^-$: 254.0858, found: 254.0856.

5.1.2.3 General Procedure C (selective alkylation of thio group of 3-mercaptophenol)
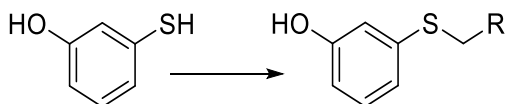
Benzyl bromide (1.1eq) and 3-mercaptophenol (1.0 eq) were added to a stirred suspension of potassium carbonate (3 eq) in acetonitrile (2 mL). The resulting solution was heated to 60 °C under nitrogen. After 2 hours, the reaction mixture was cooled to room temperature, diluted with EtOAc (50 mL), quenched with acetic acid (172 μL), absorbed onto silica and purified by flash chromatography (Biotage SP4, SiO$_2$, 10-12% EtOAc in petroleum ether) to afford the target compounds.

3-Benzylthiophenol (50)
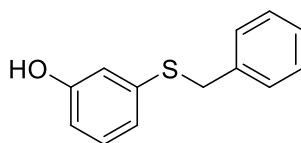
The reaction was carried out according to general procedure **C** using benzyl bromide (392 μL, 3.30 mmol, 1.1 eq), 3-mercaptophenol (306 μL, 3.00 mmol, 1 eq) and potassium carbonate (415 mg, 3 mmol, 3 eq) in acetonitrile (2 mL). The crude residue was purified by flash chromatography (10-12% EtOAc in petroleum ether) to afford the title compound (620 mg, 95% yield) as a white solid. ^{1}H NMR (400 MHz, DMSO-d_6) δ 4.24 (s, 2H), 6.53 – 6.61 (m, 1H), 6.73 (d, J = 1.9 Hz, 1H), 6.80-6.93 (m, 1H), 7.08 (t, J = 7.9 Hz, 1H), 7.20 – 7.26 (m, 1H), 7.26 – 7.33 (m, 2H), 7.33 – 7.38 (m, 2H), 9.58 (s, 1H). ESI-HRMS calculated for C$_{13}$H$_{11}$OS (M-H)$^-$: 215.0536, found: 215.0539.

3-(4-Chlorobenzylthio)phenol (51)
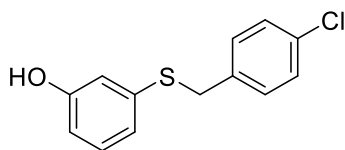
The reaction was carried out according to general procedure **C** using 4-chlorobenzyl bromide (678 mg, 3.30 mmol, 1.1 eq), 3-mercaptophenol (306 μL, 3.00 mmol, 1.0 eq) and potassium carbonate (212 mg, 3.00 mmol, 1.0 eq) in acetonitrile (2 mL). The crude residue was purified by flash chromatography (10-12% EtOAc in petroleum ether) to afford the title compound (328 mg, 44% yield) as a red solid. ^{1}H NMR (400 MHz, DMSO-d_6) δ 4.20 (s, 2H), 6.58 (dd, J = 2.4, 7.9 Hz, 1H), 6.70 (t, J = 2.1 Hz, 1H), 6.74 (dd, J = 2.0, 7.6 Hz, 1H), 7.09 (t, J = 7.9 Hz, 1H), 7.26 – 7.36 (m, 3H), 7.41 (d, J = 1.6 Hz, 1H), 9.52 (s, 1H). ^{13}C NMR (100 MHz, DMSO-d_6) δ 39.1, 112.2, 113.5, 121.8, 128.8, 130.4, 130.8, 132.7, 135.2, 136.5, 157.7. ESI-HRMS calculated for $C_{13}H_{10}OClS$ (M-H)$^-$: 249.0146, found: 249.0150.

3-(4-Fluorobenzylthio)phenol (52)
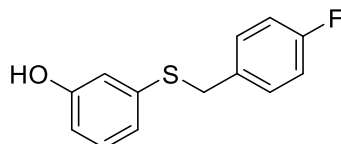
The reaction was carried out according to general procedure **C** using 4-fluorobenzyl bromide (624 mg, 411 μL, 3.30 mmol, and 1.1 eq) and 3-mercaptophenol (306 μL, 3.00 mmol, 1.0 eq) and potassium carbonate (415 mg, 3.00 mmol) in acetonitrile (2 mL). The crude was purified by flash column chromatography using a gradient (10-12% EtOAc in petroleum ether) to afford the title compound (700 mg, 96% yield) as a brown oil. ^{1}H NMR (400 MHz, DMSO-d6) δ 4.18 (s, 2H), 6.57 (ddd, J = 0.9, 2.4, 8.1 Hz, 1H), 6.70 (t, J = 2.0 Hz, 1H), 6.74 (ddd, J = 1.0, 1.8, 7.8 Hz, 1H), 7.06 – 7.11 (m, 2H), 7.11 – 7.16 (m, 2H), 7.34 – 7.42 (m, 2H), 9.50 (s, 1H). ^{13}C NMR (100 MHz,

DMSO-d_6) δ 36.2, 113.7, 115.4, 115.6, 115.8, 119.3, 130.4, 131.3, 134.4, 137.4, 158.2, 160.6, 163.0.

3-(4-Trifluoromethylbenzyl)thiophenol (53)
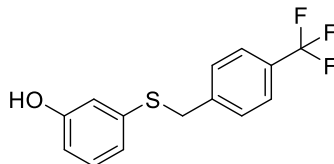
The reaction was carried out according to general procedure **C** using *p*-trifluoro methyl benzylbromide (788 mg, 510.2 uL, 3.30 mmol, 1.1 eq) and 3- thiophenol (414.6 mg, 306 uL, 3.00 mmol, 1.0 eq) to afford the title compound (456 mg, 53% yield) as a yellow oil. ^{1}H NMR (400 MHz, DMSO-d_6) δ 4.32 (s, 2H), 6.55-6.60 (dd, *J* = 8.2, 2.3, 0.8 Hz, 1H), 6.68 -6.69 (m, 2H), 7.84-7.91 (m, 1H), 6.92 (d, *J* = 8.0 Hz, 2H), 7.17 (d, *J* =8.0 Hz, 2H), 9.47 (s, 1H).^{13}C NMR (100 MHz, DMSO-d_6) 40.0, 112.1, 113.1, 121.2, 124.4, 125.1, 129.1, 129.3, 131.2, 137. 8, 140.4, 158.7.

3-Cyclohexylmethylthiophenol (54)
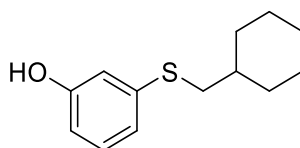
The reaction was carried out according to general procedure **C** using cyclohexanmethane bromide (584 mg, 460 μL, 3.30 mmol, 1.1 eq), 3-mercaptophenol (306 μL, 3.00 mmol, 1.1 eq) and potassium carbonate (415 mg, 3.00 mmol, 1.0 eq) in acetonitrile (2 mL). The crude residue was purified by flash chromatography (10-12% EtOAc in petroleum ether) to afford the title compound (438 mg, 65% yield) as a yellow oil.^{1}H NMR (400 MHz, DMSO-d_6) δ 0.98 (qd, *J* = 3.4, 11.9 Hz, 2H), 1.08 – 1.17 (m, 3H), 1.55 – 1.63 (m, 1H), 1.68 (dq, *J* = 3.4, 12.9 Hz, 2H), 1.83 (dd, *J* = 3.4, 13.5 Hz, 3H), 2.79 (d, *J* = 6.9 Hz, 2H), 2.89 (s, 2H), 6.54 (dd, *J* = 2.3, 7.9 Hz, 1H), 6.65 – 6.72 (m, 2H), 7.08 (t, *J* = 7.9 Hz, 1H), 9.49 (s, 1H). ^{13}C NMR (100 MHz, DMSO-

d_6) δ 25.8, 26.5, 31.5, 32.7, 37.5, 113.0, 114.7, 118.7, 130.4, 138.5, 158.3. ESI-HRMS calculated for $C_{13}H_{19}O\ S$ (M+H) $^+$: 223.1149, found: 223.1151.

5.1.2.4 Synthesis of 3-(methoxymethoxy) phenol (61)
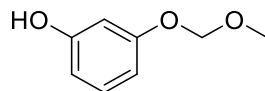
Caesium carbonate (8.88 g, 27.24 mmol, 1.0 eq) was added to a solution of resorcinol (3.30 g, 30.00 mmol, and 1.1 eq) in acetone (30 ml) at 0 °C under argon. Then, chloromethyl methyl ether (2.07 ml, 27.24 mmol, 1.0 eq) was added dropwise to the resulting white suspension and the mixture was maintained at 0 °C for 1.5 h. Solid material was filtered off and the filtrate was purified by flash chromatography (15% EtOAc in petroleum ether) to afford the title compound (1.5 g, 36% yield) as a colourless oil. ^{1}H NMR (400 MHz, DMSO-d_6) δ 3.36 (s, 3H), 5.11 (s, 2H), 6.59 – 6.62 (m, 1H), 6.63 – 6.65 (m, 1H), 6.65 (d, J = 1.7 Hz, 1H), 7.12 – 7.25 (m, 1H), 9.49 (s, 1H). ^{13}C NMR (100 MHz, DMSO-d_6) δ 54.6, 94.4, 103.8, 108.6, 109.1, 158.5, 159.9. ESI-HRMS calculated for $C_8\ H_{11}\ O_3$ (M+H)$^+$: 155.0703, found: 155.0703.

5.1.2.5 Synthesis of 4-bromomethyl benzaldehyde (39) [271]
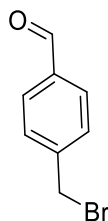
Diisobutylaluminium hydride (DIBAL-H) (1.0 eq) was added to a stirred solution of 4-(bromomethyl) benzonitrile (1.0 eq) in toluene (40 mL). After 1 hour, the reaction mixture was quenched with HCl (3 M) extracted with EtOAc to afford the target compound as white solid. ^{1}H NMR (400 MHz, DMSO-d6) δ 4.79 (s, 2H), 7.67 (d, J = 8.3 Hz, 2H), 7.91 (d, J = 8.3 Hz, 2H), 10.01 (s, 1H).^{13}C NMR (100 MHz, DMSO-d_6) δ 33.3, 129.2, 130.4, 138.1, 145.5. 190.1.

5.1.2.6 General procedure D (alkylation of phenols)

X=S, NH or O

X=S, NH or O
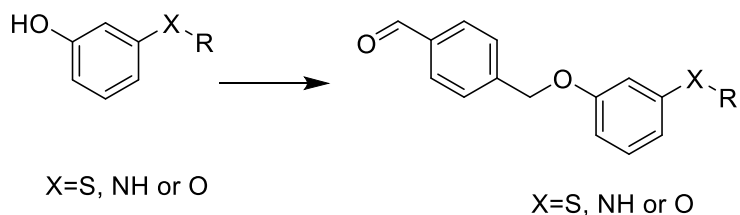
To a solution of desired phenol (1 eq) and potassium carbonate (2.75 eq) in MeCN (2.5 mL), 4-bromomethyl benzaldehyde (1.1 eq) was added at room temperature and then the reaction mixture was heated at 60° C for 3 h. After cooling down, the solvent was evaporated, and the crude was dissolved in EtOAc and water. The organic layer was separated, washed with brine, dried over anhydrous $MgSO_4$ and concentrated. The residue was purified by flash column chromatography (Biotage SP4, SiO_2, 15-25% EtOAc in petroleum ether) to afford the desired alkylated derivatives.

3-(4-Formylbenzyloxy)phenyl-4-methoxybenzenesulfonate (40)
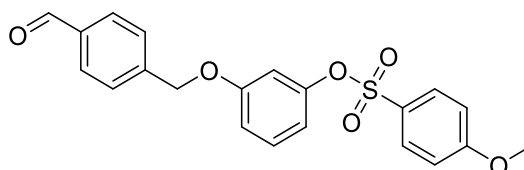
The reaction was carried out according to general procedure **D** using compound **29** (500 mg, 1.78 mmol, 1.0 eq) and 4-bromomethyl benzaldehyde (390 mg, 1.96 mmol, 1.1eq). The crude product was purified by flash column chromatography using a gradient (15→2%EtOAc in petroleum ether) to afford the title compound (600 mg, 85% yield) as a reddish-brown oil. ^{1}H NMR (400 MHz, DMSO-d_6) δ 3.87 (s, 3H), 5.18 (s, 2H), 6.59 (dd, J = 8.4, 3.1 Hz, 1H), 6.71 (m, 1H), 6.99 (dd, J = 8.4, 3.1 Hz, 1H), 7.12-7.18 (m, 1H), 7.30 (d, J = 8.1 Hz, 2H), 7.62 (d, J = 8.1 Hz, 2H), 7.80 (d, J = 8.3 Hz, 2H), 7.90 (d, J = 8.3 Hz, 2H), 10.03 (s, 1H).^{13}C NMR (100 MHz, DMSO-d_6) 58.1, 106.3, 114.5, 115.6, 115.9, 128.3,129.5, 130.1, 131.1, 132.8, 135.8, 142.5, 154.7,

159.3, 161.2., 190.1. ESI-HRMS calculated for $C_{21}H_{19}O_6S$ (M+H)$^+$: 399.0942, found: 399.0948.

3-(4-Formylbenzyloxy)phenyl butane-1-sulfonate (41)
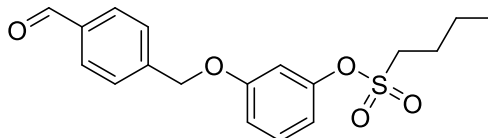
The reaction was carried out according to general procedure **D** using compound **30** (231 mg, 0.99 mmol, 1.0 eq) and 4-bromomethyl benzaldehyde (218 mg, 1.09 mmol, 1.1 eq). The crude product was purified by flash column chromatography using a gradient from 15 to 25% EtOAc in petroleum ether to afford the title compound (241 mg, 70% yield) as a yellow oil. ^{1}H NMR (400 MHz, DMSO-d_6) δ 0.90 (t, J = 7.3 Hz, 3H), 1.43-1.49 (m, 2H), 1.70 – 1.82 (m, 2H), 3.45 – 3.56 (m, 2H), 5.46 (s, 2H), 6.94 (dd, J = 2.3, 8.1 Hz, 1H), 7.00 (t, J = 2.4 Hz, 1H), 7.03 – 7.08 (m, 1H), 7.41 (t, J = 8.3 Hz, 1H), 7.67 (q, J = 3.3, 3.9 Hz, 2H), 7.92 – 7.97 (m, 2H), 10.34 (s, 1H).^{13}C NMR (100 MHz, DMSO-d_6) δ 13.1, 20.4, 24.8, 49.4, 68.8, 108.8, 113.8, 114.5, 126.8, 127.8, 129.8, 130.8, 135.5, 143.4, 149.4, 158.8, 193.3. ESI-HRMS calculated for $C_{18}H_{21}O_5S$ (M+H)$^+$: 349.1103, found: 349.1104.

3-(4-Formylbenzyloxy)phenyl 4-chlorobenzenesulfonate (42)
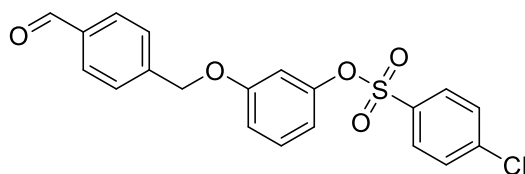
The reaction was carried out according to general procedure **D** using compound **31** (200 mg, 0.70 mmol, 1.0 eq) and 4-bromomethyl benzaldehyde (153 mg, 0.77 mmol, 1.1 eq) to afford the title compound as a yellow oil. The product was used in the next step without further purification (248 mg, 88% yield). ^{1}H NMR (400 MHz, DMSO-d_6) δ 5.19 (s, 2H), 6.64 (dd, J = 2.3, 8.1 Hz, 1H), 6.75 (t, J = 2.4 Hz, 1H), 7.01 (dd, J = 2.6, 8.4 Hz, 1H), 7.32 (t, J = 8.3 Hz, 1H), 7.62 (d, J = 8.1 Hz, 2H), 7.75(d, J = 8.1 Hz, 2H), 7.87 (d, J = 8.4 Hz, 2H), 7.92 (d, J = 8.4 Hz, 2H), 10.03 (s, 1H). ^{13}C NMR (100 MHz, DMSO-d_6) 70.4, 106.2, 114.2, 117.3, 129.6, 129.8, 130.0, 130.1, 135.4, 137.1, 137.2, 137.9, 150.1, 157.7, 192.4. ESI-HRMS calculated for $C_{20}H_{16}O_5$ Cl S (M+H)$^+$: 403.0400, found: 403.0401.

3-(4-Formylbenzyloxy)phenyl 4-methylbenzenesulfonate (43)

The reaction was carried out according to general procedure **D** using compound **32** (161 mg, 0.60 mmol, 1.0 eq) and 4-bromomethyl benzaldehyde (133 mg, 0.67 mmol, 1.1 eq). The crude product was purified by flash column chromatography using a gradient from 15 to 25% EtOAc in petroleum ether to afford the title compound (181 mg, 78% yield) as a yellowish-brown oil. ^{1}H NMR (400 MHz, DMSO-d_6) δ 2.42 (s, 3H), 5.17 (s, 2H), 6.60 (dd, J = 2.3, 8.1 Hz, 1H), 6.71 (t, J = 2.3 Hz, 1H), 6.99 (dd, J = 2.5, 8.1 Hz, 1H), 7.26 – 7.32 (m, 1H), 7.46 (d, J = 8.0 Hz, 2H), 7.62 (d, J = 7.7 Hz, 2H), 7.70 (d, J = 8.1 Hz, 2H), 7.91 (d, J = 8.1 Hz, 2H), 10.01 (s, 1H).^{13}C NMR (100 MHz, DMSO-d_6) δ 21.2, 70.3, 102.7, 108.7, 115.5, 126.7, 130.0, 130.4, 131.1, 132.4,

135.8, 138.2, 142.4, 152.7, 160.2, 191.1. ESI-HRMS calculated for $C_{21}H_{19}O_5S$ $(M+H)^+$: 383.0942, found: 383.0948.

3-(4-Formylbenzyloxy)phenylcyclohexanesulfonate (44)
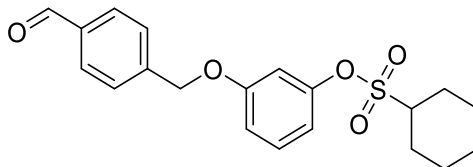
The reaction was carried out according to general procedure **D** using compound **33** (60 mg, 0.23 mmol, 1.0 eq) and 4-bromomethyl benzaldehyde (51 mg, 0.27 mmol, 1.1 eq) to afford the title compound as a yellow oil. The product was used in the next step without further purification (84 mg, 95% yield).^{1}H NMR (400 MHz, DMSO-d_6) δ 1.12 – 1.26 (m, 1H), 1.26 – 1.42 (m, 2H), 1.44 – 1.70 (m, 3H), 1.68 – 1.89 (m, 2H), 2.10 – 2.28 (m, 2H), 3.51 (tt, J = 3.5, 11.9 Hz, 1H), 5.28 (s, 2H), 6.88 – 6.93 (m, 1H), 6.93 – 6.97 (m, 1H), 7.05 (dd, J = 2.4, 8.3 Hz, 1H), 7.40 (t, J = 8.3 Hz, 1H), 7.68 (d, J = 7.8 Hz, 2H), 7.95 (d, J = 8.0 Hz, 2H), 10.02 (s, 1H). ^{13}C NMR (100 MHz, DMSO-d_6) δ 24.1, 25.2, 28.1, 54.0, 69.9, 102.8, 110.5, 113.2, 129.2, 130.1, 131.2, 135.1, 142.2, 152.1, 161.4, 190.1. ESI-HRMS calculated for $C_{20}H_{23}O_5S$ $(M-H)^-$: 375.1256, found: 375.1257.

N-(3-((4-Formylbenzyl)oxy)phenyl)-4-methoxybenzenesulfonamide (45)
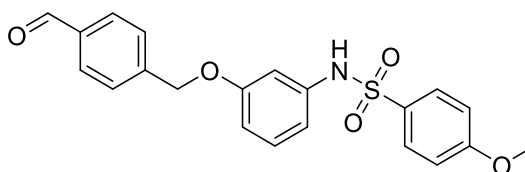
The reaction was carried out according to general procedure **D** using compound **34** (500 mg, 1.79 mmol, 1.0 eq) and 4-bromomethyl benzaldehyde (391 mg, 1.96 mmol, 1.1 eq). The crude was purified by flash column chromatography using a gradient from 15 to 25% EtOAc in petroleum ether to afford the title compound (200 mg, 28% yield) as a colourless oil. ^{1}H NMR (400 MHz, DMSO-d_6) δ 3.87 (s, 3H), 4.84 (s, 2H), 6.49 (ddd, J = 0.9, 2.1, 7.9 Hz, 1H), 6.51 (t, J = 2.2 Hz, 1H), 6.61 (ddd, J = 0.9, 2.4, 8.2 Hz, 1H), 7.03 (t, J = 8.0 Hz, 1H), 7.14 (d, J = 8.9 Hz, 2H), 7.50 (d, J = 8.2 Hz, 2H), 7.61 (d, J = 8.9 Hz, 2H), 7.83 (d, J = 8.3 Hz, 2H), 9.52 (s, 1H), 9.94 (s, 1H). ^{13}C NMR (100 MHz, DMSO-d_6) δ 53.3, 55.7, 114.4, 114.7, 115.6, 118.2, 128.5, 129.4, 129.6, 135.3, 139.8, 143.6, 157.5, 162.7, 192.6. ESI-HRMS calculated for $C_{21}H_{20}NO_5S$ (M+H)$^+$: 398.1057, found: 398.1046.

N-(3-((4-Formylbenzyl)oxy)phenyl)butane-1-sulfonamide (46)
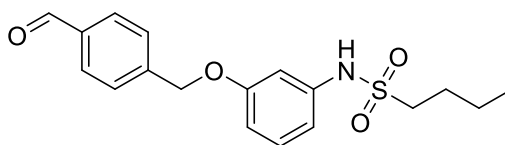
The reaction was carried out according to general procedure **D** using compound **35** (500 mg, 1.44 mmol, 1.0 eq) and 4-bromomethyl benzaldehyde (828 mg, 4.16 mmol, 1.1 eq). The crude was purified by flash column chromatography using a gradient (CH$_2$Cl$_2$: EtOAc 90:10) to afford the title compound as a white solid (274 mg, 36% yield).^{1}H NMR (400 MHz, DMSO-d_6) δ 0.89 (t, J = 7.1 Hz, 3H), 1.31 (m, 2H), 1.61 (m, 2H), 3.06-3.10 (m, 2H), 5.16 (s, 2H), 6.19 (dd, J = 8.2, 2.3 Hz, 1H), 6.35 -6.40 (m, 1H), 6.94 (dd, J = 8.0, 2.0, Hz, 1H), 7.09-7.25 (m, 1H), 7.55(d, J = 8.3 Hz, 2H), 7.82 (d, J = 8.3 Hz, 2H), 9.90 (s, 1H), 10.02 (s, 1H). ^{13}C NMR (100 MHz, DMSO-d_6) δ 13.8, 21.0, 21.6, 56.3, 71.4, 106.3, 115.2, 129.8, 131.1, 131.8, 134.8, 139.8, 145.3, 158.8, 193.3.

4-Chloro-N-(3-(4-formylbenzyloxy)phenyl)benzenesulfonamide (47)
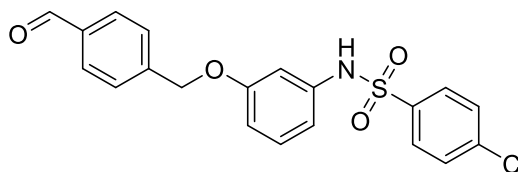
The reaction was carried out according to general procedure **D** using compound **36** (500 mg, 1.76 mmol, 1.0 eq) and 4-bromomethyl benzaldehyde (386 mg, 1.94 mmol, 1.1 eq) to afford the title compound as a white solid. The product was used in the next step without further purification (250 mg, 35% yield). ^{1}H NMR (400 MHz, DMSO-d_6) 4.87 (s, 2H), 6.48-6.51 (m, 1H), 6.61-6.63 (m, 1H), 6.99-7.05 (m, 1H)), 7.49 (d, J = 7.8 Hz, 2H), 7.62-7.75 (m, 5H), 7.83 (d J = 8.0 Hz, 2H), 9.55 (s, 1H) 9.93 (s, 1H).^{13}C NMR (100 MHz, DMSO-d_6) 70.4, 106.2, 114.2, 117.3, 129.6, 129.8, 130.0, 130.1, 135.4, 137.1, 137.2, 137.9, 150.1, 157.7, 192.4.

N-(3-(4-Formylbenzyloxy)phenyl)-4-methylbenzenesulfonamide (48)
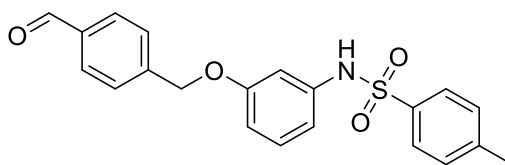
The reaction was carried out according to general procedure **D** using compound **37** (150 mg, 0.57 mmol, 1.0 eq) and 4-bromomethyl benzaldehyde (124 mg, 0.62 mmol, 1.1 eq). The residue was purified by flash column chromatography using 0→5% MeOH in CH_2Cl_2 to afford the title compound as a white solid (100 mg, 26% yield). ^{1}H NMR (400 MHz, DMSO-d_6) δ 2.43 (s, 3H), 4.87 (s, 2H), 6.46 (dd, J = 8.0, 1.8 Hz, 1H), 6.48 – 6.50 (m, 2H), 6.61 (dd, J = 8.2, 2.3 Hz, 1H), 7.50 (d, J = 8.1 Hz, 2H), 7.63 (d, J = 7.3 Hz, 2H), 7.66 – 7.71 (m, 2H), 7 .82 (d, J = 8.1 Hz, 2H), 9.54 (s, 1H), 9.93 (s, 1H). ^{13}C NMR (100 MHz, DMSO-d_6) δ 21.3, 53.5, 114.9, 115.6, 118.3, 127.3, 128.5, 129.3, 129.43, 129.6, 135.4, 137.7, 139.6, 143.4, 157.5, 192.6. ESI-HRMS calculated for $C_{21}H_{20}NO_4S$ (M+H)$^+$: 382.0962, found 382.0951.

N-(3-(4-Formylbenzyloxy)phenyl)cyclohexanesulfonamide (49)
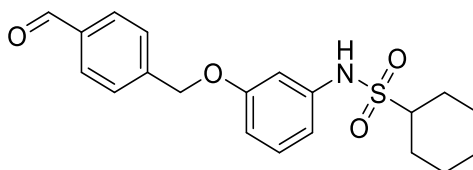
The reaction was carried out according to general procedure **D** using compound **38** (500 mg, 2.08 mmol, 1.0 eq) and 4-bromomethyl benzaldehyde (445 mg, 2.28 mmol, 1.1 eq). The residue was purified by flash column chromatography using 10→15% EtOAc in to petroleum ether to afford the title compound (250 mg, 34% yield) as a white solid. ^{1}H NMR (400 MHz, DMSO-d_6) δ 1.11 - 1.22 (m, 1H), 1.26 - 1.36 (m, 2H), 1.49 - 1.55 (m, 2H), 1.57 - 1.65 (m, 1H), 1.78 (m, 2H), 2.17-2.22 (m, 2H), 3.45 - 3.57 (m, 1H) 5.28 (s, 2H), 6.90 (ddd, J=8.2, 2.3, 0.8 Hz, 1H), 6.96 (s, 1H), 7.05 (ddd, J = 8.2, 2.3, 0.8 Hz, 1H), 7.40 (m, 1H), 7.67 (d, J = 8.0 Hz, 2H), 7.96 (d, J = 8.0 Hz, 2H), 9.60 (s, 1H), 10.02 (s, 1H). ^{13}C NMR (100 MHz, DMSO-d_6) δ 21.8, 24.0, 24.4, 27.1, 28.0, 51.2, 54.5, 60.0, 62.3, 65.4, 70.0, 109.1, 114.1, 114.8 127.6, 129.0, 131.1, 135.2, 137.8 150.1, 160.1. ESI-HRMS calculated for C$_{20}$H$_{22}$NO$_4$S (M-H)$^-$: 372.1348, found: 372.1357.

4-(3-(Benzylthiophenoxymethyl)benzaldehyde (55)
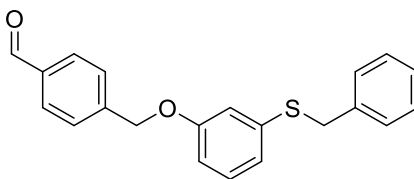
The reaction was carried out according to general procedure **D** using compound **50** (600 mg, 2.79 mmol, 1.0 eq), 4-bromomethyl benzaldehyde (155 mg, 3.01 mmol, 1.3 eq) and potassium carbonate (249 mg, 4.33 mmol, 3 eq) in acetonitrile (2.5 mL). The resulting residue was purified by flash chromatography (25→60% CH_2Cl_2 in petroleum ether) to yield the title compound (700 mg, 75% yield) as a dark yellow oil. ^{1}H NMR (400 MHz, DMSO-d_6) δ 4.22 (s, 2H), 5.18 (s, 2H), 6.83 (dd, J = 2.4, 8.3 Hz, 1H), 6.91 (d, J = 7.8 Hz, 1H), 6.95 – 7.01 (m, 1H), 7.20 (d, J = 8.0 Hz, 1H), 7.24 (d, J = 7.8 Hz, 1H), 7.28 (d, J = 7.5 Hz, 1H), 7.33 (t, J = 8.2 Hz, 2H), 7.64 (s, 1H), 7.67 (d, J = 10.3 Hz, 2H), 7.90 – 7.97 (m, 2H), 9.98 (s, 1H).^{13}C NMR (100 MHz, DMSO-d_6) δ 36.3, 68.5, 112.5, 114.1, 120.6, 126.7, 127.8, 128.4, 129.5, 129.7, 129.9, 135.6, 137.4, 143.9, 158.3, 192.8. ESI-HRMS calculated for $C_{21}H_{19}O_2S$ (M+H) [+]: 335.1053, found: 335.1059.

4-(3-(4-Chlorobenzylthiophenoxy)methyl)benzaldehyde (56)
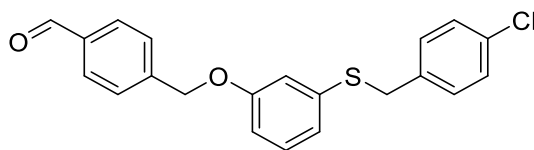
The reaction was carried out according to general procedure **D** using compound **51** (150 mg, 0.60 mmol, 1.0 eq), 4-bromomethyl benzaldehyde (155 mg, 0.78 mmol, 1.3 eq) and potassium carbonate (248 mg, 1.80 mmol, 3.0 eq) in acetonitrile (3 mL). The crude residue was purified by flash chromatography (30% CH_2Cl_2 in petroleum ether) to yield the title compound (189 mg, 86% yield) as a brownish red oil. ^{1}H NMR (400 MHz, DMSO-d_6) δ 4.24 (s, 2H), 5.22 (s, 2H), 6.84 (dd, J = 3.0, 8.2 Hz, 1H), 6.90 (d, J = 7.7 Hz, 1H), 6.96- 6.98 (m, 1H), 7.20 (t, J = 8.0 Hz, 1H), 7.30-7.38 (m, 4H), 7.64 (d, J = 8.0 Hz, 2H), 7.94 (d, J = 8.0 Hz, 2H), 10.02 (s, 1H). ^{13}C NMR (100 MHz, DMSO-d_6) δ 36.2, 69.1, 110.3, 115.1, 121.5, 128.2, 129.9, 130.3, 130.8, 133.4, 135.2, 136.2, 137.1, 142.4, 158.5, 190.4.

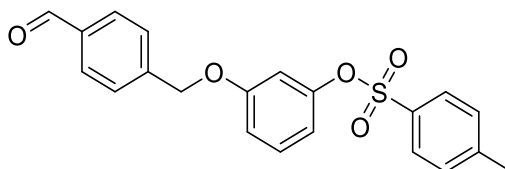**4-(3-(4-Fluorobenzylthiophenoxy)methyl)benzaldehyde (57)**
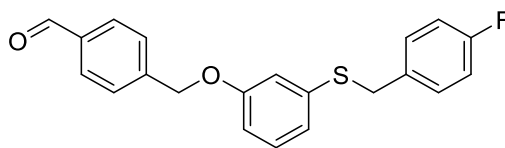
The reaction was carried out according to general procedure **D** using compound **52** (150 mg, 0.64 mmol, 1.0 eq), 4-Bromomethyl benzaldehyde (165 mg, 0.83 mmol, 1.3 eq), and potassium carbonate (265 mg, 1.92 mmol, 3.0 eq) in acetonitrile (3 mL). The crude product was purified by flash column chromatography (0 →30% CH_2Cl_2 in petroleum ether) to yield the title compound (200 mg, 89% yield) as a yellow oil. ^1H NMR (400 MHz, DMSO-d_6) δ 4.24 (s, 2H), 5.23 (s, 2H), 6.84 (ddd, J = 0.9, 2.6, 8.3 Hz, 1H), 6.91 (dt, J = 1.3, 7.8 Hz, 1H), 6.96 – 7.01 (m, 1H), 7.06 – 7.15 (m, 2H), 7.21 (t, J = 8.0 Hz, 1H), 7.33 – 7.41 (m, 2H), 7.65 (d, J = 8.1 Hz, 2H), 7.94 (d, J = 8.3 Hz, 2H), 10.02 (s, 1H). ^{13}C NMR (100 MHz, DMSO-d_6) δ 36.0, 69.1, 113.2, 114.9, 115.6, 115.8, 121.4, 128.4, 130.4, 131.3, 134.3, 134.3, 138.0, 144.5, 158.9, 163.0, 193.4. ^{19}F NMR (471 MHz, DMSO-d_6) δ -115.51. ESI-HRMS calculated for $C_{21}H_{16}FO_2S$ (M-H)$^-$: 351.0861, found: 351.0866.

4-(3-(4-Trifluoromethylbenzylthiophenoxy)methyl)benzaldehyde (58)
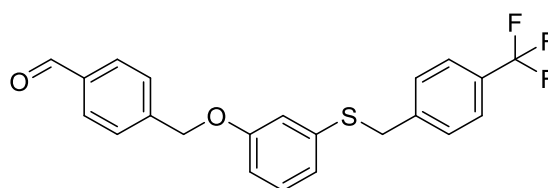
The reaction was carried out according to general procedure **D** using compound **53** (150 mg, 0.39 mmol, 1.0 eq), 4-bromomethyl benzaldehyde (102 mg, 0.51 mmol, 1.3 eq) and potassium carbonate (414 mg, 1.18 mmol, 3.0 eq) in acetonitrile (3 mL). The crude residue was purified by flash chromatography (25→60% CH_2Cl_2 in petroleum ether) to yield the title compound (156 mg, 99% yield) as a brown oil. ^{1}H NMR (400 MHz, DMSO-d_6) δ 4.32 (s, 2H), 5.15 (s, 2H), 6.54 – 6.71 (m, 3H), 6.71 – 6.86 (m, 1H), 7.07 (ddd, J = 2.5, 5.1, 10.4 Hz, 1H), 7.13 – 7.37 (m, 3H), 7.51 – 7.69 (m, 3H), 7.84 (d, J = 8.1 Hz, 1H), 9.76 (s, 1H).^{13}C NMR (100 MHz, DMSO-d_6) δ 39.5, 70.5, 110.5, 115.2, 121.2, 124.1, 125.1, 129.2, 129.4, 129.9, 130.1, 135.5, 137.2, 139.9, 143.0, 160.3, 191.1.

4-(3-(Cyclohexylmethylthiophenoxy)methyl)benzaldehyde (59)

The reaction was carried out according to general procedure **D** using compound **54** (350 mg, 1.57 mmol, 1.0 eq), 4-bromomethyl benzaldehyde (407 mg, 2.04 mmol, 1.3 eq) and potassium carbonate (653 mg, 4.27 mmol, 3.0 eq) in acetonitrile (7 mL). The crude residue was purified by flash chromatography (25→60% CH_2Cl_2 in petroleum ether) to yield the title compound (200 mg, 37% yield) as a brown oil. ^{1}H NMR (400 MHz, DMSO-d_6) δ 0.95 (q, J = 12.1 Hz, 2H), 1.12 (d, J = 9.5 Hz, 3H), 1.32 – 1.52 (m, 1H), 1.52 – 1.70 (m, 2H), 1.78 (d, J = 13.0 Hz, 3H), 2.62 – 2.95 (m, 2H), 5.25 (d, J = 4.9 Hz, 2H), 6.79 – 6.84 (m, 1H), 6.86 – 6.92 (m, 2H), 7.22 (t, J = 8.0 Hz, 1H), 7.65 (dd, J = 8.0, 11.1 Hz, 2H), 7.85 – 7.88 (m, 1H), 7.94 (d, J = 8.2 Hz, 1H), 10.01 (s, 1H). ESI-HRMS calculated for $C_{21}H_{25}O_2S$ (M+H)$^+$: 341.1499, found: 341.1500.

5.1.2.7 Synthesis of 4-(3-(methoxymethoxyphenoxy) methyl) benzaldehyde (62).
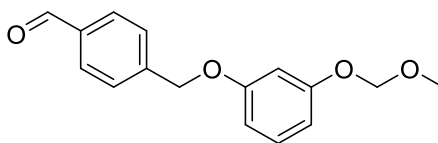
4-Bromomethyl benzaldehyde (165 mg, 9.98 mmol, 1.3 eq) was added to a stirred suspension of compound **61** (1.4 g, 9.08 mmol, 1.0 eq) and potassium carbonate (265 mg, 1.92 mmol, 3.0 eq) in acetonitrile (3 mL). The resulting mixture was heated to 60 °C under nitrogen. After 3 hours, the reaction mixture was cooled to room temperature and diluted with dichloromethane, absorbed onto silica and purified by flash chromatography (30% CH_2Cl_2 in petroleum ether) to yield the title compound (200 mg, 89% yield) as a yellow oil. ^{1}H NMR (400 MHz, DMSO-d_6) δ 3.36 (s, 3H), 5.90 (s, 2H), 6.05 (s, 2H), 6.59 – 6.62 (m, 1H), 6.63 – 6.65 (m, 1H), 6.65 (d, J = 1.7 Hz, 1H), 7.12 – 7.25 (m, 1H), 7.47 (d, J = 8.0 Hz, 2H), 7.88 (d, J = 8.0 Hz, 2H), 9.89 (s, 1H). ^{13}C NMR (100 MHz, DMSO-D_6) δ 54.6, 69.7, 94.4, 103.8, 108.6, 109.1, 129.9, 130.1, 130.7, 135.8, 142.1, 158.5, 160.1, 190.2. ESI-HRMS calculated for $C_{16}H_{17}O_4$ $(M+H)^+$: 273.1121, found: 273.1121.

5.1.2.8 General procedure E (reductive amination) [272]

X=S, NH or O

X=S, NH or O
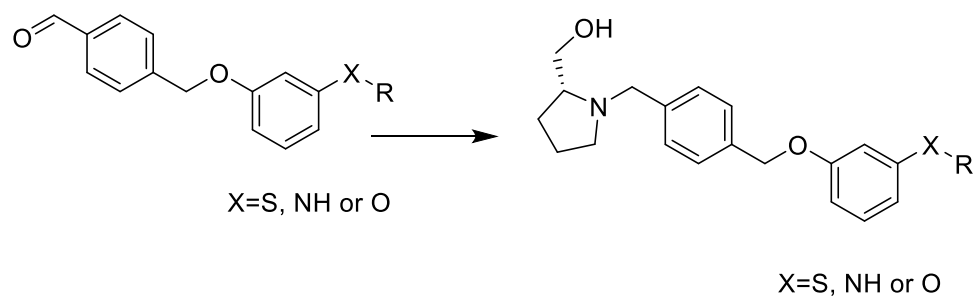
To a solution of a previousely synthesised aldehydes (1.0 eq), utilizing general procedure D, in 1,2-dichloroethane (5 mL) was added (R)-(-)-2-pyrrolidinemethanol (1.5 eq) and sodium triacetoxyborohydride (1.5 eq). After the reaction mixture was stirred overnight, the mixture was diluted with CH_2Cl_2 and washed with saturated aqueous sodium carbonate solution. The organic layer was dried over anhydrous $MgSO_4$ and concentrated. The residue was purified by flash column chromatography (Biotage SP4, SiO_2, 0.1% Et_3N in EtOAc) to afford the desired compounds.

(*R*)-3-((4-((2-(Hydroxymethyl)pyrrolidin-1-yl)methyl)benzyl)oxy)phenyl4-methoxybenzenesulfonate (3)
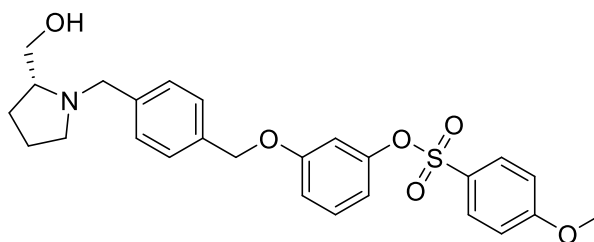
The reaction was carried out according to general procedure **E** using compound **40** (200 mg, 0.50 mmol, 1.0 eq), (*R*)-(-)-2-pyrrolidinemethanol (54 µL, 0.55 mmol, 1.1 eq) and sodium triacetoxyborohydride (159 mg, 0.75 mmol, 1.5 eq). The crude product was purified by flash column chromatography (0 →10% MeOH in EtOAc buffered with 1% Et$_3$N) to afford the title compound as a yellow oil (85 mg, 35%). ^{1}H NMR (400 MHz, DMSO-d_6) δ 1.28 – 1.61 (m, 3H), 1.72 – 1.80 (m, 1H), 2.07 - 2.10 (m, 1H), 2.34 – 2.47 (m, 1H), 2.69 – 3.00 (m, 1H), 3.32 – 3.45 (m, 2H), 3.87 (s, 3H), 3.55-3.61 (m, 1H), 4.04 (d, J = 13.3 Hz, 1H), 4.40 (br.s, 1H), 5.00 (s, 2H), 6.58 (dd, J = 8.2, 2.3 Hz, 1H), 6.07 6.66 (m, 1H), 6.95 (dd, J = 8.0, 2.0 Hz, 1H), 7.16-7.18 (m, 1H), 7.26 (d, J = 8.0 Hz, 2H), 7.33 (d, J = 8.0 Hz, 2H), 7.77 (d, J = 8.0 Hz, 2H), 7.79 (d, J = 8.0 Hz, 2H). ^{13}C NMR (100 MHz, DMSO-d_6) 23.8, 28.7, 54.3, 59.2, 64.1, 66.2, 70.1, 106.3, 114.5, 117.6, 127.2, 128.3, 129.1, 134.8, 134.7, 136.1, 151.8, 159.3, 161.2. ESI-HRMS calculated for C$_{26}$H$_{30}$NO$_6$S (M+H)$^+$: 484.1788, found: 484.1782.

(*R*)-3-((4-((2-(Hydroxymethyl)pyrrolidin-1-yl)methyl)benzyl)oxy)phenyl4-chlorobenzenesulfonate (4)
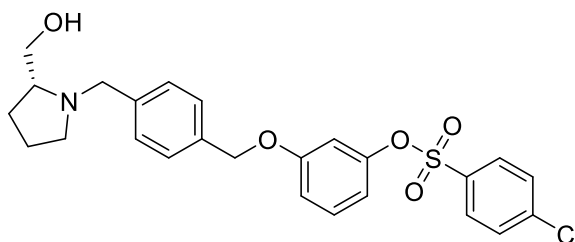
The reaction was carried out according to general procedure **E** using compound **42** (150 mg, 0.37 mmol, 1.0 eq), (*R*)-(-)-2-pyrrolidinemethanol (40 µL, 0.41 mmol, 1.1 eq) and sodium triacetoxyborohydride (117 mg, 0.55 mmol, 1.5 eq). The crude residue was purified by flash column chromatography (0 → 10% MeOH in EtOAc buffered with 1% Et$_3$N) to afford the title compound as a colorless oil (67 mg, 37% yield). ^{1}H NMR (400 MHz, DMSO-d_6) δ 1.29 – 1.57 (m, 4H), 1.72 – 1.90 (m, 1H), 2.07 - 2.10 (m, 1H), 2.49 – 2.67 (m, 1H), 2.69 – 3.00 (m, 1H), 3.32 – 3.37(m, 1H), 3.40-3.45 (m, 1H), 4.03 (d, *J* = 13.3 Hz, 1H), 4.42 (br.s, 1H), 5.00 (s, 2H),6.58 (dd, *J* = 8.2, 2.3 Hz, 1H), 6.71 (m, 1H), 6.95 (dd, *J* = 8.0, 2.0 Hz, 1H), 7.18-7.20 (m, 1H), 7.29 (d, *J* = 8.2 Hz, 2H), 7.32 (d, *J* = 8.2 Hz, 2H), 7.78 (d, *J* = 8.4 Hz, 2H), 7.87 (d, *J* = 8.4 Hz, 2H). ^{13}C NMR (100 MHz, DMSO-d_6) 22.9, 27.3, 55.1, 58.5, 63.0, 65.2, 69.6, 105.0, 114.4, 118.7, 127.5, 128.7, 129.3, 130.1, 134.5, 136.9, 138.1, 151.6, 159.5. HRMS- ESI calculated for C$_{25}$H$_{27}$NO$_5$ClS (M+H)$^+$: 488.1291, found: 488.1293.

(*R*)-3-((4-((2-(Hydroxymethyl)pyrrolidin-1-yl)methyl)benzyl)oxy)phenyl4-methylbenzenesulfonate (5)
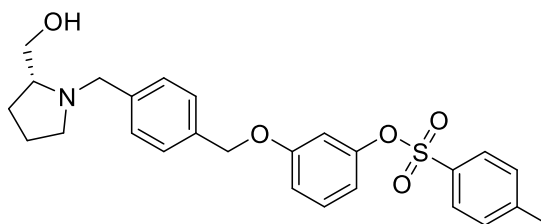
The reaction was carried out according to general procedure **E** using compound **43** (161 mg, 0.42 mmol, 1.0 eq), (*R*)-(-)-2-pyrrolidinemethanol (46 μL, 0.38 mmol, 1.1eq) and sodium triacetoxyborohydride (136 mg, 0.62 mmol, 1.5 eq). The crude product was purified by flash column chromatography (0 to 10% MeOH in EtOAc with 1% Et₃N) to afford the title compound as a colourless oil (88 mg, 45% yield). ^{1}H NMR (400 MHz, DMSO-d_6) δ 1.41-1.58 (m, 3H), 1.77-1.83 (m, 1H), 2.12-2.23 (m, 1H), 2.42 (s, 3H), 2 .47 – 2.55 (m, 1H), 2.61- 2.76 (m, 1H), 3.29- 3.31 (m, 1H), 3.45 (m, 2H), 4.05 (d, *J* = 13.2 Hz, 1H), 4.42 (br. s, 1H), 4.99 (s, 2H), 6.58 (dd, *J* = 2.2, 8.1 Hz, 1H), 6.67 (t, *J* = 2.3 Hz, 1H), 6.96 (dd, *J* = 2.3, 8.1 Hz, 1H), 7.27 (t, *J* = 8.3 Hz, 1H), 7.32 (app s, 4H), 7.47 (d, *J* = 8.2 Hz, 2H), 7.73 (d, *J* = 8.3 Hz, 2H).^{13}C NMR (100 MHz, DMSO-d_6) δ 21.4, 22.4, 27.9, 53.5, 54.0, 58.4, 64.1, 64.8, 110.7, 114.7, 115.4, 127.2, 127.7, 130.3, 131.1, 132.6, 135.0, 137.1, 138.6, 152.4, 159.4. ESI-HRMS calculated for $C_{26}H_{30}NO_5S$ (M+H)$^+$: 468.1838, found: 468.1839.

(*R*)-3-((4-((2-(Hydroxymethyl)pyrrolidin-1-yl)methyl)benzyl)oxy)phenylbutane-1-sulfonate (8)

The reaction was carried out according to general procedure **E** using compound **41** (150 mg, 0.43 mmol, 1.0 eq) and (*R*)-(-)-2-pyrrolidinemethanol (47 µL, 0.47 mmol, 1.5 eq) and sodium triacetoxyborohydride (158 mg, 0.42 mmol, 1.5 eq). The crude was purified by flash column chromatography (0 → 10% MeOH in EtOAc buffered with 1% Et₃N) to afford the title compound as a colourless oil (100 mg, 54% yield). ¹H NMR (400 MHz, DMSO-*d₆*) δ 0.90 (t, *J* = 7.5 Hz, 3H), 1.30-1.38 (m, 2H), 1.43 (t, *J* = 7.4 Hz, 2H), 1.59 (s, 3H), 1.71-1.82 (m, 2H), 1.85-2.09 (m, 2H), 2.54 - 2.78 (m, 2H), 2.96-3.04 (m, 2H), 3.43 – 3.52 (m, 2H), 4.45 (s, 1H), 5.11 (s, 2H), 6.91 (dd, *J* = 2.2, 8.1 Hz, 1H), 6.73 -6.80 (m, 1H), 6.97 (t, *J* = 2.2 Hz, 1H), 7.03 (dd, *J* = 2.5, 8.3 Hz, 1H), 7.39 (dd, *J* = 7.5, 9.2 Hz, 4H). ¹³C NMR (100 MHz, DMSO-*d₆*) δ 13.3, 21.0, 22.4, 28.0, 35.7, 54.9, 58.4, 64.2, 64.8, 69.1, 112.7, 115.5, 120.6, 124.9, 127.5, 128.6, 129.9, 130.3, 137.0, 158.6. ESI-HRMS calculated for C₂₃H₃₂O₅NS (M+H)⁺ : 434.1994, found : 434.1996.

(*R*)-3-((4-((2-(Hydroxymethyl)pyrrolidin-1-yl)methyl)benzyl)oxy)phenyl cyclohexanesulfonate (9)

The reaction was carried out according to general procedure **E** using compound **44** (60 mg, 0.16 mmol, 1.0 eq), (*R*)-(-)-2-pyrrolidinemethanol (17 µL, 0.176 mmol, 1.1 eq) and sodium triacetoxyborohydride (51 mg, 0.24 mmol, 1.5 eq). The crude was purified by flash column chromatography (0 → 10% MeOH in EtOAc buffered with 1% Et$_3$N) to afford the title compound as a colourless oil (55 mg, 74% yield). ^{1}H NMR (400 MHz, DMSO-*d6*) δ 1.20 – 1.27 (m, 2H), 1.25 – 1.44 (m, 1H), 1.47 – 1.69 (m, 5H), 1.76 – 1.87 (m, 4H), 2.17 (d, *J* = 13.2 Hz, 3H), 2.55 (m, 1H), 2.76 (m, 1H), 3.25 – 3.29 (m, 1H), 3.30 – 3.32 (m, 1H), 3.43 – 3.47 (m, 1H), 3.51 (td, *J* = 4.2, 8.3 Hz, 1H), 4.06 (d, *J* = 4.7 Hz, 1H), 4.42 (br.s, 1H), 5.10 (s, 2H), 6.89 (dd, *J* = 8.0, 2.3 Hz, 1H), 6.92 (t, *J* = 2.3 Hz, 1H), 7.02 (dd, *J* = 2.5, 8.3 Hz, 1H), 7.33 (d, *J* = 7.8 Hz, 2H), 7.38-7.40 (m, 3H). ^{13}C NMR (100 MHz, DMSO-*d6*) δ 22.4, 24.1, 24.5, 26.1, 27.6, 50.5, 54.0, 59.0, 61.3, 64.4, 69.5, 108.8, 113.5, 114.2, 127.2, 128.7, 130.5, 134.9, 137.2, 149.6, 159.4. ESI-HRMS calculated for C$_{25}$H$_{34}$O$_5$NS (M+H)$^+$: 460.2152, found: 460.2151.

(*R*)-*N*-(3-((4-((2-(Hydroxymethyl)pyrrolidin-1-yl)methyl)benzyl)oxy)phenyl)butane-1-sulfonamide (10)
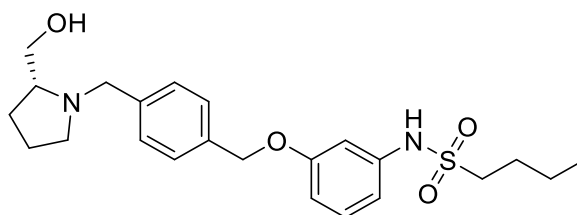
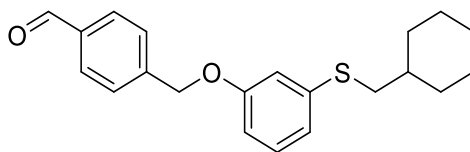The reaction was carried out according to general procedure **E** using compound **46** (150 mg, 0.44 mmol, 1.0 eq), (*R*)-(-)-2-pyrrolidinemethanol (48 µL, 0.47 mmol, 1.5 eq) and sodium triacetoxyborohydride (180 mg, 0.86 mmol, 1.5 eq). The crude was purified by flash column chromatography (0 → 10% MeOH in EtOAc buffered with 1% Et$_3$N) to afford the title compound as a white solid (120 mg, 65% yield). ^{1}H NMR (400 MHz, DMSO-d_6) δ 0.89 (t, *J* = 7.5 Hz, 3H), 1.34 (m, 2H), 1.43 – 1.54 (m, 2H), 1.60 (m, 2H), 1.61 - 168 (m, 2H), 2.20 - 2.30 (m, 1H), 2.33 (m, 1H), 3.11 (t, *J* = 7.1 Hz, 2H) , 3.43 (d, *J* = 13.3 Hz, 2H), 3.62 (t, *J* = 6.7 Hz, 2H), 4.01 (s,1H), 5.16 (s, 2H), 6.19 (dd, *J* = 8.2, 2.3 Hz, 1H), 6.35(s, 1H), 6.94 (dd, *J* = 8.0, 2.0,0.8 Hz, 1H), 7.09 (m, 1H), 7.11 (d, *J* = 8.3 Hz, 2H), 7.16 (d, *J* = 8.3 Hz, 2H), 10.02 (s, 1H).). ^{13}C NMR (100 MHz, DMSO-d_6) δ 14.2, 22.1, 22.6, 25.2, 28.1, 60.1, 60.2, 70.2, 70.7, 80.3, 114.3, 117.3, 125.2, 127.1, 129.8, 130.8, 132.1, 134.6, 139.8, 162.5. ESI-HRMS calculated for C$_{23}$H$_{33}$N$_2$O$_4$S (M+H)$^+$: 433.2194, found: 433.2196.

(*R*)-*N*-(3-((4-((2-(hydroxymethyl)pyrrolidin-1-yl)methyl)benzyl)oxy)phenyl)-4-methylbenzenesulfonamide (11)

The reaction was carried out according to general procedure **E** using compound **48** (80 mg, 0.21 mmol, 1.0 eq), (*R*)-(-)-2-pyrrolidinemethanol (23 µL, 0.23 mmol, 1.1 eq) and sodium triacetoxyborohydride (59.5 mg, 0.31 mmol, 1.5 eq). The crude product was purified by flash column chromatography (0 → 10% MeOH in EtOAc buffered with 1% Et$_3$N) to afford the title compound as a yellow oil (50 mg, 51% yield). ^{1}H NMR (400 MHz, DMSO-d_6) 1.50 – 1.61 (m, 3H), 1.78 – 1.85 (m, 1H), 2.03 - 2.10 (m, 1H), 2.43 (s, 3H), 2.47 – 2.55 (m, 1H), 2.64 – 2.71 (m, 1H), 3.18 – 3.29 (m, 1H), 3.36 – 3.51 (m, 2H), 3.96 (d, *J* = 13.3 Hz, 1H), 4.40 (br.s, 1H), 4.71 (s, 2H), 6.41 (d, *J* = 7.6 Hz, 1H), 6.44 – 6.45 (m, 1H), 6.59 (dd, *J* = 7.8, 2.1 Hz, 1H), 6.98 - 7.02 (m, 1H), 7.21 (d, *J* = 8.3 Hz, 2H), 7.27 (d, *J* = 8.3 Hz, 2H), 7.58 – 7.68 (app s, 4H), 9.51 (s, 1H). ^{13}C NMR (100 MHz, DMSO-d_6) δ 22.4, 27.9, 53.5, 54.0, 58.4, 64.1, 64.8, 114.7, 115.7, 118.4, 127.2, 127.7, 128.4, 128.5, 129.3, 134.6, 138.0, 139.1, 139.6, 157.4. ESI-HRMS calculated for C$_{26}$H$_{31}$N$_2$O$_4$S (M+H)$^+$: 467.1834, found: 467.1838.

(*R*)-*N*-(3-((4-((2-(Hydroxymethyl)pyrrolidin-1-yl)methyl)benzyl)oxy)phenyl)-4-methoxybenzenesulfonamide (12)
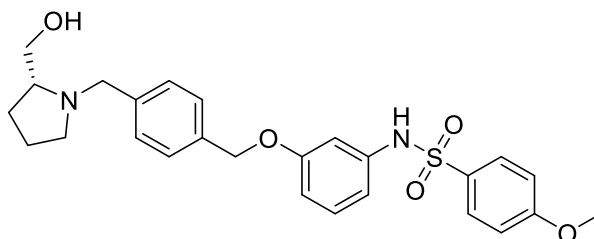
The reaction was carried out according to general procedure **E** using compound **45** (150 mg, 0.37 mmol, 1eq), (*R*)-(-)-2-pyrrolidinemethanol (41 µL, 0.41 mmol, 1.1eq) and sodium triacetoxyborohydride (119 mg, 0.56 mmol, 1.5 eq). The crude was purified by flash column chromatography (0 → 10% MeOH in EtOAc buffered with 1% Et$_3$N) to afford the title compound as a yellow oil (104 mg, 57% yield). ^{1}H NMR (400 MHz, CDCl$_3$) δ 1.68– 1.77 (m, 3H), 2.44– 2.82 (m, 2H), 3.08– 3.21 (m, 2H), 3-66-3.73 (m 2H), 3.91 (s, 3H), 4.60 (d, *J* = 13.9 Hz, 1H), 4.77 (d, *J* = 13.9 Hz, 1H), 6.05 (t, *J* = 2.2 Hz, 1H), 6.47 (ddd, *J* = 1.0, 2.0, 7.9 Hz, 1H), 6.73 (ddd, *J* = 1.0, 2.5, 8.2 Hz, 1H), 6.95 – 7.00 (m, 2H), 7.08 (t, *J* = 8.1 Hz, 1H), 7.18 (d, *J* = 8.1 Hz, 2H), 7.23 (d, *J* = 8.1 Hz, 2H), 7.61 – 7.76 (m, 2H). ^{13}C NMR (100 MHz, CDCl$_3$) 23.8, 28.7, 55.3, 58.2, 62.5, 64.1, 66.2, 70.1, 113.3, 115.5, 117.6, 119.50, 128.3, 129.0, 129.2, 129.3, 132.7, 139.1, 149.8, 155.9, 161.2. ESI-HRMS calculated for C$_{26}$H$_{31}$ N$_2$O$_5$S (M+H)$^+$: 483.1948, found: 483.1939.

(R)-4-Chloro-N-(3-((4-((2-(hydroxymethyl)pyrrolidin-1-yl)methyl)benzyl)oxy)phenyl)benzenesulfonamide (13)

The reaction was carried out according to general procedure **E** using compound **47** (150 mg, 0.37 mmol, 1.0 eq), (*R*)-(-)-2-pyrrolidinemethanol (43 µL, 0.41 mmol, 1.1 eq) and sodium triacetoxyborohydride (119 mg, 0.56 mmol, 1.5 eq). The crude product was purified by flash column chromatography (0 → 10% MeOH in EtOAc buffered with 1% Et₃N) to afford the title compoundas a yellow solid (100 mg, 55% yield). ^{1}H NMR (400 MHz, DMSO-*d₆*) δ 1.51-1.60 (m, 3H), 1.77 – 1.87 (m, 1H), 2.66-2.08 (m, 1H), 2.66 – 2.73 (m, 1H), 3.00 – 3.18 (m, 2H), 3.24 (d, *J* = 12.9 Hz, 1H), 3.38 – 3.46 (m, 1H), 3.98 (d, *J* = 13.3 Hz, 1H), 4.37 (br.s, 1H), 4.73 (s, 2H), 6.44 -6.46 (m, 2H), 6.60 – 6.64 (m, 1H), 7.03 (t, *J* = 8.0 Hz, 1H), 7.16 (d, *J* = 8.1 Hz, 2H), 7.20 (d, *J* = 8.2 Hz, 2H), 7.66 (d, *J* = 8.8 Hz, 2H), 7.70 (d, *J* = 8.8 Hz, 2H), 9.53 (s, 1H). ^{13}C NMR (100 MHz, DMSO-*d₆*) δ 22.4, 28.0, 53.5, 54.0, 58.4, 64.1, 64.8, 114.9, 115.8, 118.5, 127.7, 128.5, 129.2, 129.4, 134.4, 136.8, 138.0, 139.4, 157.5. ESI-HRMS calculated for C₂₅H₂₈N₂O₄ClS (M+H) $^+$: 487.1458, found: 487.1458.

(*R*)-*N*-(3-((4-((2-(Hydroxymethyl)pyrrolidin-1-yl)methyl)benzyl)oxy)phenyl)cyclohexanesulfonamide (14)
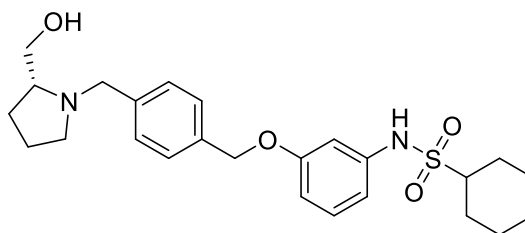
The reaction was carried out according to general procedure **E** using compound **49** (150 mg, 0.40 mmol, 1.0 eq), (*R*)-(-)-2-pyrrolidinemethanol (36 µL, 0.44 mmol, 1.1 eq) and sodium triacetoxyborohydride (139 mg, 0.66 mmol, 1.5 eq). The crude product was purified by flash column chromatography (0 → 10% MeOH in EtOAc buffered with 1% Et$_3$N) to afford the title compound as a yellow oil (110 mg, 60% yield). ^{1}H NMR (400 MHz, DMSO-d_6) 1.09 – 1.34 (m, 5H), 1.44 (td, J = 3.5, 12.3 Hz, 2H), 1.49 – 1.65 (m, 3H), 1.79 – 1.84 (m, 1H), 2.04 – 2.14 (m, 4H), 2.63 – 2.73 (m, 1H), 3.11 (td, J = 4.2, 8.5 Hz, 1H), 3.18 (d, J = 5.1 Hz, 1H), 3.20 – 3.28 (m, 2H), 3.39 – 3.46 (m, 1H), 3.98 (d, J = 13.3 Hz, 1H), 4.36 (br.s, 1H), 4.86 (s, 2H), 6.61 (dd, J = 2.3, 8.0 Hz, 1H), 6.74 (t, J = 2.2 Hz, 1H), 6.83 (dd, J = 2.0, 7.8 Hz, 1H), 7.10 (t, J = 8.1 Hz, 1H), 7.15 (d, J = 8.2 Hz, 2H), 7.21 (d, J = 8.2 Hz, 2H), 9.52 (s, 1H). ^{13}C NMR (100 MHz, DMSO-d_6) δ 22.4, 24.5, 24.8, 26.2, 28.0, 54.0, 58.4, 59.7, 64.1, 64.8, 114.1, 115.5, 118.3, 127.5, 128.4, 129.5, 135.5, 140.2, 157.5. ESI-HRMS calculated for C$_{25}$H$_{35}$O$_4$N$_2$S (M+H)$^+$: 459.2312, found: 459.2317.

(*R*)-(1-(4-((3-((4-Chlorobenzyl)thio)phenoxy)methyl)benzyl)pyrrolidin-2-yl)methanol (20)
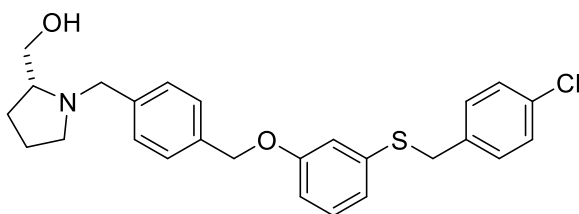
The reaction was carried out according to general procedure **E** using compound **56** (100 mg, 0.27 mmol, 1.0 eq), (*R*)-(-)-2-pyrrolidinemethanol (29 μL, 0.29 mmol, 1.1 eq) and sodium triacetoxyborohydride (172 mg, 0.81 mmol, 3.0 eq) in 1,2-dichloroethane (5 mL). The crude residue was purified by flash chromatography (1% Et₃N in EtOAc) to afford the title compound (122 mg, 99% yield) as a yellow oil. ^{1}H NMR (500 MHz, CDCl₃-d) δ 1.88 – 2.05 (m, 2H), 2.07 – 2.19 (m, 2H), 3.04 (dt, *J* = 7.5, 11.5 Hz, 1H), 3.59 (dt, *J* = 5.8, 11.3 Hz, 1H), 3.62 – 3.69 (m, 1H), 3.86 (d, *J* = 3.3 Hz, 1H), 3.95 (dd, *J* = 8.2, 13.2 Hz, 1H), 4.08 (s, 2H), 4.19 (d, *J* = 13.0 Hz, 1H), 4.63 (d, *J* = 13.0 Hz, 1H), 5.03 (s, 2H), 6.81 (dd, *J* = 2.5, 8.1 Hz, 1H), 6.88 (t, *J* = 2.1 Hz, 1H), 6.90 – 6.96 (m, 1H), 7.21 (dd, *J* = 8.3, 16.7 Hz, 3H), 7.28 (d, *J* = 4.0 Hz, 2H), 7.48 (app s, 4H). ^{13}C NMR (126 MHz, CDCl₃) δ 23.3, 26.4, 38.3, 59.7, 61.1, 68.7, 69.2, 113.2, 116.2, 122.7, 128.2, 128.6, 129.9, 130.2, 131.2, 133.0, 136.0, 137.2, 158.7. ESI-HRMS calculated for C₂₆H₂₉O₂NClS (M+H)$^+$: 454.1602, found: 454.1603.

(*R*)-(1-(4-((3-((4-Fluorobenzyl)thio)phenoxy)methyl)benzyl)pyrrolidin-2-yl)methanol (21)
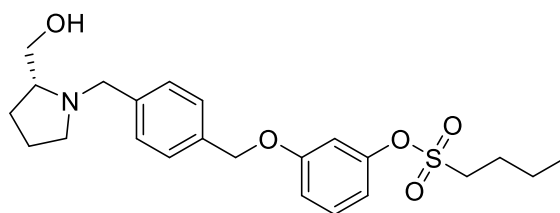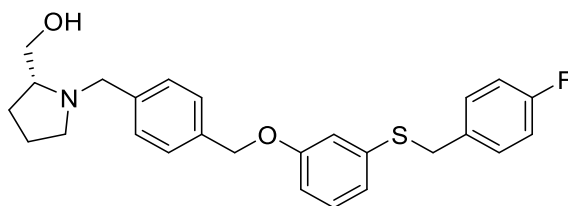

The reaction was carried out according to general procedure **E** using compound **57** (155 mg, 0.44 mmol, 1.0 eq), (*R*)-(-)-2-pyrrolidinemethanol (48 μL, 0.48 mmol, 1.1 eq) and sodium triacetoxyborohydride (279 mg, 1.32 mmol, 3.0 eq) in 1,2-dichloroethane (4 mL). The crude residue was purified by flash chromatography (1% Et$_3$N in EtOAc) to afford the title compound (70 mg, 36% yield) as a light-yellow oil. ^{1}H NMR (400 MHz, DMSO-d_6) δ 1.58 (t, J = 8.5 Hz, 3H), 1.83 (dd, J = 4.4, 8.2 Hz, 1H), 2.11 (t, J = 8.1 Hz, 1H), 2.56 (d, J = 6.2 Hz, 1H), 2.75 (t, J = 8.1 Hz, 1H), 3.24 – 3.32 (m, 2H), 3.45 (dd, J = 4.6, 10.5 Hz, 1H), 4.04 (d, J = 13.3 Hz, 1H), 4.23 (s, 2H), 4.41 (br.s, 1H), 5.04 (s, 2H), 6.81 (dd, J = 2.5, 8.3 Hz, 1H), 6.88 (d, J = 7.8 Hz, 1H), 6.95 (d, J = 2.7 Hz, 1H), 7.11 (t, J = 8.6 Hz, 2H), 7.19 (t, J = 8.1 Hz, 1H), 7.34 (p, J = 7.6 Hz, 6H). ^{13}C NMR (100 MHz, DMSO-d_6) δ 23.0, 28.6, 39.5, 54.6, 59.1, 64.8, 65.4, 69.7, 113.2, 114.9, 115.6, 115.8, 121.1, 128.1, 129.2, 130.4, 131.3, 134.3, 135.7, 137.8, 140.3, 159.2, 160.6, 163.0. ^{19}F NMR (471 MHz, DMSO-d_6) δ–115.55. ESI-HRMS calculated for C$_{26}$H$_{29}$FNO$_2$S (M+H)$^+$: 438.1896, found: 438.1898.

(*R*)-(1-(4-(3((4-Trifluoromethylbenzyl)thio)phenoxy)methyl)benzyl)pyrrolidin-2-yl)methanol (22)
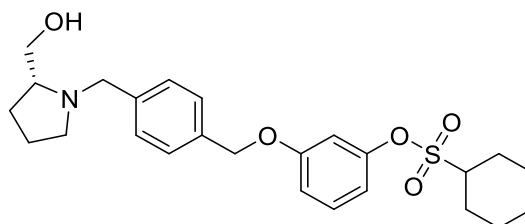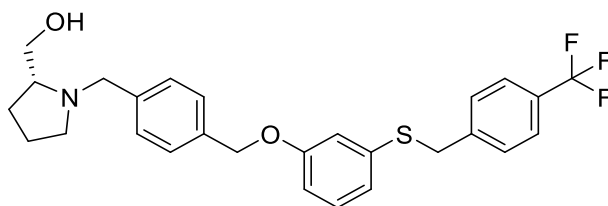

The reaction was carried out according to general procedure **E** using compound **58** (150 mg, 0.36 mmol, 1.0 eq), (*R*)-(-)-2-pyrrolidinemethanol (43 μL, 0.40 mmol, 1.1 eq) and sodium triacetoxyborohydride (254 mg, 1.09 mmol, 3.0 eq), in 1,2-dichloroethane (2 mL). The crude residue was purified by flash chromatography (1% Et$_3$N in EtOAc) to afford the title compound (92 mg, 52% yield) as yellow oil. ^{1}H NMR (400 MHz, DMSO-d_6) δ 1.57-1.63 (m, 3H), 1.79 – 1.87 (m, 1H), 2.09 – 2.14 (m, 1H), 2.52 – 2.60 (m, 1H), 2.75 (m, 1H), 3.24 – 3.29 (m, 1H), 3.30 (s, 1H), 3.39 – 3.51 (m, 1H), 4.01 – 4.06 (m, 1H), 4.24 (s, 2H), 4.42 (br.s, 1H), 5.21 (s, 2H), 6.81 (ddd, *J* = 2.4, 5.4, 7.9 Hz, 1H), 6.90 (t, *J* = 2.2 Hz, 1H), 6.87 – 6.93 (m, 1H), 6.93 – 6.96 (m, 1H), 7.19 (d, *J* = 8.0 Hz, 2H), 7.21 (d, *J* = 8.1 Hz, 2H), 7.30 (d, *J* = 8.1 Hz. 2H), 7.46 (d, *J* = 8.0 Hz, 2H). ^{13}C NMR (100 MHz, DMSO-d6) δ 21.0, 26.9, 38.3, 58.3, 60.2, 62.1, 69.0, 73.0, 110.5, 115.2, 121.2, 124.1, 125.1, 129.2, 129.4, 129.9, 130.1, 135.5, 137.2, 139.9, 143.0, 160.3. ESI-HRMS calculated for C$_{27}$H$_{29}$O$_2$NF$_3$S (M+H+): 488.1860, found: 488.1866.

**(*R*)-(1-(4-((3-((Cyclohexylmethyl)thio)phenoxy)methyl)benzyl)pyrrolidin-2-yl)methanol (23)**
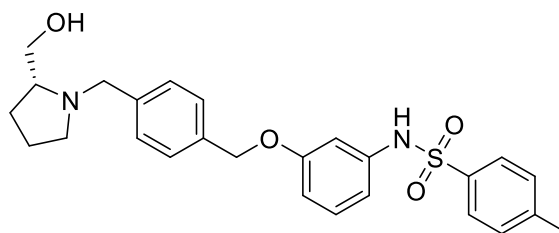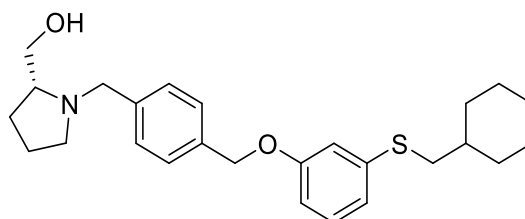

The reaction was carried out according to general procedure **E** using compound **59** (100 mg, 0.29 mmol, 1.0 eq), (*R*)-(-)-2-pyrrolidinemethanol (31 μL, 0.32 mmol, 1.1 eq) and sodium triacetoxyborohydride (186 mg, 0.88 mmol, 3.0 eq) in 1,2-dichloroethane (5 mL). The crude residue was purified by flash chromatography (1% Et₃N in EtOAc) to afford the title compound (50 mg, 40% yield) as a colourless oil.
^{1}H NMR (400 MHz, DMSO-d_6) δ 0.96 (dd, J = 9.5, 17.3 Hz, 2H), 1.13 (d, J = 9.0 Hz, 1H), 1.24-1.26 (m, 1H), 1.33 – 1.48 (m, 1H), 1.54 – 1.71 (m, 4H), 1.80 (t, J = 12.0 Hz, 3H), 1.97 – 1.99 (m, 1H), 2.01 (m, 1H), 2.58 (m, 1H), 2.83 (d, J = 6.7 Hz, 2H), 3.31 (s, 1H), 3.35 (s, 2H), 3.35 – 3.45 (m, 1H), 4.42 (br.s, 1H), 5.24 (s, 2H), 6.78 – 6.83 (m, 1H), 6.87 – 6.92 (m, 2H), 7.22 (t, J = 8.0 Hz, 1H), 7.61 – 7.65 (m, 2H), 7.85 – 7.89 (m, 2H). ^{13}C NMR (100 MHz, DMSO-d_6) δ 25.4, 32.0, 45.0, 58.0, 68.2, 75.1, 110.4, 115.1, 115.7, 118.7, 120.2, 123.6, 128.0, 132.4, 135.4, 138.5, 142.9, 149.8, 158.2. ESI-HRMS calculated for C₂₆H₃₆O₂NS (M+H)⁺ : 426.2460, found: 426.2461.

**Tert-butyl(*R*)-((1-(4-((3-(benzylthio)phenoxy)methyl)benzyl)pyrrolidin-2-yl)methyl)carbamate(60)**
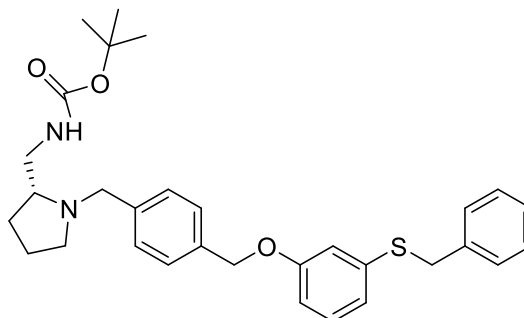
The reaction was carried out according to general procedure **E** using compound **55** (150 mg, 0.44 mmol, 1.0 eq), *tert*-butyl (*R*)-(pyrrolidin-2-ylmethyl) carbamate (98 mg, 99 μL, 0.49 mmol, 1.1eq) and sodium triacetoxyborohydride (0.28 mg, 1.34 mmol, 3.0 eq). The crude residue was purified by flash column chromatography (0 → 10% MeOH in EtOAc buffered with 1% Et$_3$N) to afford the title compound as a yellow oil (115 mg, 50% yield). ^{1}H NMR (400 MHz, DMSO-d_6) 1.37 (s, 9H), 1.49 - 1.60 (m, 3 H), 1.74-1.81 (m, 1 H), 2.03 - 2.11 (m, 1 H), 2.50 – 2.52 (m, 1H), 2.60 – 2.70 (m, 1H), 3.07 – 3.12 (m, 2H), 3.15 (d, *J* = 13.3 Hz, 1H), 3.40-3.62 (m.1H), 4.24 (s, 2 H), 5.04 (s, 1 H), 5.23 (s, 1 H), 6.09 (dd, J = 8.4, 3.1 Hz, 1H), 6.17-6.19 (m, 1H), 6.48 (dd, J = 8.4, 3.1 Hz, 1H), 6.51-6.54 (m, 1H), 6.95-6.99 (m , 1H), 7.18 (d, *J* = 8.0 Hz, 2H), 7.24 (d, *J* = 8.0 Hz, 2H), 7.28 (s, 1H), 7.60 – 7.67 (m, 2H), 7.75 – 7.87 (m, 2H). ^{13}C NMR (100 MHz, DMSO-d_6) 22.9, 27.3, 55.1, 58.5, 63.0, 65.2, 69.6, 105.0, 114.4, 118.7, 127.5, 128.7, 129.3, 130.0, 130.1, 134.5, 136.9, 138.1, 151.6, 159.5. ESI-HRMS calculated for C$_{31}$H$_{39}$O$_3$N$_2$S (M+H)$^+$: 519.2573, found: 519.2576.

5.1.2.9 Synthesis of (*R*)-(1-(4-((3(benzylthio) phenoxy) methyl) benzyl) pyrrolidin-2-yl) methanamine (24).
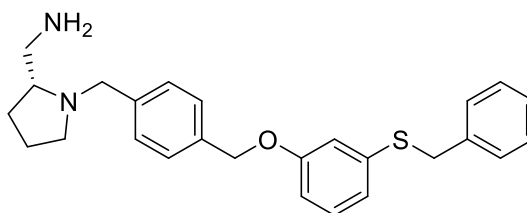
To a solution of compound **60** (150 mg, 0.45 mmol, 1.0 eq) in CH_2Cl_2 trifluoroacetic acid (TFA) (1 mL) was added at room temperature. After the mixture was stirred at room temperature for 4 h, water was added and the organic layer was separated, washed with saturated aqueous potassium carbonated solution, dried over anhydrous $MgSO_4$ and concentrated. The crude was purified by flash column chromatography (0 → 10% MeOH in EtOAc buffered with 1% Et_3N) to afford the title compound as a yellow oil (115 mg, 60% yield). ^1H NMR (400 MHz, DMSO-*d6*) 1.36-1.73 (m, 3H), 1.65-1.95 (m, 2 H), 2.03 - 2.11 (m, 1 H), 2.50 – 2.52 (m, 1H), 2.60 – 2.70 (m, 1H), 3.07 – 3.12 (m, 1H), 3.15 (d, *J* = 13.3 Hz, 1H), 3.30-3.45 (m, 1 H), 4.24 (s, 2 H), 5.04 (s, 1 H), 5.23 (s, 1 H), 6.79 (m, 1H), 6.88-6.90 (m, 1H), 6.94-6.98 (dd, J = 8.4, 3.1 Hz, 1H), 7.10 (m, 1H), 7.18 (d, *J* = 8.0 Hz, 2H), 7.24 (d, *J* = 8.0 Hz, 2H), 7.25 (s, 1H), 7.30 (d, *J* = 8.1 Hz, 2H),7.42 (d, *J* = 8.1Hz, 2H). ^{13}C NMR (100 MHz, DMSO-*d6*) 22.4, 26.5, 45.1, 50.5, 60.0, 65.2, 70.6, 70.9, 110.0, 120.7, 126.5, 127.0, 127.7, 128.3, 129.8, 130.1, 135.5, 137.2, 137.8, 160.5. ESI-HRMS calculated for $C_{26}H_{31}N_2OS$ (M+H)$^+$: 419.2078, found: 419.2073.

(*S*)-(1-(4-((3-(Benzylthio)phenoxy)methyl)benzyl)pyrrolidin-2-yl)methanol(25)
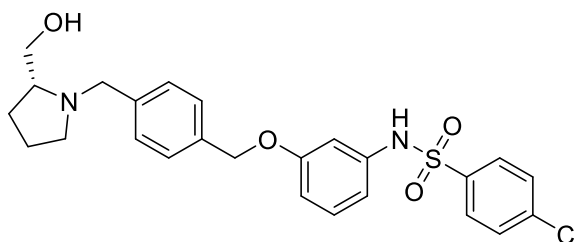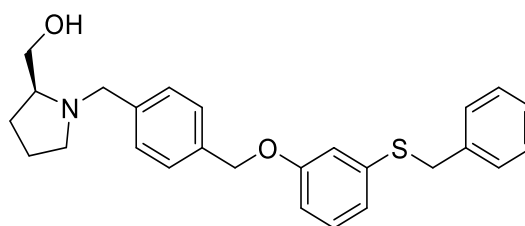

The reaction was carried out according to general procedure **E** using compound **55** (110 mg, 0.32 mmol, 1.0 eq), (*S*)-(-)-2-pyrrolidinemethanol (48 μL, 0.49 mmol, 1.5eq) and sodium triacetoxyborohydride (204 mg, 0.97 mmol, 3.0 eq) in 1, 2-dichloroethane (2 mL). The crude residue was purified by flash chromatography (1% Et$_3$N in EtOAc) to afford the title compound (49 mg, 36% yield) as a yellow oil. ^{1}H NMR (400 MHz, DMSO-*d*$_6$) δ 1.57-1.63 (m, 3H), 1.79 – 1.87 (m, 1H), 2.09 – 2.14 (m, 1H), 2.52 – 2.60 (m, 1H), 2.75 (m, 1H), 3.24 – 3.29 (m, 1H), 3.30 (s, 1H), 3.39 – 3.51 (m, 1H), 4.01 – 4.06 (m, 1H), 4.24 (s, 2H), 4.42 (br.s, 1H), 5.21 (s, 2H), 6.81 (ddd, *J* = 2.4, 5.4, 7.9 Hz, 1H), 6.90 (t, *J* = 2.2 Hz, 1H), 6.87 – 6.93 (m, 1H), 6.93 – 6.96 (m, 1H), 7.19 (dd, *J* = 5.9, 8.0 Hz, 1H), 7.19 (dd, *J* = 5.9, 8.0 Hz, 1H), 7.22 – 7.25 (m, 1H), 7.21-7.28 (dd, *J* = 1.7, 7.5 Hz, 1H), 7.30 – 7.33 (m, 2H), 7.35 (td, *J* = 1.6, 3.7 Hz, 3H). ^{13}C NMR (100 MHz, DMSO-*d*$_6$) δ 20.5, 27.5, 36.3, 49.8, 58.3, 62.1, 69.0, 73.0, 110.3, 114.0, 114.4, 118.8, 121.1, 124.0, 127.1, 128.0, 128.4, 128.7, 130.0, 130.3, 130.4, 137.5, 139.8, 142.7, 157.5. ESI-HRMS calculated for C$_{26}$ H$_{30}$ O$_2$ N S (M+H)$^+$: 420.1992, found: 420.1992.

(*R*)-(1-(4-((3-(Benzylthio)phenoxy)methyl)benzyl)piperidin-2-yl)methanol (26)
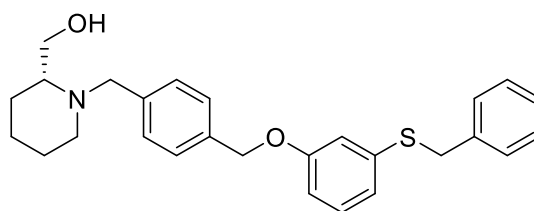
The reaction was carried out according to general procedure **E** using compound **55** (110 mg, 0.32 mmol, 1.0 eq), (*R*)-piperidin-2-ylmethanol (41 μL, 0.36 mmol, 1.1 eq), and sodium triacetoxyborohydride (204 mg, 0.98 mmol, 3.0 eq) in 1,2-dichloroethane (5 mL). The crude residue was purified by flash chromatography (1% Et$_3$N in EtOAc) to afford the title compound (40 mg, 24% yield) as a colourless oil. ^{1}H NMR (400 MHz, DMSO-*d$_6$*) δ 1.48 – 1.24 (m, 3H). 1.63 (d, *J* = 17.2 Hz, 3H), 2.28-2.30 (m, 1H), -2.50-2.63 (m, 1H), 3.24 (d, *J* = 13.9 Hz, 1H), 3.45 (s, 2H), 3.64 (d, *J* = 11.3 Hz, 1H), 4.08 (d, *J* = 13.2 Hz, 1H), 4.23 (s, 2H), 4.44 (br.s, 1H), 5.04 (s, 2H), 6.81 (dd, *J* = 2.5, 8.2 Hz, 1H), 6.89 (dd, *J* = 1.6, 7.6 Hz, 1H), 6.95 (t, *J* = 2.2 Hz, 1H), 7.18 (d, *J* = 8.0 Hz, 1H), 7.25 – 7.21 (m, 1H), 7.39 – 7.27 (m, 8H). ESI-HRMS calculated for C$_{27}$H$_{32}$O$_2$NS (M+H)$^+$: 434.2148, found: 434.2142.

2-((4-((3-(Benzylthio)phenoxy) methyl) benzyl) amino) ethan-1-ol (27)
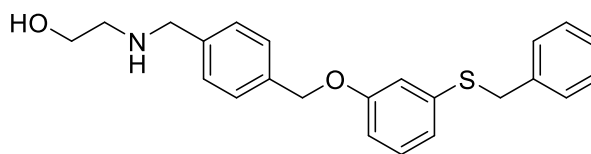
The reaction was carried out according to general procedure **E** using compound **55** (150 mg, 0.44 mmol, 1.0 eq), 2-methoxyethan-1-amine (54.9 mg, 0.47 mmol, 1.5 eq) and sodium triacetoxyborohydride (308 mg, 1.46 mmol, 3.0 eq). The crude product was purified by flash column chromatography ($0 \rightarrow 10\%$ MeOH in EtOAc buffered with 1% Et$_3$N) to afford the title compound as a colourless oil (90 mg, 53% yield). ^{1}H NMR (400 MHz, DMSO-d$_6$) 2.29 (t, J = 7.1 Hz, 2H), 3.40 (t, J = 7.1 Hz, 2H), 3.50 (s, 2 H), 4.16 (s, 2 H), 4.50 (s, 1 H), 5.04 (s, 2 H), 6.25 (m, 1H), 6.65-6.79 (m, 1H), 6.88-6.90 (m, 1H), 6.94-6.98 (dd, J = 8.4, 3.1 Hz, 1H), 7.-09-7.12 (m, 1H), 7.15 (d, J = 8.0 Hz, 2H), 7.20 (d, J = 8.0 Hz, 2H), 7.29 (m, 1H), 7.35 (d, J = 8.0 Hz, 2H), 7.41 (dd, J = 8.4, 3.1 Hz, 2H) . ^{13}C NMR (100 MHz, DMSO-d_6) 40.0, 52.6, 59.5, 70.8, 72.9, 110.7, 115.1, 121.6, 126.9, 126.9, 127.1, 127.7, 127.7, 128.7, 128.7, 129.4, 129.4, 129.9, 135.0, 137.1, 137.4, 139.1, 160.8. ESI-HRMS calculated for C$_{23}$ H$_{26}$O$_2$NS (M+H)$^+$: 380.1579, found: 380.1585.

1-(4-((3-(Benzylthio)phenoxy)methyl)benzyl)pyrrolidine (28)
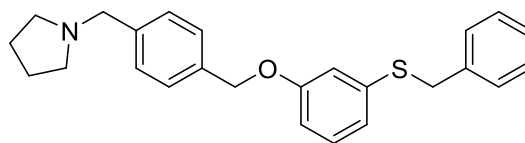
The reaction was carried out according to general procedure **E** using compound **55** (110 mg, 0.32 mmol, 1.0 eq), pyrrolidin (30 μL, 0.36 mmol, 1.1 eq) and sodium triacetoxyborohydride (204 mg, 0.988 mmol, 3.0 eq) in 1, 2-dichloroethane (5 mL). The crude residue was purified by flash chromatography (1% Et$_3$N in EtOAc) to afford the title compound (122 mg, 99% yield yield) as a yellow oil. ^{1}H NMR (400 MHz, DMSO-d_6) δ 1.67-1.70 (m, 4H), 2.38-2.41 (m, 4H), 3.33 (s, 2H),4.23 (s, 2H), 5.05 (s, 2H), 6.76 – 6.82 (m, 1H), 6.89 (dd, J = 1.6, 8.3 Hz, 1H), 6.96 (dt, J = 2.1, 9.1 Hz, 1H), 7.16 – 7.21 (m, 1H), 7.21 – 7.25 (m, 1H), 7.26 – 7.30 (m, 2H), 7.31 – 7.34 (m, 2H), 7.34 – 7.38 (m, 2H), 7.50 (q, J = 1.9 Hz, 1H), 7.62 (d, J = 8.3 Hz, 1H). ^{13}C NMR (100 MHz, DMSO-d_6) δ 22.8, 36.3, 53.2, 59.7, 68.5, 112.5, 114.1, 118.7, 126.9, 127.6, 128.3, 128.8, 129.8, 137.4, 137.7, 158.5. ESI-HRMS calculated for C$_{25}$H$_{28}$ONS (M+H) $^+$: 390.1900, found: 390.1886.

**(*R*)-(1-(4-((3-(Methoxymethoxy)phenoxy)methyl)benzyl)pyrrolidin-2-yl)methanol (15)**
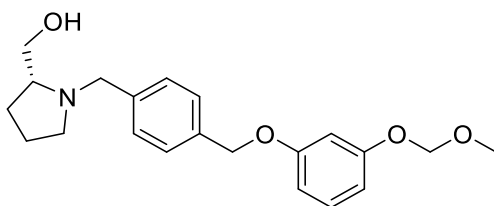
The reaction was carried out according to general procedure **E** using compound **62** (250 mg, 0.91 mmol, 1.0 eq) (*R*)-(-)-2-pyrrolidinemethanol (40 µL, 0.40 mmol, 1.1 eq) and sodium triacetoxyborohydride (583 mg, 2.75 mmol, 3.0 eq) and (*R*)-(-)-2 pyrrolidinemethanol (99 µL, 1.01 mmol, 1.1 eq) in 1, 2-dichloroethane (6 mL). The crude residue was purified by flash chromatography (1% Et₃N in EtOAc) to afford the title compound (150 mg, 43% yield) as a pale yellow oil. ^{1}H NMR (400 MHz, DMSO-d_6) δ 1.59-1.65 (m, 3H), 1.76 – 1.90 (m, 1H), 2.06 – 2.17 (m, 1H), 2.55 (dd, J = 5.1, 8.2 Hz, 1H), 2.72 – 2.79 (m, 1H), 3.24 – 3.30 (m, 1H), 3.33 (s, 1H), 3.36 (s, 3H), 3.42 – 3.48 (m, 1H), 4.05 (d, J = 13.1 Hz 1H), 4.41 (br.s, 1H), 5.04 (s, 2H), 5.16 (s, 2H), 6.59 – 6.62 (m, 1H), 6.63 – 6.65 (m, 1H), 6.65 (d, J = 1.7 Hz, 1H), 7.12 – 7.25 (m, 1H), 7.32 (d, J = 8.0 Hz, 2H), 7.37 (d, J = 8.0 Hz, 2H). ^{13}C NMR (100 MHz, DMSO-d_6) δ 23.0, 28.6, 54.6, 56.1, 59.1, 64.8, 65.4, 69.7, 94.4, 103.8, 108.6, 109.1, 128.2, 129.2, 130.5, 135.8, 137.2, 158.5, 160.1. ESI-HRMS calculated for C_{21} H_{28} O_4 N $(M+H)^+$: 358.2007, found: 358.2013.

5.1.3 Molecular modelling using the docking program GOLD 4.0

All structures were first drawn in ChemDraw® and subsequently processed using Pipeline Pilot® to add hydrogen atoms, minimize molecules and calculate 3D co-ordinates before being docked using Genetic Optimisation for Ligand Docking (GOLD) software. GOLD is a genetic algorithm for docking ligands into protein binding sites that allows partial protein flexibility. The process allows for the optimization of hydroxyl groups during docking for optimal H-bonding to the ligands. The same can be done with NH_3^+ groups unless they are held strongly by H-bonds of neighbouring protein residues. Ligand rotatable bonds are treated flexibly during the docking and only the non-rotatable bonds in the ligand were held.

The docking procedure involved the following; protein crystal structures were downloaded from protein data bank Pdb and prepared in Discovery Studio, removing the co-crystallised ligand and non-structural waters. The hydrogen atoms were added and water molecules were deleted. The binding site was defined as the centroid around the approximate centre of the orthosteric binding site. The radius of the binding site was set as 10 Å to include all the important amino acids that form the binding site. Ligands were prepared by subjecting them to ionization, following which each ligand was docked 10 times. The Gold scoring fitness function was selected and ChemPLP with default parameters was used as the scoring function and no early termination was allowed. The slow speed option was used to perform 100,000 operations, and automatic search option was enabled to perform 100% efficiency searches. All the output files were written as sdf files. The best 10 solutions of all the ligands were saved.

5.1.4 ADMET compound profiling (assays performed by Cyprotex Ltd)

5.1.4.1 Solubility

Aqueous solubility was measured using a high throughput turbidimetric assay. Initially, a stock DMSO solution is diluted in DMSO to produce a range of concentrations. These are then added to buffer, typically phosphate buffered saline at pH 7.4 (final test compound concentrations= 1 µM, 3 µM, 10 µM, 30 µM, 100 µM, final DMSO concentration = 1%, 7 replicates per concentration) and incubated for 2h at 37°C. At the end of the incubation period, the absorbance at 620nm is read for each concentration and each replicate.

5.1.4.2 Hepatocyte stability

Hepatocytes were incubated with compounds at 37°C. Samples were moved at the appropriate time points into methanol containing internal standard to terminate the reaction. Following centrifugation, the supernatant was analysed by LC-MS/MS.

5.1.4.3 Microsomal stability

The microsomes were incubated with the test compounds at 37°C in the presence of the co-factor, NADPH or (NADPH + UDPGA), which initiated the reaction. The reaction was terminated by the addition of methanol containing internal standard. Following centrifugation, the supernatant was analysed on the LC-MS/MS. The disappearance of test compound was monitored over a 45 minute timescale.

5.1.4.4 Cytochrome P450 inhibition

Isoform-specific substrates were incubated individually with human liver microsomes and a range of test compound concentrations (typically 0 - 25 µM). At the end of the incubation, the formation of metabolite was monitored by LC-MS/MS at each of the test compound concentrations and the IC_{50}'swere calculated with reference to the substrate.

5.2 Biological evaluation of compounds

5.2.1 General reagents

All biochemical reagents were purchased from Sigma-Aldrich (UK) unless otherwise stated. Pierce BCA Protein Assay kit (BCA) kit was purchased from Thermo Scientific, UK. Beta-glycerophosphate disodium salt was purchased from Merck Chemicals, UK. Hybond™ ECL™ Nitrocellulose membrane; Kodak X-ray Films (X-Omat LS) were obtained from GE Healthcare (UK) Prestained blue marker (#SDS7B2) was purchased from Sigma (Poole, UK).The caspase substrate DEVD-AMC was purchased from Cayman Chemical Company (#14986). MG132 (#PD98059) was obtained from Enzo Life Sciences (Exeter, UK). 2-(p-Hydroxyanilino)-4-(p-chlorophenyl) thiazole (SKi) was obtained from Calbiochem (Nottingham, UK), CA074Me was obtained from Merck Biosciences (Nottingham, UK). PF-543 was obtained from Calbiochem (Nottingham, UK). (R)-FTY720 methyl ether (ROMe) was gifted from Professor Robert Bittman (Queens College of the City University of New York, New York, USA).

5.2.2 Antibodies

Antibodies were obtained as follows: anti-actin (#A2066); reporter horseradish peroxidase-conjugated anti-mouse IgG (#A9169), reporter horseradish peroxidase-conjugated anti-rabbit IgG (#A0545).;and anti-p53 (#P8999) were purchased from Sigma (Poole, UK); anti-Myc (#9E10) was purchased from Santa Cruz Biotechnology (Santa Cruz, CA), Polyclonal anti-PARP antibody (#9542S), and anti-p21 (#2947) were purchased from New England Bio labs Ltd. (Hitchin, UK), Anti-SK1 (lab reference number 48:2) antibody was custom made by Abcam[273]Monoclonal anti-ERK-2 antibody (#610104) was purchased fromBD Transduction Laboratories (Oxford, UK) and Rabbit monoclonal antibody to Des1 (#EPR9680) was purchased from Abcam (UK).

5.2.3 Radioisotopes

PerkinElmer (UK)

[Methyl-3H] thymidine (37MBq/mL)

5.2.4 Cell Culture

RPMI1640, European foetal calf serum (EFCS), penicillin- streptomycin (10,000 units/mL penicillin and 10,000 μg/mL streptomycin), L- glutamine, and trypsin /EDTA solution were from Invitrogen (Paisley, UK). Charcoal filtered foetal bovine serum was from Lonza (Switzerland). Human prostate cancer LNCaP (androgen-dependent) and LNCaP-AI (androgen- independent) were gifted from Professor Hing Leung (Beatson Institute, Glasgow, UK). Smooth Muscle Cell Medium (SMCM, #1101), Trypsin/EDTA neutralization solution (TNS, #0113), fetal serum (FBS, #0010), smooth muscle cell growth supplement (SMCGS,#1152), penicillin / streptomycin (P/S, #0503) and hPASMC were obtained from Promo Cells (hPASMC, #C-12522).

5.2.4.1 Maintenance of LNCaP and LNCaP-AI cells

LNCaP and LNCaP-AI cell lines were maintained in RPMI1640 medium supplemented with 10% (v/v) EFCS or 10% (v/v) delipidated serum, respectively, 50 U/mL penicillin/50 μg/mL streptomycin and 1% (v/v) L-glutamine. Cells were cultured in T-75 cell culture flasks and incubated at a temperature of 37°C in a humidified atmosphere with 5% CO_2. Confluent cells were detached from the flask surface by incubating them in a trypsin/EDTA solution for 2-3 mins at 37°C, after removing medium and washing once with serum-free RPMI 1640 medium. Complete medium was then added to the cell/trypsin mixture and the new cell suspensions was diluted appropriately in complete medium (1:8-1:10) before being transferred to a new flask. LNCaP and LNCaP-AI cells between passage 20 and 30 were used for the experiments reported in this study.

5.2.4.2 Maintenance of hPASMC

Smooth Muscle Cell Medium (SMCM), fetal serum (FBS), smooth muscle cell growth supplement, and penicillin/streptomycin (P/S) were used to maintain the hPASMC. Cells were cultured in T-75 cell culture flasks and incubated at a temperature of 37 °C in a humidified atmosphere with 5% CO_2. Confluent cells were then washed with serum free medium before being incubated in 3 mL of a trypsin/EDTA solution for 2-3 mins at 37 °C to get them detached from the flask. Then, 3 mL of Trypsin Blocking Solution (TBS) were added to the flask and cells were transferred into a 15 mL tube. The flask was rinsed with a further 2 mL TBS to collect residual cells and added to other cells in centrifuge tube. Then cells were centrifuged at ~200G for 4-5 mins, after which the medium was aspirated, complete medium added and cells then re-suspended. The cell suspension was then diluted in complete medium (appropriately 1:5) before transfer to a new flask.

5.2.4.3 Treatment protocol

Cells were maintained until approximately 60-70% confluence, before being treated as described in each figure legend in the **Results** sections. Cells were treated with inhibitors or vehicle for 24-48 h, as indicated for each experiment. When cells were treated for 48 h, the inhibitors or vehicles were replaced after 24 h. All inhibitors were reconstituted in DMSO before being added to the culture medium for cell stimulation at a final concentration of DMSO<0.1%.

5.2.5 Preparation of cell lysates of the LNCaP and LNCaP-AI cell lines for Western blotting analysis of protein expression

Treated cells (as described in **Results** section) were harvested in their culture medium using a cell scraper and transferred to a 15 mL tube. This was followed by centrifugation at 1,000 rpm for 3 mins, before being washed with ice-cold phosphate buffer solution (PBS) and re-suspended in ice-cold lysis buffer (250 mL) [137 mMNaCl, 2.7 mMKCl, 1 mM $MgCl_2$, 1 mM $CaCl_2$, 1% (v/v) Nonidet P-40 (NP-40, IGEPAL), 10% (v/v) glycerol, 20 mM Tris-base, 0.5 mM Na_3VO_4, 0.2 mM PMSF, 10 µg/mL leupeptin and 10 µg/mL aprotinin; pH 8.0], keeping the tubes on

ice. Using a 0.24 mm gauge needle and syringe, cell lysates were homogenised by repeated passages (10 times) through the needle. The homogenised cell lysate was then transferred into micro-centrifuge tubes and mixed for 30 mins at 4°C and then centrifuged at 15,300 rpm for 10 mins at 4°C. The supernatant was transferred without disturbing the pellet into a fresh micro-centrifuge tube and stored at -20°C to be used for protein concentration assay.

The BCA assay was performed for each sample to determine protein concentration of the cell lysates. Protein concentrations of cell lysates were normalised (by adjusting the volume and thereby protein concentration) with lysis buffer. For each sample, 12 μg of protein of cell lysate were used for SDS-PAGE and western blotting. Lysate corresponding to this amount of protein was calculated before the required volume of sample buffer (0.5 mM Tris, 2 mM $Na_4P_2O_7$, 5 mM EDTA, 2% w/v SDS,1% (w/v) bromophenol blue, and mM 50 DTT, pH 6.7) was added. Sample buffer consists of several ingredients useful for extracting proteins and conducting gel electrophoresis. Tris is a buffer, which helps keep pH constant during the experiment. SDS (sodium dodecyl sulfate, also known as lauryl sulfate) is a detergent that dissolves cell and nuclear membranes by breaking down lipids (fat), as well as unfolding the proteins in the sample. The bromophenol blue was used to the sample solution tomake it easy to be seen when it loaded into the gel and to determine when the gel has run far enough (the dye is 6-8 cm from the wells). Glycerol is a very dense liquid that makes the samples dense so they sink to the bottom of the wells in the gel. Samples were boiled samples for 5 mins to completely denaturise the proteins before being loaded into polyacrylamide gels and assayed by Western blotting analysis.

5.2.5.1 Determination of protein concentration

Protein content in cell lysates was determined using a bicinchoninicacid (BCA) assay. [274]

5.2.5.1.1 Bicinchoninic acid assay

BCA assay is a spectrophotometric method for the determination of protein concentration. The BCA assay mainly relies on two reactions. First, there is a reduction of Cu^{2+} ions in the peptide bonds in protein from the cupric sulphate to form Cu^+. Secondly, two molecules of bicinchoninic acid chelate with each Cu^+ion, and form a purple-coloured product that absorbs at 562 nm. At this wavelength (OD562), there is a linear correlation between the amount of Cu^{2+} reduced and the amount of protein present in the solution that can be determined by comparison with a standard curve constructed using known concentrations of bovine serum albumin (BSA). The BCA assay was performed in duplicates in parallel with a standard curve employing BSA using the Pierce® BCA Protein Assay Kit according to the instructions provided by the manufacturer.

5.2.6 SDS-PAGE Western blotting

5.2.6.1 Preparation of polyacrylamide gels

Each polyacrylamide gel used for resolving proteins by electrophoresis consists of two layers: the separating gel, in which the resolutionof proteins by electrophoresis occurs, and the stacking gel, which allows the proteins to concentrate before entering the separating layer.

The separating gel consisting of 10% (v/v) acrylamide: bis-acrylamide, 0.375 M Tris-Base (pH8.8), 0.1% (w/v) SDS, 0.05% (w/v) ammonium persulfate and 0.025% (w/v) tetramethylethylenediamine (TEMED), while the stacking gel consisting of 4.5% (v/v) acrylamide-bis-acrylamide, 0.125 M Tris-Base (pH 6.7), 0.1% (w/v) SDS, 0.05% (w/v) ammonium persulfate and 0.1% (v/v) of TEMED.

5.2.6.2 Polyacrylamide gel electrophoresis

The principle behind gel-electrophoresis is based on the migration of negatively charged proteins (due to presence of SDS) towards the positive anode through the polyacrylamide gel. Due to the pores produced by the acrylamide, smaller proteins move faster than the large ones, thus proteins are separated by the polyacrylamide gel according to their molecular weight.

The Bio-Rad Mini-Protean II electrophoresis kit was used to perform polyacrylamide gel electrophoresis while a Hamilton syringe was used to load samples into thegel. Also, to identify the band corresponding to the protein of interest, pre-stained molecular weight marker contains a lyophilized mixture of seven prestained proteins, molecular weight range 26,600-180,000 Da (**Table 5.1**) were also loaded on the gel.

Table 5.1. Prestained molecular weight marker used in Western blotting. Table showing molecular weight of seven pre-stained proteins

Standard	Molecular weight (kDa)
α2-macroglobulin	180
β-galactosidase	116
Lactoferrin	90
Pyruvate kinase	58
Fumarase	48.5
Lactic dehydrogenase	36.5
Triosephosphate isomerase	26.6

A buffer having 25 mMTris-Base, 0.21 M glycine and 0.1% (w/v) sodium dodecyl sulfate (SDS) was used and electrophoresis was performed at a voltage of 120 V for about 2 h.

5.2.6.3 Transfer to nitrocellulose membranes

Bio-Rad Mini Trans-Blot kit filled with a buffer containing 25 mM Tris-Base, 0.21 M glycine and 20% (v/v) methanol at voltage of 100 V for 60 mins was used for electrophoretic transfer of the resolved proteins from the gel to a nitrocellulose membrane. A reservoir was included in the tank to minimize the high temperature of the transfer buffer. As proteins were charged negatively by SDS in the gel, the transfer process was conducted from the gel (negative/cathode) to the nitrocellulose (positive/anode).

5.2.6.4 Immunological detection of protein

The blocking solution consisted of 3% (w/v) non-fat dry milk in TBST [10 mM Tris-Base, 100 mM NaCl, 0.1% (v/v) Tween-20; pH 7.4] or 5% (w/v) bovine serum albumin (BSA) in TBST. Membranes were incubated for 60 mins at room temperature in order to reduce non-specific binding of the antibody. Following this, the membrane was incubated overnight with gentle agitation at 4°C with the specific primary antibody to detect a specific protein. Primary antibodies and conditions are listed in **Table 5.2**. The membrane was washed three times (10 mins each) with TBST to remove any unbound antibody. This washing was followed by incubation with the appropriate horseradish peroxidase-conjugated secondary antibody (anti-mouse or anti-rabbit, depending on the primary antibody origin) diluted 1:80,000 in 1% (w/v) non-fat dry milk in TBST for 60 mins at room temperature. The membrane was washed three times in TBST (10 mins each) to remove any excess antibody, before incubating the membranes in the enhanced chemiluminescence (ECL) reagent for 2 mins at room temperature. The reagent was prepared by mixing equal volumes of solution 1 containing 0.04% (w/v) luminol, 0.1 M Tris-Base (pH 8.5) and solution 2 containing 0.016% (w/v) p-coumaric acid, 2% (v/v) H_2O_2 and 0.1 M Tris-Base (pH 8.5). The main role of (ECL) reagent is to allow the detection of immunereactive proteins by delivering the substrate for the peroxidase. Membranes were then inserted between two transparent plastic sheets in a metal cassette and exposed to an X-ray film, which was then developed by passing it through the X-Omat machine. There was variation in the exposure time depending on the intensity of the chemiluminescence signal. After exposure, molecular weights of

immune reactive proteins were estimated by comparing their mobility on SDS-PAGE to that of pre-stained molecular weight markers (**Table 5.2**).

Table 5.2. Primary antibodies used in immunoblotting and optimal conditions.

Target Proteins	Dilution	Species	Blocking Conditions
Anti-SK1	1:1000	Rabitt	5% BSA in TBST
Anti-ERK2	1:1000	Mouse	3% (w/v) non-fat dry milk in TBST
Anti-DEGS1	1:1000	Rabitt	3% BSA in TBST
Anti-p21	1:1000	Rabitt	3% BSA in TBST
Anti-p53	1:10000	Mouse	3% (w/v) non-fat dry milk in TBST
Anti-Actin	1:1000	Rabitt	3% BSA in TBST
Anti-c-Myc	1:500	Mouse	3% (w/v) non-fat dry milk in TBST
Anti-PARP	1:1000	Rabitt	3% (w/v) non-fat dry milk in TBST

5.2.6.5 Stripping and re-probing of nitrocellulose membranes

Stripping buffer containing 62.5 mM Tris-HCl (pH 6.7), 2% (w/v) SDS and 100 mM β-mercaptoethanol was used to remove bound antibodies before being re-probed with a different antibody. Membranes were stripped for 1h at 70°C with gentle agitation. Before incubating membranes overnight with the primary antibody specific for the protein of interest, membranes were rinsed with distilled water and washed with TBST (3 times for 10 mins) with mild agitation.

5.2.6.6 Quantification

Band density was determined using the Image J software program (Scion Corporation, Frederick, MD) and expressed as integrated density units (IDU).

5.3 Cell based assays

5.3.1 [3H] Thymidine uptake proliferation assay

Cells were seeded in 1mL of complete media on to 24 well plates. When cells became 70% confluent, they were treated with inhibitors or vehicle (DMSO, 0.1% v/v final) and incubated for 24 h or as described in the legends in the **Results** section. [^{3}H] Thymidine (9.25 kBq per well) was added to each well 5 h before the end of the incubation period. Incubations were then stopped by aspirating media and immediate washing of the cells three times for 10 mins with 1 mL of 10% (w/v) ice cold trichloroacetic acid (TCA) solution and placed on ice for 10 mins. Then 0.25 mL of 0.1% SDS/ 0.3 M NaOH was added to dissolve the residual nuclear material. The contents of each well were transferred to separate scintillation vials and mixed with 2 mL of scintillation cocktail. [^{3}H] Thymidine uptake was quantified by using liquid-scintillation counting. The results were presented as the mean percentage of DNA synthesis (mean ± SEM) compared with untreated control wells of three independent experiments (GraphPad Software Inc, CA, USA).

5.3.2 MTT Assay

Assays incorporated a colorimetric growth indicator 2-(4,5-dimethylthiazol-2-yl)-3,5-diphenyl-2H-tetrazol-3-iumbromide (MTT) that is used for measuring the cell viability based on the detection of metabolic activity. It is among the several alternative assays available for monitoring cell viability. MTT is a yellow tetrazole colorimetric dye that is reduced to purple formazan in the presence of NADH and NADPH (**Figure 5.1**). Cells were seeded onto 96 well plates at a density of 10,000 cells per well in 50 μL of complete media. The plates were incubated overnight at 37°C for the cells to adhere. Treatments were added to each well as indicated in 50 μL serum media and incubated for 24 h. Media was then aspirated and replaced with 50 μL MTT reagents (5 mg/ mL in sterile PBS). Plates were then wrapped in foil and incubated at 37 ºC for 2 h.

The MTT reagent was then discarded and replaced with 100 µL of MTT-stop reagent (containing 4 mM hydrochloric acid and 0.1% (w/v) NP-40 in propan-2-ol). Plates were then re-wrapped in foil and formazan crystals were solubilised by gentle agitation for 30 mins before absorbance was read at 620 nm. The results were presented as the mean percentage of cell viability (mean ± SEM) compared with untreated control wells of three independent experiments. The results were plotted as percentage of cell viability against the logarithmic dose, and IC_{50} values were calculated by using non-linear regression curve fitting using GraphPad Prism software, version 6.01, 2014 (GraphPad Software Inc, CA, USA).

2-(4,5-dimethylthiazol-2-yl)-3,5-diphenyl-2*H*-tetrazol-3-ium bromide

MTT

(*E*,*Z*)-5-(4,5-dimethylthiazol-2-yl)-1,3-diphenylformazan
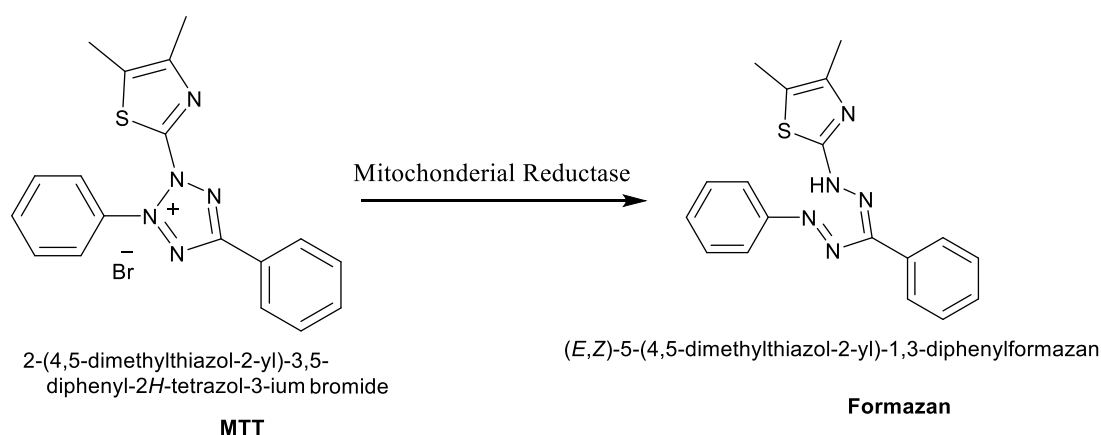
Formazan

Figure 5.1. MTT reaction that occurs in the mitochondria of the living cells leading to a change in the colour of the MTT from yellow to purple (Formazan).

5.3.3 One-step cellular caspase-3/7 assay

This is a fast, simple and amenable to high throughput cell-based screening and employs DEVD-AMC that can be cleaved by caspase-3 or caspase-7 to produce a highly fluorescent signal. [275]

Cells were seeded onto 96 well plates at a density of 10,000 cells per well in 50 µL of complete media. The plates were incubated overnight at 37°C for the cells to adhere. The following day, compounds under investigation in a 50-µL culture media were added to each well and incubated at 37°C for the required period. 50 µL of one-step caspase-3/7 assay buffer was added to each well and incubated at 37°C for 1h. Caspase-3/7 assay buffer components are:150 mM HEPES, pH 7.44,

50 mM NaCl, 150 mM KCl, 30 mM MgCl, 21.2 mM EGTA, 1.5% Nonidet P400, 3% CHAPS and 30% sucrose. Just before using the assay, the following reagents (150 μM DEVD-AMC, 30 mM DTT, and 3.0 mM PMSF) were added to 6 mL of the assay bufer. Caspase-3/7 activity was measured by reading proteolyticaly-released fluorochrome from the DEVD-AMC substrate using a plate-reading fluorimeter with an excitation at 360 nm and an emission at 460 nm [275]. Results were presented as the mean fold increase (mean ± SEM) in caspase 3/7 activity by comparing and normalising the mean fluorescence intensity for each treated group with the fluorescence intensity of untreated control wells in three independent experiments.

5.3.4 Statistical analysis

Experiments were repeated at least three times, unless otherwise stated. Data was analysed using Graph Pad Prism software and is expressed as mean with standard error of the mean (SEM) or mean with standard deviation (SD) as indicated. Statistical analysis was performed using One Way Anova with a Dunnett's post-test. A p-value <0.05 was considered significant.

5.4 ADP-Glo™ kinase assay

5.4.1 Chemicals and assay components

Recombinant human SK1 and recombinant human SK2 were purchased from R&D Systems, Inc. (#5536-SK-010 and # 5298-SK-010. The ADP-Glo™ kinase assay kit was purchased from Promega Coorporation, UK (#v9102), composed of ADP-Glo reagent, kinase detection reagent (made by mixing kinase detection buffer with a lyophilized kinase detection substrate), ultra-pure ATP and ADP. White, and *U* or *V*shape 96 -well assay plates were obtained from Greiner, UK (# 650101, 651101, and # 675075).

5.4.2 Buffer preparation

Generally, kinase assay reactions were performed in a reaction buffer of pH 7.5 consisting of 40 mM Tris-HCl (#T5941), 20 mM $MgCl_2$ (#M1028), 2 mM DTT (#T5941) with 0.01 mg/mL lipid free Bovine Serum Albumin (BSA) (#A2153) for the SK2 assay (BSA was not added to SK1 assay buffer), in a total volume of 50 mL. The pH was measured at 30 °C. The buffer was prepared on the day of the assay. The final volume of the assay per the well is 20 µL; 5 µL of substrate + 5 µL of ATP + 5 µL of SK1/or SK2 + buffer/or inhibitor.

5.4.3 Enzyme preparation

Recombinant human SK1 and SK2 with a stock concentration of (200 mg/ mL (SK1) and 267 µg/mL (SK2) was stored at -80ºC. Assay optimisation was used to determine that final concentrations of 0.2 µg/mLof SK1 and 5µg/mL of SK2 were required. A working solution containing 2.2 µL of the enzyme solution was therefore added to 550 µL of the SK1 buffer and 37 µl of SK2 was added to 500 µL of the SK2 buffer to obtain desired final concentrations of both SK1 and SK2 for 96 well plates.

5.4.4 Sphingosine substrate preparation

Sphingosine substrate is presented differently for the SK1 and SK2 assays. For the SK1 assay, sphingosine was presented as micelles in Triton X-100 solution. Since Triton X-100 suppresses SK2 activity, [50] the sphingosine for SK2 assays was mixed with fatty acid free BSA.

5.4.5 Substrate preparation for SK1

Sphingosine substrate (D-*erythro* sphingosine) was purchased from TOCRIS bioscience, UK (#0633), dissolved (at 5 mM) in DMSO and stored at -20ºC. The K_m of SK1 for sphingosine is 3 μM, which was the concentration chosen for screening our compounds for activity. A final concentration of 3 µM of the substrate in a final volume of 20 µL of the assay constituent in the well was prepared. For each 96 well plate, a total volume of 1.2 µL of 5 mM sphingosine stock was added to in 498.8 µL of Triton X-100 (final concentration 0.313% w/v).

5.4.6 Substrate preparation for SK2

The K_m of SK2 for sphingosine is 10 μM, which was the concentration chosen for screening our compounds for activity. A final concentration of 10 µM of the substrate in a total volume of 20 µL of the assay component in the wellwas prepared. Therefore, for each 96 well plate 4 µL of 5 mM stock were added to in 496 µL of 4mg/mL fatty acid free BSA buffer and these were sufficient for one 96 well plate.

5.4.7 ATP preparation

Ultra-Pure ATP from the ADP-Glo kit was used. Other sources of ATP may contain ADP that could result in high background readings and give false results. A stock concentration of 10 mM was stored at -20ºC. A final concentration of 250 μM, which is above the K_m value (77 μM) in order to saturate the ATP binding site, was used in the total assay volume of 20 µL: 50 µL of a 10 mM stock concentration was dissolved in 450 µL of assay buffer for one 96 well plate.

5.4.7.1 Inhibitor preparation

The standard selective SK1 inhibitor (**PF-543**) was used in the SK1 assay. It was dissolved in DMSO at a stock concentration of 10 mM. A 1:10 dilution was made for the displacement curve, with a concentration range between 1 nM to 3 µM. ROMe, or FO-2 selective SK2 inhibitors were used in the SK2 assay. It was dissolved in DMSO at a stock concentration of 10 mM. A 1:10 dilution was made for the displacement curve, with a concentration range between 100 nM to 30 µM.

5.4.7.2 Compound preparation

Compounds for assay were prepared at 10mM in DMSO (stored at -20 ºC). In all the enzyme assays, compounds were screened at 3 µM (final concentration of DMSO is < 0.1%). For active hits, a 1:10 dilution was made for the displacement curve, 5 µL of the prepared sample was added to 5 µL of the enzyme and 5 µL of the substrate in the enzyme assay plate with a concentration range between 1 nM and 3 µM.

5.4.8 ADP-Glo™ kinase assay method (IC$_{50}$)

The ADP-Glo™ Kinase assay was performed in three steps; kinase reaction, ATP deletion and signal detection.

ADP-Glo™ Kinase assay protocol is:

1. The total volume of the kinase reaction is 20 µL and the components were added in each well of the 96 well V bottom plate using a Multi drop Combi™.
2. To a 5 µL of substrate (3 µM final concentration for SK1 and 10 µM for SK2) was added 5 µL of ultra-pure ATP (250 µM final concentration) followed by 5 µL of the buffer or the test compounds (1nM -3µM final concentration). Then, 5 µL of enzyme (final concentration 0.2 µg / mL for SK1, and 5 µg / mL for SK2) was added. The plate was then incubated at 30°C for 90 mins.
3. 10 µL of the reaction mix was transferred into a white 96 well assay plate (# 675075), before adding 10 µL of ADP-Glo reagent (Reagent I). The plate was then spun at 430 rpm for 30 seconds and incubated at room temperature for 40 mins to stop the kinase reaction and deplete any remaining ATP. The temperature is a vital factor that affects

the rate of this enzymatic assay; therefore, the plate was left at room temperature for 10 mins to equilibrate assay plates to room temperature before adding the ADP-Glo™ kinase assay reagents.

4. At the end of incubation, 20 µL of ADP-Glo detection (Reagent II) was added and spun at 430 rpm for 30 seconds. The plate was then incubated at room temperature for 40 mins to allow the highest concentrations of ADP to fully convert to ATP. [223] The luminescence was recorded on a Wallac Victor plate reader (Perkin-Elmer, UK) using Iso96lum.

5.4.8.1 *Z´ Factor method*

Using 0.2 µg/mL of SK1 or 5 µg/ mL of SK2, 250 µM of ATP and 3 µM or 10 µM of D-*erythro* sphingosine for SK1 and SK2 respectively, all the assay components were dispensed into the first four rows of a 96 well white plate as positive control, while all the assay components but without the enzyme were added to second lower four rows as negative control. The plate was incubated for 90 mins at 37 ºC in an atmosphere containing 5% CO_2. The luminescence was tested on Wallac Victor using Iso96lum. The Z´ factor was calculated using the Zhang' equation .[222]

5.4.9 Results analysis

A 5 µL of buffer (with the equivalent volumes of DMSO used in preparing the target compounds) was added to the 'control' wells. The luminescence released from the hydrolysis of the substrate by the enzyme under these conditions was set to 100%. Hydrolysis of the substrate by the enzymes in the presence of test compounds (or the positive control), was calculated as a percentage of that of the control after subtraction of back ground value (buffer + substrate+ATP only). The control (substrate + buffer + ATP + SK1/or SK2) was assumed to have no inhibitory effect; thus, the substrate underwent 100% hydrolysis. The results were presented as the mean percentage of inhibition of three independent experiments. The results were plotted as the percentage of enzyme inhibition against the logarithmic dose and IC_{50} values were calculated by using non-linear regression curve fitting using GraphPad Prism software, version 6.01, 2014 (GraphPad Software Inc, CA, USA).

Chapter 6. References

(1)   Sato, K.; Malchinkhuu, E.; Horiuchi, Y.; Mogi, C.; Tomura, H.; Tosaka, M.; Yoshimoto, Y.; Kuwabara, A.; Okajima, F. Critical Role of ABCA1 Transporter in Sphingosine 1-Phosphate Release from Astrocytes. *J. Neurochem.* **2007**, *103* (6), 2610–2619.

(2)   Kihara, A.; Mitsutake, S.; Mizutani, Y.; Igarashi, Y. Metabolism and Biological Functions of Two Phosphorylated Sphingolipids, Sphingosine 1-Phosphate and Ceramide 1-Phosphate. *Prog. Lipid Res.* **2007**, *46* (2), 126–144.

(3)   Hannun, Y. A.; Obeid, L. M. Principles of Bioactive Lipid Signalling: Lessons from Sphingolipids. *Nat. Rev. Mol. Cell Biol.* **2008**, *9* (2), 139–150.

(4)   Gault, C. R.; Obeid, L. M.; Hannun, Y. A. An Overview of Sphingolipid Metabolism: From Synthesis to Breakdown. *Adv. Exp. Med. Biol.* **2010**, *688*, 1–23.

(5)   Venkataraman, K.; Riebeling, C.; Bodennec, J.; Riezman, H.; Allegood, J. C.; Cameron Sullards, M.; Merrill, A. H.; Futerman, A. H. Upstream of Growth and Differentiation Factor 1 (uog1), a Mammalian Homolog of the Yeast Longevity Assurance Gene 1 (LAG1), Regulates N-Stearoyl-Sphinganine (C18-(dihydro)ceramide) Synthesis in a Fumonisin B1-Independent Manner in Mammalian Cells. *J. Biol. Chem.* **2002**, *277* (38), 35642–35649.

(6)   Michel, C.; van Echten-Deckert, G.; Rother, J.; Sandhoff, K.; Wang, E.; Merrill, A. H. Characterization of Ceramide Synthesis. *J. Biol. Chem.* **1997**, *272* (36), 22432–22437.

(7)   Hanada, K.; Kumagai, K.; Yasuda, S.; Miura, Y.; Kawano, M.; Fukasawa, M.; Nishijima, M. Molecular Machinery for Non-Vesicular Trafficking of Ceramide. *Nature.* **2003**, *426* (6968), 803–809.

(8)   Mandon, E. C.; Ehses, I.; Rother, J.; Van Echten, G.; Sandhoff, K. Subcellular Localization and Membrane Topology of Serine Palmitoyltransferase, 3-Dehydrosphinganine Reductase, and Sphinganine N- Acyltransferase in Mouse Liver. *J. Biol. Chem.* **1992**, *267* (16), 11144–11148.

(9)   Dai, Q.; Liu, J.; Chen, J.; Durrant, D.; McIntyre, T. M.; Lee, R. M. Mitochondrial Ceramide Increases in UV-Irradiated HeLa Cells and Is Mainly Derived from Hydrolysis of Sphingomyelin. *Oncogene.* **2004**, *23* (20), 3650–3658.

(10)   Spence, M. W.; Clarke, J. T. R.; Cook, H. W. Pathways of Sphingomyelin Metabolism in Cultured Fibroblasts from Normal and Sphingomyelin Lipidosis Subjects. *J. Biol. Chem.* **1983**, *258* (14), 8595–8600.

(11)   Andrieu-Abadie, N.; Levade, T. Sphingomyelin Hydrolysis during Apoptosis. *Biochim. Biophys. Acta - Mol. Cell Biol. Lipids.* **2002**, *1585* (2-3), 126–134.

(12)   Kolesnick, R. Critical Review The Therapeutic Potential of Modulating the Ceramide / Sphingomyelin Pathway. *J. Clin. Invest.* **2002**, *110* (1), 3–8.

(13)   Ogretmen, B.; Hannun, Y. A. Biologically Active Sphingolipids in Cancer Pathogenesis and Treatment. *Nat. Rev. Cancer* **2004**, *4* (8), 604–616.

(14)   Bartke, N.; Hannun, Y. A. Bioactive Sphingolipids: Metabolism and Function. *J. Lipid Res.* **2009**, *50 Suppl* (Supplement), S91–S96.

(15)   Maceyka, M.; Harikumar, K. B.; Milstien, S.; Spiegel, S. Sphingosine-1-Phosphate Signaling and Its Role in Disease. *Trends Cell Biol.* **2012**, *22* (1), 50–60.

(16)   Ichikawa, S.; Sakiyama, H.; Suzuki, G.; Hidari, K. I.; Hirabayashi, Y. Expression Cloning of a cDNA for Human Ceramide Glucosyltransferase That Catalyzes the First Glycosylation Step of Glycosphingolipid Synthesis. *Proc. Natl. Acad. Sci. U. S. A.* **1996**, *93* (10), 4638–4643.

(17)   Tafesse, F. G.; Ternes, P.; Holthuis, J. C. M. The Multigenic Sphingomyelin Synthase Family. *J. Biol. Chem.* **2006**, *281* (40), 29421–29425.

(18)   Maceyka, M.; Payne, S. G.; Milstien, S.; Spiegel, S. Sphingosine Kinase, Sphingosine-1-Phosphate, and Apoptosis. *Biochim Biophys Acta* **2002**, *1585* (2-3), 193–201.

(19)   Cuvillier, O. (CUL-ID:1484434) Sphingosine in Apoptosis Signaling. *Biochim. Biophys. Acta.* **2002**, *1585* (2-3), 153–162.

(20)   Pettus, B. J.; Bielawski, J.; Porcelli, A. M.; Reames, D. L.; Johnson, K. R.; Morrow, J.; Chalfant, C. E.; Obeid, L. M.; Hannun, Y. A. The Sphingosine Kinase 1/sphingosine-1-Phosphate Pathway Mediates COX-2 Induction and PGE2 Production in Response to TNF-Alpha. *FASEB J.* **2003**, *17* (11), 1411–1421.

(21)   Shida, D.; Fang, X.; Kordula, T.; Takabe, K.; Lépine, S.; Alvarez, S. E.; Milstien, S.; Spiegel, S. Cross-Talk between lpa1 and Epidermal Growth Factor Receptors Mediates up-Regulation of Sphingosine Kinase 1 to Promote Gastric Cancer Cell Motility and Invasion. *Cancer Res.* **2008**, *68* (16), 6569–6577.

(22)   Cuvillier, O.; Pirianov, G.; Kleuser, B.; Vanek, P. G.; Coso, O. A.; Gutkind, S.; Spiegel, S. Suppression of Ceramide-Mediated Programmed Cell Death by Sphingosine-1-Phosphate. *Nature.* **1996**, *381* (6585), 800–803.

(23)   Gangoiti, P.; Granado, M. H.; Alonso, A.; Goni, F. M.; Gomez-Munoz, A. Implication of Ceramide, Ceramide 1-Phosphate and Sphingosine 1-Phosphate in Tumorigenesis. *Transl Oncogenomics.* **2008**, *2008* (3), 81–98.

(24) Alemany, R.; Van Koppen, C. J.; Danneberg, K.; Ter Braak, M.; Meyer Zu Heringdorf, D. Regulation and Functional Roles of Sphingosine Kinases. *Naunyn. Schmiedebergs. Arch. Pharmacol.* **2007**, *374* (5-6), 413–428.

(25) Furuya, H.; Shimizu, Y.; Kawamori, T. Sphingolipids in Cancer. *Cancer Metastasis Rev.* **2011**, *30* (3-4), 567–576.

(26) Alvarez, S. E.; Harikumar, K. B.; Hait, N. C.; Allegood, J.; Strub, G. M.; Kim, E. Y.; Maceyka, M.; Jiang, H.; Luo, C.; Kordula, T.; Milstien, S.; Spiegel, S. Sphingosine-1-Phosphate Is a Missing Cofactor for the E3 Ubiquitin Ligase TRAF2. *Nature.* **2010**, *465* (7301), 1084–1088.

(27) Newton, J.; Lima, S.; Maceyka, M.; Spiegel, S. Revisiting the Sphingolipid Rheostat: Evolving Concepts in Cancer Therapy. *Exp. Cell Res.* **2015**, *333* (2), 195–200.

(28) Pyne, N. J.; Pyne, S. Sphingosine 1-Phosphate and Cancer. *Nat. Rev. Cancer* **2010**, *10* (7), 489–503.

(29) Augé, N.; Nikolova-Karakashian, M.; Carpentier, S.; Parthasarathy, S.; Nègre-Salvayre, A.; Salvayre, R.; Merrill, A. H.; Levade, T. Role of Sphingosine 1-Phosphate in the Mitogenesis Induced by Oxidized Low Density Lipoprotein in Smooth Muscle Cells via Activation of Sphingomyelinase, Ceramidase, and Sphingosine Kinase. *J. Biol. Chem.* **1999**, *274* (31), 21533–21538.

(30) Aarthi, J. J.; Darendeliler, M. a; Pushparaj, P. N. Dissecting the Role of the S1P/S1PR Axis in Health and Disease. *J. Dent. Res.* **2011**, *90* (7), 841–854.

(31) Abuhusain, H. J.; Matin, A.; Qiao, Q.; Shen, H.; Kain, N.; Day, B. W.; Stringer, B. W.; Daniels, B.; Laaksonen, M. a.; Teo, C.; McDonald, K. L.; Don, A. S. A Metabolic Shift Favoring Sphingosine 1-Phosphate at the Expense of Ceramide Controls Glioblastoma Angiogenesis. *J. Biol. Chem.* **2013**, *288* (52), 37355–37364.

(32) Olivera, A.; Kohama, T, Tu, J.; Milstiein, S.; Spiegel, S. Purification and Characterization of Rat Kidney Sphingosine Kinase. *FASEB J.* **1998**, *12* (8), 12576–12583.

(33) Xia, P.; Gamble, J. R.; Wang, L.; Pitson, S. M.; Moretti, P. A. B.; Wattenberg, B. W.; D'Andrea, R. J.; Vadas, M. A. An Oncogenic Role of Sphingosine Kinase. *Curr. Biol.* **2000**, *10* (23):1527-30.

(34) Nava, V. Sphingosine Kinase Type 1 Promotes Estrogen-Dependent Tumorigenesis of Breast Cancer MCF-7 Cells. *Exp. Cell Res.* **2002**, *281* (1), 115–127.

(35)   French, K. J.; Schrecengost, R. S.; Lee, B. D.; Zhuang, Y.; Smith, S. N.; Eberly, J. L.; Yun, J. K.; Smith, C. D. Discovery and Evaluation of Inhibitors of Human Sphingosine Kinase. *Cancer Res.* **2003**, *63* (18), 5962–5969.

(36)   Pitson, S. M.; Moretti, P. A. B.; Zebol, J. R.; Lynn, H. E.; Xia, P.; Vadas, M. A.; Wattenberg, B. W. Activation of Sphingosine Kinase 1 by erk1/2-Mediated Phosphorylation. *EMBO J.* **2003**, *22* (20), 5491–5500.

(37)   Taha, T. A.; Osta, W.; Kozhaya, L.; Bielawski, J.; Johnson, K. R.; Gillanders, W. E.; Dbaibo, G. S.; Hannun, Y. A.; Obeid, L. M. Down-Regulation of Sphingosine Kinase-1 by DNA Damage: Dependence on Proteases and p53. *J. Biol. Chem.* **2004**, *279* (19), 20546–20554.

(38)   Maceyka, M.; Sankala, H.; Hait, N. C.; Le Stunff, H.; Liu, H.; Toman, R.; Collier, C.; Zhang, M.; Satin, L. S.; Merrill, A. H.; Milstien, S.; Spiegel, S. SphK1 and SphK2, Sphingosine Kinase Isoenzymes with Opposing Functions in Sphingolipid Metabolism. *J. Biol. Chem.* **2005**, *280* (44), 37118–37129.

(39)   McNaughton, M.; Pitman, M.; Pitson, S. M.; Pyne, N. J.; Pyne, S. Proteasomal Degradation of Sphingosine Kinase 1 and Inhibition of Dihydroceramide Desaturase by the Sphingosine Kinase Inhibitors, SKi or ABC294640, Induces Growth Arrest in Androgen-Independent LNCaP-AI Prostate Cancer Cells. *Oncotarget.* **2016**, *7* (13), 16663–16675.

(40)   Takabe, K.; Paugh, S. W.; Milstien, S.; Spiegel, S. "Inside-Out" Signaling of Sphingosine-1-Phosphate: Therapeutic Targets. *Pharmacol. Rev.* **2008**, *60* (2), 181–195.

(41)   Hla, T.; Lee, M. J.; Ancellin, N.; Paik, J. H.; Kluk, M. J. Lysophospholipids [mdash] Receptor Revelations. *Science.* **2001**, *294* , 1875–1878.

(42)   Hisano, Y.; Kobayashi, N.; Yamaguchi, A.; Nishi, T. Mouse SPNS2 Functions as a Sphingosine-1-Phosphate Transporter in Vascular Endothelial Cells. *PLoS One* **2012**, *7* (6).

(43)   Sato, M.; Ikeda, H.; Uranbileg, B.; Kurano, M.; Saigusa, D.; Aoki, J.; Maki, H.; Kudo, H.; Hasegawa, K.; Kokudo, N.; Yatomi, Y. Sphingosine Kinase-1, S1P Transporter Spinster Homolog 2 and S1P2 mRNA Expressions Are Increased in Liver with Advanced Fibrosis in Human. *Sci. Rep.* **2016**. 32119.

(44)   Neubauer, H. A.; Pitson, S. M. Roles, Regulation and Inhibitors of Sphingosine Kinase 2. *FEBS J.* **2013**, *280* (21), 5317–5336.

(45)   Spiegel, S. and; Milstien, S. Sphingosine-1-Phosphate: An Enigmatic Signalling Lipid. *Nat. Rev. Mol. Cell Biol.* **2003**, *4* (5), 397–407.

(46)   Pyne, N.; Pyne, S. Sphingosine 1-Phosphate Receptor 1 Signaling in Mammalian Cells. *Molecules.* **2017**, *22* (3), 344.

(47) Limaye, V.; Li, X.; Hahn, C.; Xia, P.; Berndt, M. C.; Vadas, M. A.; Gamble, J. R. Sphingosine Kinase-1 Enhances Endothelial Cell Survival through a PECAM-1-Dependent Activation of PI-3K/Akt and Regulation of Bcl-2 Family Members. *Blood.* **2005**, *105* (8), 3169–3177.

(48) Sauer, B.; Gonska, H.; Manggau, M.; Kim, D. S.; Schraut, C.; Schäfer-Korting, M.; Kleuser, B. Sphingosine 1-Phosphate Is Involved in Cytoprotective Actions of Calcitriol in Human Fibroblasts and Enhances the Intracellular Bcl-2/Bax Rheostat. *Pharmazie.* **2005**, *60* (4), 298–304.

(49) Li, J.; Guan, H.-Y.; Gong, L.-Y.; Song, L.-B.; Zhang, N.; Wu, J.; Yuan, J.; Zheng, Y.-J.; Huang, Z.-S.; Li, M. Clinical Significance of Sphingosine Kinase-1 Expression in Human Astrocytomas Progression and Overall Patient Survival. *Clin. Cancer Res.* **2008**, *14* (21), 6996–7003.

(50) Liu, H.; Sugiura, M.; Nava, V. E.; Edsall, L. C.; Kono, K.; Poulton, S.; Milstien, S.; Kohama, T.; Spiegel, S. Molecular Cloning and Functional Characterization of a Novel Mammalian Sphingosine Kinase Type 2 Isoform. *J. Biol. Chem.* **2000**, *275* (26), 19513–19520.

(51) Sanna, M. G.; Wang, S.-K.; Gonzalez-Cabrera, P. J.; Don, A.; Marsolais, D.; Matheu, M. P.; Wei, S. H.; Parker, I.; Jo, E.; Cheng, W.-C.; Cahalan, M. D.; Wong, C.-H.; Rosen, H. Enhancement of Capillary Leakage and Restoration of Lymphocyte Egress by a Chiral S1P1 Antagonist in Vivo. *Nat. Chem. Biol.* **2006**, *2* (8), 434–441.

(52) Singleton, P. a; Dudek, S. M.; Chiang, E. T.; Garcia, J. G. N. Regulation of Sphingosine 1-Phosphate-Induced Endothelial Cytoskeletal Rearrangement and Barrier Enhancement by S1P1 Receptor, PI3 Kinase, Tiam1/Rac1, and Alpha-Actinin. *FASEB J.* **2005**, *19* (12), 1646–1656.

(53) Spiegel, S.; Milstien, S. Sphingosine 1-Phosphate, a Key Cell Signaling Molecule. *J. Biol. Chem.* **2002**, *277* (29), 25851–25854.

(54) Takuwa, Y.; Okamoto, Y.; Yoshioka, K.; Takuwa, N. Sphingosine-1-Phosphate Signaling in Physiology and Diseases. *BioFactors.* **2012**, *38* (5), 329–337.

(55) Christian Waeber, Nicolas Blondeau, S. S.; S. Vascular Sphingosine-1-Phosphate S1P1 and S1P3 Receptors. *Drug News Perspect.* **2004**, *17* (6), 1–18.

(56) Blom, T.; Bergelin, N.; Meinander, A.; Löf, C.; Slotte, J. P.; Eriksson, J. E.; Törnquist, K. An Autocrine Sphingosine-1-Phosphate Signaling Loop Enhances NF-kappaB-Activation and Survival. *BMC Cell Biol.* **2010**, *11* (1), 45.

(57) Maclennan, A. J.; Carney, P. R.; Zhu, W. J.; Chaves, A. H.; Garcia, J.; Grimes, J. R.; Anderson, K. J.; Roper, S. N.; Lee, N. An Essential Role for the H218 / AGR16 / Edg-5 / LP B2 Sphingosine 1-Phosphate Receptor in Neuronal Excitability. **2001**, *14*(2), 203–209.

(58) Herr, D. R.; Grillet, N.; Schwander, M.; Rivera, R.; Müller, U.; Chun, J. Sphingosine 1-Phosphate (S1P) Signaling Is Required for Maintenance of Hair Cells Mainly via Activation of S1P2. *J. Neurosci.* **2007**, *27* (6), 1474–1478.

(59) Kono, M.; Belyantseva, I. A.; Skoura, A.; Frolenkov, G. I.; Starost, M. F.; Dreier, J. L.; Lidington, D.; Bolz, S. S.; Friedman, T. B.; Hla, T.; Proia, R. L. Deafness and Stria Vascularis Defects in S1P2 Receptor-Null Mice. *J. Biol. Chem.* **2007**, *282* (14), 10690–10696.

(60) Ishii, I.; Friedman, B.; Ye, X.; Kawamura, S.; McGiffert, C.; Contos, J. J. A.; Kingsbury, M. A.; Zhang, G.; Brown, J. H.; Chun, J. Selective Loss of Sphingosine 1-Phosphate Signaling with No Obvious Phenotypic Abnormality in Mice Lacking Its G Protein-Coupled Receptor, LP B3/EDG-3. *J. Biol. Chem.* **2001**, *276* (36), 33697–33704.

(61) Gräler, M. H.; Bernhardt, G.; Lipp, M. EDG6, a Novel G-Protein-Coupled Receptor Related to Receptors for Bioactive Lysophospholipids, Is Specifically Expressed in Lymphoid Tissue. *Genomics* **1998**, *53* (2), 164–169.

(62) Graler, M. H.; Bernahardt, G.; Lipp, M. A Lymphoid Tissue-Specific Receptor, EDG6, with Potential Immune Modulatory Functions Mediated by Extracellular Lysophospholipids. *Curr Top Microbiol Immunol.* **1999**, *246* (10), 131–136.

(63) Hu, W.-M.; Li, L.; Jing, B.-Q.; Zhao, Y.-S.; Wang, C.-L.; Feng, L.; Xie, Y.-E. Effect of S1P5 on Proliferation and Migration of Human Esophageal Cancer Cells. *World J. Gastroenterol.* **2010**, *16* (15), 1859–1866.

(64) Im, D. S.; Clemens, J.; Macdonald, T. L.; Lynch, K. R. Characterization of the Human and Mouse Sphingosine 1-Phosphate Receptor, S1P5 (Edg-8): Structure-Activity Relationship of sphingosine1-Phosphate Receptors. *Biochemistry.* **2001**, *40* (46), 14053–14060.

(65) Shida, D.; Takabe, K.; Kapitonov, D.; Milstien, S.; Spiegel, S. Targeting sphk1 as a New Strategy against Cancer. *Curr. Drug Targets.* **2008**, *9*, 662.

(66) Choi, O. No TitleCalcium Mobilization via Sphingosine Kinase in Signalling by the Fc Epsilon RI Antigen Receptor. *Nature.* **1996**, *380* (6575), 634.

(67) Müller, C. W.; Rey, F. a; Sodeoka, M.; Verdine, G. L.; Harrison, S. C. Structure of the NF-Kappa B p50 Homodimer Bound to DNA. *Nature.* **1995**, *373*, 311–317.

(68) Huang, S.; Robinson, J. B.; Deguzman, A.; Bucana, C. D.; Fidler, I. J. Blockade of Nuclear Factor-kappaB Signaling Inhibits Angiogenesis and Tumorigenicity of Human Ovarian Cancer Cells by Suppressing Expression of Vascular Endothelial Growth Factor and Interleukin 8. *Cancer Res.* **2000**, *60* (19), 5334–5339.

(69) Hait, N. C.; Allegood, J.; Maceyka, M.; Strub, G. M.; Harikumar, K. B.; Singh, S. K.; Luo, C.; Marmorstein, R.; Kordula, T.; Milstien, S.; Spiegel, S. Regulation of Histone Acetylation in the Nucleus by Sphingosine-1-Phosphate. *Science.* **2009**, *325* (5945), 1254–1257.

(70) Strub, G. M.; Paillard, M.; Liang, J.; Gomez, L.; Allegood, J. C.; Hait, N. C.; Maceyka, M.; Price, M. M.; Chen, Q.; Simpson, D. C.; Kordula, T.; Milstien, S.; Lesnefsky, E. J.; Spiegel, S. Sphingosine-1-Phosphate Produced by Sphingosine Kinase 2 in Mitochondria Interacts with Prohibitin 2 to Regulate Complex IV Assembly and Respiration. *FASEB J.* **2011**, *25* (2), 600–612.

(71) Kohama, T.; Olivera, A.; Edsall, L.; Nagiec, M. M.; Dickson, R.; Spiegel, S. Molecular Cloning and Functional Characterization of Murine Sphingosine Kinase. *J Biol Chem.* **1998**, *273*.

(72) Nava, V. E.; Lacana', E.; Poulton, S.; Liu, H.; Sugiura, M.; Kono, K.; Milstien, S.; Kohama, T.; Spiegel, S. Functional Characterization of Human Sphingosine Kinase-1. *FEBS Lett.* **2000**, *473* (1), 81–84.

(73) Okada, T.; Ding, G.; Sonoda, H.; Kajimoto, T.; Haga, Y.; Khosrowbeygi, A.; Gao, S.; Miwa, N.; Jahangeer, S.; Nakamura, S. I. Involvement of N-Terminal-Extended Form of Sphingosine Kinase 2 in Serum-Dependent Regulation of Cell Proliferation and Apoptosis. *J. Biol. Chem.* **2005**, *280* (43), 36318–36325.

(74) Pitson, S. M. Regulation of Sphingosine Kinase and Sphingolipid Signaling. *Trends Biochem. Sci.* **2011**, *36* (2), 97–107.

(75) Pitson, S. M.; Moretti, P. a B.; Zebol, J. R.; Zareie, R.; Derian, C. K.; Darrow, A. L.; Qi, J.; D'Andrea, R. J.; Bagley, C. J.; Vadas, M. a; Wattenberg, B. W. The Nucleotide-Binding Site of Human Sphingosine Kinase 1. *J. Biol. Chem.* **2002**, *277* (51), 49545–49553.

(76) Yokota, S.; Taniguchi, Y.; Kihara, A.; Mitsutake, S.; Igarashi, Y. Asp177 in C4 Domain of Mouse Sphingosine Kinase 1a Is Important for the Sphingosine Recognition. *FEBS Lett.* **2004**, *578* (1-2), 106–110.

(77) Sugiura, M.; Kono, K.; Liu, H.; Shimizugawa, T.; Minekura, H.; Spiegel, S.; Kohama, T. Ceramide Kinase, a Novel Lipid Kinase: Molecular Cloning and Functional Characterization. *J. Biol. Chem.* **2002**, *277* (26), 23294–23300.

(78) Liu, H.; Toman, R. E.; Goparaju, S. K.; Maceyka, M.; Nava, V. E.; Sankala, H.; Payne, S. G.; Bektas, M.; Ishii, I.; Chun, J.; Milstien, S.; Spiegel, S. Sphingosine Kinase Type 2 Is a Putative bh3-Only Protein That Induces Apoptosis. *J. Biol. Chem.* **2003**, *278*, 40330.

(79) Pitson, S. M.; Moretti, P. A. B.; Zebol, J. R.; Xia, P.; Gamble, J. R.; Vadas, M. A.; D'Andrea, R. J.; Wattenberg, B. W. Expression of a Catalytically Inactive Sphingosine Kinase Mutant Blocks Agonist-Induced Sphingosine Kinase

Activation. A Dominant-Negative Sphingosine Kinase. *J. Biol. Chem.* **2000**, *275* (43), 33945–33950.

(80)   Leclercq, T.; Pitson, S. Cellular Signalling by Sphingosine Kinase and Sphingosine 1-Phosphate. *IUBMB Life (International Union Biochem. Mol. Biol. Life.* **2006**, *58* (8), 467–472.

(81)   Wang, Z.; Min, X.; Xiao, S. H.; Johnstone, S.; Romanow, W.; Meininger, D.; Xu, H.; Liu, J.; Dai, J.; An, S.; Thibault, S.; Walker, N. Molecular Basis of Sphingosine Kinase 1 Substrate Recognition and Catalysis. *Structure.* **2013**, *21* (5), 798–809.

(82)   Wang, J.; Knapp, S.; Pyne, N. J.; Pyne, S.; Elkins, J. M. Crystal Structure of Sphingosine Kinase 1 with PF-543. *ACS Med. Chem. Lett.* **2014**, *5* (12), 1329–1333.

(83)   Melendez, A. J.; Carlos-Dias, E.; Gosink, M.; Allen, J. M.; Takacs, L. Human Sphingosine Kinase: Molecular Cloning, Functional Characterization and Tissue Distribution. *Gene.* **2000**, *251* (1), 19–26.

(84)   Olivera, A.; Rosenfeldt, H. M.; Bektas, M.; Wang, F.; Ishii, I.; Chun, J.; Milstien, S.; Spiegel, S. Sphingosine Kinase Type 1 Induces G12/13-Mediated Stress Fiber Formation, yet Promotes Growth and Survival Independent of G Protein-Coupled Receptors. *J. Biol. Chem.* **2003**, *278* (47), 46452–46460.

(85)   Ding, G.; Sonoda, H.; Yu, H.; Kajimoto, T.; Goparaju, S. K.; Jahangeer, S.; Okada, T.; Nakamura, S. Protein Kinase D-Mediated Phosphorylation and Nuclear Export of Sphingosine Kinase 2. *J Biol Chem.* **2007**, *282* (37), 27493–27502.

(86)   Gijsbers, S.; Van Der Hoeven, G.; Van Veldhoven, P. P. Subcellular Study of Sphingoid Base Phosphorylation in Rat Tissues: Evidence for Multiple Sphingosine Kinases. *Biochim. Biophys. Acta - Mol. Cell Biol. Lipids.* **2001**, *1532* (1-2), 37–50.

(87)   Stahelin, R. V; Hwang, J. H.; Kim, J. H.; Park, Z. Y.; Johnson, K. R.; Obeid, L. M.; Cho, W. The Mechanism of Membrane Targeting of Human Sphingosine Kinase 1. *J Biol Chem.* **2005**, *280* (52), 43030–43038.

(88)   Delon, C.; Manifava, M.; Wood, E.; Thompson, D.; Krugmann, S.; Pyne, S.; Ktistakis, N. T. Sphingosine Kinase 1 Is an Intracellular Effector of Phosphatidic Acid. *J. Biol. Chem.* **2004**, *279* (43), 44763–44774.

(89)   Xia, P.; Wang, L.; Moretti, P. A. B.; Albanese, N.; Chai, F.; Pitson, S. M.; D'Andrea, R. J.; Gamble, J. R.; Vadas, M. A. Sphingosine Kinase Interacts with TRAF2 and Dissects Tumor Necrosis Factor-A Signaling. *J. Biol. Chem.* **2002**, *277* (10), 7996–8003.

(90) Ren, R.; Mayer, B. J.; Cicchetti, P.; Baltimore, D. Identification of a Ten-Amino Acid Proline-Rich SH3 Binding Site. *Science*.**1993**, *259* (5098), 1157–1161.

(91) Yu, H.; Chen, J. K.; Feng, S.; Dalgarno, D. C.; Brauer, A. W.; Schrelber, S. L. Structural Basis for the Binding of Proline-Rich Peptides to SH3 Domains. *Cell*. **1994**, *76* (5), 933–945.

(92) Inagaki, Y.; Li, P.-Y.; Wada, A.; Mitsutake, S.; Igarashi, Y. Identification of Functional Nuclear Export Sequences in Human Sphingosine Kinase 1. *Biochem. Biophys. Res. Commun.* **2003**, *311* (1), 168–173.

(93) Ancellin, N.; Colmont, C.; Su, J.; Li, Q.; Mittereder, N.; Chae, S. S.; Stefansson, S.; Liau, G.; Hla, T. Extracellular Export of Sphingosine Kinase-1 Enzyme. Sphingosine 1-Phosphate Generation and the Induction of Angiogenic Vascular Maturation. *J. Biol. Chem.* **2002**, *277* (8), 6667–6675.

(94) Hait, N. C.; Bellamy, A.; Milstien, S.; Kordula, T.; Spiegel, S. Sphingosine Kinase Type 2 Activation by ERK-Mediated Phosphorylation. *J. Biol. Chem.* **2007**,282,12058-12065.

(95) Le Stunff, H.; Giussani, P.; Maceyka, M.; Lépine, S.; Milstien, S.; Spiegel, S. Recycling of Sphingosine Is Regulated by the Concerted Actions of Sphingosine-1-Phosphate Phosphohydrolase 1 and Sphingosine Kinase 2. *J. Biol. Chem.* **2007**, *282* (47), 34372–34380.

(96) Weigert, A.; Cremer, S.; Schmidt, M. V.; Von Knethen, A.; Angioni, C.; Geisslinger, G.; Brüne, B. Cleavage of Sphingosine Kinase 2 by Caspase-1 Provokes Its Release from Apoptotic Cells. *Blood.* **2010**, 115 (17), 3531-3540.

(97) Chan, H.; Pitson, S. M. Post-Translational Regulation of Sphingosine Kinases. *Biochim. Biophys. Acta - Mol. Cell Biol. Lipids.* **2013**, *1831* (1), 147–156.

(98) Don, A. S.; Rosen, H. A Lipid Binding Domain in Sphingosine Kinase 2. *Biochem. Biophys. Res. Commun.* **2009**, *380* (1), 87–92.

(99) Snider, A. J.; Kawamori, T.; Bradshaw, S. G.; Orr, K. A.; Gilkeson, G. S.; Hannun, Y. A.; Obeid, L. M. A Role for Sphingosine Kinase 1 in Dextran Sulfate Sodium-Induced Colitis. *FASEB J.* **2009**, *23* (1), 143–152.

(100) Jolly, P. S.; Bektas, M.; Olivera, A.; Gonzalez-Espinosa, C.; Proia, R. L.; Rivera, J.; Milstien, S.; Spiegel, S. Transactivation of Sphingosine-1-Phosphate Receptors by FcepsilonRI Triggering Is Required for Normal Mast Cell Degranulation and Chemotaxis. *J. Exp. Med.* **2004**, *199* (7), 959–970.

(101) Sanchez, T.; Thangada, S.; Wu, M.-T.; Kontos, C. D.; Wu, D.; Wu, H.; Hla, T. PTEN as an Effector in the Signaling of Antimigratory G Protein-Coupled Receptor. *Proc. Natl. Acad. Sci. U. S. A.* **2005**, *102* (12), 4312–4317.

(102) Colombini, M. Ceramide Channels and Their Role in Mitochondria-Mediated Apoptosis. *Biochimica et Biophysica Acta - Bioenergetics*. **2010**, *1797* (6-7) 1239-1244.

(103) Ohotski, J.; Long, J. S.; Orange, C.; Elsberger, B.; Mallon, E.; Doughty, J.; Pyne, S.; Pyne, N. J.; Edwards, J. Expression of Sphingosine 1-Phosphate Receptor 4 and Sphingosine Kinase 1 Is Associated with Outcome in Oestrogen Receptor-Negative Breast Cancer. *Br. J. Cancer.* **2012**, *106* (8), 1453–1459.

(104) Watson, C.; Long, J. S.; Orange, C.; Tannahill, C. L.; Mallon, E.; McGlynn, L. M.; Pyne, S.; Pyne, N. J.; Edwards, J. High Expression of Sphingosine 1-Phosphate Receptors, S1P1 and S1P3, Sphingosine Kinase 1, and Extracellular Signal-Regulated Kinase-1/2 Is Associated with Development of Tamoxifen Resistance in Estrogen Receptor-Positive Breast Cancer Patients. *Am. J. Pathol.* **2010**, *177* (5), 2205–2215.

(105) Hsu, A.; Zhang, W.; Lee, J. F.; An, J.; Ekambaram, P.; Liu, J.; Honn, K. V.; Klinge, C. M.; Lee, M. J. Sphingosine-1-Phosphate Receptor-3 Signaling up-Regulates Epidermal Growth Factor Receptor and Enhances Epidermal Growth Factor Receptor-Mediated Carcinogenic Activities in Cultured Lung Adenocarcinoma Cells. *Int. J. Oncol.* **2012**, *40* (5), 1619–1626.

(106) Long, J. S.; Edwards, J.; Watson, C.; Tovey, S.; Mair, K. M.; Schiff, R.; Natarajan, V.; Pyne, N. J.; Pyne, S. Sphingosine Kinase 1 Induces Tolerance to Human Epidermal Growth Factor Receptor 2 and Prevents Formation of a Migratory Phenotype in Response to Sphingosine 1-Phosphate in Estrogen Receptor-Positive Breast Cancer Cells. *Mol. Cell. Biol.* **2010**, *30* (15), 3827–3841.

(107) Yoshida, Y.; Nakada, M.; Harada, T.; Tanaka, S.; Furuta, T.; Hayashi, Y.; Kita, D.; Uchiyama, N.; Hayashi, Y.; Hamada, J. I. The Expression Level of Sphingosine-1-Phosphate Receptor Type 1 Is Related to MIB-1 Labeling Index and Predicts Survival of Glioblastoma Patients. *J. Neurooncol.* **2010**, *98* (1), 41–47.

(108) Sanders, L. C.; Matsumura, F.; Bokoch, G. M.; de Lanerolle, P. Inhibition of Myosin Light Chain Kinase by p21-Activated Kinase [see Comments]. *Science (80-.).* **1999**, *283* (5410), 2083–2085.

(109) Radeff-Huang, J.; Seasholtz, T. M.; Matteo, R. G.; Brown, J. H. G Protein Mediated Signaling Pathways in Lysophospholipid Induced Cell Proliferation and Survival. *J. Cell. Biochem.* **2004**, *92* (5), 949–966.

(110) Yamashita, H.; Kitayama, J.; Shida, D.; Yamaguchi, H.; Mori, K.; Osada, M.; Aoki, S.; Yatomi, Y.; Takuwa, Y.; Nagawa, H. Sphingosine 1-Phosphate Receptor Expression Profile in Human Gastric Cancer Cells: Differential Regulation on the Migration and Proliferation. *J Surg Res.* **2006**, *130* (1), 80–87.

(111) Okamoto, Y.; Wang, F.; Yoshioka, K.; Takuwa, N.; Takuwa, Y. Sphingosine-1-Phosphate-Specific G Protein-Coupled Receptors as Novel Therapeutic Targets for Atherosclerosis. *Pharmaceuticals* **2011**, *4* (1), 117–137.

(112) Long, J. S.; Fujiwara, Y.; Edwards, J.; Tannahill, C. L.; Tigyi, G.; Pyne, S.; Pyne, N. J. Sphingosine 1-Phosphate Receptor 4 Uses HER2 (ERBB2) to Regulate Extracellular Signal Regulated Kinase-1/2 in MDA-MB-453 Breast Cancer Cells. *J. Biol. Chem.* **2010**, *285* (46), 35957–35966.

(113) Van Brocklyn, J. R.; Young, N.; Roof, R. Sphingosine-1-Phosphate Stimulates Motility and Invasiveness of Human Glioblastoma Multiforme Cells. *Cancer Lett.* **2003**, *199* (1), 53–60.

(114) Lepley, D.; Paik, J.; Hla, T.; Ferrer, F. The G Protein – Coupled Receptor S1P 2 Regulates Rho / Rho Kinase Pathway to Inhibit Tumor Cell Migration. **2005**, *9*(65), 3788–3796.

(115) Bryan, L.; Paugh, B. S.; Kapitonov, D.; Wilczynska, K. M.; Alvarez, S. M.; Singh, S. K.; Milstien, S.; Spiegel, S.; Kordula, T. Sphingosine-1-Phosphate and Interleukin-1 Independently Regulate Plasminogen Activator Inhibitor-1 and Urokinase-Type Plasminogen Activator Receptor Expression in Glioblastoma Cells : Implications for Invasiveness Sphingosine-1-Phosphate and Interleukin-1. *Mol. Cancer Res.* **2008**, *6* (9), 1469–1477.

(116) Arikawa, K.; Takuwa, N.; Yamaguchi, H.; Sugimoto, N.; Kitayama, J.; Nagawa, H.; Takehara, K.; Takuwa, Y. Ligand-Dependent Inhibition of B16 Melanoma Cell Migration and Invasion via Endogenous S1P2 G Protein-Coupled Receptor: Requirement of Inhibition of Cellular Rac Activity. *J. Biol. Chem.* **2003**, *278* (35), 32841–32851.

(117) Sugimoto, N.; Takuwa, N.; Yoshioka, K.; Takuwa, Y. Rho-Dependent, Rho Kinase-Independent Inhibitory Regulation of Rac and Cell Migration by LPA1 Receptor in Gi-Inactivated CHO Cells. *Exp. Cell Res.* **2006**, *312* (10), 1899–1908.

(118) Liu, C.; Okruzhnov, Y.; Li, H.; Nicholas, J. Human Herpesvirus 8 (HHV-8)-Encoded Cytokines Induce Expression of and Autocrine Signaling by Vascular Endothelial Growth Factor (VEGF) in HHV-8-Infected Primary-Effusion Lymphoma Cell Lines and Mediate VEGF-Independent Antiapoptotic Effects. *J Virol.* **2001**, *75* (22), 10933–10940.

(119) Wu, W.; Shu, X.; Hovsepyan, H.; Mosteller, R. D.; Broek, D. VEGF Receptor Expression and Signaling in Human Bladder Tumors. *Oncogene.* **2003**, *22*, 3361–3370.

(120) Yatomi, Y.; Ruan, F.; Megidish, T.; Toyokuni, T.; Hakomori, S.; Igarashi, Y. N, N-Dimethylsphingosine Inhibition of Sphingosine Kinase and Sphingosine 1-Phosphate Activity in Human Platelets. *Biochemistry.* **1996**, *Jan*, A – H.

(121) Gao, Z.; Wang, H.; Xiao, F. J.; Shi, X. F.; Zhang, Y. K.; Xu, Q. Q.; Zhang, X. Y.; Ha, X. Q.; Wang, L. S. SIRT1 Mediates Sphk1/S1P-Induced Proliferation and Migration of Endothelial Cells. *Int. J. Biochem. Cell Biol.* **2016**, *74*, 152–160.

(122) Chae, S. S.; Paik, J. H.; Furneaux, H.; Hla, T. Requirement for Sphingosine 1-Phosphate Receptor-1 in Tumor Angiogenesis Demonstrated by in Vivo RNA Interference. *J. Clin. Invest.* **2004**, *114* (8), 1082–1089.

(123) Visentin, B.; Vekich, J. A.; Sibbald, B. J.; Cavalli, A. L.; Moreno, K. M.; Matteo, R. G.; Garland, W. A.; Lu, Y.; Yu, S.; Hall, H. S.; Kundra, V.; Mills, G. B.; Sabbadini, R. A. Validation of an Anti-Sphingosine-1-Phosphate Antibody as a Potential Therapeutic in Reducing Growth, Invasion, and Angiogenesis in Multiple Tumor Lineages. *Cancer Cell.* **2006**, *9* (3), 225–238.

(124) O'Brien, N.; Jones, S. T.; Williams, D. G.; Cunningham, H. B.; Moreno, K.; Visentin, B.; Gentile, A.; Vekich, J.; Shestowsky, W.; Hiraiwa, M.; Matteo, R.; Cavalli, A.; Grotjahn, D.; Grant, M.; Hansen, G.; Campbell, M.-A.; Sabbadini, R. Production and Characterization of Monoclonal Anti-Sphingosine-1-Phosphate Antibodies. *J. Lipid Res.* **2009**, *50* (11), 2245–2257.

(125) Brinkmann, V.; Davis, M. D.; Heise, C. E.; Albert, R.; Cottens, S.; Hof, R.; Bruns, C.; Prieschl, E.; Baumruker, T.; Hiestand, P.; Foster, C. A.; Zollinger, M.; Lynch, K. R. The Immune Modulator FTY720 Targets Sphingosine 1-Phosphate Receptors. *J. Biol. Chem.* **2002**, *277* (24), 21453–21457.

(126) Brinkmann, V.; Billich, A.; Baumruker, T.; Heining, P.; Schmouder, R.; Francis, G.; Aradhye, S.; Burtin, P. Fingolimod (FTY720): Discovery and Development of an Oral Drug to Treat Multiple Sclerosis. *Nat. Rev. Drug Discov.* **2010**, *9* (11), 883–897.

(127) Wendler, D. S. Problems with the Consensus Definition of the Therapeutic Misconception. *J. Clin. Ethic.* **2013**, *24* (4), 387–394.

(128) Lim, K. G.; Tonelli, F.; Li, Z.; Lu, X.; Bittman, R.; Pyne, S.; Pyne, N. J. FTY720 Analogues as Sphingosine Kinase 1 Inhibitors: Enzyme Inhibition Kinetics, Allosterism, Proteasomal Degradation and Actin Rearrangement in MCF-7 Breast Cancer Cells. *J. Biol. Chem.* **2011**, *286* (21), 18633–18640.

(129) Loveridge, C.; Tonelli, F.; Leclercq, T.; Lim, K. G.; Long, J. S.; Berdyshev, E.; Tate, R. J.; Natarajan, V.; Pitson, S. M.; Pyne, N. J. The Sphingosine Kinase 1 Inhibitor 2-(p-Hydroxyanilino)-4-(p-Chlorophenyl) Thiazole Induces Proteasomal Degradation of Sphingosine Kinase 1 in Mammalian Cells. *J. Biol. Chem.* **2010**, *285* (50), 38841–38852.

(130) Azuma, H.; Takahara, S.; Ichimaru, N.; Wang, J. D.; Itoh, Y.; Otsuki, Y.; Morimoto, J.; Fukui, R.; Hoshiga, M.; Ishihara, T.; Nonomura, N.; Suzuki, S.; Okuyama, A.; Katsuoka, Y. Marked Prevention of Tumor Growth and

Metastasis by a Novel Immunosuppressive Agent, FTY720, in Mouse Breast Cancer Models. *Cancer Res.* **2002**, *62* (5), 1410–1419.

(131) Gräler, M. H.; Goetzl, E. J. The Immunosuppressant FTY720 down-Regulates Sphingosine 1-Phosphate G-Protein-Coupled Receptors. *FASEB J.* **2004**, *18* (3), 551–553.

(132) Ohmori, T.; Yatomi, Y.; Osada, M.; Kazama, F.; Takafuta, T.; Ikeda, H.; Ozaki, Y. Sphingosine 1-Phosphate Induces Contraction of Coronary Artery Smooth Muscle Cells via S1P2. *Cardiovasc. Res.* **2003**, *58* (1), 170–177.

(133) Davis, M. D.; Clemens, J. J.; Macdonald, T. L.; Lynch, K. R. Sphingosine 1-Phosphate Analogs as Receptor Antagonists. *J. Biol. Chem.* **2005**, *280* (11), 9833–9841.

(134) Ruckhäberle, E.; Rody, A.; Engels, K.; Gaetje, R.; Von Minckwitz, G.; Schiffmann, S.; Grösch, S.; Geisslinger, G.; Holtrich, U.; Karn, T.; Kaufmann, M. Microarray Analysis of Altered Sphingolipid Metabolism Reveals Prognostic Significance of Sphingosine Kinase 1 in Breast Cancer. *Breast Cancer Res. Treat.* **2008**, *112* (1), 41–52.

(135) Guo, X. Z.; Zhang, W. W.; Wang, L. S.; Lu, Z. Z.; Wang, H.; Xu, J. H.; Tian, H. [Adenovirus-Mediated Overexpression of KAI1 Suppresses Sphingosine Kinase Activation and Metastasis of Pancreatic Carcinoma Cells]. *Zhonghua Nei Ke Za Zhi.* **2006**, *45* (9), 752–754.

(136) Sarkar, S.; Maceyka, M.; Hait, N. C.; Paugh, S. W.; Sankala, H.; Milstien, S.; Spiegel, S. Sphingosine Kinase 1 Is Required for Migration, Proliferation and Survival of MCF-7 Human Breast Cancer Cells. *FEBS Lett.* **2005**, *579* (24), 5313–5317.

(137) Sutherland, C. M.; Moretti, P. A. B.; Hewitt, N. M.; Bagley, C. J.; Vadas, M. A.; Pitson, S. M. The Calmodulin-Binding Site of Sphingosine Kinase and Its Role in Agonist-Dependent Translocation of Sphingosine Kinase 1 to the Plasma Membrane. *J. Biol. Chem.* **2006**, *281* (17), 11693–11701.

(138) Hait, N. C.; Sarkar, S.; Le Stunff, H.; Mikami, A.; Maceyka, M.; Milstien, S.; Spiegel, S. Role of Sphingosine Kinase 2 in Cell Migration toward Epidermal Growth Factor. *J. Biol. Chem.* **2005**, *280* (33), 29462–29469.

(139) Le Scolan, E.; Pchejetski, D.; Banno, Y.; Denis, N.; Mayeux, P.; Vainchenker, W.; Levade, T.; Moreau-Gachelin, F. Overexpression of Sphingosine Kinase 1 Is an Oncogenic Event in Erythroleukemic Progression. *Blood.* **2005**, *106* (5), 1808–1816.

(140) Tilly, J. L.; Kolesnick, R. N. Sphingolipids, Apoptosis, Cancer Treatments and the Ovary: Investigating a Crime against Female Fertility. *Biochim. Biophys. Acta - Mol. Cell Biol. Lipids.* **2002**, *1585* (2), 135–138.

(141) Xu, Y.; Xiao, Y. J.; Baudhuin, L. M.; Schwartz, B. M. The Role and Clinical Applications of Bioactive Lysolipids in Ovarian Cancer. *J Soc Gynecol Investig.* **2001**, *8* (1), 1–13.

(142) Bonhoure, E.; Pchejetski, D.; Aouali, N.; Morjani, H.; Levade, T.; Kohama, T.; Cuvillier, O. Overcoming MDR-Associated Chemoresistance in HL-60 Acute Myeloid Leukemia Cells by Targeting Shingosine Kinase-1. *Leukemia.* **2006**, *20* (1), 95–102.

(143) Shu, X.; Wu, W.; Mosteller, R. D.; Broek, D. Sphingosine Kinase Mediates Vascular Endothelial Growth Factor-Induced Activation of Ras and Mitogen-Activated Protein Kinases. *Mol. Cell. Biol.* **2002**, *22* (22), 7758–7768.

(144) Akao, Y.; Banno, Y.; Nakagawa, Y.; Hasegawa, N.; Kim, T.-J.; Murate, T.; Igarashi, Y.; Nozawa, Y. High Expression of Sphingosine Kinase 1 and s1p Receptors in Chemotherapy-Resistant Prostate Cancer pc3 Cells and Their Camptothecin-Induced up-Regulation. *Biochem. Biophys. Res. Commun.* **2006**, *342* (4), 1394–1399.

(145) Pchejetski, D.; Golzio, M.; Bonhoure, E.; Calvet, C.; Doumerc, N.; Garcia, V.; Mazerolles, C.; Rischmann, P.; Teissié, J.; Malavaud, B.; Cuvillier, O. Sphingosine Kinase-1 as a Chemotherapy Sensor in Prostate Adenocarcinoma Cell and Mouse Models. *Cancer Res.* **2005**, *65* (24), 11667 LP – 11675.

(146) Nava, V. E.; Cuvillier, O.; Edsall, L. C.; Kimura, K.; Milstien, S.; Gelmann, E. P.; Spiegel, S. Sphingosine Enhances Apoptosis of Radiation-Resistant Prostate Cancer Cells. *Cancer Res.* **2000**, *60* (16), 4468–4474.

(147) Pchejetski, D.; Doumerc, N.; Golzio, M.; Naymark, M.; Teissié, J.; Kohama, T.; Waxman, J.; Malavaud, B.; Cuvillier, O. Chemosensitizing Effects of Sphingosine Kinase-1 Inhibition in Prostate Cancer Cell and Animal Models. *Mol. Cancer Ther.* **2008**, *7* (7), 1836–1845.

(148) Sauer, L.; Nunes, J.; Salunkhe, V.; Skalska, L.; Kohama, T.; Cuvillier, O.; Waxman, J.; Pchejetski, D. Sphingosine Kinase 1 Inhibition Sensitizes Hormone-resistant Prostate Cancer to Docetaxel. *Int. J. cancer* **2009**, *125* (11), 2728–2736.

(149) Pchejetski, D.; Bohler, T.; Brizuela, L.; Sauer, L.; Doumerc, N.; Golzio, M.; Salunkhe, V.; Teissié, J.; Malavaud, B.; Waxman, J. FTY720 (fingolimod) Sensitizes Prostate Cancer Cells to Radiotherapy by Inhibition of Sphingosine Kinase-1. *Cancer Res.* **2010**, *70* (21), 8651–8661.

(150) Chipuk, J. E.; McStay, G. P.; Bharti, A.; Kuwana, T.; Clarke, C. J.; Siskind, L. J.; Obeid, L. M.; Green, D. R. Sphingolipid Metabolism Cooperates with BAK and BAX to Promote the Mitochondrial Pathway of Apoptosis. *Cell.* **2012**, *148* (5), 988–1000.

(151) Sankala, H. M.; Hait, N. C.; Paugh, S. W.; Shida, D.; Lépine, S.; Elmore, L. W.; Dent, P.; Milstien, S.; Spiegel, S. Involvement of Sphingosine Kinase 2 in p53-Independent Induction of p21 by the Chemotherapeutic Drug Doxorubicin. *Cancer Res.* **2007**, *67* (21), 10466–10474.

(152) Nemoto, S.; Nakamura, M.; Osawa, Y.; Kono, S.; Itoh, Y.; Okano, Y.; Murate, T.; Hara, A.; Ueda, H.; Nozawa, Y.; Banno, Y. Sphingosine Kinase Isoforms Regulate Oxaliplatin Sensitivity of Human Colon Cancer Cells through Ceramide Accumulation and Akt Activation. *J. Biol. Chem.* **2009**, *284* (16), 10422–10432.

(153) Gao, P.; Smith, C. D. Ablation of Sphingosine Kinase-2 Inhibits Tumor Cell Proliferation and Migration. *Mol Cancer Res.* **2011**, *9* (11), 1509–1519.

(154) Van Brocklyn, J. R.; Jackson, C. A.; Pearl, D. K.; Kotur, M. S.; Snyder, P. J.; Prior, T. W. Sphingosine Kinase-1 Expression Correlates with Poor Survival of Patients with Glioblastoma Multiforme: Roles of Sphingosine Kinase Isoforms in Growth of Glioblastoma Cell Lines. *J Neuropathol Exp Neurol* **2005**, *64* (8), 695–705.

(155) French, K. J.; Zhuang, Y.; Maines, L. W.; Gao, P.; Wang, W.; Beljanski, V.; Upson, J. J.; Green, C. L.; Keller, S. N.; Smith, C. D. Pharmacology and Antitumor Activity of ABC294640, a Selective Inhibitor of Sphingosine Kinase-2. *J. Pharmacol. Exp. Ther.* **2010**, *333* (1), 129–139.

(156) Chumanevich, A. A.; Poudyal, D.; Cui, X.; Davis, T.; Wood, P. A.; Smith, C. D.; Hofseth, L. J. Suppression of Colitis-Driven Colon Cancer in Mice by a Novel Small Molecule Inhibitor of Sphingosine Kinase. *Carcinogenesis.* **2010**, *31* (10), 1787–1793.

(157) Qin, Z.; Dai, L.; Trillo-Tinoco, J.; Senkal, C.; Wang, W.; Reske, T.; Bonstaff, K.; Del Valle, L.; Rodriguez, P.; Flemington, E. Targeting Sphingosine Kinase Induces Apoptosis and Tumor Regression for KSHV-Associated Primary Effusion Lymphoma. *Mol. Cancer Ther.* **2014**, *13* (1), 154–164.

(158) Maines, L. W.; Fitzpatrick, L. R.; French, K. J.; Zhuang, Y.; Xia, Z.; Keller, S. N.; Upson, J. J.; Smith, C. D. Suppression of Ulcerative Colitis in Mice by Orally Available Inhibitors of Sphingosine Kinase. *Dig. Dis. Sci.* **2008**, *53*, 997.

(159) Antoon, J. W.; White, M. D.; Slaughter, E. M.; Driver, J. L.; Khalili, H. S.; Elliott, S.; Smith, C. D.; Burow, M. E.; Beckman, B. S. Targeting NFκB Mediated Breast Cancer Chemoresistance through Selective Inhibition of Sphingosine Kinase-2. *Cancer Biol. Ther.* **2011**, *11* (7), 678–689.

(160) Schrecengost, R. S.; Keller, S. N.; Schiewer, M. J.; Knudsen, K. E.; Smith, C. D. Downregulation of Critical Oncogenes by the Selective SK2 Inhibitor ABC294640 Hinders Prostate Cancer Progression. *Mol. Cancer Res.* **2015**, *13* (12), 1591–1601.

(161) Oskouian, B.; Saba, J. D. Cancer Treatment Strategies Targeting Sphingolipid Metabolism. *Adv. Exp. Med. Biol.* **2010**, *688* (2010), 185–205.

(162) Modrak, D. E.; Gold, D. V; Goldenberg, D. M. Sphingolipid Targets in Cancer Therapy. *Mol. Cancer Ther.* **2006**, *5* (2), 200–208.

(163) Saelens, X.; Festjens, N.; Walle, L. Vande; Gurp, M. van; Loo, G. van; Vandenabeele, P. Toxic Proteins Released from Mitochondria in Cell Death. *Oncogene.* **2004**, *23* (16), 2861–2874.

(164) Kong, J. Y.; Klassen, S. S.; Rabkin, S. W. Ceramide Activates a Mitochondrial p38 Mitogen-Activated Protein Kinase: A Potential Mechanism for Loss of Mitochondrial Transmembrane Potential and Apoptosis. *Mol. Cell. Biochem.* **2005**, *278* (1-2), 39–51.

(165) Martínez, R.; Navarro, R.; Lacort, M.; Ruiz-Sanz, J. I.; Ruiz-Larrea, M. B. Doxorubicin Induces Ceramide and Diacylglycerol Accumulation in Rat Hepatocytes through Independent Routes. *Toxicol. Lett.* **2009**, *190* (1), 86–90.

(166) Xin, M.; Deng, X. Nicotine Inactivation of the Proapoptotic Function of Bax through Phosphorylation. *J. Biol. Chem.* **2005**, *280* (11), 10781–10789.

(167) Lin, C. F.; Chen, C. L.; Lin, Y. S. Ceramide in Apoptotic Signaling and Anticancer Therapy. *Curr Med Chem* **2006**, *13* (14), 1609–1616.

(168) Pastorino, J. G.; Tafani, M.; Rothman, R. J.; Marcineviciute, A.; Hoek, J. B.; Farber, J. L. Functional Consequences of the Sustained or Transient Activation by Bax of the Mitochondrial Permeability Transition Pore. *J. Biol. Chem.* **1999**, *274* (44), 31734–31739.

(169) Phillips, D. C.; Martin, S.; Doyle, B. T.; Houghton, J. A. Sphingosine-Induced Apoptosis in Rhabdomyosarcoma Cell Lines Is Dependent on Pre-Mitochondrial Bax Activation and Post-Mitochondrial Caspases. *Cancer Res.* **2007**, *67* (2), 756–764.

(170) Kanno, T.; Nishimoto, T.; Fujita, Y.; Gotoh, A.; Nakano, T.; Nishizaki, T. Sphingosine Induces Apoptosis in MKN-28 Human Gastric Cancer Cells in an SDK-Dependent Manner. *Cell. Physiol. Biochem.* **2012**, *30* (4), 987–994.

(171) Fabrias, G.; Muñoz-Olaya, J.; Cingolani, F.; Signorelli, P.; Casas, J.; Gagliostro, V.; Ghidoni, R. Dihydroceramide Desaturase and Dihydrosphingolipids: Debutant Players in the Sphingolipid Arena. *Prog. Lipid Res.* **2012**, *51* (2), 82–94.

(172) Gagliostro, V.; Casas, J.; Caretti, A.; Abad, J. L.; Tagliavacca, L.; Ghidoni, R.; Fabrias, G.; Signorelli, P. Dihydroceramide Delays Cell Cycle G1/S Transition via Activation of ER Stress and Induction of Autophagy. *Int. J. Biochem. Cell Biol.* **2012**, *44* (12), 2135–2143.

(173) Kraveka, J. M.; Li, L.; Szulc, Z. M.; Bielawski, J.; Ogretmen, B.; Hannun, Y. A.; Obeid, L. M.; Bielawska, A. Involvement of Dihydroceramide Desaturase in Cell Cycle Progression in Human Neuroblastoma Cells. *J. Biol. Chem.* **2007**, *282* (23), 16718–16728.

(174) Malavaud, B.; Pchejetski, D.; Mazerolles, C.; de Paiva, G. R.; Calvet, C.; Doumerc, N.; Pitson, S.; Rischmann, P.; Cuvillier, O. Sphingosine Kinase-1 Activity and Expression in Human Prostate Cancer Resection Specimens. *Eur. J. Cancer* **2010**, *46* (18), 3417–3424.

(175) Duan, R.-D.; Nilsson, Å. Metabolism of Sphingolipids in the Gut and Its Relation to Inflammation and Cancer Development. *Prog. Lipid Res.* **2009**, *48* (1), 62–72.

(176) Abbas, T.; Dutta, A. p21 in Cancer: Intricate Networks and Multiple Activities. *Nat. Rev. Cancer.* **2009**, *9* (6), 400–414.

(177) Heffernan-Stroud, L. A.; Obeid, L. M. P53 and Regulation of Bioactive Sphingolipids. *Adv. Enzyme Regul.* **2011**, *51* (1), 219–228.

(178) Cancer statistics http://www.statistics.gov.uk. Http://www.statistics.gov.uk (accessed Apr 15, 2017).

(179) Cancer Research UK. Http://globocan.iarc.fr/old/FactSheets/cancers/prostate-new.asp.http://globocan.iarc.fr/old/FactSheets/cancers/prostate-New.asp (accessed Apr 8, 2017).

(180) Denmeade, S. R.; Isaacs, J. T. Activation of Programmed (Apoptotic) Cell Death for the Treatment of Prostate Cancer. *Adv. Pharmacol.* **1996**, *35* (C), 281–306.

(181) Denis, L. J.; Griffiths, K. Endocrine Treatment in Prostate Cancer. *Semin. Surg. Oncol.* **2000**, *18* (1), 52–74.

(182) Lee, J. T.; Lehmann, B. D.; Terrian, D. M.; Chappell, W. H.; Stivala, F.; Libra, M.; Martelli, A. M.; Steelman, L. S.; McCubrey, J. A. Targeting Prostate Cancer Based on Signal Transduction and Cell Cycle Pathways. *Cell Cycle* **2008**, *7* (12), 1745–1762.

(183) Brizuela, L.; Dayon, A.; Doumerc, N.; Ader, I.; Golzio, M.; Izard, J.-C.; Hara, Y.; Malavaud, B.; Cuvillier, O. The Sphingosine Kinase-1 Survival Pathway Is a Molecular Target for the Tumor-Suppressive Tea and Wine Polyphenols in Prostate Cancer. *FASEB J.* **2010**, *24* (10), 3882–3894.

(184) Tonelli, F.; Lim, K. G.; Loveridge, C.; Long, J.; Pitson, S. M.; Tigyi, G.; Bittman, R.; Pyne, S.; Pyne, N. J. {FTY720} and (S)-FTY720 Vinylphosphonate Inhibit Sphingosine Kinase 1 and Promote Its Proteasomal Degradation in Human Pulmonary Artery Smooth Muscle, Breast Cancer and

Androgen-Independent Prostate Cancer Cells. *Cell. Signal.* **2010**, *22* (10), 1536–1542.

(185) Garavaglia, S.; Raffaelli, N.; Finaurini, L.; Magni, G.; Rizzi, M. A Novel Fold Revealed by Mycobacterium Tuberculosis NAD Kinase, a Key Allosteric Enzyme in NADP Biosynthesis. *J. Biol. Chem.* **2004**, *279* (39), 40980–40986.

(186) Mori, S.; Yamasaki, M.; Maruyama, Y.; Momma, K.; Kawai, S.; Hashimoto, W.; Mikami, B.; Murata, K. NAD-Binding Mode and the Significance of Intersubunit Contact Revealed by the Crystal Structure of Mycobacterium Tuberculosis NAD Kinase-NAD Complex. *Biochem. Biophys. Res. Commun.* **2005**, *327* (2), 500–508.

(187) Poncet-Montange, G.; Assairi, L.; Arold, S.; Pochet, S.; Labesse, G. NAD Kinases Use Substrate-Assisted Catalysis for Specific Recognition of NAD. *J. Biol. Chem.* **2007**, *282* (47), 33925–33934.

(188) Bakali, H. M. A.; Herman, M. D.; Johnson, K. A.; Kelly, A. A.; Wieslander, A.; Hallberg, B. M.; Nordlund, P. Crystal Structure of YegS, a Homologue to the Mammalian Diacylglycerol Kinases, Reveals a Novel Regulatory Metal Binding Site. *J. Biol. Chem.* **2007**, *282*, 19644.

(189) Nichols, C. E.; Lamb, H. K.; Lockyer, M.; Charles, I. G.; Pyne, S.; Hawkins, A. R.; Stammers, D. K. Characterization of Salmonella Typhimurium YegS, a Putative Lipid Kinase Homologous to Eukaryotic Sphingosine and Diacylglycerol Kinases. *Proteins* **2007**, *68* (1), 13–25.

(190) Miller, D. J.; Jerga, A.; Rock, C. O.; White, S. W. Analysis of the Staphylococcus Aureus DgkB Structure Reveals a Common Catalytic Mechanism for the Soluble Diacylglycerol Kinases. *Structure.* **2008**, *16* (7), 1036–1046.

(191) Labesse, G.; Douguet, D.; Assairi, L.; Gilles, A. M. Diacylglyceride Kinases, Sphingosine Kinases and NAD Kinases: Distant Relatives of 6-Phosphofructokinases. *Trends Biochem. Sci.* **2002**, *27* (6), 273–275.

(192) Coward, J.; Ambrosini, G.; Musi, E.; Truman, J. P.; Haimovitz-Friedman, A.; Allegood, J. C.; Wang, E.; Merrill, A. H.; Schwartz, G. K. Safingol (L-Threo-Sphinganine) Induces Autophagy in Solid Tumor Cells through Inhibition of PKC and the PI3-Kinase Pathway. *Autophagy.* **2009**, *5* (2), 184–193.

(193) Sakakura, C.; Sweeney, E. a; Shirahama, T.; Hagiwara, A.; Yamaguchi, T.; Takahashi, T.; Hakomori, S.; Igarashi, Y. Selectivity of Sphingosine-Induced Apoptosis. Lack of Activity of DL-Erythyro-Dihydrosphingosine. *Biochem. Biophys. Res. Commun.* **1998**, *246* (3), 827–830.

(194) Jin, Y.-X.; Yoo, H.-S.; Kihara, A.; Choi, C.-H.; Oh, S.; Moon, D.-C.; Igarashi, Y.; Lee, Y.-M. Sphingosine Kinase Assay System with Fluorescent Detection

in High Performance Liquid Chromatography. *Arch. Pharm. Res.* **2006**, *29* (11), 1049–1054.

(195) Sugiura, R.; Sio, S. O.; Shuntoh, H.; Kuno, T. Calcineurin Phosphatase in Signal Transduction: Lessons from Fission Yeast. *Genes to Cells.* **2002**, *7* (7), 619–627.

(196) Igarashi, Y.and Hakomori, S. Enzymatic Synthesis of N,N-Dimethyl-Sphingosine:demonstration of the Sphingosine: N-Methyltransferase in Mouse Brain. *Biochem. Biophys. Res. Commun.* **1989**, *164*, 1411–1416.

(197) King, C. C.; Zenke, F. T.; Dawson, P. E.; Dutil, E. M.; Newton, A. C.; Hemmings, B. A.; Bokoch, G. M. Sphingosine Is a Novel Activator of 3-Phosphoinositide-Dependent Kinase 1. *J. Biol. Chem.* **2000**, *275* (24), 18108–18113.

(198) Megidish, T.; White, T.; Takio, K.; Titani, K.; Igarashi, Y.; Hakomori, S. The Signal Modulator Protein 14-3-3 Is a Target of Sphingosine- or N,N-Dimethylsphingosine-Dependent Kinase in 3T3(A31) Cells. *Biochem.Biophys.Res.Commun.* **1995**, *216* (3), 739–747.

(199) Edsall, L. C.; Van Brocklyn, J. R.; Cuvillier, O.; Kleuser, B.; Spiegel, S. N,N-Dimethylsphingosine Is a Potent Competitive Inhibitor of Sphingosine Kinase but Not of Protein Kinase C: Modulation of Cellular Levels of Sphingosine 1-Phosphate and Ceramide. *Biochemistry.* **1998**, *37* (37), 12892–12898.

(200) Valentine, W. J.; Godwin, V. I.; Osborne, D. A.; Liu, J.; Fujiwara, Y.; Van Brocklyn, J.; Bittman, R.; Parrill, A. L.; Tigyi, G. FTY720 (gilenya) Phosphate Selectivity of Sphingosine 1-Phosphate Receptor Subtype 1 (S1P 1) G Protein-Coupled Receptor Requires Motifs in Intracellular Loop 1 and Transmembrane Domain. *J. Biol. Chem.* **2011**, *286* (35), 30513–30525.

(201) Lim, K. G.; Tonelli, F.; Berdyshev, E.; Gorshkova, I.; Leclercq, T.; Pitson, S. M.; Bittman, R.; Pyne, S.; Pyne, N. J. Inhibition Kinetics and Regulation of Sphingosine Kinase 1 Expression in Prostate Cancer Cells: Functional Differences between Sphingosine Kinase 1a and 1b. *Int. J. Biochem. Cell Biol.* **2012**, *44* (9), 1457–1464.

(202) Gustin, D. J.; Li, Y.; Brown, M. L.; Min, X.; Schmitt, M. J.; Wanska, M.; Wang, X.; Connors, R.; Johnstone, S.; Cardozo, M.; Cheng, A. C.; Jeffries, S.; Franks, B.; Li, S.; Shen, S.; Wong, M.; Wesche, H.; Xu, G.; Carlson, T. J.; Plant, M.; Morgenstern, K.; Rex, K.; Schmitt, J.; Coxon, A.; Walker, N.; Kayser, F.; Wang, Z. Structure Guided Design of a Series of Sphingosine Kinase (SphK) Inhibitors. *Bioorganic Med. Chem. Lett.* **2013**, *23* (16), 4608–4616.

(203) Rex, K.; Jeffries, S.; Brown, M. L.; Carlson, T.; Coxon, A.; Fajardo, F.; Frank, B.; Gustin, D.; Kamb, A.; Kassner, P. D.; Li, S.; Li, Y.; Morgenstern, K.; Plant, M.; Quon, K.; Ruefli-Brasse, A.; Schmidt, J.; Swearingen, E.; Walker, N.;

Wang, Z.; Watson, J. E. V.; Wickramasinghe, D.; Wong, M.; Xu, G.; Wesche, H. Sphingosine Kinase Activity Is Not Required for Tumor Cell Viability. *PLoS One.* **2013**, *8* (7).

(204) Adachi, K.; Chiba, K. FTY720 Story. Its Discovery and the Following Accelerated Development of Sphingosine 1-Phosphate Receptor Agonists as Immunomodulators Based on Reverse Pharmacology. *Perspect. Medicin. Chem.* **2008**, *I*, 11–23.

(205) Keng Lim, Chaode Sun, Robert Bittman, Nigel Pyne, and S. P. (R)-FTY720 Methyl Ether Is a Specific Sphingosine Kinase 2 Inhibitor: Effect on Sphingosine Kinase 2 Expression in HEK 293 Cells and Actin Rearrangement and Survival of MCF-7 Breast Cancer Cells. *Cell Signal.* **2011**, *23* (10), 1590–1595.

(206) Raje, M. R.; Knott, K.; Kharel, Y.; Bissel, P.; Lynch, K. R.; Santos, W. L. Design, Synthesis and Biological Activity of Sphingosine Kinase 2 Selective Inhibitors. *Bioorg. Med. Chem.* **2012**, *20* (1), 183–194.

(207) Paugh, S. W.; Paugh, B. S.; Rahmani, M.; Kapitonov, D.; Almenara, J. A.; Kordula, T.; Milstien, S.; Adams, J. K.; Zipkin, R. E.; Grant, S. A Selective Sphingosine Kinase 1 Inhibitor Integrates Multiple Molecular Therapeutic Targets in Human Leukemia. *Blood.* **2008**, *112* (4), 1382–1391.

(208) Xiang, Y.; Asmussen, G.; Booker, M.; Hirth, B.; Kane, J. L.; Liao, J.; Noson, K. D.; Yee, C. Discovery of Novel Sphingosine Kinase 1 Inhibitors. *Bioorg. Med. Chem. Lett.* **2009**, *19* (21), 6119–6121.

(209) Xiang, Y.; Hirth, B.; Kane, J. L.; Liao, J.; Noson, K. D.; Yee, C.; Asmussen, G.; Fitzgerald, M.; Klaus, C.; Booker, M. Discovery of Novel Sphingosine Kinase-1 Inhibitors. Part 2. *Bioorg. Med. Chem. Lett.* **2010**, *20*, 4550.

(210) Schnute, M. E.; McReynolds, M. D.; Kasten, T.; Yates, M.; Jerome, G.; Rains, J. W.; Hall, T.; Chrencik, J.; Kraus, M.; Cronin, C. N.; Saabye, M.; Highkin, M. K.; Broadus, R.; Ogawa, S.; Cukyne, K.; Zawadzke, L. E.; Peterkin, V.; Iyanar, K.; Scholten, J. A.; Wendling, J.; Fujiwara, H.; Nemirovskiy, O.; Wittwer, A. J.; Nagiec, M. M. Modulation of Cellular S1P Levels with a Novel, Potent and Specific Inhibitor of Sphingosine Kinase-1. *Biochem. J.* **2012**, *444* (1), 79–88.

(211) Lynch, K. R. Building a Better Sphingosine Kinase-1 Inhibitor. *Biochem. J.* **2012**, *444* (1), e1–e2.

(212) Evangelisti, C.; Evangelisti, C.; Teti, G.; Chiarini, F.; Falconi, M.; Melchionda, F.; Pession, A.; Bertaina, A.; Locatelli, F.; McCubrey, J. A.; Beak, D. J.; Bittman, R.; Pyne, S.; Pyne, N. J.; Martelli, A. M. Assessment of the Effect of Sphingosine Kinase Inhibitors on Apoptosis,unfolded Protein Response and Autophagy of T-Cell Acute Lymphoblastic Leukemia Cells; Indications for Novel Therapeutics. *Oncotarget.* **2014**, *5* (17), 7886–7901.

(213) Liu, Z.; Macritchie, N.; Pyne, S.; Pyne, N. J.; Bittman, R. Synthesis of (S)-FTY720 Vinylphosphonate Analogues and Evaluation of Their Potential as Sphingosine Kinase 1 Inhibitors and Activators. *Bioorganic Med. Chem.* **2013**, *21* (9), 2503–2510.

(214) Santos, W. L.; Lynch, K. R. Drugging Sphingosine Kinases. *ACS Chem. Biol.* **2015**, *10* (1), 225–233.

(215) Byun, H.-S.; Pyne, S.; MacRitchie, N.; Pyne, N. J.; Bittman, R. Novel Sphingosine-Containing Analogues Selectively Inhibit Sphingosine Kinase (SK) Isozymes, Induce SK1 Proteasomal Degradation and Reduce DNA Synthesis in Human Pulmonary Arterial Smooth Muscle Cells. *Medchemcomm.* **2013**, *4* (10), 1394–1399.

(216) Antoon, J. W.; White, M. D.; Meacham, W. D.; Slaughter, E. M.; Muir, S. E.; Elliott, S.; Rhodes, L. V; Ashe, H. B.; Wiese, T. E.; Smith, C. D. Antiestrogenic Effects of the Novel Sphingosine Kinase-2 Inhibitor ABC294640. *Endocrinology.* **2010**, *151* (11), 5124–5135.

(217) Beljanski, V.; Lewis, C. S.; Smith, C. D. Antitumor Activity of Sphingosine Kinase 2 Inhibitor ABC294640 and Sorafenib in Hepatocellular Carcinoma Xenografts. *Cancer Biol. Ther.* **2011**, *11* (5), 524–534.

(218) Gandy, K. A. O.; Obeid, L. M. Targeting the Sphingosine Kinase/Sphingosine 1-Phosphate Pathway in Disease: Review of Sphingosine Kinase Inhibitors. *Biochim. Biophys. Acta.* **2012**, *1831* (1), 1–10.

(219) MacRitchie, N.; Volpert, G.; Al Washih, M.; Watson, D. G.; Futerman, A. H.; Kennedy, S.; Pyne, S.; Pyne, N. J. Effect of the Sphingosine Kinase 1 Selective Inhibitor, PF-543 on Arterial and Cardiac Remodelling in a Hypoxic Model of Pulmonary Arterial Hypertension. *Cell. Signal.* **2016**, *28* (8), 946–955.

(220) Zegzouti, H.; Zdanovskaia, M.; Hsiao, K.; Goueli, S. a. ADP-Glo: A Bioluminescent and Homogeneous ADP Monitoring Assay for Kinases. *Assay Drug Dev. Technol.* **2009**, *7* (6), 560–572.

(221) Deanna L. Siow and Binks W. Wattenberg. NIH Public Access. *Anal Biochem. December 15; 371(2) 184–193.* **2007**, *2* (15), 184–193.

(222) Zhang, J.-H. A Simple Statistical Parameter for Use in Evaluation and Validation of High Throughput Screening Assays. *J. Biomol. Screen.* **1999**, *4* (2), 67–73.

(223) Li, H.; Totoritis, R. D.; Lor, L. a; Schwartz, B.; Caprioli, P.; Jurewicz, A. J.; Zhang, G. Evaluation of an Antibody-Free ADP Detection Assay: ADP-Glo. *Assay Drug Dev. Technol.* **2009**, *7* (6), 598–605.

(224) Cortés, A.; Cascante, M.; Cárdenas, M. L.; Cornish-Bowden, A. Relationships between Inhibition Constants, Inhibitor Concentrations for 50% Inhibition and Types of Inhibition: New Ways of Analysing Data. *Biochem. J.* **2001**, *357* (Pt 1), 263–268.

(225) Linusson, A.; Gottfries, J.; Olsson, T.; Ornskov, E.; Folestad, S.; Nordén, B.; Wold, S. Statistical Molecular Design, Parallel Synthesis, and Biological Evaluation of a Library of Thrombin Inhibitors. *J. Med. Chem.* **2001**, *44* (21), 3424–3439.

(226) Blanco, S. E.; Almandoz, M. C.; Ferretti, F. H. Determination of the Overlapping pKa Values of Resorcinol Using UV-Visible Spectroscopy and DFT Methods. *Spectrochim. Acta - Part A Mol. Biomol. Spectrosc.* **2005**, *61* (1-2), 93–102.

(227) Bordwell, F. G. Equilibrium Acidities in Dimethyl Sulfoxide Solution. *Acc. Chem. Res.* **1988**, *21* (12), 456–463.

(228) Abdel-magid, A. F.; Mehrman, S. J. A Review on the Use of Sodium Triacetoxyborohydride in the Reductive Amination of Ketones and Aldehydes. *Org. Process Res. Dev.* **2006**, *10* (5), 971–1031.

(229) Gordon W. Gribble & C.F. Nutaitis. borohydride.in.carboxylic.acid.media (2). *Org. Prep. Proced. INT.* **1985**, *17* (5), 317–384.

(230) Green, T. W; Wuts, P. G. M. *Protective Groups in Organic Synthesis*; Wiley-Interscience: New York, 1999.

(231) Bleicher, K. H.; Böhm, H.-J.; Müller, K.; Alanine, A. I. A Guide to Drug Discovery: Hit and Lead Generation: Beyond High-Throughput Screening. *Nat. Rev. Drug Discov.* **2003**, *2* (5), 369–378.

(232) Liang, C.; Lian, H. Recent Advances in Lipophilicity Measurement by Reversed-Phase High-Performance Liquid Chromatography. *TrAC Trends Anal. Chem.* **2015**, *68*, 28–36.

(233) Yu, J.; Li, N.; Lin, P.; Li, Y.; Mao, X.; Bao, G.; Gu, W.; Zhao, R. Intestinal Transportations of Main Chemical Compositions of Polygoni Multiflori Radix in Caco-2 Cell Model. *Evidence-based Complement. Altern. Med.* **2014**, *2014*, 483641–483648.

(234) Lipinski, C. A.; Lombardo, F.; Dominy, B. W.; Feeney, P. J. Experimental and Computational Approaches to Estimate Solubility and Permeability in Drug Discovery and Development Settings. *Advanced Drug Delivery Reviews*. **2012**, *46* (1-3) 3–26.

(235) Defert, O.; Boland, S. Kinase Profiling in Early Stage Drug Discovery: Sorting Things out. *Drug Discov. Today Technol.* **2015**, *18*, 52–61.

(236) Barter, Z. E.; Bayliss, M. K.; Beaune, P. H.; Boobis, A. R.; Carlile, D. J.; Edwards, R. J.; Houston, J. B.; Lake, B. G.; Lipscomb, J. C.; Pelkonen, O. R.; Tucker, G. T.; Rostami-Hodjegan, A. Scaling Factors for the Extrapolation of in Vivo Metabolic Drug Clearance from in Vitro Data: Reaching a Consensus on Values of Human Microsomal Protein and Hepatocellularity per Gram of Liver. *Curr. Drug Metab.* **2007**, *8* (1), 33–45.

(237) Di, L.; Kerns, E. H. *Drug-Like Properties: Concepts, Structure Design and Methods from ADME to Toxicity Optimization*; 2016.

(238) Nelson, D. R. and Nebert, D. W. Cytochrome P450 (CYP) Gene Superfamily. *Cytochrome P450 Gene Superfamily. eLS.* **2011**, *450* (January).

(239) FDA Draft Guidance for Industry. Drug Interaction StudiesStudy Design, Data Analysis, Implications for Dosing, and L. R. http://www.fda.gov/NewsEvents/Newsroom/PressAnnouncements/ucm31783 8.htm (accessed Apr 20, 2017).

(240) Leite, C. F.; Almeida, T. R.; Lopes, C. S.; Dias da Silva, V. J. Multipotent Stem Cells of the Heart-Do They Have Therapeutic Promise? *Front. Physiol.* **2015**, *6* (123), 123.

(241) Horoszewicz, J. S. The LNCaP Cell Line-a New Model for Studies on Human Prostatic Carcinoma. *Prog. Clin. Biol. Res.* **1980**, *37*, 115–132.

(242) Horoszewicz, J. S.; Leong, S. S.; Kawinski, E.; Karr, J. P.; Rosenthal, H.; Chu, T. M.; Mirand, E. A.; Murphy, G. P. LNCaP Model of Human Prostatic Carcinoma. *Cancer Res.* **1983**, *43* (4), 1809–1818.

(243) Watson, D. G.; Tonelli, F.; Alossaimi, M.; Williamson, L.; Chan, E.; Gorshkova, I.; Berdyshev, E.; Bittman, R.; Pyne, N. J.; Pyne, S. The Roles of Sphingosine Kinases 1 and 2 in Regulating the Warburg Effect in Prostate Cancer Cells. *Cell. Signal.* **2013**, *25* (4), 1011–1017.

(244) Flanagan, L.; Meyer, M.; Fay, J.; Curry, S.; Bacon, O.; Duessmann, H.; John, K.; Boland, K. C.; McNamara, D. A.; Kay, E. W. Low Levels of Caspase-3 Predict Favourable Response to 5FU-Based Chemotherapy in Advanced Colorectal Cancer: Caspase-3 Inhibition as a Therapeutic Approach. *Cell Death Dis.* **2016**, *7* (2), e2087.

(245) Huwiler, A.; Kotelevets, N.; Xin, C.; Pastukhov, O.; Pfeilschifter, J.; Zangemeister-Wittke, U. Loss of Sphingosine Kinase-1 in Carcinoma Cells Increases Formation of Reactive Oxygen Species and Sensitivity to Doxorubicin-Induced DNA Damage. *Br. J. Pharmacol.* **2011**, *162* (2), 532–543.

(246) Klionsky, D. J. Autophagy as a Regulated Pathway of Cellular Degradation. *Science (80-.).* **2000**, *290* (5497), 1717–1721.

(247) Lavieu, G.; Scarlatti, F.; Sala, G.; Carpentier, S.; Levade, T.; Ghidoni, R.; Botti, J.; Codogno, P. Regulation of Autophagy by Sphingosine Kinase 1 and Its Role in Cell Survival during Nutrient Starvation. *J. Biol. Chem.* **2006**, *281* (13), 8518–8527.

(248) Scarlatti, F.; Bauvy, C.; Ventruti, A.; Sala, G.; Cluzeaud, F.; Vandewalle, A.; Ghidoni, R.; Codogno, P. Ceramide-Mediated Macroautophagy Involves Inhibition of Protein Kinase B and up-Regulation of Beclin 1. *J. Biol. Chem.* **2004**, *279* (18), 18384–18391.

(249) Lavieu, G.; Scarlatti, F.; Sala, G.; Carpentier, S.; Levade, T.; Ghidoni, R.; Botti, J.; Codogno, P. Sphingolipids in Macroautophagy. *Autophagosome and Phagosome.* **2008**, *445* (3), 159–173.

(250) Yamamoto, A.; Tagawa, Y.; Yoshimori, T.; Moriyama, Y.; Masaki, R.; Tashiro, Y. Bafilomycin A_1 Prevents Maturation of Autophagic Vacuoles by Inhibiting Fusion between Autophagosomes and Lysosomes in Rat Hepatoma Cell Line, H-4-II-E Cells. *Cell Struct. Funct.* **1998**, *23* (1), 33–42.

(251) Klionsky, D. J.; Elazar, Z.; Seglen, P. O.; Rubinsztein, D. C. Does Bafilomycin A 1 Block the Fusion of Autophagosomes with Lysosomes ? *Autophagy* **2008**, *4* (7), 849–850.

(252) Acosta, J. C.; Gil, J. Senescence: A New Weapon for Cancer Therapy. *Trends Cell Biol.* **2012**, *22* (4), 211–219.

(253) Kihara, A.; Anada, Y.; Igarashi, Y. Mouse Sphingosine Kinase Isoforms SPHK1a and SPHK1b Differ in Enzymatic Traits Including Stability, Localization, Modification, and Oligomerization. *J Biol Chem.* **2006**, *281* (7), 4532–4539.

(254) Cingolani, F.; Casasampere, M.; Sanllehi, P.; Casas, J.; Bujons, J.; Fabrias, G. Inhibition of Dihydroceramide Desaturase Activity by the Sphingosine Kinase Inhibitor SKI II. *J. Lipid Res.* **2014**, *55* (8), 1711–1720.

(255) Casasampere, M.; Ordoñez, Y. F.; Pou, A.; Casas, J. Inhibitors of Dihydroceramide Desaturase 1: Therapeutic Agents and Pharmacological Tools to Decipher the Role of Dihydroceramides in Cell Biology. *Chem. Phys. Lipids.* **2016**, *197*, 33–44.

(256) Venant, H.; Rahmaniyan, M.; Jones, E. E.; Lu, P.; Lilly, M. B.; Garrett-Mayer, E.; Drake, R. R.; Kraveka, J. M.; Smith, C. D.; Voelkel-Johnson, C. The Sphingosine Kinase 2 Inhibitor ABC294640 Reduces the Growth of Prostate Cancer Cells and Results in Accumulation of Dihydroceramides in Vitro and in Vivo. *Mol. Cancer Ther.* **2015**, *14* (12), 2744–2752.

(257) Aurelio, L.; Scullino, C. V.; Pitman, M. R.; Sexton, A.; Oliver, V.; Davies, L.; Rebello, R. J.; Furic, L.; Creek, D. J.; Pitson, S. M.; Flynn, B. L. From

Sphingosine Kinase to Dihydroceramide Desaturase: A Structure-Activity Relationship (SAR) Study of the Enzyme Inhibitory and Anticancer Activity of 4-((4-(4-Chlorophenyl)thiazol-2-Yl)amino)phenol (SKI-II). *J. Med. Chem.* **2016**, *59* (3), 965–984.

(258) Holliday, R. Cancer and Cell Senescence. *Nature.* **2001**, *306* (5945), 742.

(259) Carnero, A. *Cell Senescence*; **2013**; 965.

(260) Dick, T. E.; Hengst, J. A.; Fox, T. E.; Colledge, A. L.; Kale, V. P.; Sung, S.-S.; Sharma, A.; Amin, S.; Loughran, T. P.; Kester, M.; Wang, H.-G.; Yun, J. K. The Apoptotic Mechanism of Action of the Sphingosine Kinase 1 Selective Inhibitor SKI-178 in Human Acute Myeloid Leukemia Cell Lines. *J. Pharmacol. Exp. Ther.* **2015**, *352* (3), 494–508.

(261) Beljanski, V.; Knaak, C.; Smith, C. D. A Novel Sphingosine Kinase Inhibitor Induces Autophagy in Tumor Cells. *J Pharmacol Exp Ther.* **2010**, *333* (2), 454–464.

(262) Jiang, Q.; Wong, J.; Fyrst, H.; Saba, J. D.; Ames, B. N. Gamma-Tocopherol or Combinations of Vitamin E Forms Induce Cell Death in Human Prostate Cancer Cells by Interrupting Sphingolipid Synthesis. *Proc. Natl. Acad. Sci. U. S. A.* **2004**, *101* (51), 17825–17830.

(263) Holliday, M. W.; Cox, S. B.; Kang, M. H.; Maurer, B. J. C22:0- and C24:0-Dihydroceramides Confer Mixed Cytotoxicity in T-Cell Acute Lymphoblastic Leukemia Cell Lines. *PLoS One.* **2013**, *8* (9).

(264) Carroll, B.; Donaldson, J. C.; Obeid, L. Sphingolipids in the DNA Damage Response. *Adv. Biol. Regul.* **2015**, *58*, 38–52.

(265) Heffernan-Stroud, L. A.; Helke, K. L.; Jenkins, R. W.; De Costa, A.-M.; Hannun, Y. A.; Obeid, L. M. Defining a Role for Sphingosine Kinase 1 in p53-Dependent Tumors. *Oncogene.* **2012**, *31* (9), 1166–1175.

(266) Lovat, P. E.; Corazzari, M.; Goranov, B.; Piacentini, M.; Redfern, C. P. F. Molecular Mechanisms of Fenretinide-Induced Apoptosis of Neuroblastoma Cells. *Ann. N. Y. Acad. Sci.* **2004**, *1028* (1), 81–89.

(267) Shen, J. C.; Wang, T. T.; Chang, S.; Hursting, S. D. Mechanistic Studies of the Effects of the Retinoid N-(4-Hydroxyphenyl)retinamide on Prostate Cancer Cell Growth and Apoptosis. *Mol. Carcinog.* **1999**, *24* (3), 160–168.

(268) Cancer Research UK, 2016. Https://www.cancerresearchuk.org/. No Title.

(269) Perletti, G.; Monti, E.; Marras, E.; Cleves, A.; Magri, V.; Trinchieri, A.; Rennie, P. S. Efficacy and Safety of Second-Line Agents for Treatment of Metastatic Castration-Resistant Prostate Cancer Progressing after Docetaxel. A Systematic

Review and Meta-Analysis. *Arch. Ital. di Urol. e Androl.* **2015**, *87* (2), 121–129.

(270) Cameron, M.; Hoerrner, R. S.; McNamara, J. M.; Figus, M.; Thomas, S. One-Pot Preparation of 7-Hydroxyquinoline. *Org. Process Res. Dev.* **2006**, *10* (1), 149–152.

(271) Gawley, R. E.; Mao, H.; Haque, M. M.; Thorne, J. B.; Pharr, J. S. Visible Fluorescence Chemosensor for Saxitoxin. *J. Org. Chem.* **2007**, *72* (6), 2187–2191.

(272) Abdel-Magid, A. F.; Carson, K. G.; Harris, B. D.; Maryanoff, C. a.; Shah, R. D. Reductive Amination of Aldehydes and Ketones with Sodium Triacetoxyborohydride. Studies on Direct and Indirect Reductive Amination Procedures. *J. Org. Chem.* **1996**, *61* (11), 3849–3862.

(273) Huwiler, A.; Döll, F.; Ren, S.; Klawitter, S.; Greening, A.; Römer, I.; Bubnova, S.; Reinsberg, L.; Pfeilschifter, J. Histamine Increases Sphingosine Kinase-1 Expression and Activity in the Human Arterial Endothelial Cell Line EA. Hy 926 by a PKC-A-Dependent Mechanism. *Biochim. Biophys. Acta (BBA)-Molecular Cell Biol. Lipids.* **2006**, *1761* (3), 367–376.

(274) Smith, P. K.; Krohn, R. I.; Hermanson, G. T.; Mallia, A. K.; Gartner, F. H.; Provenzano, M. D.; Fujimoto, E. K.; Goeke, N. M.; Olson, B. J.; Klenk, D. C. Measurement of Protein Using Bicinchoninic Acid. *Anal. Biochem.* **1985**, *150* (1), 76–85.

(275) Carrasco, R. A.; Stamm, B.; Lilly, E. Benchmark One-Step Cellular Caspase-3 / 7 Assay. *Biotechniques.* **2003**, *34* (5), 1064–1067.